UNIVERSITY OF CAPE TOWN
IYUNIVESITHI YASEKAPA • UNIVERSITEIT VAN KAAPSTAD

PROPERTIES OF WESTERN CAPE CONCRETE WITH METAKAOLIN

by

ALICE TITUS BAKERA

BKRALI003

SUBMITTED TO THE UNIVERSITY OF CAPE TOWN

In partial fulfilment of the requirements for the degree of

MSc(Eng) in Civil Engineering

Faculty of Engineering and the Built Environment

UNIVERSITY OF CAPE TOWN

Date of Submission:	04 April 2018; Rev. 10 July 2018
Supervisor:	Prof. Mark Alexander
Department:	Civil Engineering
University:	UCT

DECLARATION

I know the meaning of plagiarism and declare that all the work in the document, save for that which is properly acknowledged, is my own. This thesis/dissertation has been submitted to the Turnitin module (or equivalent similarity and originality checking software) and I confirm that my supervisor has seen my report and any concerns revealed by such have been resolved with my supervisor

Signed: Signed by candidate Date: 04 April 2018

Name: Alice Titus Bakera.

ABSTRACT

More than four billion of tons of cement are produced annually for construction purposes in the world. This is associated with high production costs and environmental pollution, since cement manufacturing requires fuel to run the processes, and emits carbon dioxide (CO_2) during the burning of raw materials. With these problems, the use of Supplementary Cementitious Materials (SCMs) is found to be an appropriate solution, as it contributes to the reduction of cement used in concrete by partially replacing cement with SCMs. However, a challenge arises as to the availability of SCMs. This is mainly because many SCMs such as slag, fly ash, and silica fume are industrial by-products. This means that any fluctuation in the production of the primary products (steel, electrical power, and silicon metal) directly affects their availability. Therefore, an alternative SCM such as metakaolin, which is obtained from calcination of kaolin clay, is a potential solution to SCM availability fluctuation, especially in the Western Cape construction industry which depends on the use of Corex slag (GGCS) from a source that can be variable. This raises the need to investigate the properties of concrete with metakaolin, in order to assess its potential for use as an alternative SCM in the Western Cape.

The properties of concrete with a locally available metakaolin were studied with the following specific objectives; i) to characterize metakaolin in terms of its morphology and pozzolanic activity, ii) to assess the influence of metakaolin on fresh and hardened concrete properties, and to compare these with the properties of concrete with GGCS, iii) to assess the influence of metakaolin on the deformation behaviour of concrete, iv) to evaluate the durability properties of concrete containing metakaolin by assessing its potential to mitigate Alkali Silica Reaction (ASR), and to reduce concrete penetrability.

The study followed two methodologies; a substantial and critical literature review of the use of metakaolin in concrete, and laboratory investigations on the performance of metakaolin in mortar and concrete. In the literature review, metakaolin was shown to enhance the properties of concrete. However, various contradictions were highlighted on the influence of metakaolin on certain properties of concrete, such as setting times and tensile splitting strength. Moreover, there were limited studies on the deformation behaviour (especially creep) of concrete with metakaolin, as well as the potential of metakaolin to mitigate ASR. Besides, the characterization of Western Cape concrete with metakaolin had not been extensively studied. Therefore, these gaps raised a need for experimental investigations.

The experimental investigations involved six categories; i) Morphology of metakaolin using Scanning Electron Microscopy (SEM) analysis, ii) pozzolanic reactivity using three tests; strength activity index test, heat of hydration test (semi-adiabatic and isothermal calorimetry tests), and thermogravimetric analysis (TGA), iii) fresh properties of concrete assessed by setting time and workability, iv) hardened properties of concrete using compressive strength, tensile splitting strength, and porosity using Mercury Intrusion Porosimetry (MIP), v) deformation behaviour of concrete using static elastic modulus, and creep and shrinkage tests, and finally, vi) durability properties of concretes assessed by Durability Index (DI) tests, accelerated mortar bar test (ASR), accelerated carbonation test, and chloride bulk diffusion test. Special mortars were designed for pozzolanic activity and accelerated mortar bar tests, while three groups of concretes i.e. with 0.4, 0.5, and 0.6 water/binder (w/b) ratios with five different replacement rates of SCMs (0%, 10%, 15%, and 20% metakaolin, and 50% GGCS) were designed and cast for hardened properties and durability tests.

Experimental results showed that metakaolin had a significant influence on Western Cape concrete properties. It was found that metakaolin had a high pozzolanic activity. Metakaolin in concrete was found to increase setting times while decreasing workability. Compressive and tensile splitting strengths were enhanced by metakaolin, with the highest strengths at 20% replacement level with an increase of approximately 47% and 41% in comparison with the controls, respectively. Metakaolin was found to have a greater influence on concrete with higher w/b ratio. Metakaolin was also found to alter the microstructure of concrete by refining the pores and minimizing their connectivity. The deformation behaviour was also affected by metakaolin. It was found that metakaolin increased the elastic modulus of concrete while decreasing creep and drying shrinkage of concrete. With increasing metakaolin content, the durability of concrete in terms of transport properties, and resistance against deleterious chemical processes was improved. It was concluded that the addition of metakaolin helped to produce concrete with excellent quality. In comparison to GGCS, it was found that in most of the investigated concrete properties, metakaolin outperformed GGCS at equivalent mix proportions.

Technically, metakaolin can therefore be used as a substitute for GGCS in concrete in the Western Cape, thereby contributing a solution to the potential scarcity of SCMs, and potentially reducing environmental effects. Nevertheless, challenges remain on the cost effectiveness, and the willingness and awareness of the construction industry in adapting its use.

ACKNOWLEDGEMENT

Foremost, I praise and give thanks to the Almighty God for His favours and blessings in my life.

I would like to express my sincere gratitude to my supervisor Prof Mark G Alexander for his patience, motivation, guidance, and continuous support of my research and studies.

I would also like to express my gratitude to Prof Pilate Moyo, Prof Hans Beushausen and all CoMSIRU members (2016-2018).

My sincere thanks go to the following organisations for their valuable support in one way or another: The Concrete Institute; Sika South Africa (Pty) Ltd; Pretoria Portland Cement (PPC) Ltd; AfriSam South Africa (Pty) Ltd; Kaolin Group; Serina Trading and The University of Dar es Salaam (Tanzania).

Moreover, I would like to express my appreciation to Nooredien Hassen, Charles May and all Civil Engineering laboratory staffs, UCT; Soraya Von Willingh of the Centre for Materials Engineering, Department of Mechanical Engineering, UCT; Miranda Waldron of the Electron Microscope Unit, Centre for Imaging and Analysis, UCT; Prof Manu Santhanam and Yuvaraj Dhandapani of IIT Madras, India; and Steve Crosswell of PPC Ltd.

Lastly, Special thanks go to my lovely family for supporting me unceasingly throughout my life.

TABLE OF CONTENTS

LIST OF FIGURES

LIST OF TABLES

1. CHAPTER ONE: INTRODUCTION

1.1. BACKGROUND

The global demand for Portland Cement (PC) in the construction industry is projected to rise from 3.27 billion tonnes in 2010 to 4.83 billion tonnes in 2030 due to healthy increases in construction activity in the developing countries (Statista, 2018). This is associated with a high energy intensive process which causes high production costs, and a high carbon dioxide (CO_2) emission to the atmosphere which leads to greenhouse gas effects. Cement production involves calcination of limestone to produce clinker which accounts for 0.8 tonnes of CO_2 per tonne of cement (Rashad, 2013), representing 5-8% of worldwide CO_2 emission (Scrivener and Kirkpatrick, 2008).

Therefore, the use of Supplementary Cementitious Materials (SCMs) has been adopted for the purpose of not only reducing the quantity of PC in construction but also improving strength and enhancing durability of concrete (Siddique and Khan, 2011). The reduction of cement reduces the demand for producing clinker, and hence a substantial decrease in CO_2 emission and production costs (Lothenbach, Scrivener and Hooton, 2011).

However, most SCMs commonly used in construction such as slag, silica fume, and fly ash are industrial by-products whose availability declines with a decrease in production of steel, silicon metal, and coal, respectively. Therefore, it is important to explore other sources of SCMs such as metakaolin from naturally occurring clay minerals (kaolinite). This will help to complement the availability of SCMs and to meet the increase in demand for cement in the construction industry in Africa and elsewhere (Scrivener, 2014).

Unlike other pozzolanic materials, metakaolin is a primary product, not a secondary product or a by-product. It is produced by controlled thermal treatment of kaolin clay (Badogiannis and Tsivilis, 2008). It consists of amorphous silica and alumina that reacts with Calcium Hydroxide (CH) in cement to produce cementitious phases such as Calcium Silicate Hydrates (CSH) and Calcium Aluminate Hydrates (CAH) (Siddique and Khan, 2011). This reaction has several advantages in concrete which are:

i. It improves the durability of concrete by reducing the ingress of water and aggressive ions (i.e. sulphate attack, acid attack, and chloride ion penetration). This is because of its reaction in concrete which leads to concrete impermeability (Sabir, Wild and Bai, 2001). Consequently, its usage in concrete may help to achieve more durable structures.

ii. It prevents expansive Alkali-Silica Reaction (ASR) in concrete when reactive aggregates are used (Ramlochan, Thomas and K. a Gruber, 2000). These aggregates react with alkalis in concrete and produce an expansive alkali-silica gel which causes deterioration of concrete. However, in the presence of metakaolin, alkalis are immobilised, resulting in less tendency for reaction with the aggregate which is harmful to concrete

iii. It enhances early strength development in precast concrete under stream-curing conditions. Instead of using cement with more than 95% clinker whose production generates large CO_2 emissions, the partial replacement by metakaolin can achieve a similar early-age strength. Therefore, its application is suitable for the precast industry. (Cassagnabère, Escadeillas and Mouret, 2008; Cassagnabère *et al.*, 2010).

iv. The energy consumed in the production of metakaolin is lower compared to the energy consumed in the production of PC. This is due to its lower calcination temperature of about between 600 – 900^{o}C, while in cement production, about 1450^{o}C is needed for clinker production (Scrivener, 2014). Therefore, it is more economical due to the lower production costs.

v. Metakaolin is regarded as a sustainable and environmentally-friendly material, due to the limited CO_2 emissions during its production process (Badogiannis *et al.*, 2015). Thus, when it is used as a replacement material for cement, a significant reduction of the total CO_2 emissions is achieved.

1.2. PROBLEM STATEMENT

In the construction industry in the Western Cape, Ground Granulated Corex Slag (GGCS) is currently used as a SCM in concrete. It is occasionally difficult to guarantee the availability of this material since it is a by-product of the iron and steel production industry (Saldanha Steel). It is possible that the decline of steel production or other global factors may lead to scarcity of this material. Nevertheless, the future iron ore extraction methods plan to operate with a slag-free steelmaking process by either designing a system that will neglect a slag process (Li, Hideaki and Tokuda, 1995; Dippenaar, 2004) or recycling slag inside the ironmaking and steelmaking process by using a so-called slag regenerator (Diao *et al.*, 2016). This indicates that in the future all over the world, slag amounts will decrease.

For example, the historical record of South African steel production in Figure 1.1 shows its fluctuation. The amount of steel produced from 2016 to 2018 was lower compared to that between 2014 and 2016. This was directly associated with less GGCS production. Therefore,

a further decline of steel production in South Africa is a threat to the Western Cape concrete construction industry which is highly dependent on GGCS.

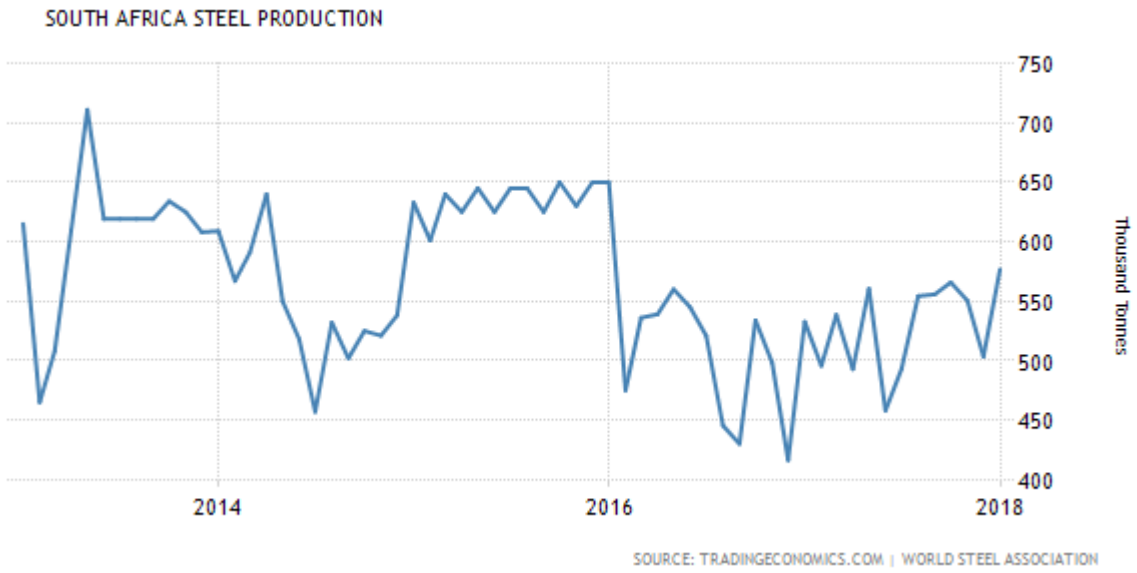

Figure 1.1: South African steel production records (TradingEconomics, 2018)

Another possible SCM that the Western Cape cement industry can use is fly ash, which is produced in large quantities by Eskom electrical power stations. However, the problem of using fly ash in the Western Cape is largely the extensive transport distances needed to freight the fly ash from the Mpumalanga region, mainly, leading to an uneconomical solution.

Therefore, there is a need to consider an alternative SCM for use in the Western Cape. A possible candidate for this material could be metakaolin. However, before metakaolin can be used confidently in concrete, its properties, and effects on the performance (structural and durability) of concrete need to be thoroughly investigated.

1.3. OBJECTIVES

1.3.1. Main objective

The main objective is: To investigate the properties of Western Cape concrete with a locally available metakaolin for use as an alternative SCM in concrete.

1.1.1. Specific objectives

The specific objectives are:

i. To characterise metakaolin in terms of its morphology and pozzolanic activity.
ii. To assess the influence of metakaolin on fresh and hardened concrete properties and compare its performance with concrete with 50% GGCS.
iii. To assess the influence of metakaolin on the deformation behaviour of concrete.

iv. To evaluate the durability properties of concrete containing metakaolin by assessing its potential to reduce concrete penetrability and to mitigate ASR.

1.4. RESEARCH QUESTIONS

From the specific objectives, the following research questions were formulated.

i. Do the physical and chemical properties of metakaolin improve the concrete properties?
ii. What is the pozzolanic activity of metakaolin? How can this best be taken advantage of in fresh and hardened concrete?
iii. What levels of metakaolin replacement are suitable in concrete as a function of the w/b ratio, and what influence do these have on the properties of concrete? How do these influences differ from those of GGCS?
iv. To what extent does metakaolin affect time-dependent properties of concrete (static elastic modulus, creep and shrinkage)?
v. Does metakaolin decrease concrete penetrability, and if so, to what degree for different transport mechanisms?
vi. To what degree does metakaolin mitigate the alkali-aggregate reaction in concrete? What levels of metakaolin are required for adequate ASR mitigation?

1.5. SCOPE AND SIGNIFICANCE OF THIS RESEARCH

This research was limited to the metakaolin obtained from a local Western Cape Supplier, being Serina Trading. The experiments also were conducted to conform to the South African environment. The significance of this study is to enlarge the body of knowledge of use of metakaolin as an SCM. Thus, it leads to awareness on the potential use of metakaolin in South Africa, particularly in the Western Cape.

1.6. RESEARCH OUTLINE

This dissertation consists of five chapters; Chapter one presents the Introduction to the study. It includes the background, problem statement, research objectives, research question, and scope and significance of the study. Chapter two presents the Literature Review on the use of metakaolin in concrete. It includes the review on the following areas; i) general understanding of metakaolin (history of metakaolin, manufacturing process and geological occurrences in South Africa), ii) influence of metakaolin on concrete properties. Chapter three presents the Experimental Methodology which includes the description of materials and various test methods used for the study. Chapter four presents the Analysis and Discussion of Results

obtained after undergoing laboratory investigation. Chapter five presents the Conclusions and Recommendations.

2. CHAPTER TWO: LITERATURE REVIEW

2.1. INTRODUCTION

This chapter gives a summary of the literature review of metakaolin. It describes metakaolin in the following aspects: history of use of metakaolin in concrete, geographical occurrence of metakaolin raw material and its availability in South Africa, manufacture of metakaolin, physical and chemical properties of metakaolin, pozzolanic activity of metakaolin, properties of fresh and hardened concrete with metakaolin, deformation behaviour of concrete with metakaolin, and durability properties of concrete with metakaolin.

Metakaolin is a unique pozzolanic material which comprises two major oxides; aluminium oxide (alumina) and silicon oxide (silica). It is neither a by-product of industrial process nor natural occurring material; it is derived from a naturally occurring material called kaolin clay. It is manufactured specifically for cementing application. When metakaolin partially replaces cement in concrete, it enhances both structural and durability performances of concrete.

2.2. HISTORY OF USE OF METAKAOLIN IN CONCRETE

The knowledge of using calcined clay or burnt clay in cementitious materials was first discovered by Romans. They applied a blended mix of lime, natural pozzolana, and crushed and burnt clay to construct historical structures such as temples, palaces, castles, and defensive ramparts. Thereafter, the development in cement technology was dormant until the eighteenth century, when PC was discovered (Barnes & Bensted 2002:372).

The use of PC in construction continued until the twentieth century, when scientists were keen to produce durable structures. They found that incorporating highly pozzolanic materials such as fly ash, slag, and metakaolin could not only assist concrete to resist sulphate attack and ASR but also to enhance its structural properties (Thomas *et al.*, 2006; Thomas, 2011; Thomas, Fournier and Folliard, 2013).

The first documented use of metakaolin was recorded in 1962 when it was incorporated in the concrete used to construct Jupia dam in the Amazon Basin, Brazil. During construction, highly alkali reactive aggregates were used. A cement blended with metakaolin was used to suppress ASR, subsequently, there has been no deterioration effect reported on its structural properties until now (Rashad, 2013).

In 1994, metakaolin concrete was used to construct structures such as foundations, marine slipways, and water diversion scheme (place not specified). This was an experiment which was done to review a high performance of metakaolin concrete subject to aggressive condition in the field. The structures were reported to perform well within the study period (Asbridge et al. 1996)

In 1975, Davidovits (2015:7) developed a geopolymer cement based on metakaolin and soluble alkali-silica. This initiated the use of metakaolin as a raw material in the production of geopolymer cement. This cement was established as an alternative to PC, thereby potentially reducing the use of PC in the construction industry. However, the application of geopolymer concrete is limited due to major technical and economic barriers.

Metakaolin has been also used recently in the construction industry. Examples of construction projects which used metakaolin are; the ongoing project of construction of new U.S Embassy compounds in Paramaribo, Suriname, South America, which is planned to use more than 500 tonnes of PowerPemba Metakaolin® (DSTN Suriname N.V., 2017). Other projects are Benicia-Martinez Bridge, Broad Contemporary Art Museum- Los Angeles, and Pinalito Hydro Project (Advanced Cement Technologies, 2017). All these projects used PowerPozz™ (high reactivity metakaolin) for purpose of strength enhancement, durability improvement, and ASR mitigation, respectively.

In conclusion, the body of knowledge of metakaolin uses in concrete is still developing worldwide, and scientists are committed to finding out more about metakaolin. Thus, the following section discusses the nature, origin, and availability of metakaolin raw material. This is to understand the nature of this material and why it is the best choice to use in the construction industry.

2.3. GEOLOGICAL OCCURRENCE OF METAKAOLIN RAW MATERIALS AND ITS AVAILABILITY IN SOUTH AFRICA

Before more closely considering the availability of the raw material for metakaolin in South Africa, it is important to understand the geological occurrence of the raw materials. Metakaolin is derived from a kaolin mineral group which comprises kaolinite, dickite, nacrite, and halloysite (Murray 1981:21). However, the most common source is kaolinite which is richly contained in the clay called kaolin clay (Diko et al. 2016).

Kaolin clay ($Al_2Si_2O_5(OH)_4$) is a common phyllosilicate mineral which consists of the so-called 1:1 alternating sheets of silica (Si_2O_5) and alumina ($A_{l2}(OH)_4$) in tetrahedral and

octahedral coordinates (Diko et al. 2016). These two sheets are strongly joined together by a common layer of oxygen and hydroxyl, see Figure 2.1. However, the kaolinite structure has a very limited substitution, in which some titanium or aluminium ions may be found substituting silicon in the tetrahedral layer. Because of this, kaolinite is characterised by low cation exchange and sorptivity capacity, relatively low surface area, good rheology, and plasticity (Murray 1981:21-23).

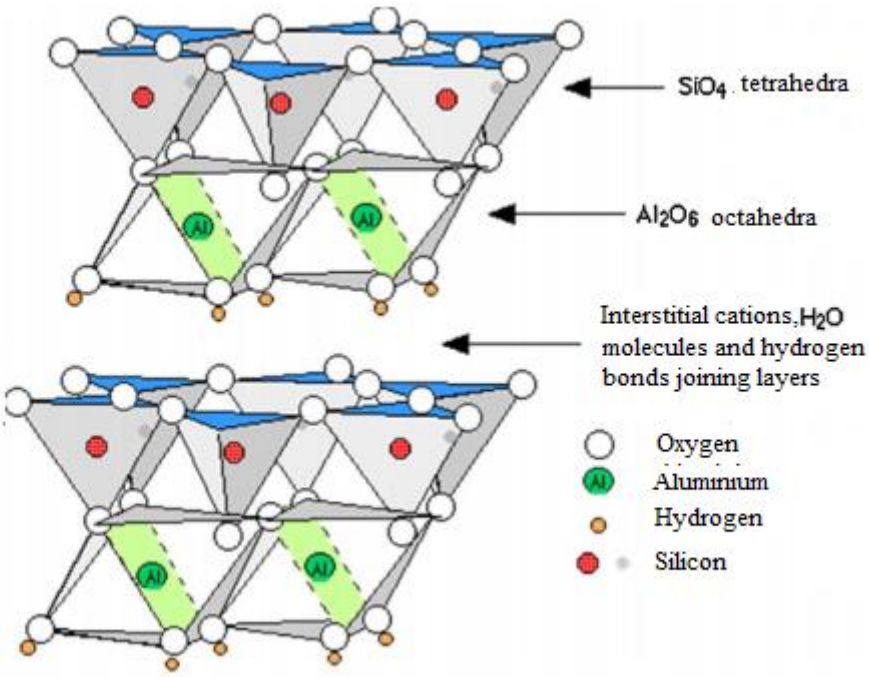

Figure 2.1: Kaolinite (kaolin clay) structure (Ravi et al., 2017)

Bloodworth et al. (1993) described this clay as either non-plastic kaolin (china clay) or plastic kaolin (ball clay). The authors define non-plastic kaolin as clay with low plasticity and low dry strength due to relatively coarse particle size, whereas plastic kaolin has high plasticity and high dry strength. They claimed that this clay can be distinguished from other clays by its whiteness, fineness, and controllable particle sizes.

Ekosse (2010) and Bloodworth et al. (1993) classified kaolin deposits or occurrences into two classifications; residual (primary) deposits and sedimentary (secondary) deposits. Residual deposits are derived from in-situ alteration of alumina-silicate-rich parent rock such as granite or granitic gneiss by weathering, hydrothermal processes, and rarely volcanic processes. On the other hand, sedimentary deposits are those which occur in sedimentary rocks and sometimes are formed by transportation and deposition of kaolin clay from in-situ formations.

In South Africa, Ekosse (2010) reported twenty kaolin deposits which are the product of residual weathering of granites, feldspathic gneiss, and shales. These are in Cape Town area, Grahamstown District, Pretoria (Bronkhorstspruit area), Limpopo, Namaqualand, Mpumalanga, North West, and KwaZulu-Natal. Hosterman et al. (1990) also reported the presence of 60 million tonnes of kaolinized tillite found in Grahamstown of which 80% is kaolin clay.

In Western Cape, kaolinite is obtained from both pure kaolin clay and plastic clay. Kaolin clay is abundantly available in Cape Town, Vredenburg peninsula, and southern Namaqualand areas. Previously, this clay was used as a filler in the ceramic and paper industries. Around the twentieth century, the high competition from calcium carbonates reduced the market of kaolin clay in those industries. Therefore, Cole et al. (2014) reported a total of eight abandoned mines and nine unexploited deposits holding about 19.7 million tonnes of kaolin in Cape Town, see Table 2.1. In Vredenburg Peninsula, they reported three unexploited deposits holding 0.6 million tonnes, and in Southern Namaqualand areas, they reported two abandoned mines, and other more seven unexploited deposits holding 11.5 million tonnes of kaolin clay.

Table 2.1: Distribution of unexploited kaolin deposits and abandoned mines in Cape Town.

Area	Location	Unexploited deposits	Abandoned mines
Cape Town	Noordhoek- Fish Hoek Valley	3	5
	Brackenfell Kuils River area	3	2
	Stellenbosch- Somerset West area	3	1
	Total	9	8

Cole et al. (2014) also reported that the amount of plastic clay found in Western Cape province and in Buffelsfontein Farms (435.3 km from east of Albertinia) is significant to be exploited for about 50 years to come. This clay is rich in kaolinite, with few amounts of quartz, mica, illite, montmorillonite and organic materials. Therefore, the future of kaolinite in Western Cape seems assured since the resources are reliable and guaranteed.

Even though resources are available, the raw material must be processed into the reactive state for construction purposes. Therefore, the means of its manufacture must be discussed.

2.4. MANUFACTURE OF METAKAOLIN

The name metakaolin consists of two words “meta” and “kaolin.” Meta means change and kaolin stands for kaolin clay. Thus, metakaolin means changing a state of kaolin clay by dehydroxylation process. Dehydroxylation of kaolin clay is an endothermic process that

involves a removal of physically absorbed water and chemically bounded hydroxyl ions in the clay by applying heat energy under controlled condition. The dehydroxylation product (metakaolin) is an amorphous mixture of silica and alumina and free of water molecules (Chakraborty, 2013).

In that case, metakaolin can be derived from the following three technical methods; mechanical activation, thermal activation, and calcination of waste paper sludge as summarised in Figure 2.2

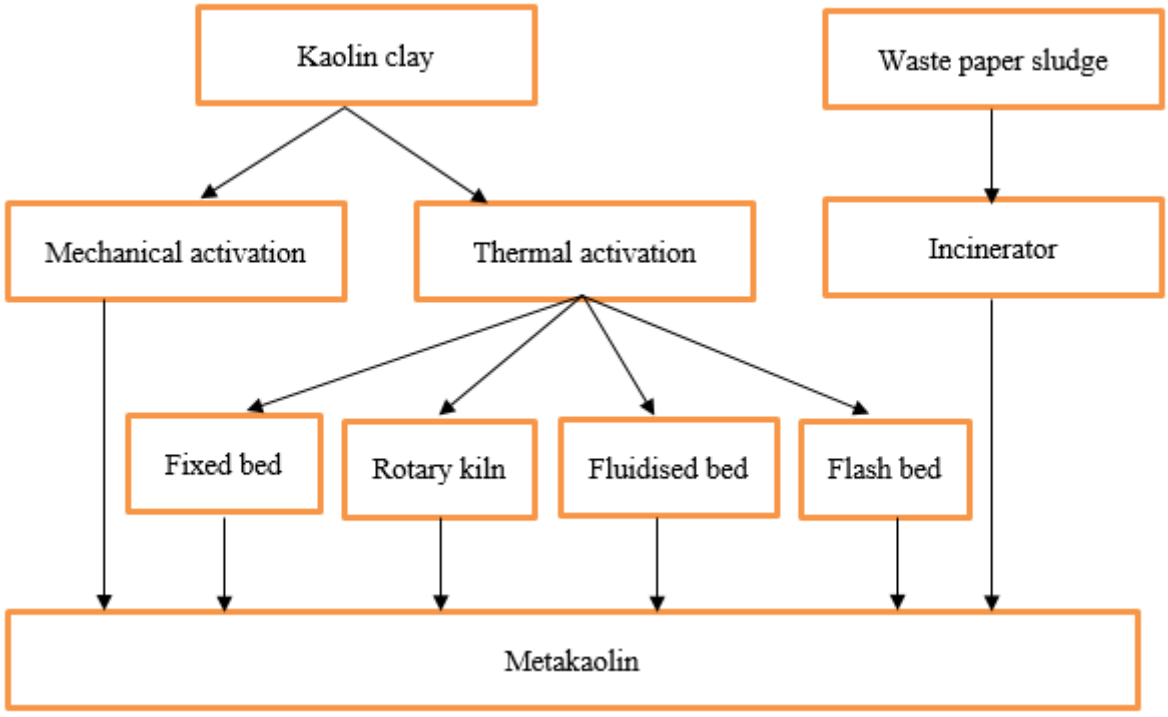

Figure 2.2: Illustration of different methods used in the production of metakaolin (Bapat 2013:94)

2.5. MECHANICAL ACTIVATION OF KAOLIN CLAY

Mechanical activation or treatment of kaolin is defined as the amorphization process of kaolin clay by applying grinding and size reduction operations. Grinding operations are applied to bend or break down the crystal structure of kaolin clay. This is followed by size reduction operation which is carried out in a vibratory, oscillatory, or planetary mill, whereby the impact and friction forces are applied to the particles to produce metakaolin. This metakaolin sometimes is called an amorphous kaolin. Its pozzolanic activity is highly dependent on the composition of its raw material as well as the grinding time. This process does not involve any combustion process and hence no greenhouses gases are emitted except those generated from electric grinding machines. Therefore, it has an environmental advantage (Bapat 2013:96).

2.5.1. Thermal activation of kaolin clay

Thermal activation of kaolin clay is mostly adapted for large scale applications. It produces a large quantity of metakaolin within a short period. This method entails dehydroxylation or calcination of kaolinite clay at a specific temperature to drive off the chemically bound water and destroy the crystalline structure of clay. The specific temperature must correspond to a range between endothermal dehydration of clay and exothermal recrystallization of high-temperature phases (Bapat 2013:96). Ramezanianpour (2014:225) specified a temperature between 650^{o}C to 900^{o}C, Rashad, (2013) a temperature between 600^{o}C to 900^{o}C, while Siddique (2008) between 500^{o}C to 800^{o}C. Therefore, a reasonable calcining temperature is considered to be lying between 500^{o}C and 900^{o}C, see equation 2.1.

$$\overset{\text{Kaolin clay}}{Al_2Si_2O_5(OH)_4} \xrightarrow{500^{o}C-900^{o}C} \overset{\text{Metakaolin}}{Al_2O_3.2SiO_2} + 2H_2O \qquad (2.1)$$

To achieve a highly reactive metakaolin, kaolin clay should be thoroughly roasted during dehydroxylation. Overheating kaolin clay should be avoided since it results in sintering and formation of mullite which is a nonreactive material.

Nicolas et al. (2013) described three stage methods of manufacturing metakaolin, i.e. selection/grinding process, calcination process, and subsequent grinding process. In the calcination process, either of the following four processes (Figure 2.2) can be employed (Bapat 2013:96);

2.5.1.1. Fixed bed calcination

This method is preferable to produce metakaolin for laboratory purposes. It involves the use of a fixed bed furnace or technique. A dried kaolin clay is fed into the furnace and heated from the ambient temperature up to 700^{o}C for about 6 h at a rate of 250^{o}C/ h. Thereafter, the material is cooled to 450^{o}C while the furnace is closed. Finally, the material is discharged and cooled in a desiccator at ambient temperature. In this process, a reactive metakaolin is obtained by grinding the cooled material in a mortar mill until 100% of mass pass through a 45 µm sieve (Pera and Amrouz, 1998; Tironi *et al.*, 2013).

2.5.1.2. Traditional soak calcination process.

In this process, kaolin clay is calcined in a rotary kiln calciner for several hours. This kiln is a cylindrical vessel which is slightly inclined horizontally and rotated slowly about its axis. It is 60 to 90 m in length and 4 to 6 m in diameter. The clay is fed on its upper end. As it rotates, the hot gases of 650^{o}C to 900^{o}C dehydroxylate the clay for about 3 to 5 h. This process

produces agglomerate metakaolin particles of 5 to 10 cm in diameter which requires further grinding into very fine particles (Nicolas, Cyr and Escadeillas, 2013).

2.5.1.3. Fluidised bed calcination process

This process requires only few minutes of calcination (Bapat 2013:96). It can be employed using either a stationary fluidised or a circulating fluidised bed reactor. A first step involves grinding a raw kaolin clay into a finer grained material with 80% of the particles having a size ranging between 0.1 to 3 mm. Thereafter, a fluidised bed reactor is supplied with a mixture of fuel, oxygen-containing gas, and granular kaolin. The reactor is maintained at a calcination temperature between 850^{o}C to 950^{o}C, then, the mixture stays in a combustion zone for about 3 to 5 s before going through a cooling zone. In the cooling zone, a gas of 200^{o}C temperature is allowed to pass over the mixture, and finally, metakaolin is withdrawn from the reactor ready to be used as SCM (Bareuther *et al.*, 1976).

2.5.1.4. Flash calcination process.

A flash calciner with a pneumatically suspended feeder is used in this process (Teklay *et al.*, 2015). The clay is firstly pre-treated, air-dried, and ground into powdered particles. Finally, it is dried again at 100^{o}C, then sieved on a 200 μm sieve. During calcination process, the powdered clay is fed into the calciner and is rapidly heated at a temperature between 1000°C and 1200°C for a short period (0.1 to 1 s). Lastly, it is quenched rapidly with a counterflow of cold gas. The final product has very fine particles, hence it does not need further grinding (Nicolas et al. 2013).

2.5.1.5. Comparisons of different calcination processes

Generally, fixed bed and rotary kiln processes are considered as traditional 'soak calcination', while fluidised bed and flash calcination process are considered similar. Nevertheless, most of the studies seemed to adapt either the use of traditional soak calcination or flash calcination process during the production of metakaolin. Therefore, in this section, these two processes are discussed.

Flash calcination process has economic, social, and environmental advantages. Firstly, it offers a minimum energy consumption, quoted as 2.5 times less than tradition soak calcination process (Argeco DéveloppementCompany, 2017). Nicolas et al. (2013) also added that flash calcination consumes 2.2 MJ of energy to produce one tonne of metakaolin which is 80% less than the energy consumption in cement production. This minimal energy consumption leads to a very competitive cost of metakaolin compared to other hydraulic binding materials.

Secondly, the flash calcination process has less emission of greenhouses gases and pollution (Argeco Développement Company 2017). Generally, it has zero CO_2 gas emission during raw material transformation. The visual and sound pollution generated on the surrounding environment is low compared to both traditional calcination and cement production industry. Hence, such plant can be installed near to the market, consequently, metakaolin becomes secure and economical.

Unlike the traditional soak calcined product, the flash-calcined product is characterised by low density, lower specific surface area, high light absorption capacity (Salvador, 1995) and mainly spherically shaped particles. These characteristics are due to the omission of final grinding process, hence, they enhance its good workability when blended with cement (Claverie *et al.*, 2015). However, soak calcined metakaolin exhibits slightly higher early strength development than flash calcined metakaolin (Nicolas, Cyr and Escadeillas, 2013). This is due to its high specific surface area associated with final grinding process. Generally, flash calcination process is preferable in the production of commercial metakaolin because it saves both production time and energy.

2.5.2. Calcination of waste paper sludge

Kaolin clay is used in the paper industries as filler. Therefore, the waste products from those industries are believed to contain high quantity of kaolinite minerals and other minor minerals such as calcite, muscovite, talc, quartz, and cellulosic matter. In that case, recycling this sludge by calcination process results in the production of highly reactive metakaolin. Bapat (2013:98) said when waste paper sludge is calcined at a temperature between 600^{o}C to 800^{o}C, the end product is metakaolin which comprises alumina, silica and minor lime. This lime is produced after decomposing calcite at 800^{o}C. The authors also said the characteristics of this metakaolin are very similar to that produced from pure natural kaolin clay. In that case, the calcined waste paper sludge is an alternative source of metakaolin as well as offering a route to the utilisation of the waste materials associated with environmental preservation.

2.6. PHYSICAL AND CHEMICAL PROPERTIES OF METAKAOLIN

Metakaolin is a pozzolanic material which is white in colour. It has very fine particles with an average size of less than 3 µm depending on the process of manufacture (Siddique and Khan, 2011). Metakaolin particles are also smaller than cement particles, but not as fine as silica fume. However, more than 99.8% of its particles pass a 45 µm sieve (Bapat 2013:100). Its mineralogy

is Al-Si in a non-crystalline form with angular and platy particles, see Figure 2.3 and Figure 2.4.

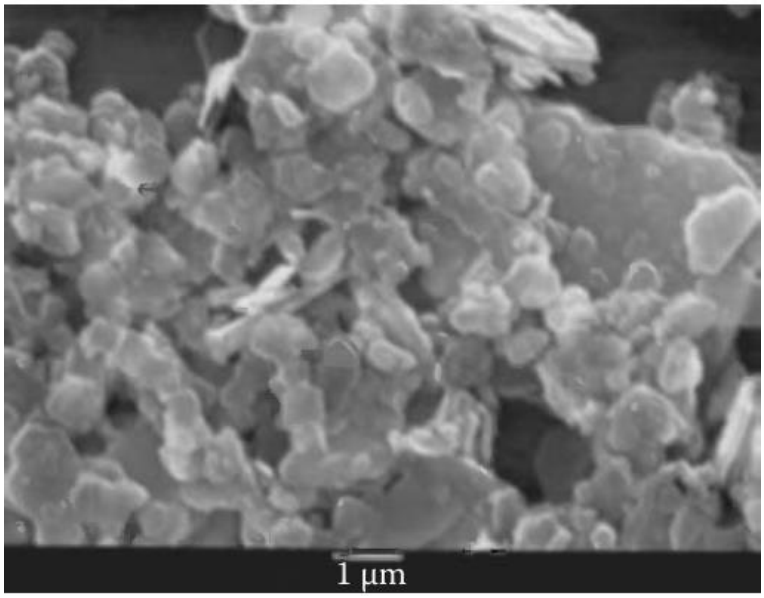

Figure 2.3: Typical scanning electron micrograph of MK manufactured by thermal activation (Bapat 2013:101)

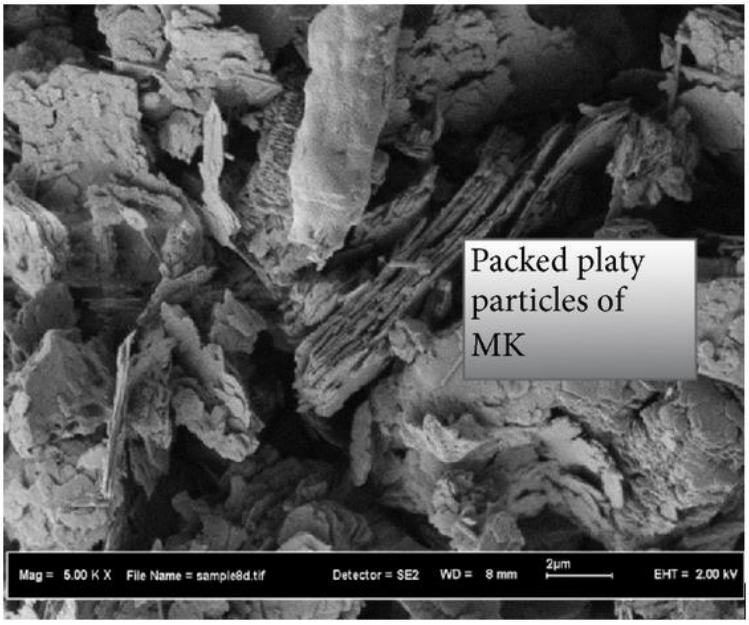

Figure 2.4: Typical scanning electron micrograph of metakaolin (Yusuf et al., 2014)

Table 2.2 shows its physical properties derived from different sources. Since the fineness of metakaolin significantly depends on calcination processes, hence the different values of fineness observed in Table 2.2 are probably due to the processes employed. When tradition soak-calcination process is used, metakaolin with a high specific surface area is produced. This

is due to the final grinding process which is omitted in flash calcination process. However, test method used to determine fineness can also explain the differences in the fineness values

Table 2.2: Physical and chemical properties of metakaolin

References	Zhang and Malhotra (1995)	Subaşı and Emiroğlu (2015)	Barnes and Bensted (2002)	Poon et al. (2001)
Specific gravity	2.5	2.56	2.6	2.62
Fineness (m^2/g)	16.8[a]	0.918[b]	10 - 25[a]	1.268[b]
Avg. Particle size (µm)	1.3	-	2	-
Particle size distribution	99.8% passed a 45µm sieve	> 90% passes a 45µm sieve	-	-

NB: [a] = BET nitrogen surface area, [b] = Blaine surface area.

Table 2.3 shows chemical composition of metakaolin from different sources. All types of metakaolin are rich in silicon oxide and aluminium oxide comprising more than 90% of metakaolin. Other minor components are ferric oxide, calcium oxide, magnesium oxide, and potassium oxide. The metakaolin in Table 2.3 contains only a small quantity of calcium oxide, therefore no capacity to undergo hydration process by themselves. Aluminium oxide also adds an advantage in concrete on resisting sulphate attack. This is due to its pozzolanic reaction which results in the production of additional alumina containing phases such as tetracalcium aluminate hydrate (C_4AH_{13}), stratlingite (C_2ASH), gehlenite hydrate (C_2ASH_8), and hydrogarnet (C_3AH_6) (Bapat 2013:100).

Table 2.3: Chemical composition of metakaolin.

Mineral component (%)	Duan et al. (2013)	Frías et al. (2000)	Poon et al. (2001)	Robayo-Salazar et al. (2016)
SiO_2	50.27	51.60	53.2	50.72
Al_2O_3	34.46	41.30	43.9	44.63
Fe_2O_3	0.75	4.64	0.38	0.37
CaO	0.29	0.09	0.02	-
MgO	-	0.16	0.05	-
SO_3	0.21	-	-	-
TiO_3	-	0.83	1.68	1.76
K_2O+Na_2O	-	0.63	0.27	-
LOI	12.65	0.60	0.50	0.86

2.7. POZZOLANIC ACTIVITY OF METAKAOLIN

Pozzolanic activity of a material is defined as the ability of that material to react with calcium hydroxide (CH). CH is also known as Portlandite, which is formed by dissolving calcium oxide (CaO) in water (equation 2.2). Thomas (2013:33) noted that pozzolanic activity can be

described as either the rate at which the material reacts with CH or as the amount of CH reacted or combined with the phases of the material. These phases are silica (S) and alumina (A).

$$CaO + H_2O = Ca(OH)_2 \quad (2.2)$$

Thomas (2013:33) indicated that the rate of reaction depends upon the specific surface area of the material, water/binder (w/b) ratio of the mix, and temperature. High specific surface makes pozzolanic reaction easier, however, this applies only at the early stage of the reaction. In the long term, the rate of reaction remains controlled by the phases of the pozzolan (Walker and Pavı´a, 2011). Moreover, high w/b ratio provides a better dispersion of pozzolanic particles and temperature accelerates their movement, consequently, increases the rate of reaction (Mindess et al. 2003:96).

The amount of CH reacted depends on the nature and content of the reactive phases in the material, CH /pozzolan ratio of the mix, and mix curing duration. Reactivity of the phases significantly depends on the calcination temperature during production, purity of its raw materials (Sabir et al. 2001), and the amorphousness of the material; mostly or totally amorphousness phases are considered to be more reactive than crystalline phases (Walker and Pavı´a, 2011). These influence a high consumption of CH, although a low CH/pozzolan ratio also ensures that CH produced in cement paste is completely consumed. Besides, the consumption of CH is also affected by the curing time, as curing time increases, the rate of CH production keeps decreasing compared to the early stages of curing.

2.7.1. Metakaolin pozzolanic reaction mechanism

PC consists of four clinker compounds; C_3S (tricalcium silicate or alite), C_2S (dicalcium silicate or belite), C_3A (tricalcium aluminate), and C_4AF (calcium aluminate ferrite). C_3S is about 50-90% content into cement, whereby C_2S is 10-40%, and the remaining percentage is the total of C_3A, C_4AF and other oxides (Barnes & Bensted 2002:29&33).

During hydration process, C_3S and C_2S react with water to produce calcium silicate hydrate (CSH) and CH (equations 2.3 and 2.4), whereby a substantial portion of CH is produced by C_3S. This is because, firstly, the quantity of C_3S is higher in cement compared to the rest of clinker compounds, and secondly, its C/S molar ratio (=3.0) is greater than that of CSH formed (between 1.4 and 2.0) (Hewlett 2004:249). Therefore, the remaining CaO is significant to produce CH compared to C_2S. Nevertheless, a small portion of CH produced reacts with alumina (C_3A and C_4AF) to form C_3AH_6 and C_4AH_{19} (equation 2.5). In the presence of gypsum, C_3A reacts with gypsum to form compounds such as ettringite (not in excess) which

contributes to early strength. Therefore, the remaining CH is responsible for the pozzolanic reaction.

$$2C_3.S + 11H = C_3.S_2.H_8 + 3CH \quad (2.3)$$

$$2C_2.S + 9H = C_3.S_2.H_8 + CH \quad (2.4)$$

$$2C_3A + 24H + CH = C_3AH_6 + C_4AH_{19} \quad (2.5)$$

Metakaolin (AS_2, A = $A1_20_3$; S = SiO_2) in concrete or mortar reacts with the remaining CH and produces more cementitious phase mainly calcium silicate hydrate (CSH) and gehlenite hydrate (C_2ASH_8 (see equation 2.6) (Hewlett 2004:496). The composition of CSH produced here is similar to that produced by C_3A, although its C/S molar ratio is slightly lower.

$$3CH + AS_2 + 6H = CSH + C_2ASH_8 \quad (2.6)$$

Note:

Abbreviations	*CH*	*A*	*C*	*F*	*H*	*S*
Formula	*$Ca(OH)_2$*	*Al_2O_3*	*CaO*	*Fe_2O_3*	*H_2O*	*SiO_2*

Nevertheless, the pozzolanic reaction tends to slow down due to the presence of a strong concentration of metal ions such as Potassium (K^+) and Sodium (Na^+) from the dissolved oxides in cement. These ions react with the reactive phase of metakaolin to produce an amorphous alkali silicate. However, an abundance of calcium ions and low solubility of CSH in the system cause the alkali-silicate phase to be short-lived (Thomas 2013:33). Thus, pozzolanic reaction continues until either CH or pozzolanic phases (S and A) are completely consumed.

2.7.2. Test methods for pozzolanic activity

Ramezanianpour (2014) categorised the means of evaluating the pozzolanic activity of pozzolanic materials into three categories: chemical, physical, and mechanical. Chemical evaluation includes, firstly, the measurement of the total amount of silicon oxide, aluminium oxide and iron oxide reduced during the pozzolanic reaction, and secondly, the measurement of the reduced amount of calcium ions in the pozzolan-saturated lime solution. Physical evaluation includes the use of X-ray diffraction analysis (XRD), while mechanical evaluation is divided in two ways; by measuring the heat evolved during the pozzolanic reaction, and by determining the compressive strength of mortar containing pozzolan, bearing in mind that compressive strength also depends on the nature of cement used.

Donatello et al. (2010) divided the evaluation techniques into two categories; direct methods and indirect methods. Direct methods determine the presence of CH and its reduction with time. These include analytical methods such as X-ray diffraction (XRD), thermogravimetric analysis (TGA), differential thermal analysis (DTA), or classical chemical titration such as the Frattini test and the saturated lime method. Indirect methods involve evaluation of physical properties of a test sample that indicates the extent of pozzolanic activity such as compressive strength, electrical conductivity, and heat evolution using calorimetry.

The following two subsections discuss work done by different researchers on determining the pozzolanic activity of metakaolin in terms of CH consumption and heat of hydration.

2.7.3. CH consumption

On completion of the cement hydration process, the amount of CH generated is approximately equal to 28%, although in practice complete hydration is difficult to achieve, hence, CH ranges between 16% to 20% (by cement weight) (Wild & Khatib 1997). CH is partially water soluble and chemically reactive particularly with acids, gases, sulphate ions, reactive pozzolans, and reactive aggregates. Thus, it substantially influences durability performance of mortar and concrete.

Barnes and Bensted (2002:378) claimed that a partial replacement of cement by 20% to 25% metakaolin contributes to the removal of CH in concrete. This removal plays an important role in improving the interface zone between aggregates and paste, increasing the resistance to acid attack, chloride attack, sulphate attack, and preventing ASR.

Wild and Khatib (1997) examined the strength development and CH consumption in cement paste and mortar samples with 0% to 15% metakaolin. They used TGA to determine CH content until 365 days of curing. They observed that CH amount decreased significantly with metakaolin. Likewise, CH content in 5% and 15% metakaolin mortars was at the lowest values at 14 days, while in 10% metakaolin mortar was at 7 days (see Figure 2.5). They explained this as a result of high rate of pozzolanic reaction. Furthermore, they suggested that replacement levels considerably more than 15% were required for full removal of CH. However, this idea may not be desirable since it may contribute to lowering the pH of concrete.

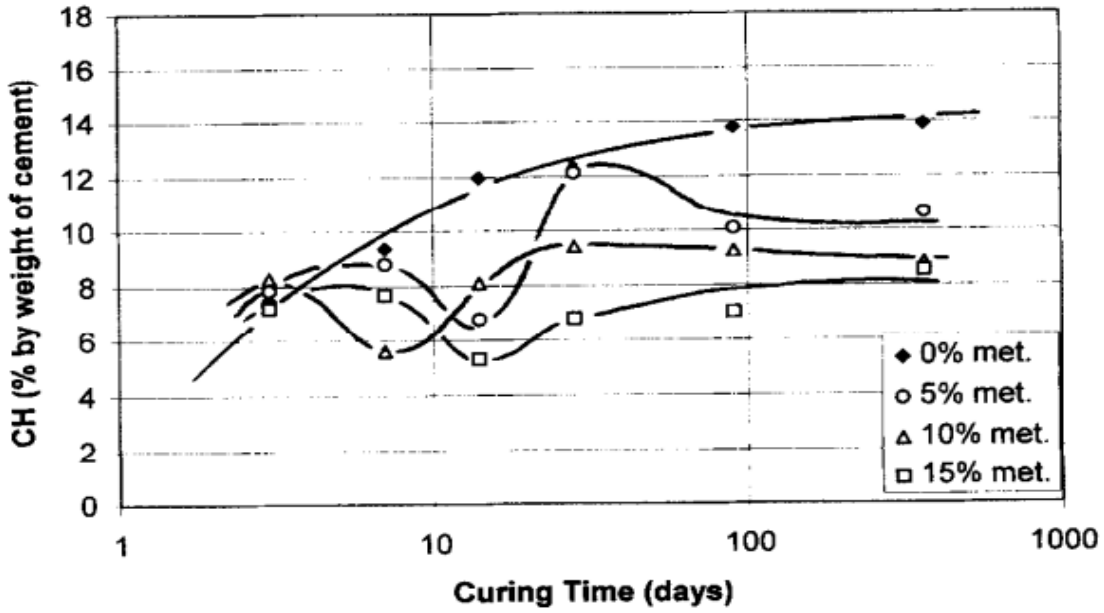

Figure 2.5: The change in calcium silicate content Vs curing time for mortar containing metakaolin (Wild and Khatib, 1997).

Frias and Cabrera (2000) also observed the same results. CH contents in the samples with metakaolin increased between 3 and 7 days (Figure 2.6), then decreased until 100 days (Figure 2.7). They explained this behaviour as the result of hydration process and pozzolanic reaction, respectively. However, they noted that the inclusion of metakaolin in cement paste accelerated hydration process, hence more CH content was produced at an early age compared to the cement paste without metakaolin. Their results showed that CH content decreased with hydration time and replacement rate up to 25%.

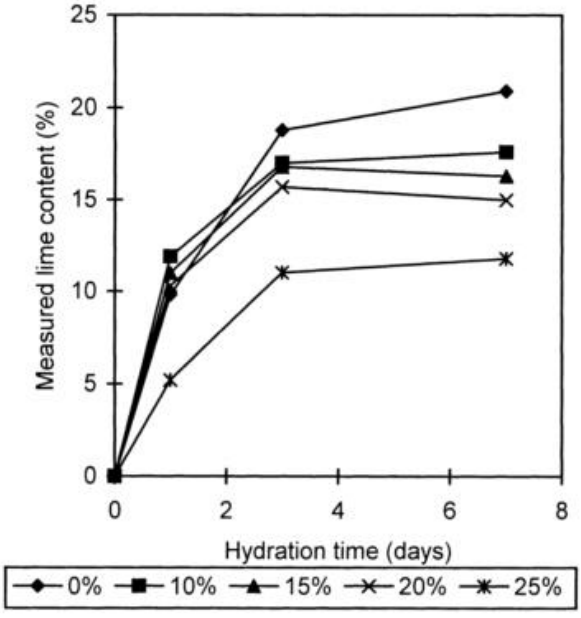

Figure 2.6: Evolution of CH with time at early ages (Frías and Cabrera, 2000)

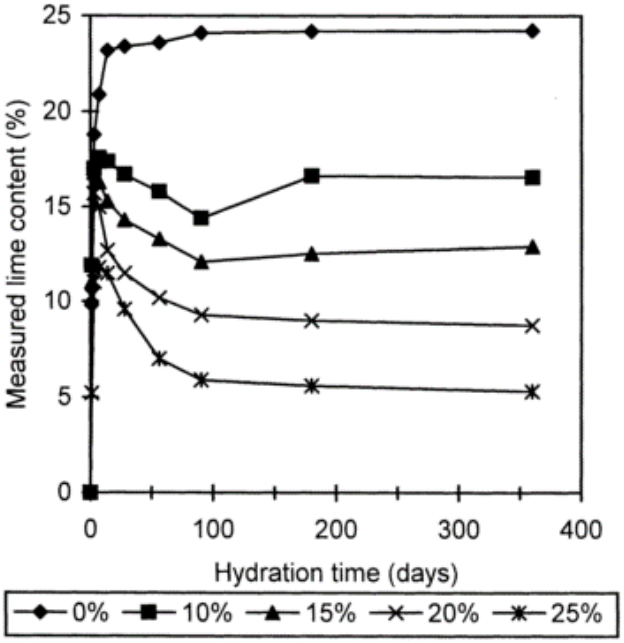

Figure 2.7: Evolution of CH with time in long term (Frías and Cabrera, 2000)

Subaşı and Emiroğlu (2015) used XRD spectroscopy to examine phase and hydration developments in cement paste samples. CH contents were measured at 28 days of hydration. The results showed the reduction of CH as metakaolin content increased in the mortar samples. The lowest CH content was determined at 30% replacement level. This was also due to metakaolin pozzolanic behaviour.

Therefore, metakaolin content between 20% and 30% is sufficient to reduce high CH content in concrete. To better understand the pozzolanic activity of metakaolin, the literature was reviewed on the influence of metakaolin on the heat of hydration.

2.7.4. Heat of hydration

Cement hydration reaction is an exothermic reaction which generates heat that impacts the performance of concrete. It mainly induces thermal stresses which cause a volume change (expansion) and microcrack formation in the mass concrete (Owens 2009:273). These microcracks increase the penetrability to aggressive ions and water which attribute to durability problems.

Reduction of cement content by replacing with pozzolanic materials reduces the content of clinker compounds, and consequently, a significant reduction in heat evolved (Newman & Choo 2003:13/26). Figure 2.8 shows the proportionality relationship between cement content and heat generated. This implies that when less cement is used due to its replacement by SCMs,

the heat generated also decreases. However, not all SCMs have the same positive influences; some such as silica fume tend to accelerate the hydration reaction and lead to high heat generation. In that case, it is important to study the effect of metakaolin.

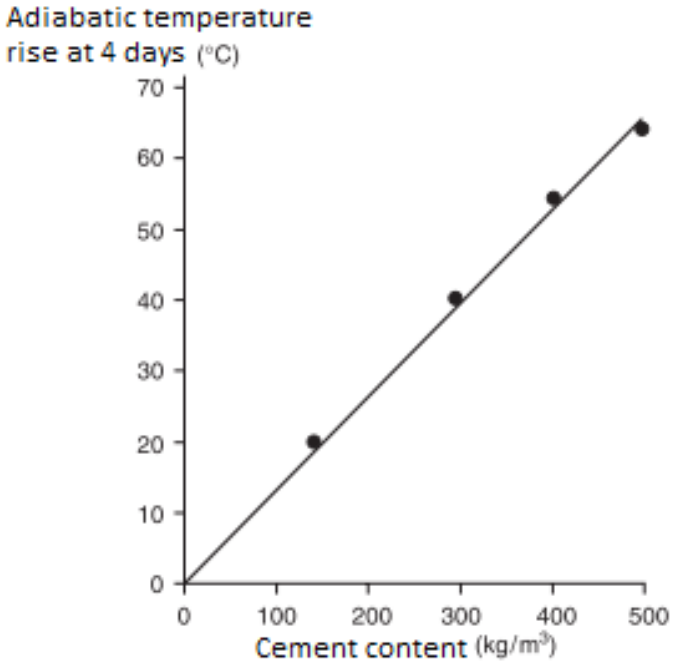

Figure 2.8: Adiabatic temperature rise as affected by cement content (Newman & Choo 2003:13/27)

According to the study done by Frías et al. (2000) who used a Langavant Calorimeter (the Spanish standard) to measure heat of hydration showed that the blended mortar with 10% and 30% metakaolin generated higher heat than PC mortar. The temperature of about 55ºC and 60ºC were measured inside 10% and 30% metakaolin blended mortars, respectively. The heat of hydration for samples with silica fume and metakaolin were approximately similar, generally produced the increasing values, while those with fly ash produced decreasing values with respect to the plain mortar. The authors reasoned this as a result of high pozzolanic activity of silica fume and metakaolin which generated more heat than plain mortar during the first few hours of hydration. This was due to an exothermic effect of pozzolanic reaction which was observed by a steep ascending slope on a curve of change in temperature of metakaolin mortar against time.

The same method was used by Bai and Wild (2002). Their results showed a greater temperature rise in the mortars with 5% to 15% metakaolin than that in the control and pulverised fuel ash mortars, see Figure 2.9. This was attributed to the increased rates of heat evolution during the first few hours of hydration resulting from the combined effect of both pozzolanic and

hydration reactions. However, temperature declined with increase in hydration time. The authors explained this as the result of CH reduction in the mortars.

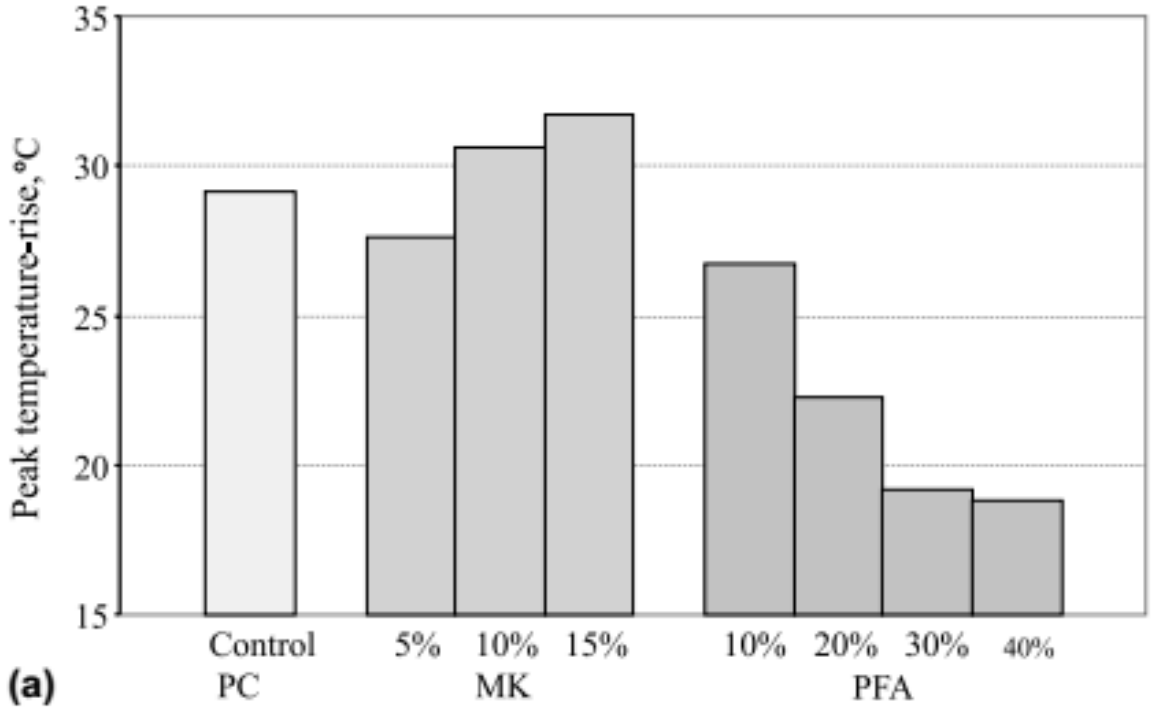

Figure 2.9: The peak temperature rise in metakaolin and pulverized-fuel ash mortars (Bai and Wild, 2002)

Similar influences of metakaolin on the heat evolution were observed by Zhang and Malhotra (1995). They measured a temperature rise in concrete mixtures at a 20°C room temperature and found that a 10% metakaolin concrete had a maximum temperature of 52.8°C after 15 h which was higher than that of the silica fume concrete (46.1°C after 20 h) and the control concrete (45.6°C after 19 h). They claimed that this high-temperature rise was due to a high pozzolanic reactivity of metakaolin.

Therefore, the addition of metakaolin in concrete generally produces high heat evolution at early hours of hydration. However, a question is whether the total heat is increased or just accelerated by metakaolin. Materials such as fly ash and blast furnace slag tend to reduce the heat of hydration, this is due to their low pozzolanic reactivity. Hence, the use of metakaolin can result in increasing heat of hydration since it has high pozzolanic reactivity approximately equal to silica fume (Newman & Choo 2003:13/28).

2.8. PROPERTIES OF FRESH CONCRETE MADE WITH METAKAOLIN

Concrete is in a fresh state from the time it is mixed until it sets. When concrete is in this state, it affects not only the choice of equipment for handling and compaction, and uniformity of

distribution of its constituents (Owens 2009:83) but also its properties in the hardened state (Ramezanianpour 2014:230). There are several factors affecting its properties which are type of cement, type of aggregate, type of pozzolanic material, mixing time and method, etc. Thus, metakaolin as a pozzolanic material has its effects on the properties of fresh concrete. In this section, workability/flow and setting time of cement paste, mortar, and concrete containing metakaolin are reviewed.

2.8.1. Workability

Workability is defined by American Concrete Institute (ACI) Committee as "*that property of freshly mixed concrete or mortar which determines the ease with which it can be mixed, placed, consolidated and finished to a homogeneous condition*". It is commonly described by using two qualitative terms; consistency and cohesiveness. Consistency means mobility or the ease of flow, which is related to the wetness or dryness of concrete, while Cohesiveness describes the tendency of concrete to resist segregation and bleeding (Owens 2009:83).

Fresh concrete with good workability allows full compaction, and minimum segregation and bleeding, thus, the essential desired strength and durability are achieved. However, its workability is affected by various factors, namely, w/b ratio, aggregate properties, mix proportions, characteristics of cement, chemical admixture, mixing temperature and time, and type of pozzolanic material (Owens 2009:83&84). Therefore, various researchers studied workability of fresh concrete with metakaolin, and the following were their findings.

Ding and Li (2002) found that metakaolin concrete offered a better workability than plain and silica fume concrete when a constant amount of Superplasticizer (SP) (also known as High-range Water Reducers, HRWR) was added into the concrete mixture with 0.35 w/b ratio, see Figure 2.10. The mixtures with 5% to 10% metakaolin had slightly higher slump values than those of silica fume and control mixtures. As the replacement levels increased to 15%, a small decrease in slump was observed, however, it was greater than the control by 150 mm. The slump values of concrete with silica fume were however much lower than the control and decreasing linearly as its replacement levels increased up to 15%.

The same results were obtained by Hassan et al. (2012); they observed that metakaolin concrete required lower SP content compared to silica fume concrete to achieve a slump flow of 650 mm. As metakaolin replacement levels increased from 0% to 25%, the demand of SP also increased. Apart from that, the control required a slightly lower SP than metakaolin concrete.

Thus, they concluded that metakaolin has a better workability than silica fume but not than control concrete.

The difference in the effect of the SP between Ding and Li and Hassan et al. on plain cement and MK cement can be explained by the SP addition easily. Ding and Li used a constant SP amount, and the workability enhanced at low additions and then went down at additions beyond a certain threshold. They used significantly lower dosage of SP than Hassan (at least the different slump values indicate this). This means, the SP dosage was far below saturation dosage for cement. Since MK attracts less SP than cement (where the aluminate phases and the ettringite cause the highest consumption) at low dosages of MK, at equal SP dosage, the SP available for cement dispersion is relatively higher, therefore the slump increases, but goes down at higher dosages, where the negative effect of MK (due to high water demand) outweighs the cement adsorption effect. Hassan et al. used identical slump values. The values are very high indicating a very high dosage of SP in all systems, close to the cement saturation dosage. Therefore, the addition of MK does no more cause a relative higher dosage of SP for cement, thus only the negative (water consumption effect) occurs.

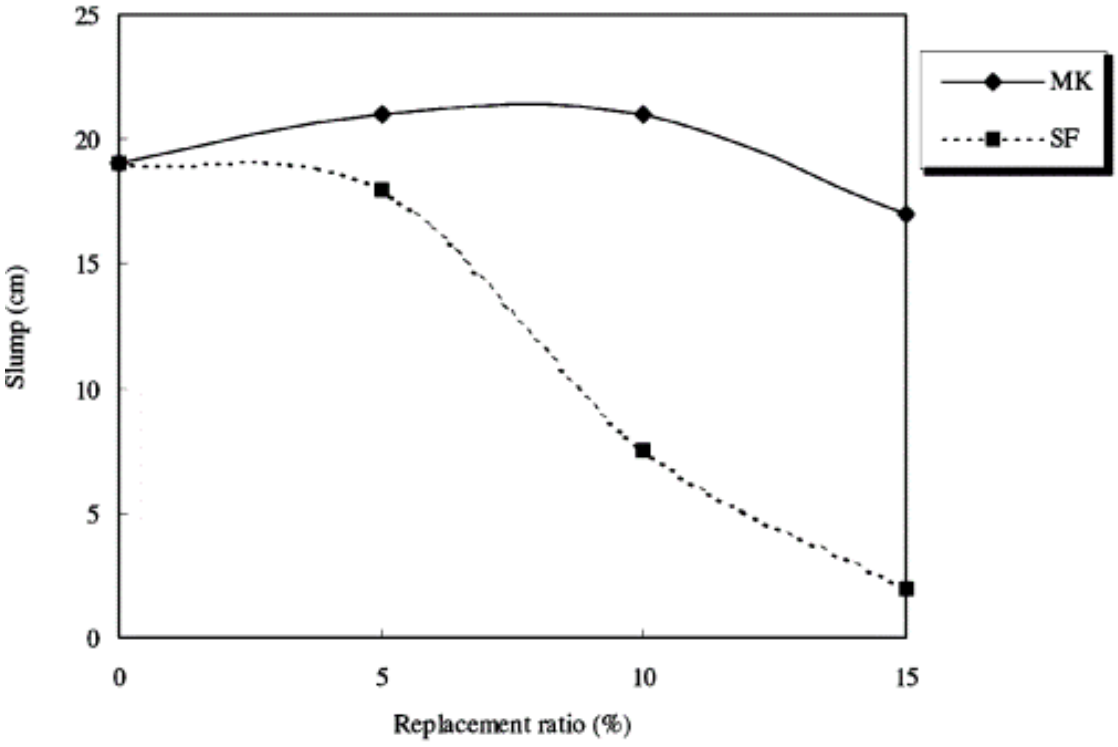

Figure 2.10: Effect of metakaolin(MK) or silica fume(SF) on slump at different levels by mass of cement (Ding and Li, 2002).

There were similar results when metakaolin was added to cement mortar. Courard et al. (2003) found that the consistency of mixes with metakaolin decreased as the replacement rate

increased from 0% to 20%. They explained this decrease was due to the fineness of metakaolin. Thus, it reflected the reduction of workability in relating to that of the reference mortar.

In cement paste, the observation was similar to that in concrete and mortar. Subaşı and Emiroğlu (2015) asserted that the addition of metakaolin in cement paste (with 0.5 w/b ratio) did not increase its workability. Much water was needed to obtain a uniform consistency. In the samples with 20%, 25% and 30% metakaolin, further water demand of 3%, 3% and 6% with respect to sample with 0% to 15% metakaolin were observed, respectively. This was caused by a high specific surface of metakaolin which increased the specific surface area of the mixture. Thus, it was concluded that metakaolin can be safely used up to the rate of 15% without requiring any increase in water; however, it still depends on metakaolin nature. Otherwise, the use of admixtures or the increase of w/b ratio is required to achieve a good workability.

Generally, incorporating metakaolin in concrete decreases workability of concrete. The literature explained this is due to its fineness compared to cement. Nevertheless, metakaolin does not only decrease workability of fresh concrete but also affects setting time of concrete.

2.8.2. Setting times

Concrete setting is defined as the onset of rigidity in fresh concrete. Hence, it can be viewed as the transition period between a state of true fluidity to true rigidity of fresh concrete that precedes a hardening process. In that case, Setting is completely different from hardening which describes the development of useful and measurable strength. Time of setting is therefore described as initial setting time and final setting time (Mindess et al. 2003:210).

Initial setting time is the time interval from the addition of water into a cementitious mixture until the mixture attains a certain degree of hardness. At this stage, the mixture tends to loss its workability, but it can still be handled or replaced. Final setting time is defined as the time at which the mixture had attained sufficient strength and hardness. It indicates when the mixture has completely lost its plasticity and hardening has begun, thus, it is no longer workable (Mindess et al. 2003:211). These setting times give a proper time indication at which concrete can be transported, placed, and consolidated. This is much related to the start of cement hydration reaction which means that the longer setting time indicates the delay of hydration reaction, and vice versa is true. Therefore, the addition of metakaolin in concrete may affect the time of set since it affects the hydration reaction.

Studies observed that the addition of metakaolin in concrete affects the setting time. Brooks et al. (2000) and Brooks and Johari (2001) reported that both initial and final setting times were extended as the amount of metakaolin increased up to 10% in high strength concrete, see Figure 2.11. However, they reported a marginal reduction in setting times particularly the initial set when compared to concrete with 5% to 10% metakaolin. Authors explained this reduction as a result of the formation of denser binding phases due to the increase in water demand, although this explanation remained questionable because it did not appear on the corresponding silica fume replacement level.

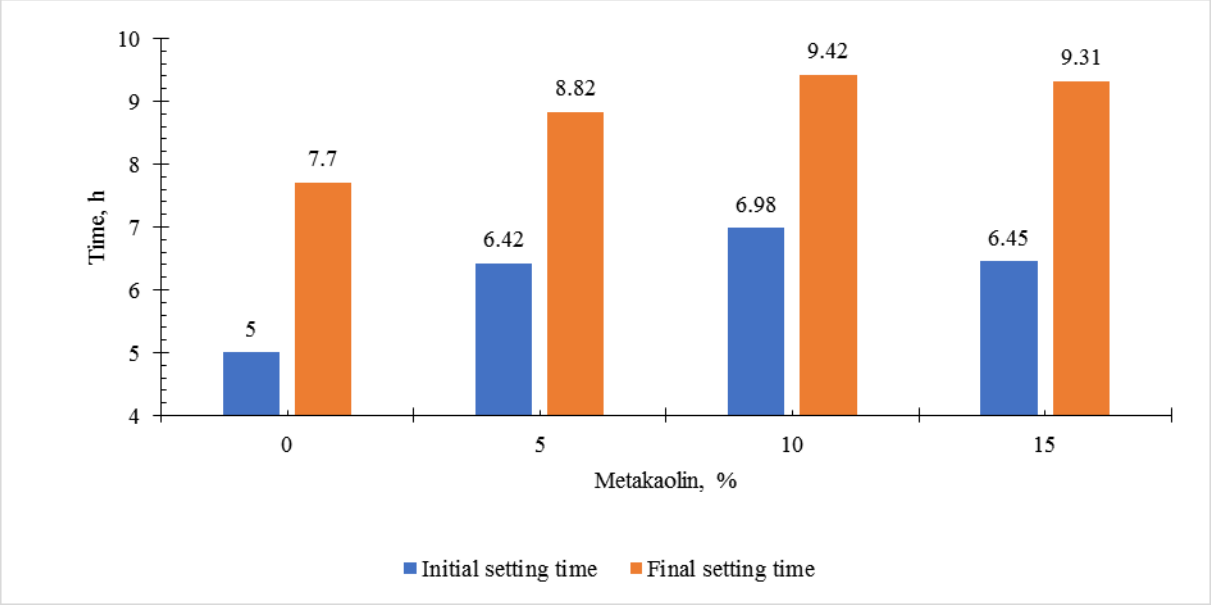

Figure 2.11: Setting times results of concrete containing metakaolin(derived from the data obtained by Brooks & Johari (2001).

However, a different observation was observed by Mobasher et al. (2010) who determined setting time of concrete sample by using ASTM C-403 standard. They reported the decrease in initial setting time up to 20% for concrete mix with 15% metakaolin, whereas for final setting time no significant changes were observed in different concrete samples, see Figure 2.12.

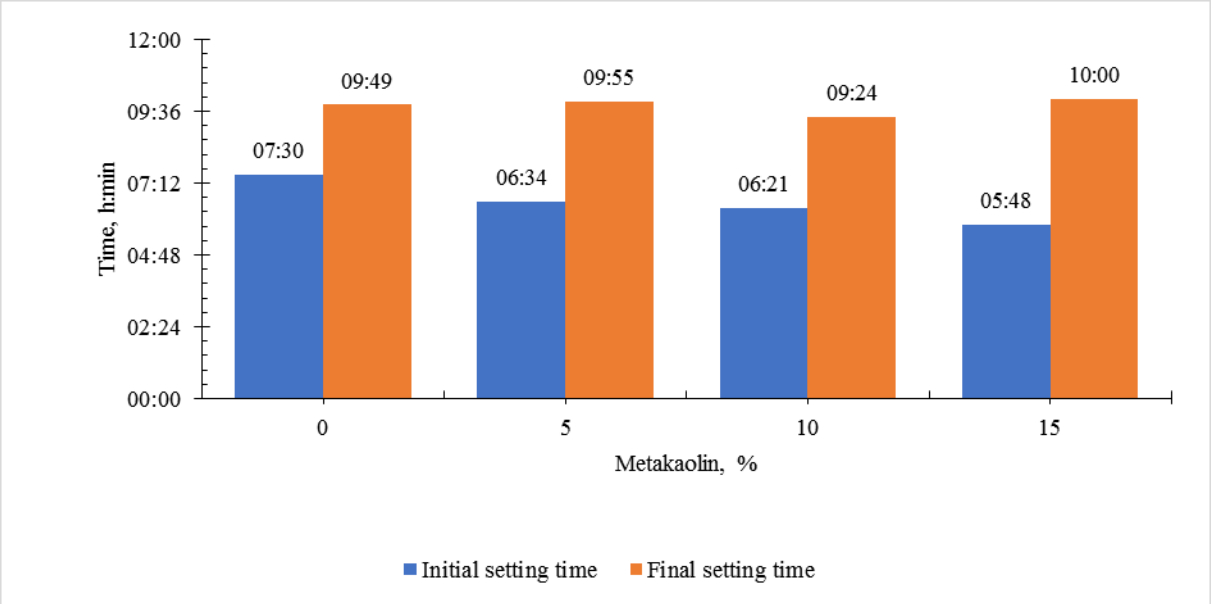

Figure 2.12: Initial and final setting time of concrete with metakaolin (Mobasher et al., 2010).

In cement paste, the influence of metakaolin seemed to support that obtained in concrete. Subaşı and Emiroğlu (2015) observed that initial and final setting times of all metakaolin-cement paste were higher than that of the reference. They increased as the replacement rate increased, see Figure 2.13. A small decrease in setting times at 15% replacement was noted. Afterwards, the setting times increased up to the replacement rate of 30%, whereby the highest initial and final setting times of 110 min and 130 min were determined, respectively.

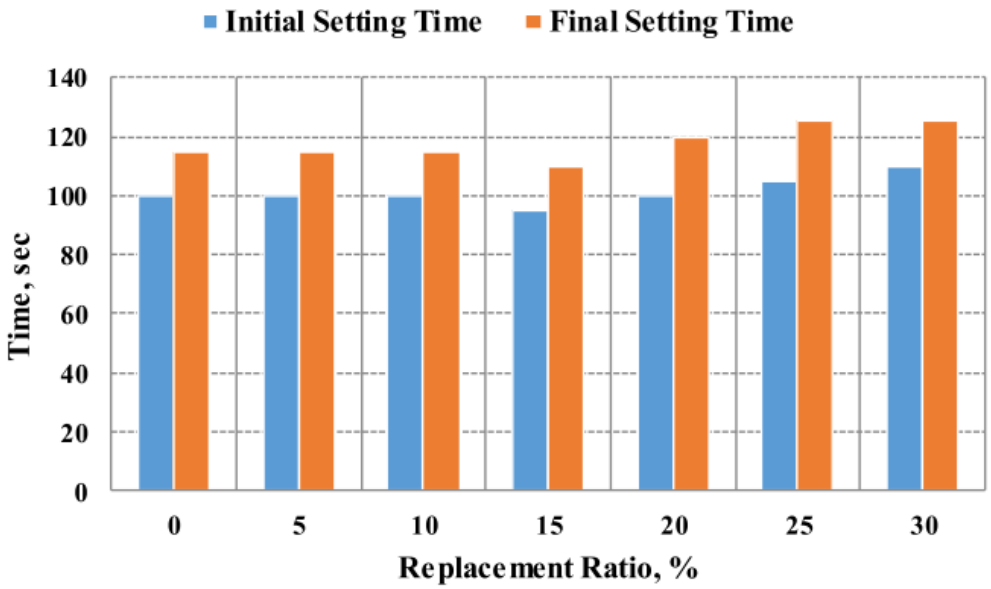

Figure 2.13: setting time of cement paste with metakaolin (Subaşı and Emiroğlu, 2015).

Therefore, the inclusion of metakaolin to some extent increases final setting times in both concrete and cement paste, however, there are contradictions on its influence on initial setting time. Besides, a slightly decreased initial setting time was observed at 15% metakaolin, and

the reason behind this decrease is still questionable. Similarly, no proportional influence of metakaolin on setting times was observed. Possibly setting time depends on a particular type of cement and admixture used. Therefore, further study about setting time of metakaolin concrete is required.

2.9. HARDENED CONCRETE MADE WITH METAKAOLIN

Concrete is a three-dimensional combination of fine and coarse aggregates filled by cement paste with interfaces separating the components. Cement paste is characterised by low modulus of elasticity and high compressive strength. Therefore, its influence in concrete is to fill the gaps between the aggregates by increasing the packing, and hence, to increase the compressive strength. Nevertheless, it is assumed that generally mechanical and permeability properties of hardened concrete are controlled by w/b ratio. Unfortunately, w/b ratio enhances only the cement paste properties, while the interface between the aggregates and cement paste remains a weak point. This is because there is a zone called interfacial transition zone (ITZ) whose structure is different from the bulk cement paste in terms of morphology, composition and density.

ITZ of concrete without SCMs consists of high porosity (large pores), largely oriented CH crystals, less CHS gel, and high concentration of ettringite (Mindess et al. 2003:305). This means improving ITZ results the improvement of the hardened properties of concrete (compression, tensile, and flexural). However, this zone is effectively improved by the addition of pozzolanic material such as silica fume (Mindess et al. 2003:305). This is due to its high pozzolanic activity and filler effect that reduce the number of large pores and CH content in the zone. This portrays that metakaolin can also influence similarly since it has approximately similar behaviour as silica fume.

The influence of metakaolin on improving the hardened properties of concrete in terms of pore structures and refinement, compressive strength, tensile strength, flexural strength, and modulus of elasticity is reviewed as follows.

2.9.1. Pore structure and refinement

Pore structure or porosity in concrete is a major component of the concrete microstructure. It is defined as capillary pores and gel pores. These pores are basically affecting mechanical and durability properties of concrete. However, their influences depend on their total volume, pore sizes, and their interconnection network. Capillary pores are defined as the remnant of water-filled space that exists between partially hydrated cement grains. They consist of macropores

and large mesopores that affect the diffusion, permeability, and shrinkage above 80% relative humidity (RH). Gel pores are an intrinsic part of CSH, generally, they are hardly seen in SEM images. They consist of small mesopores and micropores that affect creep and shrinkage of concrete at all RH as well as the strength of concrete (Mindess et al. 2003:75&88).

Pore size distribution in concrete is very difficult to assess, however, there are two methods that are often used to assess the total porosity and pore size distribution i.e. Mercury intrusion porosimetry (MIP) and adsorption method. Principally, these two methods measure different type of pores; MIP involves applying a mercury pressure into the cement paste and gives the details about capillary pore system. Adsorption method involves the condensation of vapour or gases that fill the pores through capillary effect spontaneous controlled by surface tension. This method gives the details about gel pores system (Mindess et al. 2003:76).

Porosity of hardened concrete is affected by numerous factors, namely, w/b ratio, degree of hydration, air content, consolidation, aggregate, mix proportion, and pozzolanic materials. A low w/b ratio and a high degree of hydration decrease porosity in concrete, whereby a high air content and poor consolidation increase porosity. However, the influences of aggregates depend on their shape, size, quantity, and reactivity. A high amount of largely sized aggregates with flat shape increases the amount of water in the vicinity of the aggregates that directly affects the porosity. Reactive aggregates such as dolomite and calcite tend to react with cement paste to form the compounds such as carbo-aluminates or calcium carbonate-calcium hydroxide complex in the interface region that increase the porosity (Naik, 1997).

In the case of pozzolanic materials, the inclusion of these materials in concrete leads to the densification of the microstructure that occurs as a result of pozzolanic reaction and filler effect. This contributes directly to improving the porosity and pore size distribution. Frías and Cabrera (2000) said that the evolution of porosity depends on the characteristics of pozzolanic material such as fineness, mineralogy, loss of ignition, chemical composition, and their content in the mix. This implies that different pozzolanic materials have different effects on the microstructural properties of concrete. Therefore, it is significant to study in which range metakaolin affects the pore structures of cement paste, mortar and concrete

2.9.1.1. Effect of Metakaolin on the pore structure of concrete.

Khatib and Wild (1996) examined pore size distribution in the paste containing 0% to 15% metakaolin at 0.55 w/b. They observed a proportional decrease of large pores (radius >0.02 µm) in cement paste with the increase of metakaolin content and curing time. Besides, an

increase of pore volume between 14 to 28 days of curing was noted, followed by a gradual volume decrease beyond 28 days. It was asserted that this increase was due to a renewed increase in CH content.

The decrease of large pores was also observed by Frías and Cabrera (2000) who used MIP to measure the total, capillary, and gel porosity and pore size distribution of cement paste containing metakaolin. They found that incorporating metakaolin had a positive effect on cement paste attributed to the pores refinement. Metakaolin blended paste had pore sizes less than 100 A^{o}. However, a gradual increase of very fine pores was observed as metakaolin content and hydration time increased. Hence, they concluded that metakaolin did not decrease total porosity instead, it decreased the number of large pores i.e. pore refinement.

used SEM analysis to define the pore structure of cement paste at the age of 28 days. They also observed a frequent increase of fine pores in cement paste as metakaolin content increased. Their results showed that, as the metakaolin replacement levels increased, the layers of acicular and plate- CSH phases were formed on the hydrate particles (Figure 2.14). These plate phases tended to fill the pores in the cement paste structure.

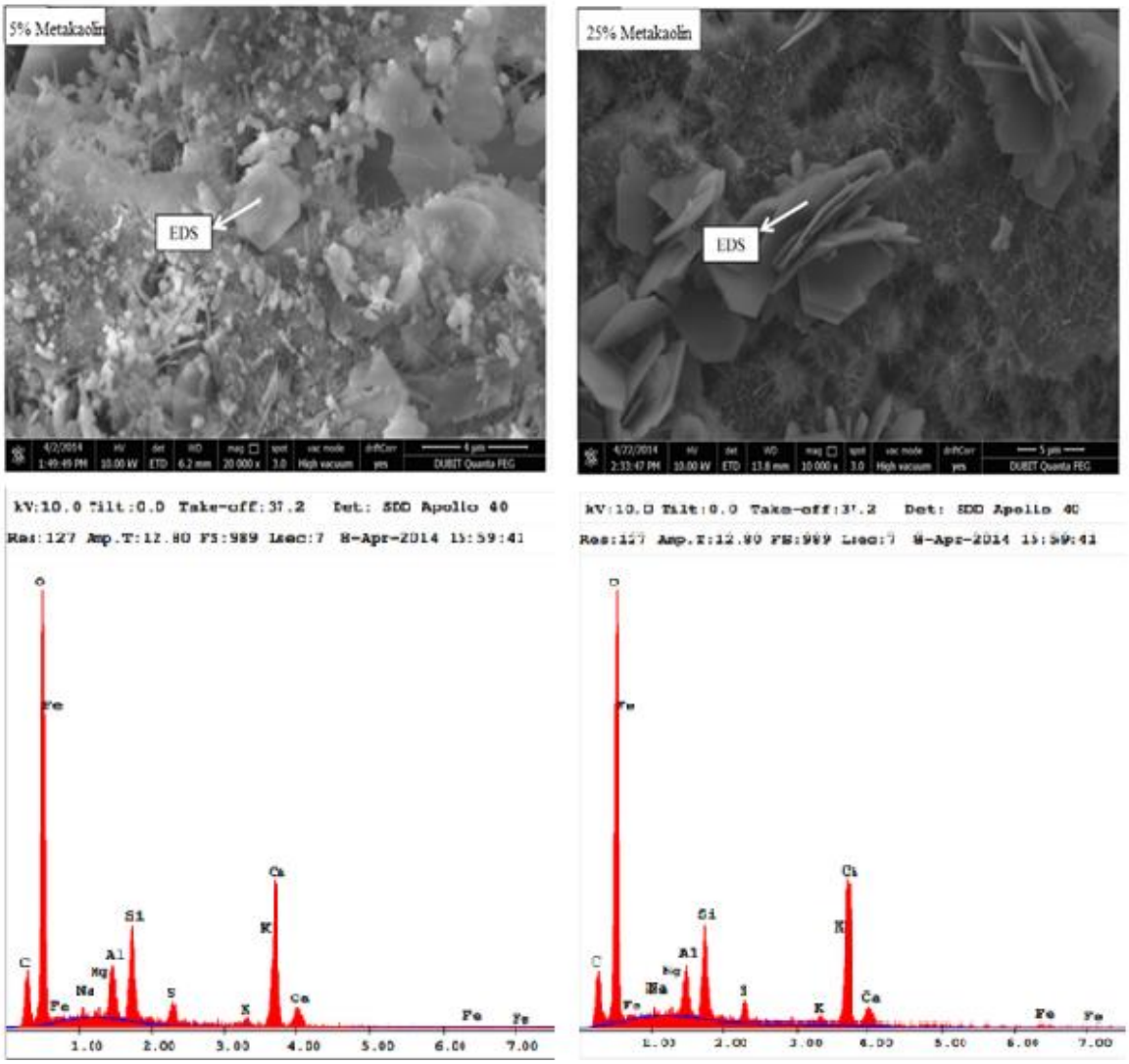

Figure 2.14: SEM image and energy distribution spectrum(EDS) of cement paste without and with 25% metakaolin (Subaşı and Emiroğlu 2015).

The increase of total porosity and pore refinement due to the increase of metakaolin content were also pronounced in the mortar studied by Jiang et al. (2015). They observed an increase in total porosity of 9.89%, 10.14%, 9.64% and 11.35% for 0%, 6%, 10%, and 14% metakaolin mortars at the age of 56 days, respectively. The critical diameter also decreased with increasing contents of metakaolin. Therefore, incorporating metakaolin in cement paste generally has nothing to do with the decrease in total porosity, instead, it improves the pore microstructures by reducing its size from large diameter to the small diameter.

2.9.2. Compressive strength

Ding and Li (2002) studied the development of compressive strength of concrete containing 0% to 15% of metakaolin and silica fume. The results showed that as the replacement level increased from 5% to 15%, the strengthening effect of metakaolin increased as did silica fume.

The compressive strengths of concrete mix with 5%, 10%, and 15% metakaolin were higher than those of control at all ages of curing. However, the results showed that the strength development for 15% metakaolin concrete was rather limited after the age of 28 days since it was approximately equal to that at 65 days.

The same observation about the limited strength development after 28 days was detected in the data collected by Wild et al. (1996), see Figure 2.15. The strength values at 28 days had a slight difference from those at 90 days. This was caused by the deceleration of pozzolanic reaction after consuming all CH produced by the cement hydration. However, the authors observed the strength increase as the replacement level increased up to 20%, then a slight decrease was seen at 25% and 30% replacement at all ages of curing.

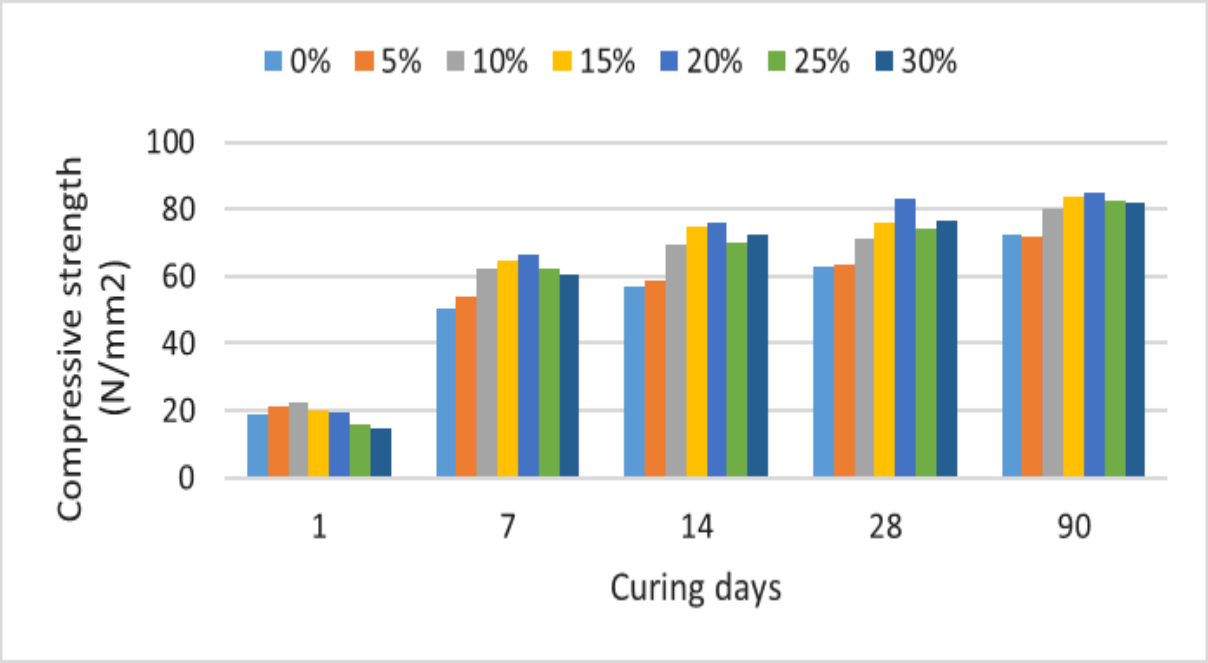

Figure 2.15: Compressive strength of concrete mixtures with metakaolin (Derived from the data obtained by Wild et al. (1996)).

The results obtained by Kim et al. (2007) differed from those obtained by Wild et al. (1996). Kim et al. found that the highest strengths were developed at the replacement rate of 10% to 15%, and less improvement in the replacement rate of 20%. Also, there was no limited strength development at the age of 28 days.

In cement paste and mortar with metakaolin, compressive strength had contradictions. Wild and Khatib (1997) showed that compressive strength of mortar and cement paste increased with increase in metakaolin replacement. The replacement levels of 10% and 15% exhibited the highest compressive strengths at all ages of curing for mortar and cement paste, respectively, see Figure 2.16 and Figure 2.17. This was supported by Khatib and Wild (1998), Poon et al.

(2001) and Batis et al. (2005), while different results were obtained by Subaşı and Emiroğlu (2015) who said that probably the difference was due to the composition of the cementitious materials used.

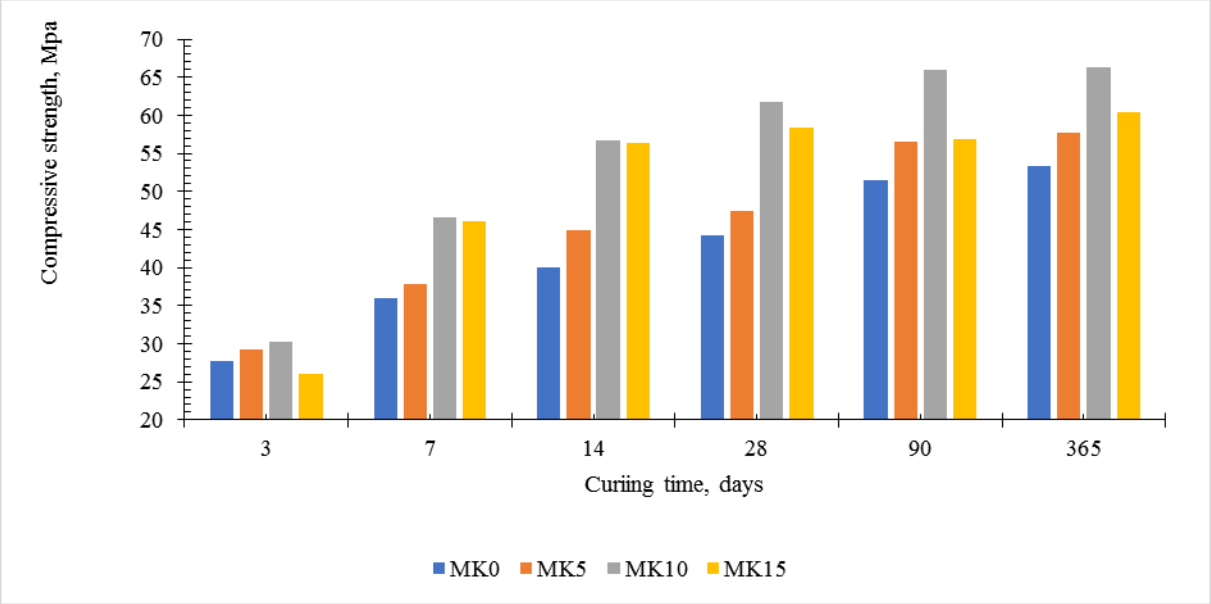

Figure 2.16: Compressive strength of the mortar with metakaolin (Wild and Khatib, 1997).

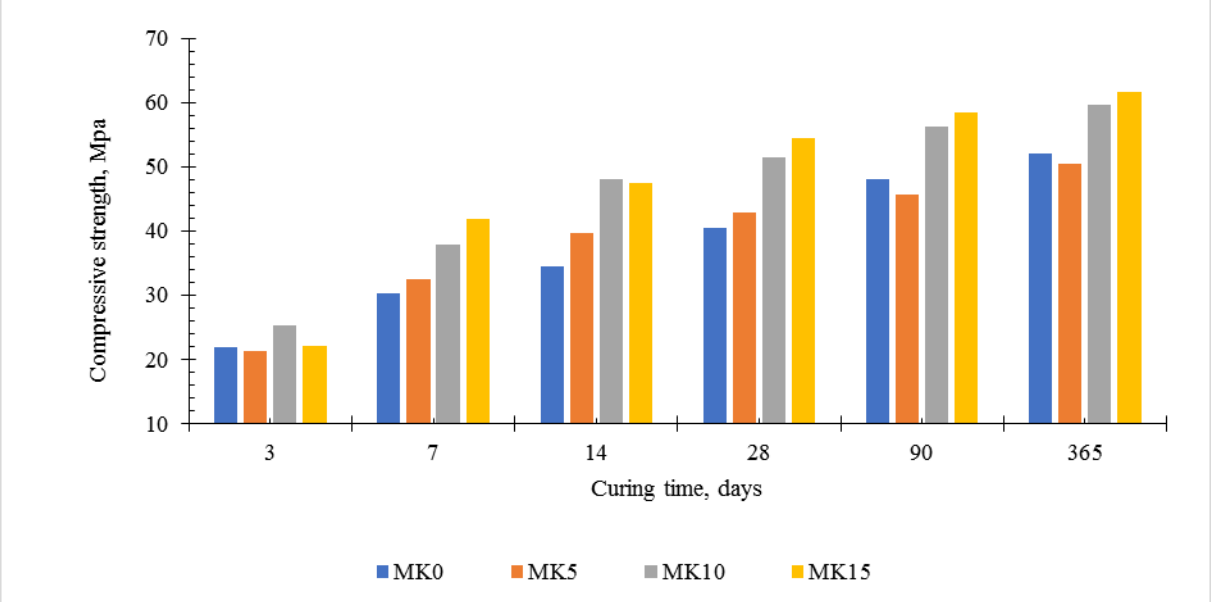

Figure 2.17: Compressive strength of the cement paste with metakaolin (Wild and Khatib, 1997).

Generally, the increase in compressive strength of concrete containing metakaolin is caused by a high pozzolanic activity of metakaolin, the acceleration of cement hydration by metakaolin, and metakaolin filler effect, whereby metakaolin particles fill the space between cement paste and aggregate hence increasing the packing density. In addition, the highest compressive

strength is obtained between 10% to 20%, whereby higher replacement levels than 20% cause the decrease in strength due to the dilution effect of PC (El-Diadamony *et al.*, 2016).

2.9.3. Tensile strength and modulus of elasticity

Qian and Li (2001) observed the effect of metakaolin on tensile strength of concrete. They conducted tensile tests on a concrete plate of 300 x 100 x 20 mm which was glued onto two steel plates that were connected to loading fixtures by pins. Their results showed that tensile strength of concrete increased with increase in metakaolin replacement, see Figure 2.18. The average tensile strength increase was 7%, 16%, and 28% with respect to that of control for 5%, 10%, and 15% metakaolin, respectively.

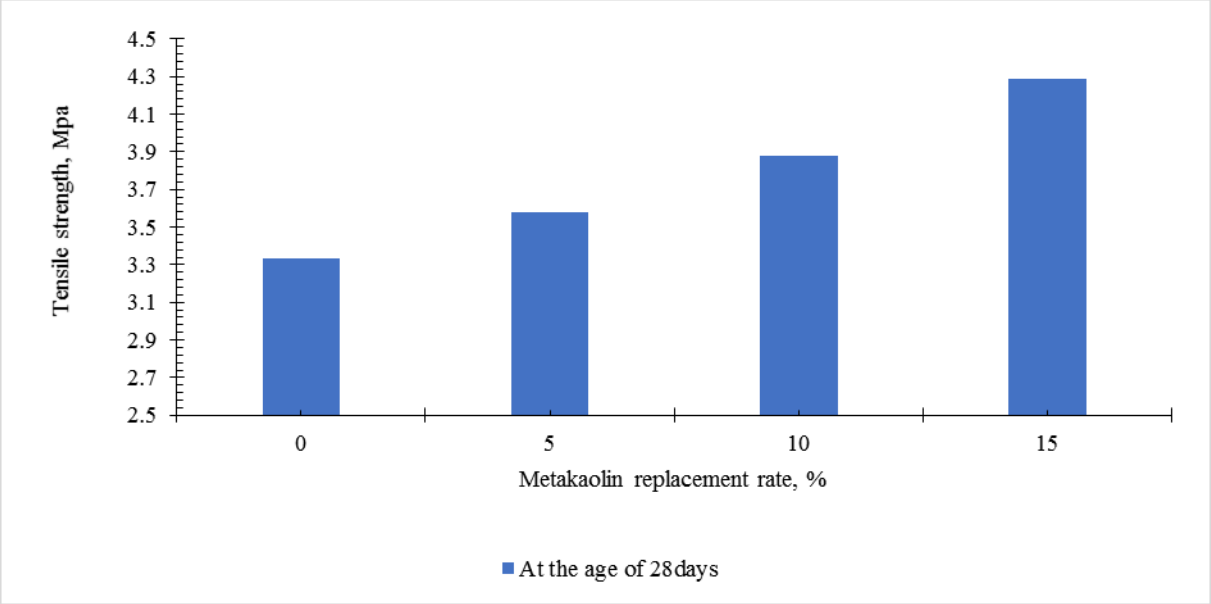

Figure 2.18: The results tensile strength of concrete containing metakaolin derived from the data obtained by Qian and Li (2001).

Aiswarya et al. (2013) investigated the development of tensile strength of different concrete grades (M20, M30, M40, and M50) containing nano metakaolin which was increased at the replacement rate of 2% up to 20%. Their results at 28 days and 56 days of curing were interesting since they observed a gradual increase in tensile strength up to 10% replacement rate, and then, the strength decreased as the rate increased to 20%, see Figure 2.19. This was also observed by Kim et al. (2007) who concluded that for the economic efficiency, 10% metakaolin would be an acceptable content to replace cement in concrete.

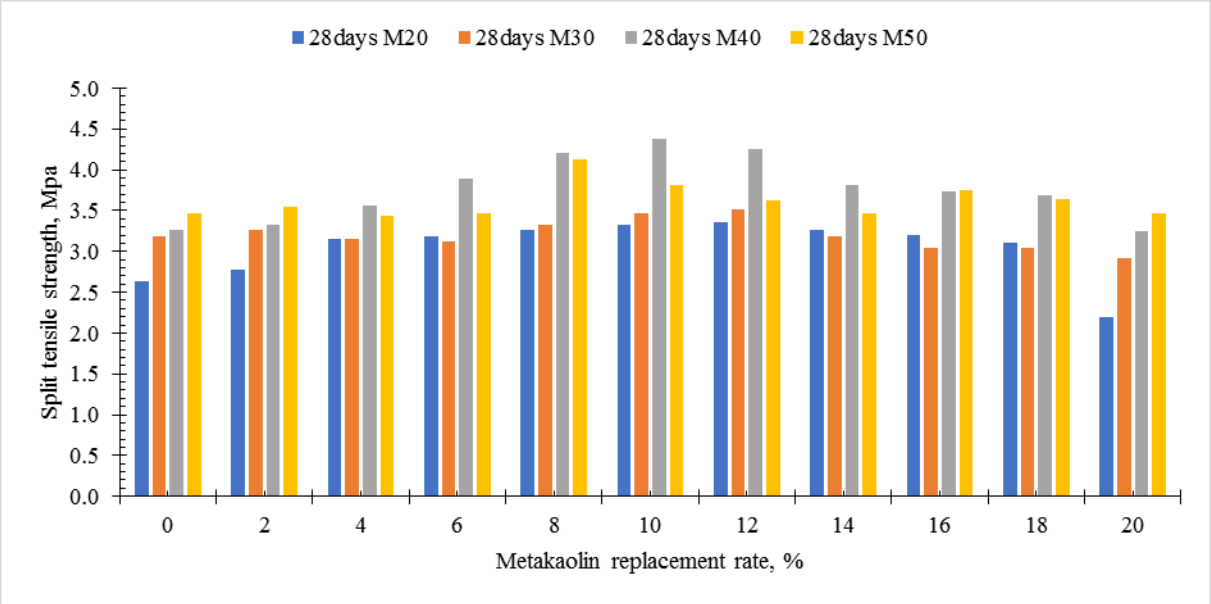

Figure 2.19: Split tensile strength of different concrete grades containing nano metakaolin derived from the data obtained by (Aiswarya et al., 2013).

The same idea of using 10% as the acceptable replacement rate of cement was agreed by Shah and Jamani (2017). They studied the influence of nano silica and metakaolin on tensile strength of high-strength concrete with 0.33 w/b ratio and 1% superplasticizer dosage. They found that 10% metakaolin concrete had a higher tensile strength than concrete with 0% and 5% metakaolin. However, nano silica tended to boost the strength at 1% and 2% replacement rate while at 3%, the strength was decreasing. The reason behind this is questionable, although, it might be due to the increase of fineness in the mixtures which could decelerate the pozzolanic reaction or nano silica fume dilution effect.

On the other hand, the study done by Shehab El-Din et al. (2017) showed that concrete containing 15% metakaolin replacement had higher tensile strength compared to concrete with 0%, 10%, 20%, 30%, and 40% metakaolin, see Figure 2.20. This also agreed with the results obtained by Qian and Li (2001). Therefore, the conclusion can be drawn that incorporating metakaolin in concrete has a positive influence on improving tensile strength of concrete, whereby a maximum strength can be obtained when cement is replaced by 10% and 15% metakaolin.

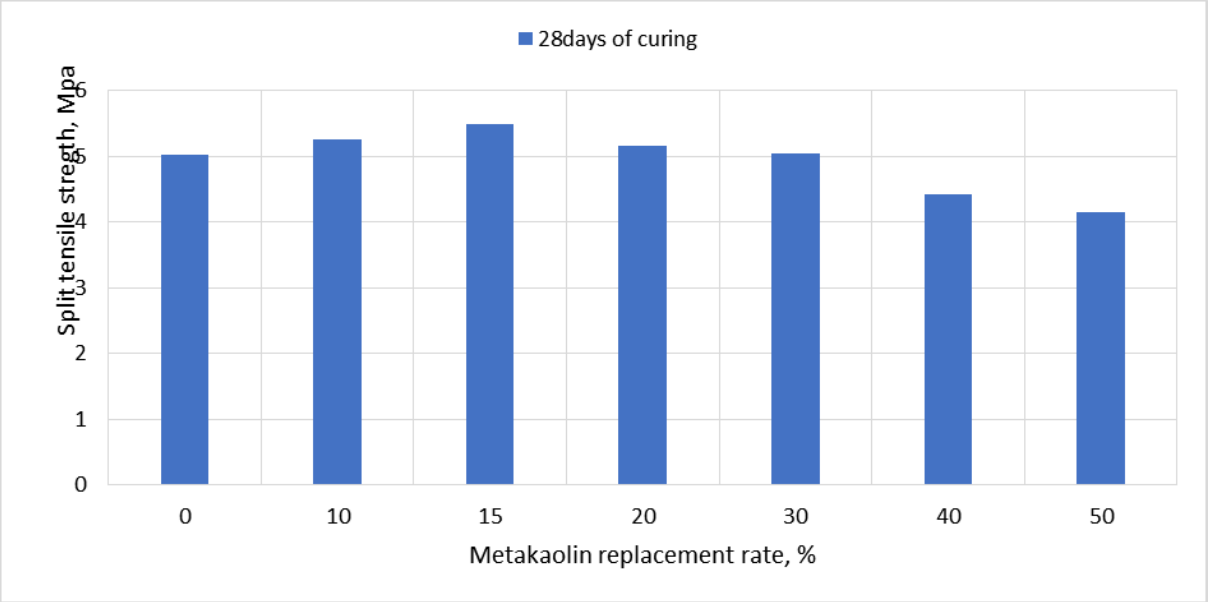

Figure 2.20: Splitting tensile strength of concrete containing metakaolin derived from data collected by Shehab El-Din et al. (2017).

In the case of modulus of elasticity, Dadsetan and Bai (2017) said that modulus of elasticity of concrete is a function of compressive strength as well as the characteristics of ITZ and moduli of elasticity of the principal constituents (paste and aggregates). Therefore, as it has been seen above metakaolin significantly increases the compressive strength of concrete so it is expected to do so in the modulus of elasticity of concrete.

Qian and Li (2001) investigated elastic modulus of concrete containing 0%, 5%, 10%, and 15% metakaolin. They found that modulus of elasticity increased with increase in metakaolin content, see Figure 2.21, although, at 10% and 15% metakaolin, the results seemed to be approximately the same at all ages. Nonetheless, the rate of increase of elastic modulus was less compared to that of compressive strength.

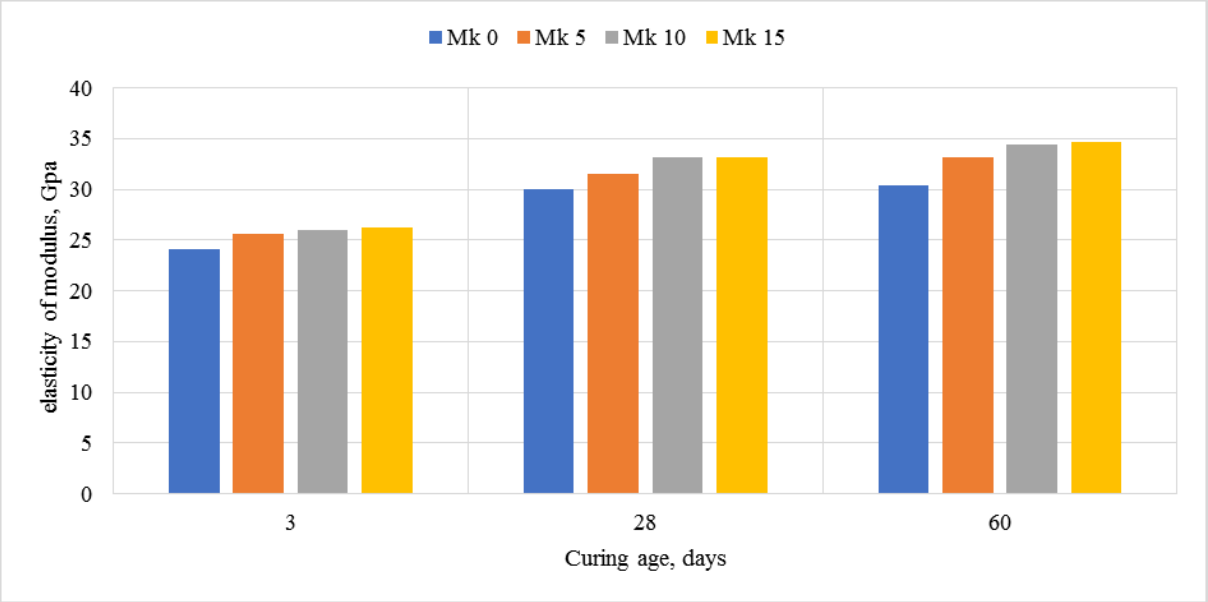

Figure 2.21: Elastic modulus of concrete containing metakaolin (Mk)at different curing age, derived from the data collected by Qian & Li (2001).

The results were different from that obtained by Khatib and Hibbert (2004) who investigated the influence of 10% and 20% metakaolin on dynamic modulus of elasticity(E_d) of concrete. They found that the inclusion of metakaolin increased E_d at all age of curing, although they concluded that further increase of metakaolin replacement level did not increase E_d, see Figure 2.22.

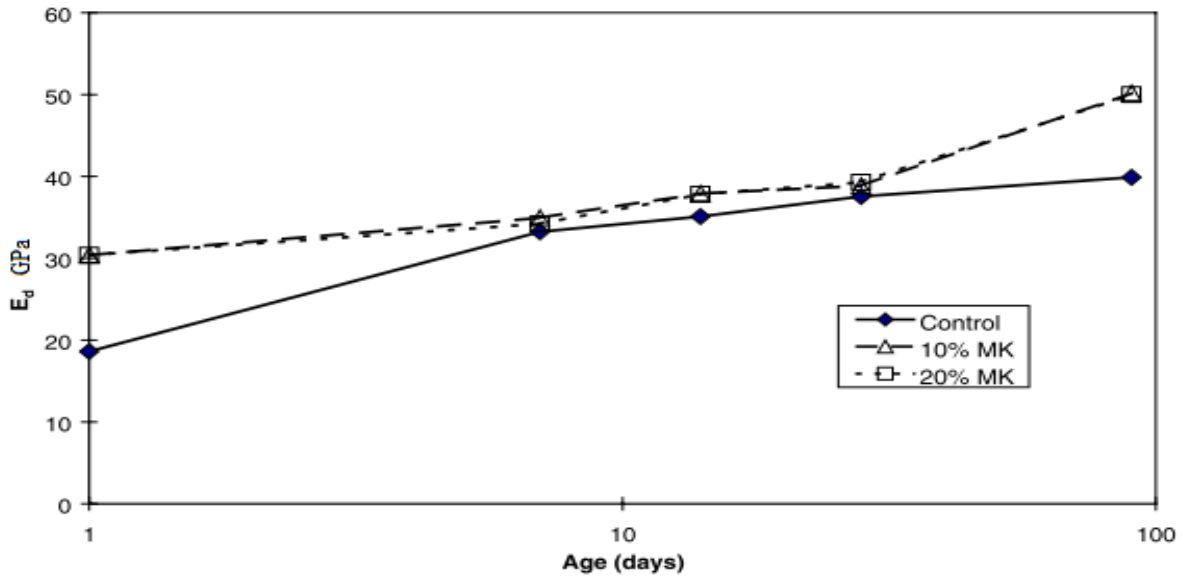

Figure 2.22: Effect of metakaolin on dynamic modulus of elasticity (E_d) of concrete (Khatib and Hibbert, 2004).

Therefore, due to the limited number of results found, more study must be done to investigate the actual effect of metakaolin on elastic modulus of concrete. Also, the reason behind a

contradiction of whether there is or there is no increase of elasticity modulus when metakaolin content is increased in concrete must be studied.

2.9.4. Flexural strength

Kim et al. (2007) also investigated flexural behaviour or bending strength of concrete with metakaolin. They revealed that flexural strength increased with the increase of metakaolin replacement levels from 10% and 15%, and then decreased for 20% metakaolin. The same results were observed by Qian and Li (2001) who observed that at 10% and 15% replacement levels, bending strength increased by 32% and 38%, and 13% and 24% (with respect to control), at 28 days and 80 days, respectively. They also observed that 5% metakaolin replacement level had a negligible effect on bending strength of concrete, see Figure 2.23. Thus, they drew the conclusion that a significant improvement in bending strength of concrete could be achieved at 10% to 15% metakaolin replacement levels.

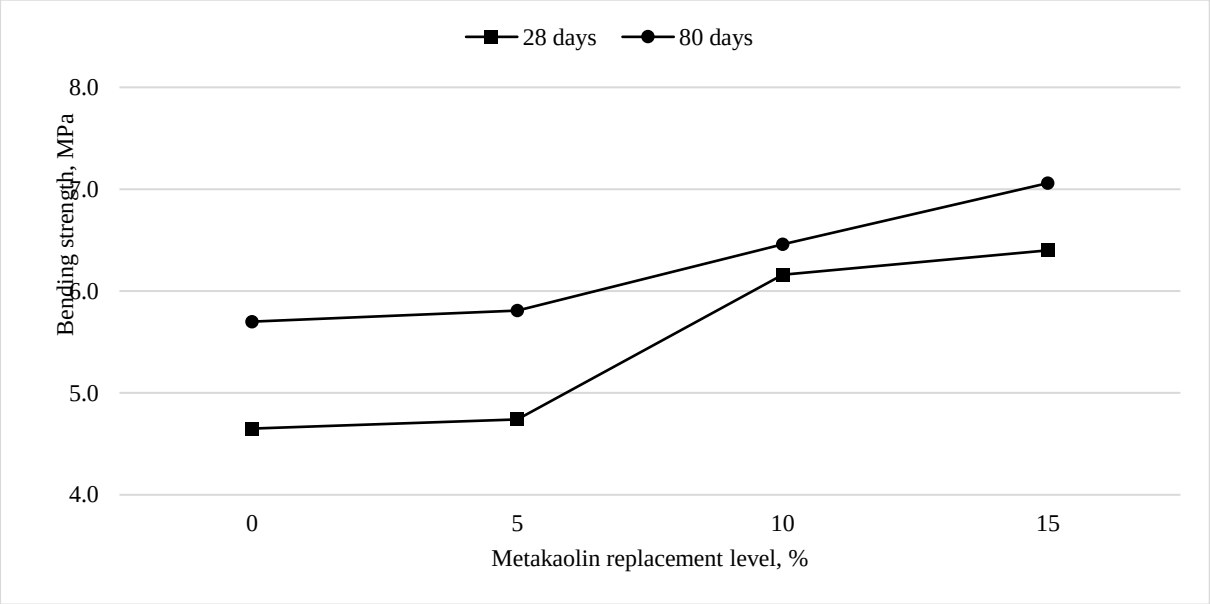

Figure 2.23: Relationships of bending strength with metakaolin replacement (Qian and Li, 2001).

The effect of metakaolin in bending strength of mortar was investigated by Courard et al. (2003). Their results showed a decrease in bending strength with the increase in metakaolin content at early curing, while achieving almost equal strength at 28 days, see Figure 2.24. The decrease was also observed by Jiang et al. (2015), although, 10% metakaolin mortar showed an ultimately higher strength compared to 6%, and 14% metakaolin mortar. Furthermore, Jiang et al. (2015) did not witness the comparable strength at 28 days but instead, they observed lower strength compared to that of plain mortar. Therefore, they said one possible reason was the discrepancy in the content of mineral admixtures.

Therefore, a clear reason behind the opposite behaviour of metakaolin on flexural strength of mortar and concrete is not yet provided in the literature. Probably a major study on this should be done to find the reason for this behaviour.

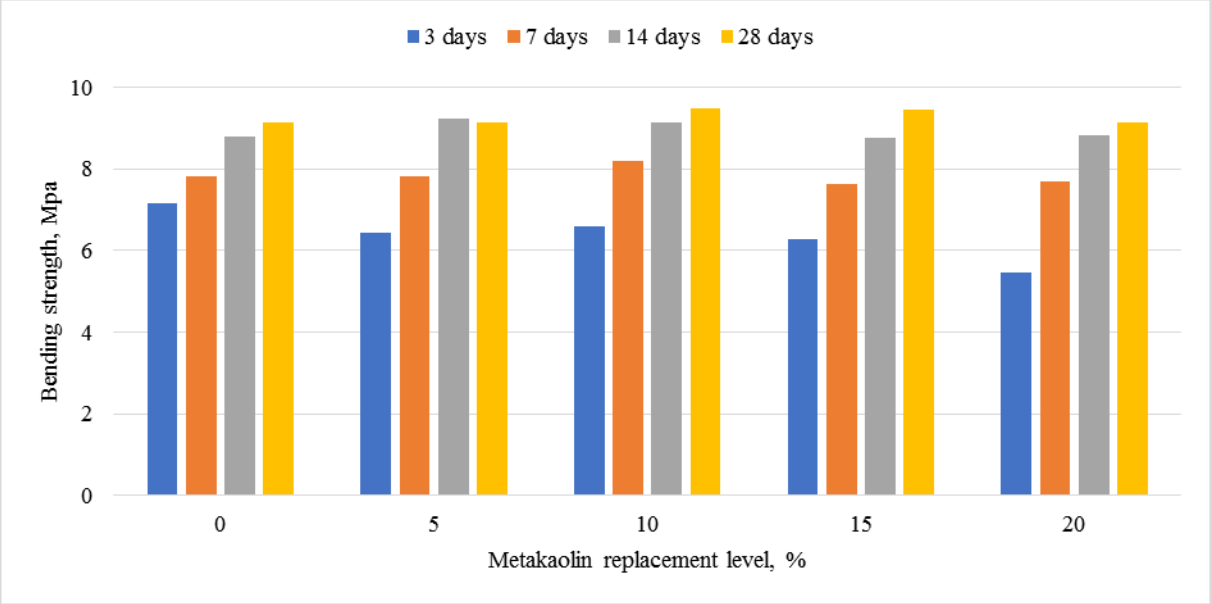

Figure 2.24: Bending strength of mortars with cement CEM I 42.5 N and metakaolin (Courard et al., 2003).

2.10. DEFORMATION BEHAVIOUR OF CONCRETE WITH METAKAOLIN

Concrete deforms due to the climatic environment (temperature and moisture) and the applied stresses i.e. loading and unloading. When concrete deforms due to change in temperature, the deformation is termed as thermal expansion/contraction. This is an abrupt phenomenon which is time independent, in contrast to the deformation due to moisture loss or gain, is classified as shrinkage or swelling, respectively. When concrete changes in volume due to loading, in long term, the deformation is termed as creep, whereas under instantaneous loading, concrete experiences elastic deformation. Elastic deformation or strain is always recovered during unloading process, whereby part of creep does not. Therefore, in long term, shrinkage and creep can lead to safety, serviceability, and economic failures of concrete structure because they are time-dependent.

2.10.1. Factors affecting deformation behaviours of hardened concrete

Shrinkage is a volumetric effect which is expressed as a linear strain. Its rate depends on the moisture gain or loss and the rate of moisture transfer from the inner core to the surface of the specimen. These two factors are influenced by the environmental temperature and RH as well as specimen geometry and size; high temperature and small specimen size result in high rate of moisture transfer and moisture loss, and finally, high shrinkage rate. If concrete is subjected

to the drying and wetting process, the maximum shrinkage will occur during the initial drying process, and it will then continue to decrease to a point where it is irreversible. The reversible shrinkage is due to moisture movement, so in case there is no rewetting, a large portion of shrinkage remains unrecovered (Illston & Domone 2002:144).

Under drying condition, shrinkage is measured as a sum of autogenous shrinkage and drying shrinkage. Autogenous shrinkage is associated with the degree of cement hydration. During hydration process especially for concrete with low water/cement (w/c) ratio < 0.4, concrete undergoes self-desiccation that creates very fine capillaries. Consequently, the surface tension within the capillaries leads to autogenous shrinkage. However, for concrete with w/c ratio > 0.4, the total shrinkage is taken as drying shrinkage since autogenous shrinkage is very little (Alexander and Beushausen, 2009).

In the case of creep of concrete, creep is substantially increased when concrete is simultaneously drying. This is because creep and shrinkage are considered interdependent (Illston & Domone 2002:157). Loading on initially dried specimen results in a significant creep reduction. Creep is highly depending on the level of applied stress, loading duration, and age of concrete at loading (Alexander and Beushausen, 2009). Creep increases proportionally to the level of applied stress up to a specific creep (stress/strength ratio) of about 0.4 and 0.6 (Illston & Domone 2002:157). This implies that applying high stress on concrete with low strength results in high creep, and vice versa is true. Likewise, working under high temperature up to 70^{o}C as well as poor quality and low content of aggregates result in increasing creep (Illston & Domone 2002:158).

In this study, the influence of SCM particularly metakaolin on shrinkage and creep of concrete is revised as follows;

2.10.2. Influence of metakaolin on shrinkage of concrete

Gleize et al. (2006) described the role of metakaolin in autogenous shrinkage in terms of the following four phenomena:

i. Dilution effects

This is associated with the decrease of cement content in the paste mixture. The replacement of cement by metakaolin leads to the decrease of cement content, which means less hydrated cement. This causes less autogenous shrinkage at least in a short term. On the other hand, for a given volume, pastes with metakaolin have higher w/c ratio than the control mixture. This

could sometimes improve the degree of hydration of the cement, and consequently, produce more hydrated cement and possibly more autogenous shrinkage.

ii. Heterogeneous nucleation

This is a physical process whereby the foreign particles that serve as a nucleation site are highly condensed by the nuclei of the hosting particles in the solution (Liu, 2000). This process leads to a chemical activation of the hosting particles. Therefore, the addition of metakaolin to replace cement causes the occurrence of the heterogeneous nucleation of cement hydrates on the surface of metakaolin particles. This is because of the fineness of metakaolin particles which serve as nucleation sites for cement hydrates. Therefore, it accelerates cement hydration process which leads to more hydrated cement, consequently, more autogenous shrinkage.

iii. Pozzolanic reaction of metakaolin

When metakaolin reacts with CH in the cement paste, it produces more hydrates which involve volume changes and autogenous shrinkage.

iv. Increase of capillary tension

The addition of metakaolin in the cement paste causes refinement of pore sizes. This is associated with the porosity decrease which leads to an increase in autogenous shrinkage (Alexander and Beushausen, 2009)

Brooks and Johari (2001) observed that autogenous shrinkage of concrete (w/b = 0.28) decreased with increasing metakaolin replacement levels at both early and long-term ages (Figure 2.25 and Figure 2.26). The decrease was reasoned as due to dilution effect. However, the curve of autogenous shrinkage of plain concrete was found to be at the highest on early ages, while at the lowest in long term. This indicates that, in long term, metakaolin increased autogenous shrinkage. Autogenous shrinkage of concrete at the age of 200 days increases by 91%, 80%, and 56% for 5%, 10%, and 15% metakaolin respectively. This phenomenon did not appear in the results obtained by Gleize et al. (2006) who studied the influence of metakaolin in cement paste.

Gleize et al. (2006) observed that the long-term autogenous shrinkage of cement-metakaolin paste, with 0.3 and 0.5 w/b ratio, decreased as metakaolin content increased by 5%, 10%, 15% and 20%, see Figure 2.27 and Figure 2.28. They also observed no overall expansion of paste at early ages. Therefore, they concluded that the clear contradiction between their results and others found in literature might be partly explained by the differences in cement and metakaolin compositions.

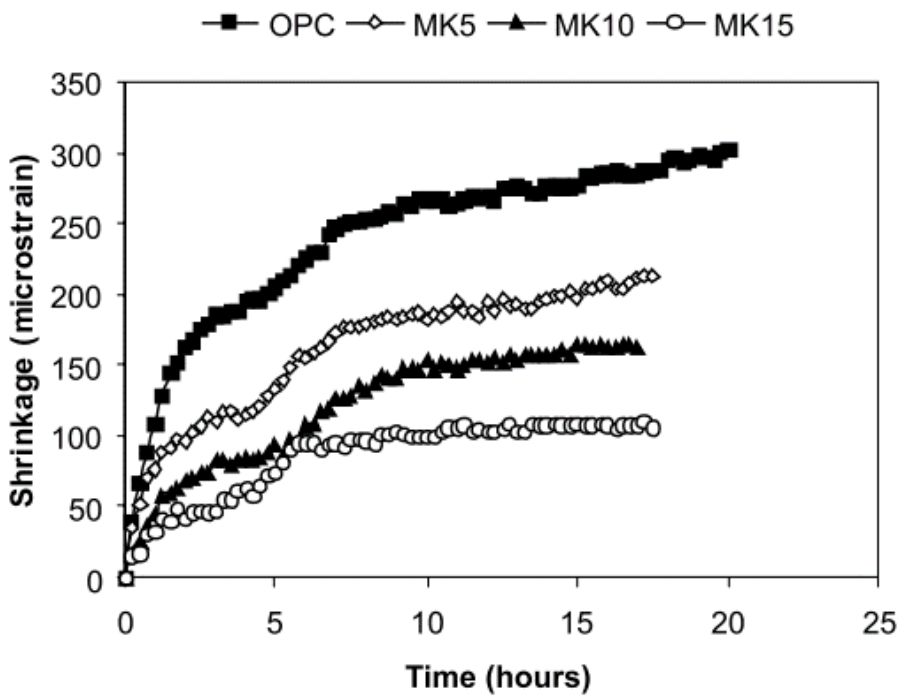

Figure 2.25: Effect of metakaolin on the early age autogenous shrinkage of concrete measured from the initial set (Brooks and Johari, 2001).

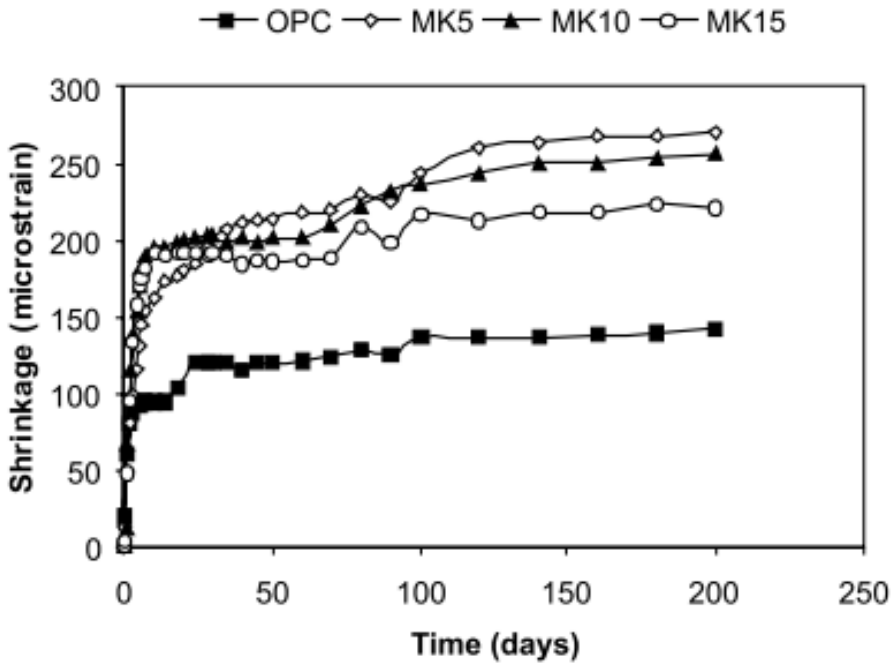

Figure 2.26: Effect of metakaolin on the long term autogenous shrinkage of concrete measured from the age of 24 h (Brooks and Johari, 2001).

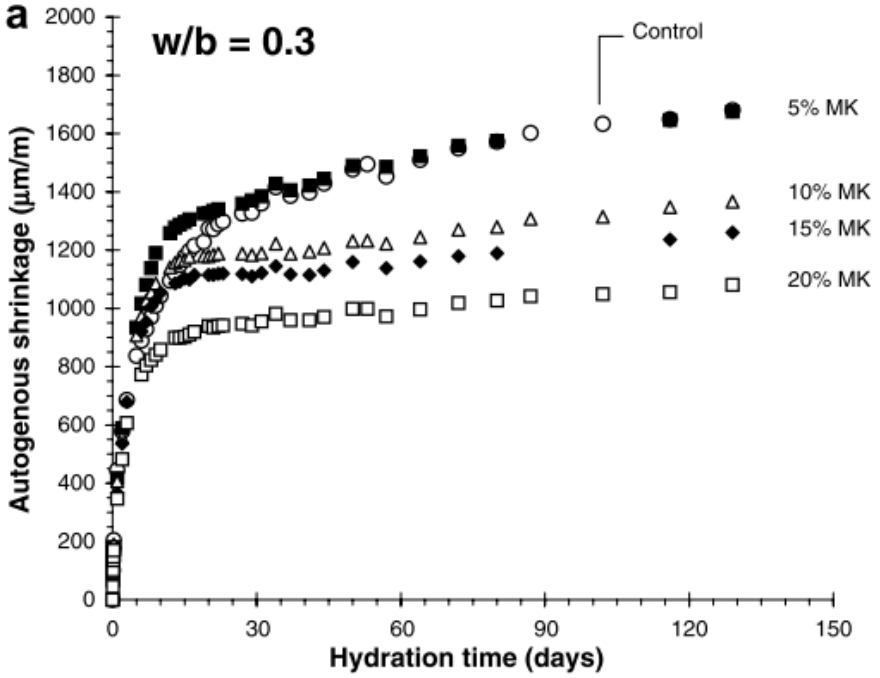

Figure 2.27: Effect of metakaolin on autogenous shrinkage of cement paste, for w/b = 0.3 (Gleize, Cyr and Escadeillas, 2006).

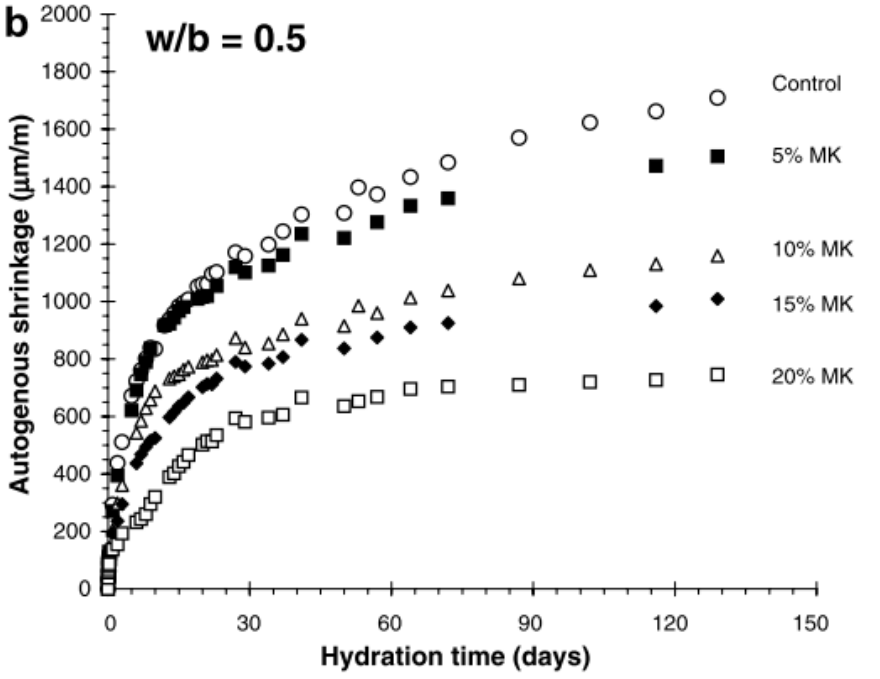

Figure 2.28: Effect of metakaolin on autogenous shrinkage of cement paste, for w/b = 0.5 (Gleize, Cyr and Escadeillas, 2006).

Other authors such as Kinuthia et al.(2000) in Gleize et al. (2006) and Wild et al. (1998) in Sabir et al. (2001) observed both tendencies of autogenous shrinkage increase and decrease with increasing metakaolin. Kinuthia et al.(2000) observed the increase in autogenous

shrinkage of cement paste (w/b = 0.5) as metakaolin increased from 5% to 10% while from 15% to 20% metakaolin exhibited a significant decrease. They reasoned that the increase was caused by the acceleration of early hydration of cement, while the decrease was due to the pozzolanic reaction products.

However, Wild et al. (1998) found that, at all hydration time, autogenous shrinkage of cement paste increased as metakaolin content increased up to a maximum of 10%, and then decreased for higher metakaolin contents. The authors believed that shrinkage increase was attributed to an optimum in the combined effect of cement hydration and pozzolanic reaction. The decrease was in part, due to the increased amount of C_2ASH_8 and reduced amounts of C_2AH_{13} as metakaolin content increased.

Brooks and Johari (2001) also found that the total shrinkage of concrete decreased with increasing metakaolin content. They reasoned that the reduction of total shrinkage was totally attributed to a low evaporation of water as hydration and pozzolanic reaction took place. This was caused by the pore structure refinement which encouraged the loss of water by self-desiccation rather than by diffusion to the outside environment. This was also supported by Khatib (2008) who observed more than half reduction of long-term shrinkage of concrete with 20% metakaolin.

Generally, the influence of metakaolin on shrinkage behaviour was contradicting. The authors obtained different results with no similarities. Hence, no conclusion could be made since there was limited number literature in this area. However, other authors suggested that the contradiction might be due to the difference in the chemical composition of metakaolin, w/b ratio, and type of cement used.

2.10.3. Influence of metakaolin on creep of concrete

Ramezanianpour (2014) related creep of concrete to the strength of concrete, and the amount and time of loading. This means that creep decreases with the increase of concrete strength, and this is best achieved in slower maturing concrete (Newman & Choo 2003). Therefore, according to section 2.9.2, the strength of concretes containing metakaolin is usually higher than control concrete, and hence a low specific creep is expected for such concretes at all ages.

Unfortunately, there was limited information to review the impact of metakaolin on creep of concrete. The only study found was Brooks and Johari (2001) who noted that the inclusion of metakaolin decreased both basic and total creep of concrete. They observed more creep decrease at the higher replacement levels. This was explained as the results of pozzolanic

reaction and filler effect which caused densification of pore structures, strong paste matrix, and improvement of ITZ in concrete. The conclusion on the influence of metakaolin on creep cannot be drawn by relying on one study, therefore, more studies are required.

2.11. DURABILITY PROPERTIES OF CONCRETE WITH METAKAOLIN

Concrete durability is the ability of concrete to remain in service for at least a required lifetime of a structure. Concrete is regarded as a most durable construction material, however, due to the exposure environment and internal causes, concrete loses its durability. This is mainly caused by chemical and physical attacks. Chemical attacks include sulphate attack, chloride attack, acid attack, sea water attack, and ASR, whereas physical attacks include abrasion and erosion, frost, and fire effects (Illston & Domone 2002:199).

The rate of concrete deterioration depends on the penetrability of aggressive ions, moisture, and gases which are accelerated by the transport mechanisms such as pressure-induced flow (permeation), diffusion, and sorption (adsorption and absorption). Permeation involves the movement of fluid under a pressure difference, which also is defined by a flow constant called "coefficient of permeability". Diffusion is the movement of ions, atoms, or molecules under a concentration gradient, also defined by "diffusivity". Sorption is the movement of a liquid into empty or partially empty pores by capillary suction, and it is defined by "sorptivity" (Mobasher et al. 2010).

Therefore, reducing the transport mechanism through concrete definitely improves the durability of concrete. This is because their flow constants (permeability, sorptivity and diffusivity) depend on two factors; chemistry of cement hydration products and pore structure of concrete. These two are improved by using low w/b ratio and SCMs such as metakaolin. SCM pozzolanic reaction adds calcium silicate hydrates that infill the skeletal structures by blocking the flow channels, consequently, reducing transport mechanism of concrete (Badogiannis and Tsivilis, 2008).

2.11.1. Water absorption and sorptivity

Khatib and Mangat (1995) described two mechanisms of water absorption of concrete which are by total immersion and by capillary action. They described water absorbed by total immersion as an indication of the total volume of the open pore in concrete. The capillary action measures the rate of absorption that provides a useful indication of the pore structure of concrete. They noted that the higher the rate of absorption means the poor the concrete quality.

However, Khatib and Clay (2004) commented that the rate of water absorption by capillary action depends on the fineness of the capillary pores, also it is a key durability index.

Khatib and Clay (2004) reported a systematic and significant reduction of the water absorption by capillary action with increasing metakaolin content from 0% to 20% in concrete. They also noted a slight increase of absorption by total immersion with increasing metakaolin content. They explained the reasons behind this reduction and increment were due to the pore refinement and the total volume increase of the pore with a diameter less than 0.02 μm, respectively. In between the curing age of 14 and 28 days, a slight increase of water absorption by capillary action and total immersion with curing time for all concrete containing metakaolin was observed, see Figure 2.29 and Figure 2.30. This was attributed to the formation of a denser hydration phase during that period of curing.

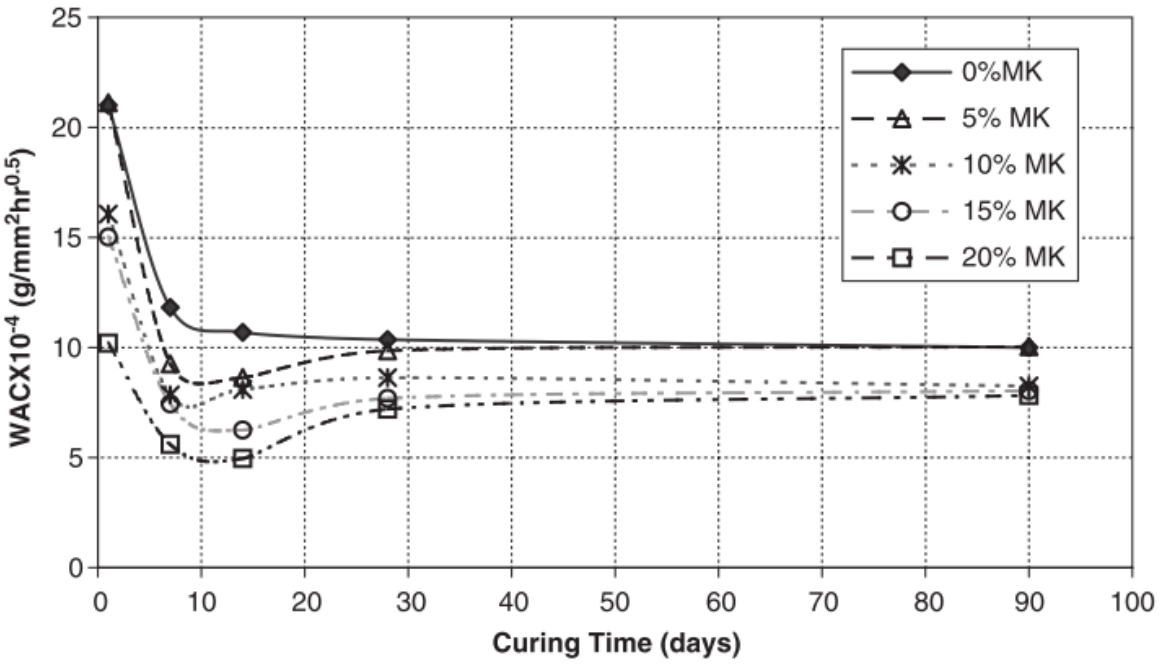

Figure 2.29: Water absorption by capillary action (WAC) of concrete containing different metakaolin content (Khatib & Clay 2004).

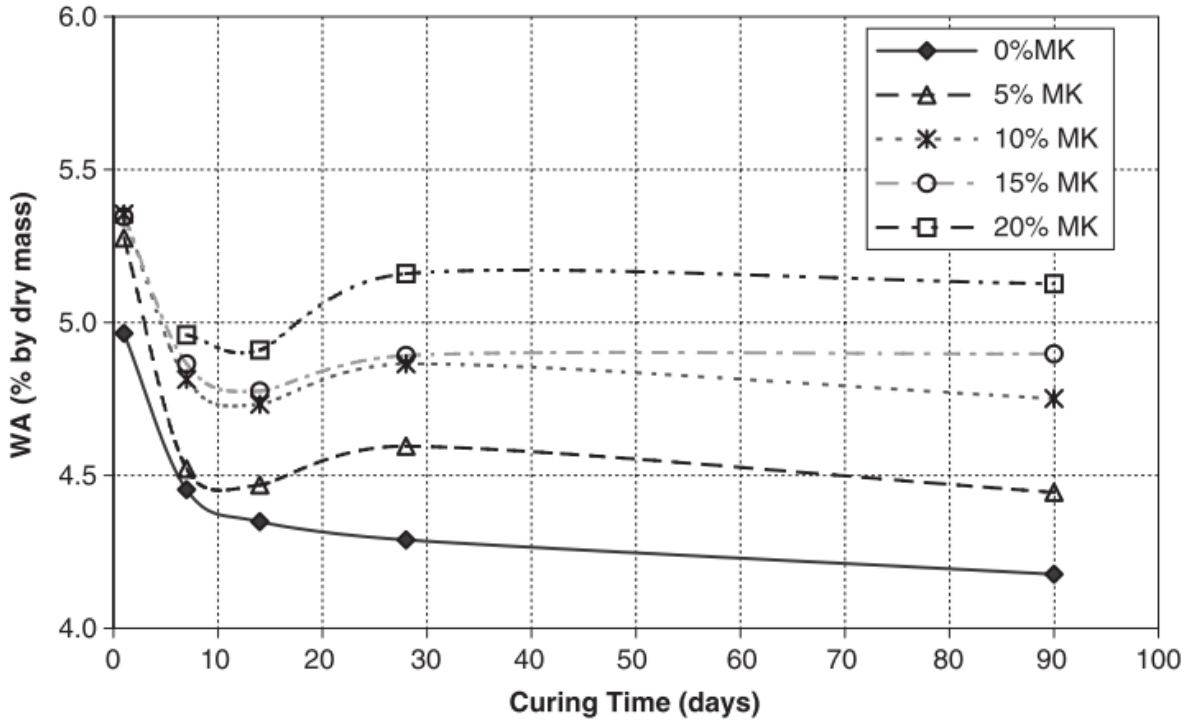

Figure 2.30: Water absorption by total immersion (WA) of concrete containing different metakaolin content (Khatib & Clay 2004).

Razak et al. (2004) said the sorptivity test measures the rate of capillary suction as opposed to the bulk effect of capillary suction in the latter at a specified time. They continued illustrating that concrete with high resistance to water absorption must have a low sorptivity value. They also described two factors which might lead to the decrease of sorptivity value; the first factor was the size of pores in concrete which means the smaller the diameter the slower the rate of sorption. The second factor was strong interconnection network of capillary pores in ITZ. This means the stronger the interconnection the slower the ingression of water. Therefore, metakaolin is expected to decrease water sorptivity value of concrete since it refines pores and strengthens ITZ.

Water sorptivity results obtained by Razak et al. (2004) showed that the inclusion of 10% metakaolin in concrete significantly decreased the sorptivity value compared to the control. Furthermore, metakaolin reduced the initial surface absorption and the water absorption of concrete within the respective curing regime i.e. air, plastic sheet, and wet burlap curing.

The same results were observed by Badogiannis and Tsivilis (2008) who found that the inclusion of metakaolin caused a relative decrease in sorptivity. The sorptivity values of concrete with metakaolin varied from 0.062 to 0.097 mm/min$^{0.5}$, while control concrete presented a sorptivity of 0.114 mm/min$^{0.5}$. Additionally, Güneyisi et al. (2012) reported that

increasing metakaolin content reduced the sorptivity value of concrete, whereby the maximum reduction was observed at 15% replacement level by 29% for both 0.25 and 0.35 w/b ratios.

Therefore, water sorptivity is inversely correlated to the replacement level of metakaolin, whereby its effect seems to be essential for capillary pore system. In addition, the review on metakaolin influence on gas permeability was studied and the following section describes the trend of its influence.

2.11.2. Gas permeability

Badogiannis and Tsivilis (2008) used a modified commercial triaxial cell operating to a maximum cell pressure of 0.7 N/mm^2 to determine of nitrogen gas (N_2) permeability in 100 mm diameter concrete specimens. They reported that gas permeability values of metakaolin concrete ranged from 1.35 to 1.85 x 10^{-16} m^2, while that of control concrete was 2.94 x 10^{-16} m^2. However, the lowest value was obtained at 10% metakaolin replacement level.

Mobasher et al. (2010) reported that gas permeability of concrete samples was improved up to 37% for 15% cement replacement by metakaolin, which was indicative of fine microstructure and low connectivity of the porosity network. The same result was reported also by Güneyisi et al. (2012) who observed the maximum reduction of 52% for concrete containing 15% metakaolin with w/b ratio of 0.25. Generally, the inclusion of metakaolin showed the positive trend on resisting the permeability of injurious gases.

2.11.3. Chloride ingress

The study of the influence of metakaolin on increasing the resistance of concrete against penetration of harmful gases and ions continued, whereby chloride ingress was studied. Various tests had been conducted to determine the influence of SCMs on chloride ingress in concrete, it showed that SCMs improve the resistance of concrete to chloride ion penetration. However, the level of improvement depends on the nature and amount of SCM, w/b ratio, cement composition, maturity of concrete, and exposure conditions.

Zhang and Malhotra (1995) studied the influence of 10% metakaolin and silica fume on concrete to resist chloride penetration as per ASTM C 1202 standard. They observed a lower chloride penetration on concrete with metakaolin and silica fume than the control. The total charges passed on concrete at the age of 28 days were 390, 410, and 3175 coulombs for concrete with metakaolin, silica fume, and control, respectively. Besides, they also observed a decrease of charges with the curing time. This might be due to the influence of SCMs on concrete pore refinement.

Boddy et al. (2001) studied the influence of high-reactivity metakaolin (at 0%, 8% and 12% replacement rate) on concrete with 0.4 and 0.3 w/b ratios to resist chloride penetration at early ages and long term. The test methods used for early age were bulk diffusion, chloride permeability, and chloride resistivity. For long-term, bulk diffusion test (at 140 days, 1 year, and 3 years), and chloride migration test were used. The results indicated that a high metakaolin content and low w/b decreased chloride diffusion, permeability, and conductivity, while increased resistivity for both early age and long term. The resistance to chloride migration increased with increasing metakaolin content and decreasing w/b as shown in Figure 2.31.

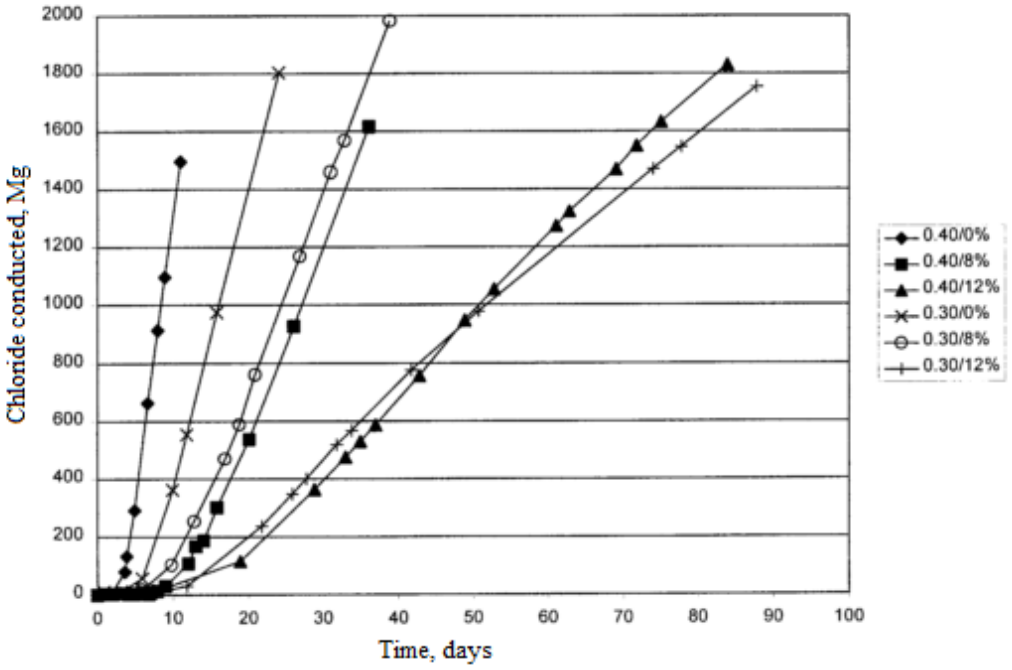

Figure 2.31: The results of chloride migration resistance on concrete containing high-reactivity metakaolin at different w/b ratios (Boddy, Hooton and Gruber, 2001).

In 2008, Badogiannis and Tsivilis also found that the addition of two metakaolin (commercial metakaolin and metakaolin derived from poor Greek kaolin) on concrete at the rate of 10% and 20% resulted in a significant increase of resistance to chloride penetration. By using AASHTO T 277 rapid chloride test, they measured the passing charges that varied from 180 to 820 coulombs in metakaolin concretes and 2460 coulombs in the control. However, slight differences were observed in between commercial metakaolin and derived metakaolin which finally they were taken as minor significance when the total chloride permeability reduction was considered.

Badogiannis et al. (2015) measured the chloride content on the same concrete mixes studied by Badogiannis and Tsivilis on 2008. They observed significantly lower chloride content on

concrete with both metakaolin in contrast to the reference concrete. The chloride content decreased as cement replacement levels increased from 10% to 20%, whereby 20% metakaolin exhibited the lowest chloride content.

Therefore, chloride diffusion, permeability, and conductivity are reduced with increasing metakaolin content in concrete. This concludes that metakaolin has a significant influence on improving the durability of concrete by lowering its permeability. Nevertheless, the influence of metakaolin on suppressing the internal causes of concrete deterioration such as ASR was studied.

2.11.4. Alkali-silica reaction (ASR)

Alkali-silica reaction (ASR) is among three types of alkali-aggregate reaction, other types are alkali-silicate reaction and alkali carbonate reaction. However, this study focuses on alkali-silica reaction since its effects are highly reported in Western Cape. This is because of the type of aggregates used; greywacke and granite aggregates.

ASR is the reaction which takes place between the alkaline pore solution of concrete and metastable forms of silica such as opal, trydimite, cristobalite, and volcanic glasses that are found in some aggregates to produce an alkali-silica gel. The alkali-silica gel formed is a hygroscopic gel which has a tendency to absorb moisture and expand within pores and micro-cracks in concrete, thereby inducing a premature distress and causing a loss in serviceability of concrete structures (Blight and Alexander, 2011). The schematic sequence of ASR is shown in Figure 2.32.

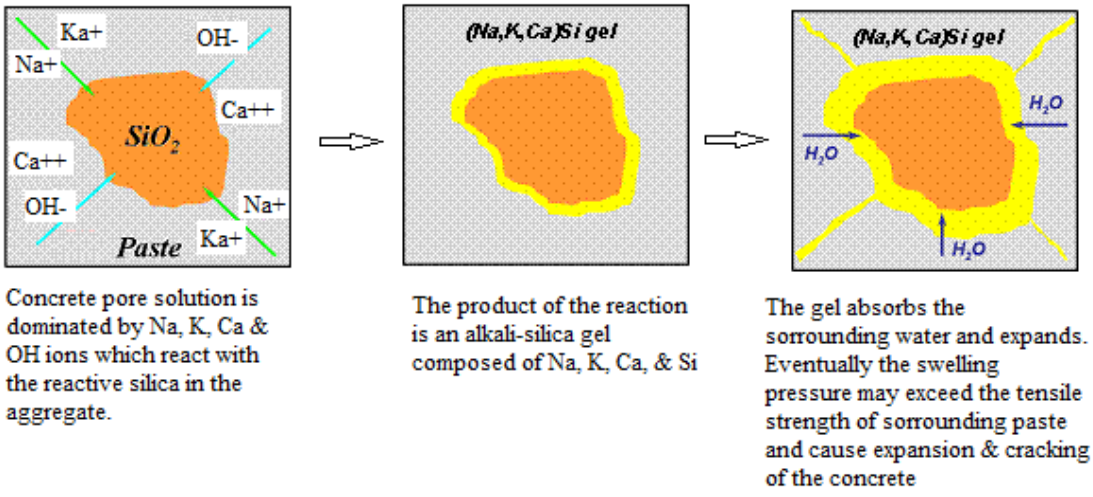

Figure 2.32: ASR sequence (Thomas et al. 2013:10)

2.11.4.1.Mechanisms of ASR

Primarily, ASR occurs under the following three conditions (Fernandes and Broekmans, 2013).

i. A sufficiently high alkalinity of the pore solution: This implies the presence of alkali metal ions such as Na^+ and K^+. These ions are responsible for dissolving CH in the pore solution, consequently, increase the alkalinity, and they react with silica in the aggregates to form alkali-silica gel.

ii. An adequate deleteriously reactive mineral(s) in the aggregate: The meant mineral is reactive silica which is glass, microporous, and unstable as well as poorly crystalline and highly disordered (amorphous). The aggregates contain such silica are susceptible to the reaction, such aggregates are greywacke, quartzite, hornfels, phyllite, argillite, granite, granite gneiss, and granodiorite.

iii. A sufficient supply of moisture: Moisture (water) acts as a transportation medium for the dissolved species, as well as for alkali–silica gel to absorb and expand. It is mostly expressed in terms of RH, whereby at 80-90% RH, ASR is preferred to occur.

In the absence of one of the above conditions, ASR cannot take place, however, a temperature at 60^{o}C in the laboratory has been proved to accelerate the reaction. A further increase of temperature by 10^{o}C is claimed to double the expansion (Owens 2009:192). Furthermore, exposing concrete with reactive aggregates in the severe environment such as freeze/thaw cycling, deicers, and sea water usually accelerates the development of ASR damage and decay (Fernandes and Broekmans, 2013).

The mechanism of ASR reaction involves a two-stage process; the hydrolysis of silica by OH^- to form alkali-silica gel, and the absorption of water by the gel which results in a volume increase. The chemical structure of silica is composed of siloxane groups (≡Si-O-Si≡), however at the surface, it consists of unsatisfied charges, loose, and disordered siloxane bonds, especially in a poorly crystalline silica, see Figure 2.33. Therefore, in the high concentration of OH^- ions, siloxane group are hydroxylated to form silanol groups (≡Si-OH) which are then, together with siloxane groups dissolved into the pore solution to from $Si\text{-}O^-$ ions, see equation 2.7 and 2.8 (Thomas et al. 2013:10-12).

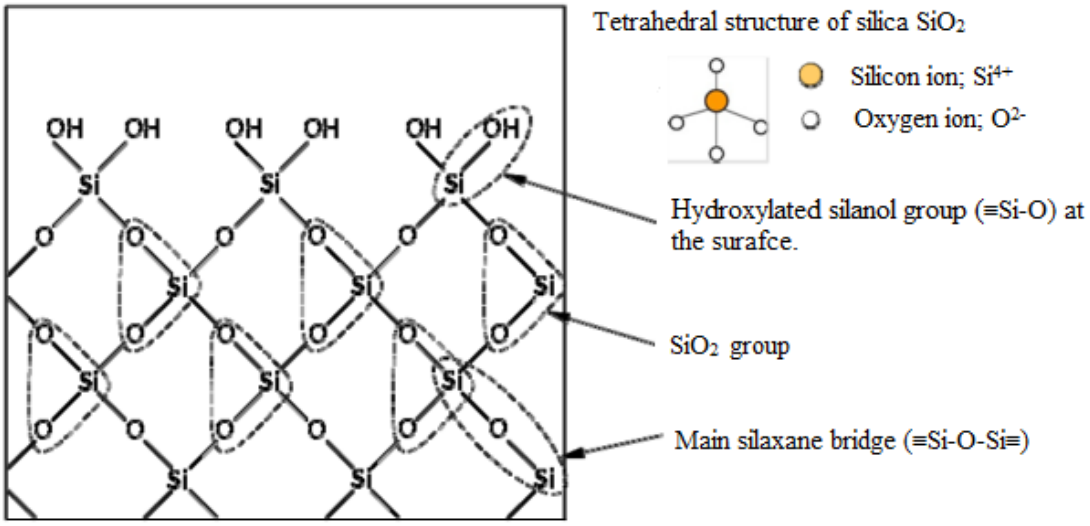

Figure 2.33: The structure of silica (Thomas, Fournier and Folliard, 2013).

$$\equiv Si\text{-}OH + OH^- = Si\text{-}O^- + H_2O \quad (2.7)$$

$$\equiv Si\text{-}O\equiv Si + OH^- \Rightarrow Si\text{-}O^- + H_2O \quad (2.8)$$

As the breaking of silica structure progress, the dissolved Si-O^- ions react with alkali metals ions (Na^+ and K^+) which are abundant in the pore solution to form a swelling alkali-silica gel, see equation 2.9. When this gel absorbs water that surrounds cement paste, it expands, and thus, it induces the swelling pressure which leads to microcracks close to the reaction site. Once the cracks are formed, they provide access to the deleterious mechanisms to operate, which finally results in the severe deterioration of concrete.

$$Si\text{-}O^- + Na^+ / K^+ = Si\text{-}O\text{-}Na \ / \ Si\text{-}O\text{-}K \quad (2.9)$$

However, in the presence of Ca^{2+}, a non-swelling gel alkali-silica gel ($CaO\text{-}Na_2O/K_2O\text{-}SiO_2\text{-}H_2O$) is formed. This gel has no effect in concrete since it greatly increases the viscosity and decreases the porosity in concrete, therefore, it is considered as CSH in concrete. Its formation is highly depending on the concentration of alkali, whereby at high alkali concentration, the possibility of not being formed is high (Blight & Alexander 2011:7).

The formation of a swelling gel depends on the relative amount of silica and alkali, and the pH of pore solution. The higher the alkalinity the greater the solubility and dissolution rate of amorphous silica. Therefore, the CH formed during hydration process in concrete is firstly act a "buffer" to maintain a high pH, i.e. high concentration of hydroxyl ions in pore solutions; and secondly, Ca^{2+} ions causes alkali recycling on the silica gel leading to further production of

swelling alkali- silica complex. In that case, reducing the formation of CH has a significant role in suppressing ASR expansion (Wang and Gillott, 1991).

2.11.4.2.Mitigation measures of ASR

Because of the problematic effects of ASR in concrete, the following mitigation measures were adopted; avoiding the use of reactive aggregates, controlling the alkali content in concrete, using lithium-based compounds, and using SCMs. Avoiding the use of reactive aggregate is found non-practicable and uneconomical especially in the certain geographical areas where there is a scarcity of nonreactive aggregates. Moreover, nonreactive aggregates cause environmental destruction during their extraction compare to reactive aggregates. Therefore, it is considered as the mitigation measure not to rely on (Thomas et al. 2013).

Limiting the alkali content was initially achieved by using of low alkali cement in concrete with the reactive aggregate. Nonetheless, the ASR expansion was still pronounced on the structures that used such cement. This was because the alkali content was controlled by the alkali content of concrete rather than cement alkali level. Controlling the concrete alkali content is somehow difficult due to alkali concentration in concrete which may be caused by drying gradients, alkali release from aggregates, or the ingress of alkalis from external sources, such as deicing salts or seawater (Thomas et al. 2013).

The use of lithium compounds is an effective way to suppress ASR. It reacts with reactive silica and forms lithium silicate which surrounds the reactive particles and protects them against alkali metal ions attack. The lithium silicate formed has low tendency to absorb water and expand, hence, low possibility of microcrack formation. However, it is challenging to use these compounds. Firstly, they are very expensive, and secondly, their effectiveness depends on the type of aggregate, whereby a certain dosage must be set for a particular aggregate. Unfortunately, there is no test method for determining an effective dosage of lithium compound for a particular aggregate. Therefore, further study on the use of lithium compounds is required (Thomas, Fournier and Folliard, 2013)

Finally, the use of SCMs such as fly ash, slag, silica fume, and metakaolin is considered as the effective and affordable method of reducing the potential of ASR. This is due to their two beneficial effects in the pore solution. Firstly, the reduction of alkalinity (and associated pH), and secondly, the depletion of portlandite, thereby reducing the number of alkalis in the system. A greater proportion of the alkalis is bound by SCMs hydration products compared to PC. This

means that alkali concentration in the pore solution is reduced which, in turn, reduces the risk of reaction with the aggregate (Sarfo-Ansah *et al.*, 2014).

Also, the use of reactive aggregate powder in concrete associated with their parent reactive aggregates is proclaimed to be the effective mitigation measure of ASR. It is believed that reactive rocks contain high silica content. When they are crushed into powder form, their silica become active, hence, they act as conventional SCMs. Therefore, they can be used as the effective and affordable mitigation measure of ASR, although, their potentiality depends on their origin, content, and fineness (Carles-Gibergues *et al.*, 2008; Cyr, Rivard and Labrecque, 2009).

All of these mitigation measures are associated with understanding the chemistry behind the occurrence of ASR. Therefore, Ballard et al. (2008) thought that, ASR problematic can be completely addressed in concrete if the following three techniques are achieved at once; lowering pH in the pore solution to suppress the initial silica solubility; reducing the concentration of free alkali metal ion (Na^+ and K^+) to restrict gel formation; and reducing the permeability of concrete to restrict water ingress, subsequently, preventing the gel from expanding.

2.11.4.3.Influences of metakaolin on suppressing ASR.

Metakaolin has a high capacity to suppress ASR expansion effect in concrete using its unique properties of pore structure refinement, consumption of CH, and entrapment of alkalis in silica-rich hydration products (Sarfo-Ansah *et al.*, 2014)

Ramlochan et al. (2000) observed ASR expansion using concrete prism test at 30^{o}C and 100% RH, and the acceleration mortar bar test at 80^{o}C in 1M NaOH with different metakaolin replacement levels. A highly reactive siliceous limestone aggregates from Spratt Quarry in Ottawa, and a lesser reactive greywacke-argillite gravel from Sudbury, Ontario were used. The results indicated the decrease in expansion as the replacement level increased for both test methods and aggregates. The concrete prisms and mortar bars containing more than 15% metakaolin had a significant high potentiality on mitigating ASR for both aggregates, and the highest reduction was observed at 20% metakaolin.

The concrete prism test (ASTM C 1293 standard) was also used by Gruber et al. (2001) to assess the influence of metakaolin to reduce ASR expansion in concrete for two years. They observed the mitigation potentiality of metakaolin on two reactive aggregates which used by Ramlochan et al. (2000). Their results showed that the expansion of concrete prisms decreased

as the metakaolin content increased from 5%, 10%, 15% and 20%, despite the type of aggregate. However, 15% and 20% metakaolin were regarded as the best replacement levels since their prisms exhibited the expansion below the limit (0.04% expansion after 2 years) for both aggregates.

Sabir et al. (2001) concluded that incorporating 10% to 15% metakaolin did not suppress only ASR expansion but also eliminated the occurrence of cracks and surface deterioration on the concrete. They also said that the role of metakaolin in mitigation ASR expansion is in reducing the freely available CH and CH/SiO_2 (active) ratio, consequently, depleting the formation of swelling gel.

Ballard et al. (2008) used ASTM C 1567 standard for evaluating the potentiality of different metakaolin submitted by Burgess Pigment Company, Holcim company, and Thiele Kaolin Company on suppressing ASR. Metakaolin from Burgess Pigment Company was tested at cement replacement levels of 5%, 10%, and 15%. The expansions after 14 days were 0.23%, 0.06% and 0.03% respectively. Holcim metakaolin was tested at the replacement levels of 10%, 15%, and 20%. Their respective expansions were 0.09%, 0.01% and 0.00% at 14 days. Metakaolin from Thiele Kaolin was also tested at replacement level of 10%, 15% and 20%, and their respective expansion after 14 days were 0.02%, 0.02% and 0.01%. Regardless of the origin, metakaolin had high potential on suppressing ASR expansion.

Mobasher et al. (2010) used ASTM C1567 standard to study the influence of metakaolin on suppressing ASR expansion. They observed the lower expansion of about 70% and 80% for the mortar bar with 10% and 15% metakaolin, respectively, compared to control. Finally, they concluded that a minimum replacement level below 5% had no significant influence to mitigate ASR, see Figure 2.34.

Sarfo-Ansah et al. (2014) found that the calcined clay pozzolana had a noticeable influence on suppressing ASR with increasing its content in blended cement, see Figure 2.35. The mortar bar with 25% revealed the lowest expansion of about 0.05% at 84 days, while the reference bar had the highest expansion of 0.35% at the age of 42 days. The recorded expansion reduction was 45% for the bars with 10% to 15% calcined clay and 70% for those with 20% to 30% calcined clay. On their XRD analysis results, the formation of a calcium silicate, $CaSi_2O_5$ increased proportionally with the increasing pozzolan content, while CH and sodium silicate ($Na_2Si_2O_5 \cdot nH_2O$) decreased. This explains the reason behind the influence of calcined clay pozzolanic reaction on suppressing ASR.

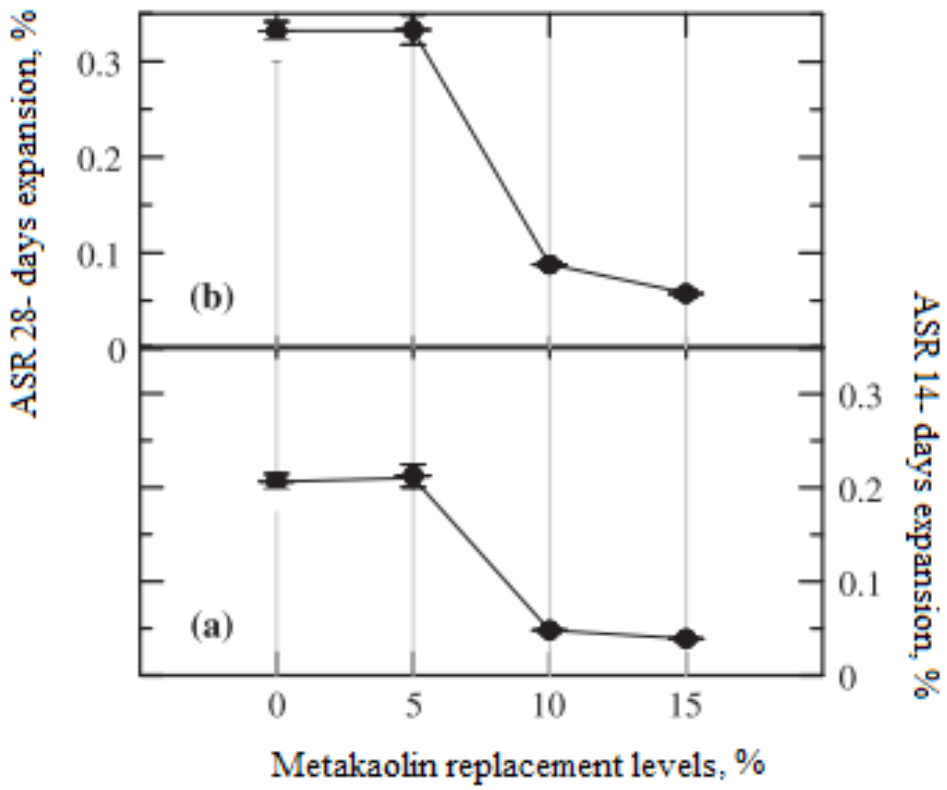

Figure 2.34: ASR expansion with increase of metakaolin content (Mobasher et al., 2010)

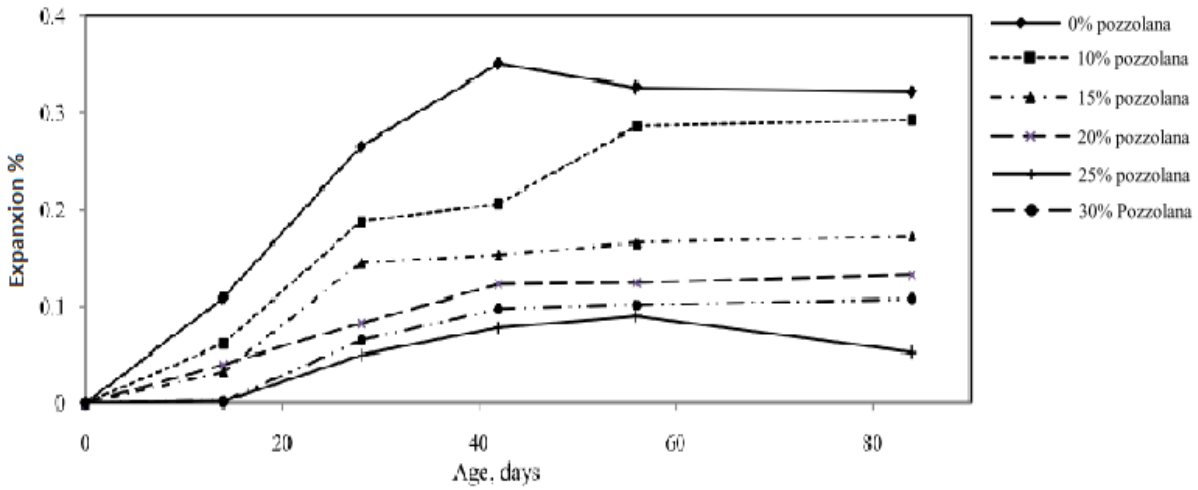

Figure 2.35: Expansion of different pozzolan(metakaolin) cement with time (Sarfo-Ansah et al., 2014)

However, there was a challenge to obtain sufficient of literature, the most obtained explained the same behaving mechanism of metakaolin when used as the SCM to suppress the effect of ASR expansion in concrete. Therefore, the conclusion can be drawn that increasing the metakaolin content at the highest level from 10% significantly reduces the ASR expansion in concrete.

2.11.5. Carbonation

Mcpolin et al. (2007) described carbonation as a progressive process that starts from the concrete surface and penetrates deeper with time. They said this process entails a combination of two processes, namely, diffusion of atmospheric carbon dioxide gas (CO_2) into concrete through pore solution, and reaction between the diffused CO_2 and CH which results in the formation of calcium carbonate (equation 2.10)

$$Ca(OH)_2 + CO_2 \rightarrow CaCO_3 + H_2O \quad (2.10)$$

However, Visser (2012) gave a detailed mechanism of the process. He said after diffusion of CO_2 in the gaseous phase of the concrete pores, it dissolves in the pore solution to form carbonic acid solution (H_2CO_3) (equation 2.11), depending on the alkalinity of the pore solution. As the dissolution proceeds, the dissolved Ca^{2+} ions from CH and cementitious matrices (calcium silicate hydrates, ettringite, and mono sulphate hydrate) react with dissolved CO_3^{2-} to form a precipitation of calcium carbonates ($CaCO_3$), see equation 2.12. The mechanism proceeds until insoluble $CaCO_3$ is formed and the equilibrium is set, then no further pH lowering.

$$CO_2 + H_2O \rightarrow 2H^+ + CO_3^{2-} \quad (2.11)$$

$$Ca^{2+} + (OH)^- + H^+ + CO_3^{2-} \rightarrow CaCO_3 + H_2O \quad (2.12)$$

2.11.5.1.Factors influencing the rate of carbonation

The overall carbonation process is a slow mechanism (Ballim et al. 2009), however, its reaction is faster compared with the diffusion of CO_2 (Meier *et al.*, 2007). This infers that whenever there are CO_2 and CH, one of them must be depleted for the reaction to stop. Even though, the process itself cannot occur if there are no acceleration factors.

Ballim et al. (2009) mentioned two factors that accelerate the reaction. These factors are sufficient moisture content (RH) and ambient temperature. Moisture content is the strongest factor because it provides a medium for chemical reaction to take place (Baker et al. 1991:29). The reaction cannot occur when concrete is completely dry as well as when it is fully saturated because water hinders diffusion of CO_2 gas by water-blocking pores. Therefore, they concluded that the maximum rate occurs when RH is between 40 and 60%, while increases with increasing the temperature.

The rate of carbonation is also influenced by the properties of concrete such as porosity and permeability. These are highly affected by the binder composition and content, and w/c ratio (Ballim, Alexander and Beushausen, 2009). Incorporating binders such as silica fume and

metakaolin tend to densify and refine the pore size, which in return, they reduce CO_2 diffusion rate. However, binders with high lime content such as fly ash decelerate the reaction rate by producing more voluminous calcium carbonates which partially fill up the pores and blocks the diffusion process (Barnes & Bensted 2002:319). Apart from that, porosity and permeability are also affected by curing age. The early the curing the higher the hydration process on the cover zone. This reduces carbonation rate by resizing the diameter of the pores thereby reducing the penetration rate and producing more CH which slows the reaction rate.

However, the formation of microcracks due to shrinkage and creep effects on concrete as well as the compaction mechanism of concrete in its fresh state can also accelerate the penetration of CO_2 into the concrete (Ballim, Alexander and Beushausen, 2009). These create the room for easy transportation of CO_2 gas into concrete, thereby speeding up the carbonation reaction.

2.11.5.2.Influence of carbonation reaction on concrete with metakaolin

Carbonation reaction has negative influences on the durability of concrete, especially reinforced concrete. This has promoted the interest in finding ways to alleviate the reaction. Considering today's concrete, whereby the use of SCMs has been given a priority due to their significance influences on improving the durability of concrete. Therefore, metakaolin potentials in influencing carbonation in concrete should be adequately quantified.

Bucher et al. (2015) indicated that 25% metakaolin in concrete could result in carbonation depth of 9 mm after 28 days of accelerated test. They argued that the main function of metakaolin in concrete is to consume CH that usually slows down carbonation, consequently, using metakaolin would increase carbonation front particularly when metakaolin does not play its role to reduce the permeability of concrete.

Kim et al. (2007) assessed the resistance of concrete with metakaolin to carbonation using the phenolphthalein indicator method at the accelerated curing conditions of 5% CO_2, 60% RH, and 30^{o}C temperature. They found that carbonation depth increased with increasing metakaolin content and exposing time, see Figure 2.36. They observed further depth increasingly at 56 days for all replacement levels; however, carbonation depth of about 100% to 370% increase was observed for 15% and 20% metakaolin-concrete regardless of the age of concrete.

Mcpolin et al. (2007) used various test methods namely accelerated carbonation test, air permeability test, pH profiling, electric conductivity, and TGA to assess the potentiality of 10% metakaolin in concrete to carbonation. All test methods showed that inclusion of metakaolin decreased the carbonation resistance. The best results were observed when the pH profiling

method was used. Figure 2.37. shows that as carbonation period increased from 0 to 6 weeks. The pH of concrete with metakaolin decreased much compared to that without metakaolin. In the inner part of concrete, the pH was higher than on its surface.

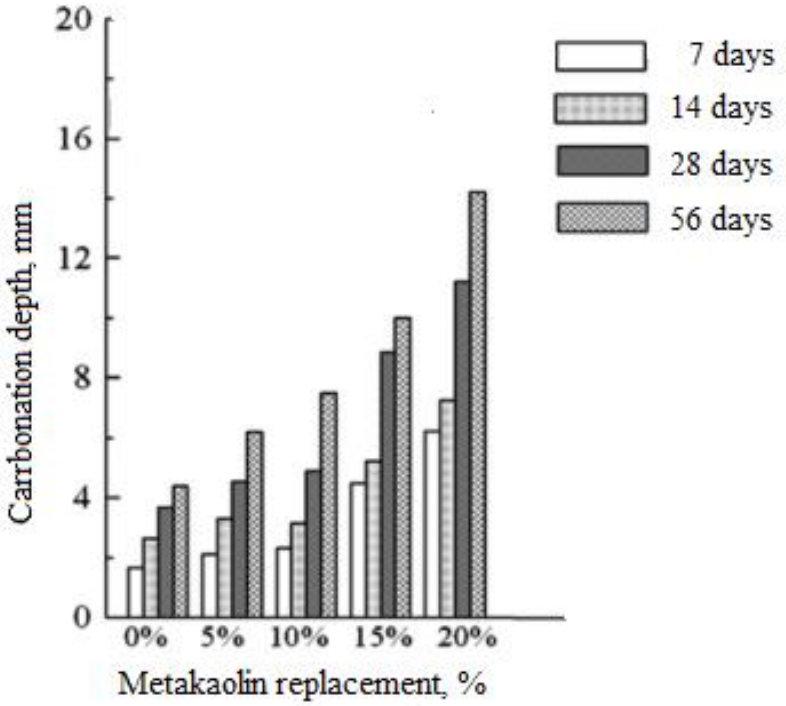

Figure 2.36: Carbonation depth of concrete with metakaolin at different replacement levels (Kim, Lee and Moon, 2007).

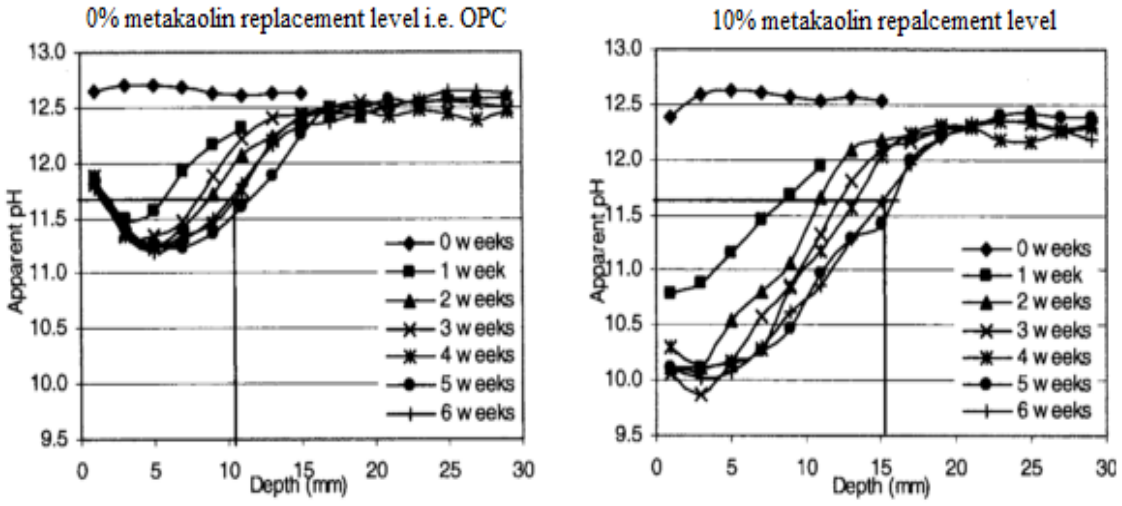

Figure 2.37: Apparent pH of concrete with 0% and 10% metakaolin at different carbonation periods with time (Mcpolin et al., 2007).

Further study was done by Nicolas et al. (2014) who used the French recommended test. Their results showed a larger carbonation depth for concrete with 25% metakaolin than the control. Additionally, they observed a decrease of CH with the increase of carbonation depth after 28

days of carbonation exposure, see Figure 2.38. The samples with metakaolin seemed to have the lowest CH of about 2% and the highest depth of carbonation of about 0.8 cm. They concluded that this phenomenon was due to the metakaolin pozzolanic reaction.

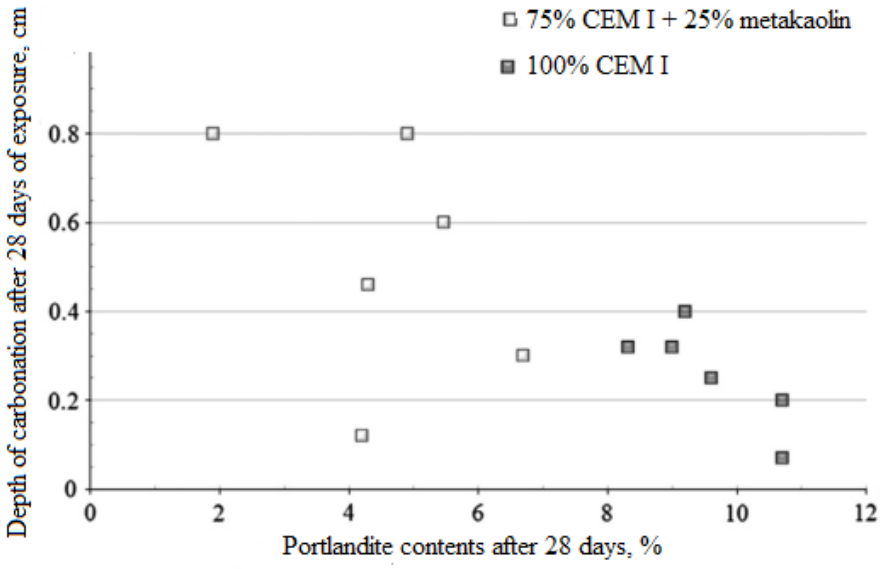

Figure 2.38: Carbonation depth after 28 days of exposure versus portlandite at 28 days (Nicolas, Cyr and Escadeillas, 2014).

The same results were observed in the cement mortar by Shi et al. (2015). They indicated that the mortar containing metakaolin had poor resistance to carbonation. This was explained as due to metakaolin influences on reducing the amount of CH in the mortar which plays an important role in slowing carbonation rate. The same reason was given by Saillio et al. (2015) who showed the trend of CH decreased with time and the variation of carbonation depth with increasing metakaolin content and time, see Figure 2.39.

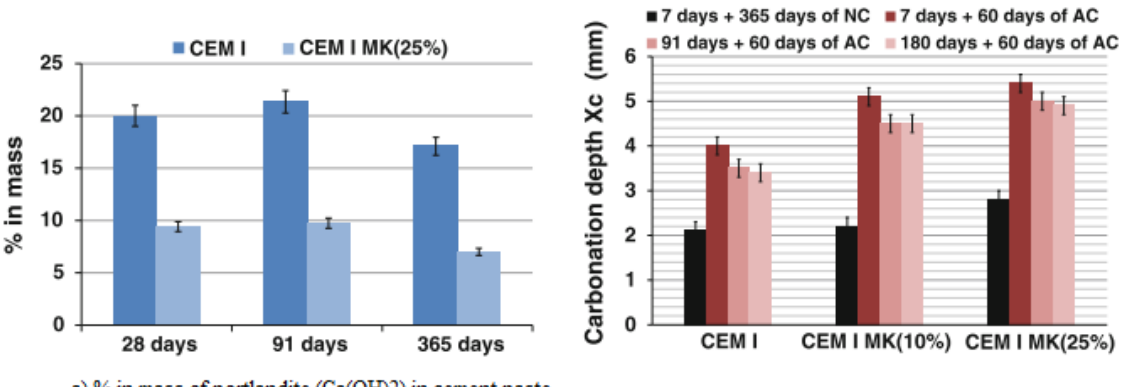

a) % in mass of portlandite ($Ca(OH)_2$) in cement paste

b)carbonation depth on the concrete with 0 to 25% metakaolin after various water curing times and natural (NC) or accelerated carbonation(AC)

Figure 2.39: Illustration of the carbonation depth increase as the consumption of CH in concrete containing metakaolin (Saillio, Baroghel-Bouny and Pradelle, 2015)

Nevertheless, Bucher et al. (2015) tested carbonation of blended binders containing metakaolin. Their results showed that the replacement of CEM I and CEM II/A-V (based on fly ash) by metakaolin leads to an increase in carbonation depth. They also observed that the combination CEM II/A-LL +MK (i.e. ternary mixture composed of clinker, limestone filler and metakaolin) intended to reduce carbonation for both accelerated and natural test. The observed carbonation depth after 50 years of natural curing condition showed that all SCMs (including MK) concrete mixes were still acceptable in terms of carbonation, especially when adequate concrete protection cover was used. This observation was supported by Tafraoui et al. (2016) who did not detect any sign of carbonation when ultra-high performance concrete (UHPC) with 20% metakaolin was subjected to accelerated carbonation test for 19 months.

Even though the inclusion of metakaolin in concrete accelerates carbonation reaction, still carbonation depth can be acceptable only if concrete with low permeability is used and a sufficient concrete cover is provided.

2.12. GENERAL CONCLUSION- LITERATURE REVIEW

This chapter has highlighted various studies on the use of metakaolin from different origins in concrete. It has been seen that metakaolin has a high potential for enhancing properties of concrete (structural and durability properties). However, there were contradictions highlighted in this chapter. Such contradictions involved the influence of metakaolin on the setting time and heat of hydration of cement, modulus of elasticity, and flexural strength of concrete with metakaolin. There were limited studies on the deformation behaviour (especially creep) of concrete with metakaolin as well as the potential of metakaolin on mitigating ASR. Moreover, the characterization of Western Cape concrete with metakaolin was not well studied. Therefore, there is a need to characterise the properties of Western Cape concrete made with metakaolin that is locally available, aiming at determining whether it can be used as an alternative SCM.

3. CHAPTER THREE: EXPERIMENTAL METHODOLOGY

3.1. INTRODUCTION

This chapter explains how the present research was conducted in the laboratory. The experimental investigation consisted of the description of materials and test methods conducted. The tests were divided into six categories, namely, pozzolanic activity of metakaolin, properties of fresh concrete with metakaolin, properties of hardened concrete with metakaolin, deformation behaviour of concrete with metakaolin, and finally, durability properties of concrete with metakaolin. All tests were conducted according to South African National Standards (SANS); however, some tests which had no corresponding SANS, were conducted according to the British Standards (BS); where both SANS and BS were not found, the American Society for Testing and Materials (ASTM) standards were used.

3.2. MATERIALS

3.2.1. Cement and water

Portland limestone cement denoted as CEM II/A-L 52.5N, a common cement collected from PPC Cement, based in the Western Cape, was used in this research. It comprises the addition of between 6% and 20% limestone extender, typically about 9%. SANS 50197-1 categorises this cement under 52.5 N strength class for common cement. Its physical and chemical properties were provided by the manufacturer and are shown in Table 3.1 and Table 3.2

Potable tap water was used for casting and curing, unless distilled water was used where the standards specified it.

3.2.2. Metakaolin (mk)

This is a highly reactive and fine material which is known as Metakaolin KG-K40. Its raw material was extracted from kaolin clay deposit at Atlantis by a company called Kaolin group. It was supplied by Serina Trading. A photograph of the metakaolin is shown in Figure 3.1.

Table 3.1 and Table 3.2 shows the physical and chemical properties of metakaolin.

Figure 3.1: Metakaolin appearance- light off-white in colour.

3.2.3. Ground Granulated Corex Slag (GGCS)

This is a type of slag currently used in the Western Cape as an SCM. It is a by-product from the iron industry, produced by the Saldanha Steel plant. It is similar to Ground Granulated Blastfurnace Slag (GGBS), however, the two slags differ in their manufacturing processes. The GGCS technology employs two reactors (reduction shaft and melting gasifier reactors), whereas, in the production of GGBS, the traditional blast furnace process is employed (Jaufeerally, 2013).

GGCS is light grey in colour. It has a higher proportion of ultrafine particles in the range 1-10 µm compared to GGBS according to South African production industries. Its particles have an angular shape with conchoidal faces (Alexander, Jaufeerally and Mackechnie, 2003). Its physical and chemical properties (provided by PPC Cement) are shown in Table 3.1 and Table 3.2.

GGCS was used in this study to produce concrete, the properties of which were determined and compared to concrete made with metakaolin. The aim was to assess whether metakaolin could be used as a substitute or replacement for GGCS.

3.2.4. Silica fume and fly ash

Silica fume and fly ash were not the main SCMs in this study, however, they were included for comparing their pozzolanic activities with that of metakaolin. Silica fume was obtained from Ferri Atlantic, while, fly ash from Ash Resources.Their physical and chemical properties are shown in Table 3.1 and Table 3.2.

Table 3.1: Physical properties of cement, metakaolin, GGCS.

Property name	CEM II A-L 53.5 N	MK	GGCS	Silica fume	Fly ash
Colour	Grey	Light off-white	Light grey	Dark grey	Tan grey
Relative density	3.14	2.30	2.90	2.10	2.36
Specific surface area (m^2/g)	0.86	-	1.29	-	1.23
D(0.5) (μm)	17.7	-	15.1	-	15.8

Table 3.2: Chemical composition of cement, metakaolin, and GGCS.

Chemical formula	Chemical composition, %				
	CEM II A-L 52.5N	GGCS	Silica fume	Metakaolin	Fly ash
SiO_2	19.77	31.32	83.91	52.81	53.72
Al_2O_3	3.24	17.04	0.85	42.02	32.94
Fe_2O_3	3.11	1.00	4.02	0.32	3.23
Mn_2O_3	0.06	0.05	0.91	0.03	0.07
TiO_2	0.19	0.58	0.02	1.30	1.71
CaO	63.84	35.15	2.52	0.02	4.32
MgO	1.28	11.76	1.29	0.07	1.07
P_2O_5	0.14	0.03	0.11	0.09	0.54
SO_3	2.55	3.04	0.00	0.00	0.00
K_2O	0.61	0.63	2.48	0.06	0.46
Na_2O	0.22	0.00	0.00	0.00	0.00
SrO	0.26	0.00	0.00	0.00	0.00
LOI	4.63	-	4.44	1.16	1.03
Total	99.9	99.3	100.5	97.9	99.1

3.2.5. Fine Aggregates

Two types of sand were used in this study; Philippi dune sand and greywacke crusher sand blended to a ratio of 60:40 (dune sand to crusher sand). Philippi dune sand originates from sand dunes which are characteristic of deserts or low-lying flat coasts. It is fine to coarse-grained. Its grains are well-rounded which resulting in a low water requirement. Greywacke crusher sand is manufactured from greywacke rock. It is characterised by a chunky particle shape (which is achieved by adoption of suitable crushing techniques) and uniform grading with high fines content. This is because it has little or no deleterious substances such as clay, being crushed from fresh rock (Fulton, 2009: 48-51).

The physical properties of the aggregates, such as particle relative density, particle size distribution, and fineness modulus were determined according to SANS 5844 and SANS 201, respectively. The results are given in Table 3.3 and Figure 3.2.

Table 3.3: Physical properties of fine aggregates

Fine aggregate type	Philippi dune sand	Greywacke crusher sand
Relative density	2.65	2.72
Fineness modulus	2.05	3.15
Percentage finer than 75 µm, %	0.07	1.32

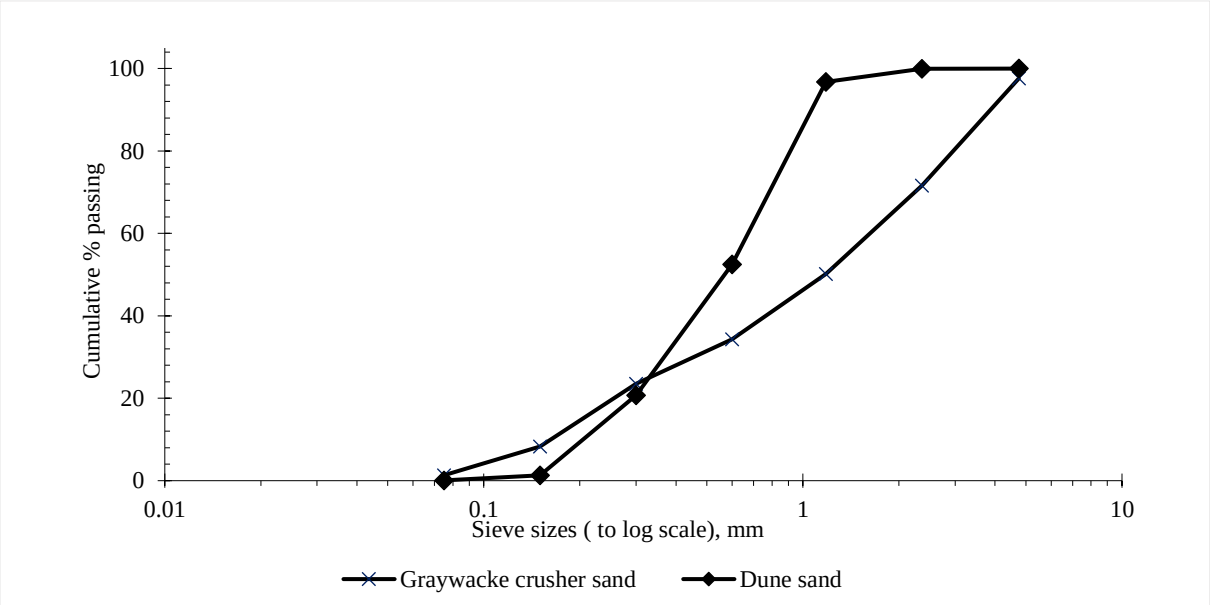

Figure 3.2: Sieve analysis results of fine aggregates

3.2.6. Coarse Aggregates

Greywacke aggregate, also known as Malmesbury shale, originates from a metamorphic rock, formed when the Cape Granite intruded into the original Malmesbury rock. Malmesbury rock consists of alternating layers of dark grey fine –grained greywacke, sandstone and slate (Cole, Ngcofe and Halenyane, 2014). The rock is a known alkali-reactive aggregate which is commonly used in Western Cape construction. However, it is usually used with cement that is blended with SCMs to suppress its reactivity. Therefore, in this study, these aggregates with a 19-mm maximum particle size were used to simulate field concrete. The physical properties, namely compacted bulk density, particle relative density, and particle size distribution were determined according to SANS 5845, SANS 5844 and SANS 201, respectively. Results are given in Table 3.4 and Figure 3.3**.**

Table 3.4: Physical properties of course aggregates.

Coarse aggregate type	Greywacke stones
Compacted bulk density (kg/m^3)	1450
Relative density	2.72
Max. nominal particle size(mm)	19

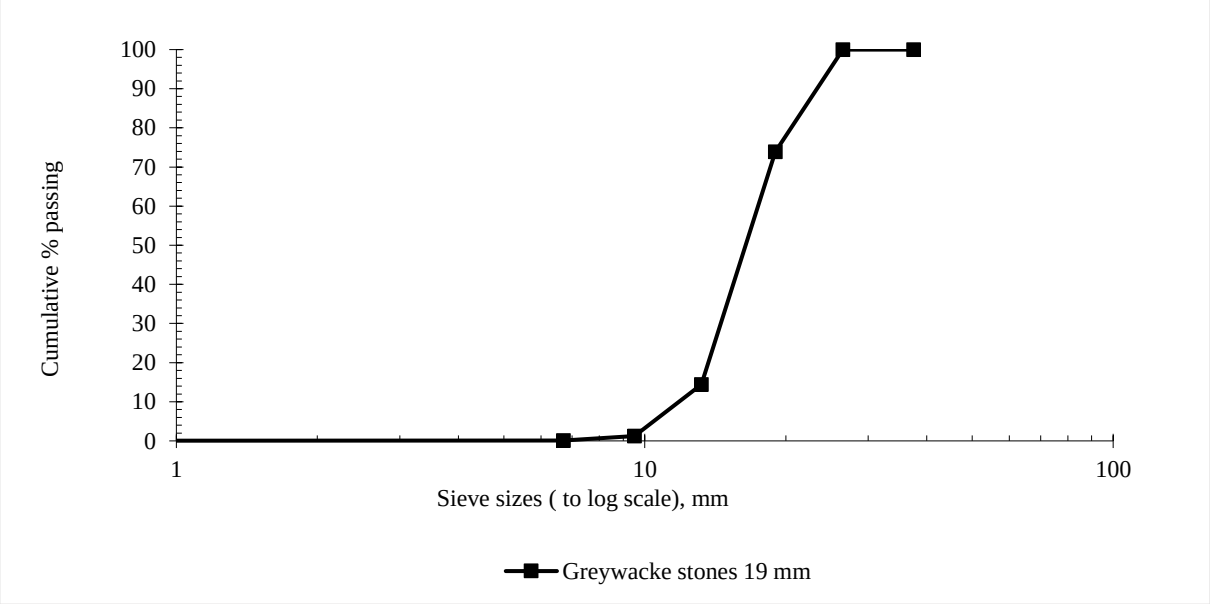

Figure 3.3: Sieve analysis of Greywacke coarse aggregate

3.2.7. Superplasticiser (SP)

The Superplasticiser used was CHRYSO® Plast Omega 103 from Chryso Southern Africa. It is a water reducing superplasticiser which is in liquid form with a relative density of 1.085 at 20°C, with a pH of 7.5. The alkali content (Na_2O) is equivalent to 2.00%. A dosage between 0.3% and 0.5% of the product by mass of cement is commonly used, however, in this study, the optimum dosage that provided a slump range of 100 ± 25 mm was established after multiple trial mixes.

3.3. SUMMARY OF TEST METHODS

Figure 3.4 summarizes the test methods, divided into five categories.

Pozzolanic activity tests were conducted to characterize the reactivity of metakaolin. Four test methods were conducted and their results were compared. Four mortar mixes (one control mix and three with 10%, 15%, and 20% metakaolin) with 0.5 w/b ratio and 1:3 binder to sand ratio were used. Besides, metakaolin was also characterized by comparing its pozzolanic reactivity with three other SCMs, namely, GGCS, silica fume, and fly ash.

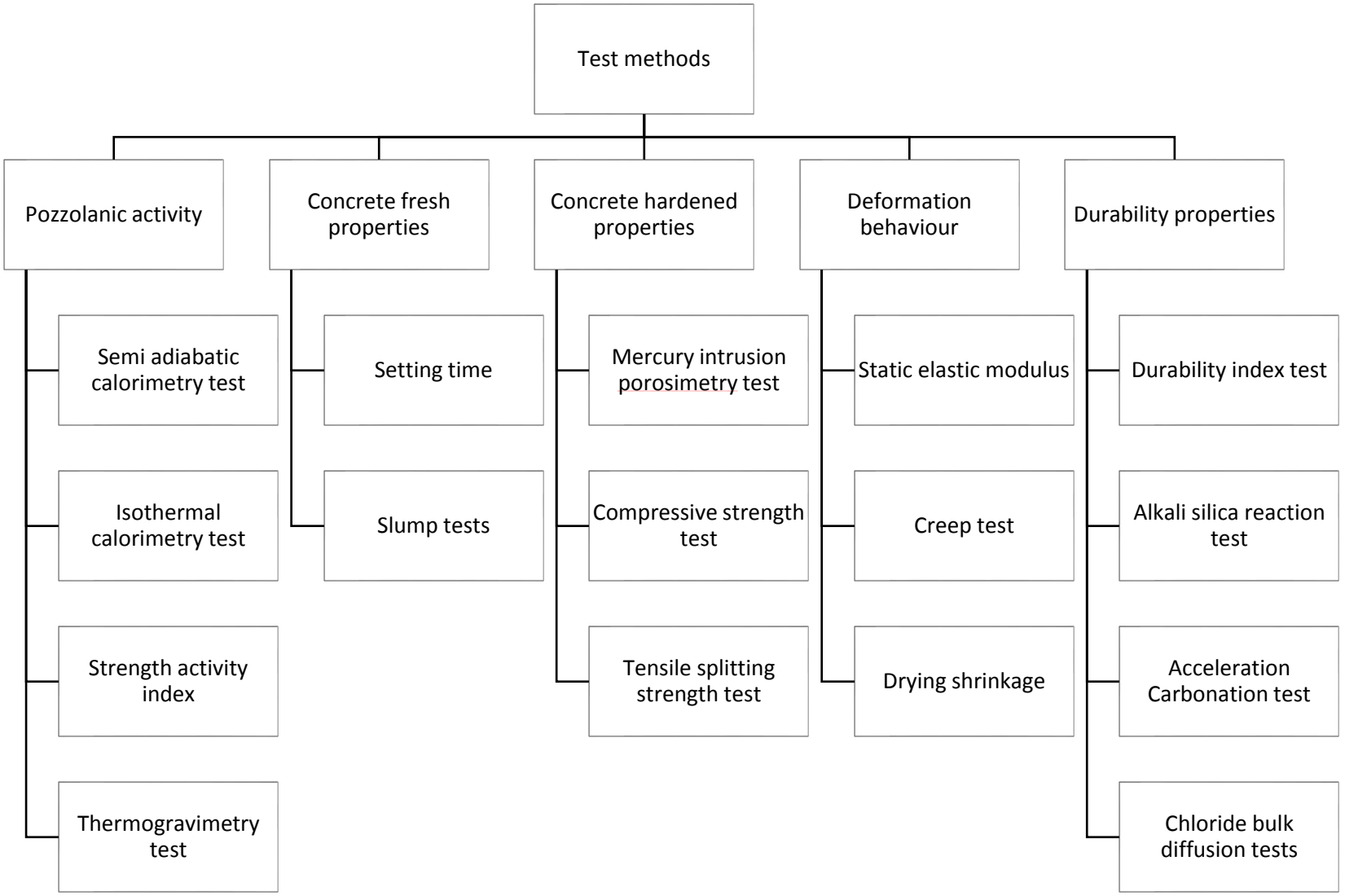

Figure 3.4: Summary of test methods divided into six categories

For the tests that involved concrete, i.e fresh and hardened concrete properties, deformation behaviour of concrete, and durability properties of concrete, a total of fifteen concrete mixes were designed. Three w/b ratios, 0.4, 0.5, and 0.6, were used. At each w/b ratio, five mixes were designed; one as a control mix, three mixes with 10%, 15% and 20% metakaolin, and one mix with 50% GGCS. Cement was replaced by metakaolin at a rate of 10%, 15%, and 20% because the literature suggested that at these replacement levels, concrete is expected to exhibit favourable engineering properties. The same reason was used to select the GGCS replacement of 50%. To avoid inconsistency, a single batch of concrete to accommodate all tests for each mix design was cast at once. However, 0.4 and 0.5 w/b mixes were re-cast four months later after 0.6 w/b mixes.

The mixes prepared for ASR testing were different since these tests required a special mortar mix. These mix designs are described in section 3.8.2.

3.4. POZZOLANIC ACTIVITY OF METAKAOLIN

The pozzolanic activity of metakaolin was assessed by three test methods; calorimetry methods that included semi-adiabatic and isothermal calorimetry tests, and strength activity index (SAI) as indirect methods, and thermogravimetric analysis (TGA) as a direct method. The reactivity of metakaolin was determined by comparing its performance in the three tests.

3.4.1. Semi adiabatic calorimetry test method

The aim of conducting this test was to determine indirectly the reactivity of metakaolin in terms of heat generated. It involved determining the amount of heat evolved in accordance with the temperature rise in the calorimeter containing a freshly made mortar. This test was performed according to the combination of two standards, ASTM C1753 and BS EN 196-9.The test procedures and equipment were developed by the UCT civil engineering department. The following sub-sections briefly outline the developed test procedures.

3.4.1.1. Inert and mortar sample preparation

The inert sample, also known as a 'reference calorimetry', was used to calculate temperature change in each mix. It was prepared by a mixture of oven-dried sand (60% dune sand: 40% crusher sand) and water at the same ratio as that used to prepare the mortar mixes.

Mortar mixes (shown in Table 3.5), sufficient to accommodate three sample containers of 0.001 m^3, were prepared. The mixing procedures involved mixing the two sand types and binder into the mixer for about 30 s at a low speed. Thereafter, water was added while continuing mixing for 60 s. Immediately after adding water, the time was recorded, and finally, the mixer was set

to high speed and the mix processed with further mixing for 60 s. The mixing environment was maintained at a temperature of 23±3^{0}C.

Table 3.5: Mortar proportions for the semi-adiabatic test method.

Content Mix	CEM II (kg/m^3)	Metakaolin (kg/m^3)	Dune Sand (kg/m^3)	Crusher sand (kg/m^3)	Water (kg/m^3)	SP /binder (%)	Slump flow (mm)
1	597	0	1075	716	299	0.0	150
2	537	60	1075	716	299	0.4	145
3	507	90	1075	716	299	0.5	155
4	478	119	1075	716	299	0.6	150
Inert sample	-	-	1075	716	299	-	-

3.4.1.2. Test procedures

Four sample containers (Figure 3.5), one with the inert sample and three with mortar samples of the same mix, were placed into the semi-adiabatic calorimeter which was insulated to avoid undue heat loss. Their corresponding temperature readings were transmitted to a 4-channel data logger using a platinum resistance thermometer, after every 10 mins for 120 h, see Figure 3.6. Readings were extracted from the data logger, and the total heat of hydration values were calculated. The heat of hydration of cement in each sample was calculated as the sum of heat accumulated in the calorimeter and heat lost into the ambient atmosphere through the period of the test. The temperature rise in the mortar was compared with the temperature of an inert sample in a reference calorimeter. The total heat evolved at a given time by unit mass of cementitious binder was determined using the relationship in equation (3.1)

$$q = Cp * \sigma T * \frac{m_s}{m_c} + \frac{1}{m_c} * \sum \alpha * \sigma t * \sigma T \qquad (3.1)$$

Where,

q Heat liberated during hydration per unit cementitious material

C_p Specific heat capacity of the sample

δT Change in temperature of the sample over the time period under consideration

α Coefficient of heat loss into the ambient atmosphere, J/h.^{o}C

δt Time elapse or increment, in h

m_s mass of the sample

m_c mass of cementitious material in the sample.

The specific heat capacity of the sample was determined as the mass-weighted sum of the specific heats of its components. The specific heat capacity of individual components shown in Table 3.6 was obtained from (Fulton, 2009:275). Distilled water at 100^{o}C was used to calibrate the equipment in which the coefficient of heat loss into the ambient atmosphere was determined. Equation 3.2 obtained from Wadsö, (2003) was used to evaluate α, which was taken from the slope of ln ΔT against time (t), using C_w as the specific heat capacity of water multiplied by its mass in the calorimeter container (0.65 kg).

$$InT = InA - \frac{\alpha}{C_W} * t \qquad (3.2)$$

The above procedures were repeated for all mixes (Table 3.5) and the influence of metakaolin on heat of hydration was observed.

Table 3.6: Specific heat capacities of individual components of mortar

Specific heat capacity	(J/kg. ^{0}C)
Cement	880
Water	4182
Philippi dune sand	910
Crusher sand	920
Metakaolin	880

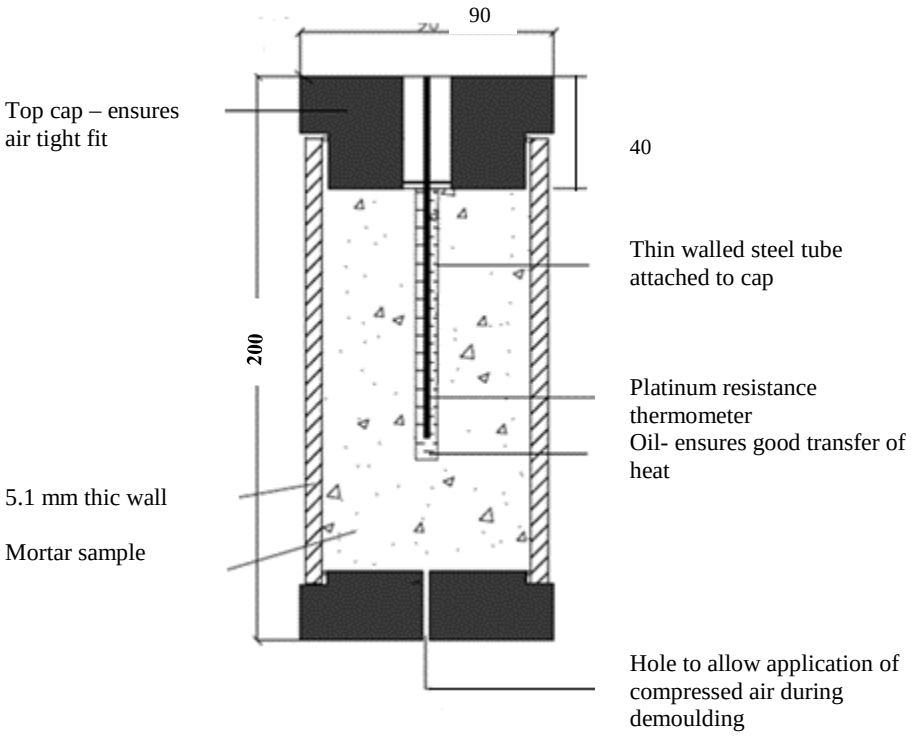

Figure 3.5: Semi-adiabatic calorimeter, sample container

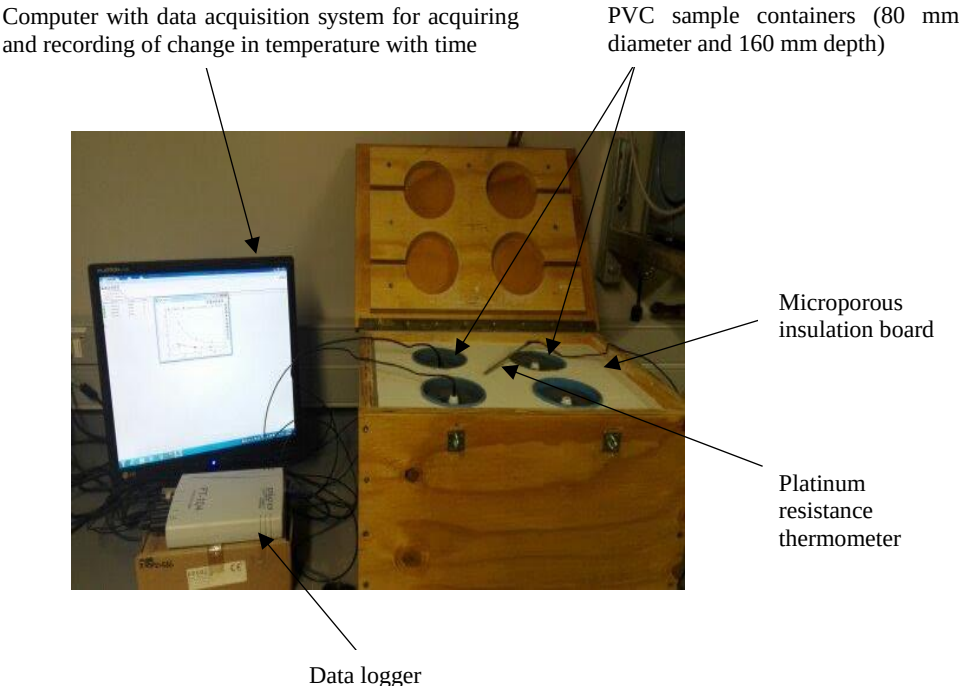

Figure 3.6: Semi adiabatic calorimetry set up

3.4.2. Isothermal calorimetry method

Isothermal calorimetry is an experimental technique to monitor heat flow through a specimen when both the specimen and the surrounding environment are kept at isothermal conditions, i.e. the same temperature. The heat flow is measured in terms of thermal power and voltage at every second from the start to the end of testing duration. Using this output, the heat of hydration of cement paste or mortar can be evaluated.

This technique was used to meet two objectives;

i) to measure the influence of different metakaolin replacement levels i.e. 10%, 15%, and 20%, on heat of hydration of cement-mortar, and

ii) to rank pozzolanic activity of metakaolin in relation to other SCMs such as GGCS, fly ash, and silica fume in terms of total heat generated.

This test was conducted using an isothermal calorimeter with software, called 'Calmetrix I-Cal 200 HPC'. The guidelines on using the equipment and software are described in the I-Cal 2000 HPC User Manual (Calmetrix Inc. 2016). Generally, the test was performed according to ASTM C 1702 and ASTM C 1679. The equipment was set to perform at a constant temperature of 20^{o}C.

To meet the first objective, mortar mixes prepared as per the semi-adiabatic test (section 3.4.1) were used. From each mix, two plastic caps were filled with 200 g of mortar and loaded into the equipment immediately after mixing. The test was then performed for 120 h.

To meet the second objective, SCM-portlandite paste were prepared according to Avet *et al.*, (2016).Two samples each with 111.1 g of paste (Table 3.7) were hand-mixed to get a homogeneous paste. Immediately after mixing the samples were filled into two plastic caps, then loaded into the calorimeter. The readings were recorded for seven (7) days. A total of four SCMs were tested; metakaolin (main SCM), GGCS, fly ash, and silica fume. Noted that potassium sulphate (K_2SO_4) and potassium hydroxide (KOH) were utilized to accelerate pozzolanic activity

Table 3.7: SCM-portlandite paste mix compositions for ranking metakaolin with other SCMs.

Mass	SCM	Portlandite	Deionized H_2O	KOH	K_2SO_4	$CaCO_3$
Type		<5% $CaCO_3$		Lab grade	Lab grade	Lab grade
(g)	11.11	33.33	60	0.24	1.2	5.56

3.4.3. Strength Activity Index (SAI) test method

This is an indirect method used to determine the pozzolanic activity of materials in terms of compressive strength development when used in conjunction with hydraulic cement. The test is based on BS 3892:1 and ASTM C 618.

Mortars with 0.5 w/b ratio and the ratio of 1 binder to 3 sand (by mass) were used (Table 3.5). Mortar was prepared in a mortar mixer and cast in 50 mm cube moulds. Superplasticizer was used to disperse metakaolin particles, and a flow test according to SANS 5862-2:2006 was conducted to maintain the flow within 150 ± 5 mm. All cubes were de-moulded 24 h after casting and placed in a water bath at 23^{o}C until ages of 3, 7, 14, 28, and 56 days. At each curing age, three cubes were removed from the bath, surface wiped clean, and tested for compressive strength according to SANS 5863:2006. The strength results were reported as the average of three tests, and presented as the percentage relative strength of the test mortar to control mortar, termed as strength activity index (SAI), see equation 3.3;

$$SAI = \frac{A}{B} * 100 \quad (3.3)$$

Where,

A Compressive strength of the test pozzolan mortar (MPa)

B Compressive strength of the control mortar (MPa).

3.4.4. Thermogravimetric analysis (TGA)

TGA is a technique in which the mass of the sample is monitored against time or temperature, while a specific rate of temperature change of the sample, in a specified atmosphere, is programmed. In this study, the technique was employed to determine the quantity of CH contained in the sample, determined from the mass loss of the sample at a temperature between 400^{o}C and 500^{o}C, where the decomposition of CH takes place. In this study, the analysis was performed to serve two objectives,

i) to determine CH consumed by different proportions of metakaolin with hydration time in mortar, and

ii) to compare the reactivity of CH with metakaolin and other SCMs.

The first objective entailed the use of crushed specimen remnants from the SAI test (section 3.4.3) after 7, 14, and 56 days of curing, while the second objective used SCM-portlandite samples of the mixes shown in Table 3.7, immediately after 7 days of performing the isothermal calorimetry test.

At the end of the hydration period of a corresponding test, the sample of approximately 100 g was immersed in isopropanol for 48 h, then dried in an oven at a temperature of 50^{o}C for another 24 h. Isopropanol was used to stop further hydration reactions and to displace water molecules, while the drying process assisted in removing free water and facilitating the grinding process. Finally, the sample was ground by using a pestle and mortar into a powder form, and sieved through a 75 μm sieve to obtain fine particles. A 10 g powdered sample was measured and stored in a plastic bag leaving no air to carbonate the sample. Thereafter, the samples were taken to the UCT Materials Engineering Laboratory for TGA.

In the TGA, a powdered sample of approximately 65 mg was measured and filled in an aluminium crucible, and set into the Netzsch (STA 409 CD) Thermal Analysis machine. The chamber was then evacuated three times and back-filled with medical air (combination of nitrogen and oxygen gas) flowing at a purge rate of 20 mL/minute in an inert environment. The sample was heated at a heating profile from 25 to 1000 °C at a heating rate of 10°C/min, and finalized by non-controlled furnace cooling. The data collected were presented in the Thermogravimetric (TG) curve showing cumulative mass loss against temperature profile and Differential Thermogravimetric analysis (DTG) showing the first derivative of cumulative mass loss by using Proteus analysis software. CH content and chemically bound water were then calculated.

3.5. CONCRETE MIX DESIGN AND FRESH STATE PROPERTIES

3.5.1. Mix design

Concrete mixes were designed according to the C & CI method (Fulton 2009:219). Aggregate properties such as particle relative density, compacted bulk density, grading, and fineness modulus of sand were determined as described in section 3.2. Water and coarse aggregate content were kept constant for all mixes i.e. water content = 185 L/m^3 and coarse aggregate content =1000 kg/m^3. Table 3.8 shows the concrete mix designs used in this study.

Superplasticiser was used to regulate the workability of concrete. This was due to the tendency of metakaolin to decrease workability. With the aid of the superplasticiser, a slump value of 100 ± 25 mm was achieved for all concrete mixes. The amount of SP used was well presented in the chapter 4 section 4.4.2.

All concrete mixes were mixed and prepared as per SANS 5861-1 and SANS 5861-2, respectively. The fresh concrete properties determined were setting time and workability.

3.5.2. Setting time

Standard consistency and setting time of cement paste samples were determined as per SANS 50196-3 in the laboratory environment at 23 ± 3^oC temperature and 50% relative humidity. Within the scope of this study, CEM II A-L 52.5 N was replaced with metakaolin at a replacement rate of 0%, 10%, 15%, and 20%.

Setting times of cement paste were determined by observing the penetration resistance of a Vicat needle into cement paste of a standard consistency. The standard consistency test was performed first to determine water content at which the distance between a plunger and base plate was 6 ± 2 mm. By using the obtained water content, cement pastes of proportions shown in Table 3.9 were prepared. The initial and final setting times were then determined using a Vicat apparatus. Noted that in this test SP was not used.

Table 3.8: Concrete mix designs – kg/m^3

w/b	Mix	Type	Variables	Cement	Metakaolin & Corex slag		Water	Coarse Aggregate	Fine Aggregate		Total	SP dosage,% by mass binder
				CEM II	mk	GGCS	Potable	Greywacke	Dune Sand	Crusher sand		
				kg/m^3								
0.4	1	Control	100% CEM II/A-L	463	-	-	185	1000	544	305	2497	0.56
	2	Metakaolin	10% mk	416	46	-	185	1000	534	300	2481	0.67
	3		15% mk	393	69	-	185	1000	529	297	2474	1.12
	4		20% mk	370	93	-	185	1000	524	294	2466	1.34
	5	Corex slag	50% GGCS	231	-	231	185	1000	533	299	2479	0.50
0.5	1	Control	100% CEM II/A-L	370	-	-	185	1000	597	335	2487	0.42
	2	Metakaolin	10% mk	333	37	-	185	1000	590	331	2475	0.57
	3		15% mk	315	56	-	185	1000	586	328	2469	0.85
	4		20% mk	296	74	-	185	1000	582	326	2463	0.94
	5	Corex slag	50% GGCS	185	-	185	185	1000	589	330	2474	0.42
0.6	1	Control	100% CEM II/A-L	308	-	-	185	1000	633	355	2481	0.04
	2	Metakaolin	10% mk	278	31	-	185	1000	626	351	2471	0.13
	3		15% mk	262	46	-	185	1000	623	350	2466	0.26
	4		20% mk	247	62	-	185	1000	620	348	2461	0.34
	5	Corex slag	50% GGCS	154	-	154	185	1000	626	351	2470	0.08

Table 3.9: Cement paste proportions

Binder proportions: total mass 500 g				
Mix	0% mk	10% mk	15% mk	20% mk
Cement, %	100	90	85	80
Metakaolin, %	0	10	15	20
Water content, % of binder	23.6	29.0	31.0	33.0

3.5.3. Workability

The workability of fresh concrete was determined by the slump test according to SANS 5862-1. This is a consistency test which is useful in detecting variations in the uniformity of a mix. It generally gives reliable results for most concretes of average workability.

3.6. HARDENED CONCRETE PROPERTIES

This section explains the tests used to determine the properties of the hardened concrete. After concrete mixing and determining the fresh state properties as described in section 3.5. Concrete was cast in the respective moulds according to SANS 5860 and cured as per SANS 5861-1.

3.6.1. Compressive and tensile splitting strength tests

Compressive strength tests were conducted according to SANS 5863, and tensile splitting strength according to SANS 6253.

Eighteen concrete cubes of 100 mm size were cast for each concrete mix and cured for 7, 28, and 56 days. At each curing age, a total of six specimens (three cubes/test) were removed from the curing bath, and tested for compressive and tensile splitting strengths (Figure 3.7) using the compressive testing machine.

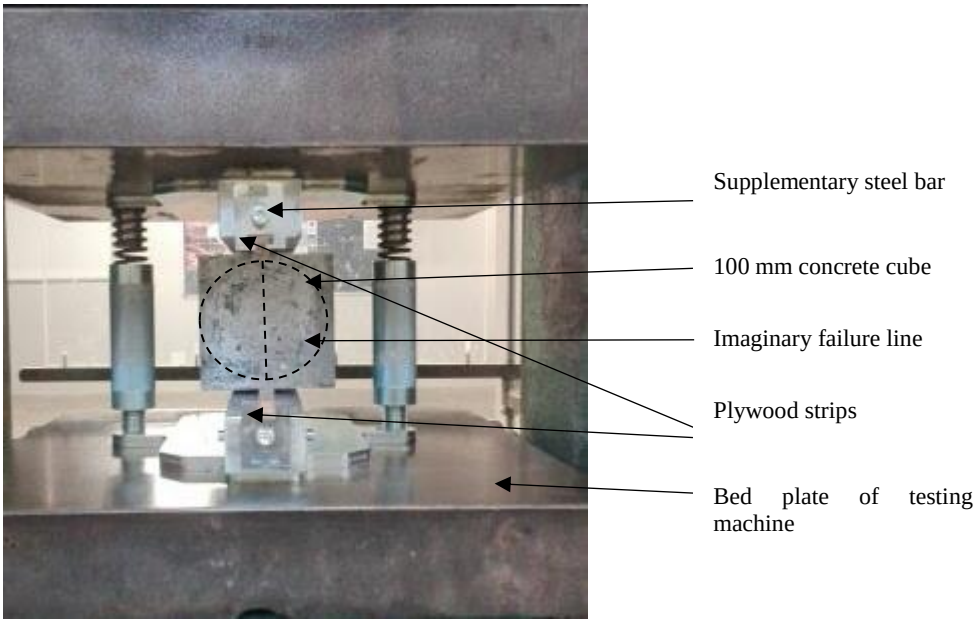

Figure 3.7: Tensile splitting strength test set up in a compressive test machine.

3.6.2. Mercury intrusion porosimetry (MIP) test

The aim of this test was to study the influence of metakaolin on the microstructure of concrete. The tests were conducted at the Indian Institute of Technology (Madras) (IITM) in Chennai, India, (under the supervision of Prof M Santhanam, an Honorary Research Associate of CoMSIRU at UCT).

3.6.2.1. Mix selection for test

Based on the observations of compressive and tensile splitting strength tests, and durability index tests, metakaolin at higher replacement levels showed higher influences. Predominantly, the highest effects were observed when 0.6 w/b was used as opposed to 0.4 and 0.5 w/b ratios which were similar. The concretes with 0.6 w/b were selected for testing pore size distribution and total porosity development at hydration periods of 7, 28, and 56 days.

3.6.2.2. Sample preparation

Sample blocks of approximately 50 x 50 mm cross-section dimension and 15 mm thick were cut from concrete cubes after the tensile splitting test at ages of 7, 28, and 56 days. To stop chemical reactions (carbonation and hydration) and to displace water molecules, the samples were immersed in isopropanol solution for 48 hours before drying in the oven at 50^{o}C for another 24 hours. Thereafter, the samples were kept in plastic bags and stored in the environmental room at 23^{o}C and 50% RH prior to the MIP test.

3.6.2.3. Summary of MIP test procedures

The MIP test was conducted at the Indian Institute of Technology (Madras) (IITM) in Chennai, India, according to Dhandapani and Santhanam (2017). It involved breaking the sample blocks into small pieces of approximately 5 mm size, then re-conditioning them in isopropanol solution for 4 days, and drying in a vacuum desiccator for a minimum period of 4 days. Thereafter, the broken pieces of sample were introduced into a chamber which was then evacuated, followed by surrounding the samples by mercury. The pressure of the mercury was gradually increased up to 400 MPa to allow mercury penetration. As the pressure increased, mercury was forced to penetrate the pores of the sample, and the change in mercury volume intrusion at each pressure step gave the pore size distribution of the samples. The test is run automatically in the Pascal 140-440 porosimeter instrument from Thermo Scientific.

3.7. DEFORMATION BEHAVIOUR OF CONCRETE

This section describes the tests used to analyse deformation behaviour of metakaolin concretes. It entails the static elastic modulus test, and creep and drying shrinkage test. The following are the detailed explanations of the tests;

3.7.1. Static elastic modulus test

This test was conducted according to BS 1881 : Part 121 : 1983. Three concrete cylinders per mix, of 100 mm diameter and 200 mm height, were cast and cured for 28 and 56 days. After each curing age, the rough-cast top surface of the specimen was ground to prepare a flat, smooth and parallel surface for testing. Thereafter, the specimen was placed in the Instron machine for static elastic modulus testing (Figure 3.8).

The test involved loading a concrete cylinder at a constant rate of 0.6 ± 0.4 MPa/s and recording load (stress) and deformation (strain) of the specimen, automatically via the Instron machine. Three load cycles from 0.5 MPa to one-third of the compressive strength at each respective loading age were carried out to reduce the effects of creep and inherent microcracks on the results. Finally, a stress-strain curve was obtained from which the secant modulus was taken as the static modulus of elasticity of concrete.

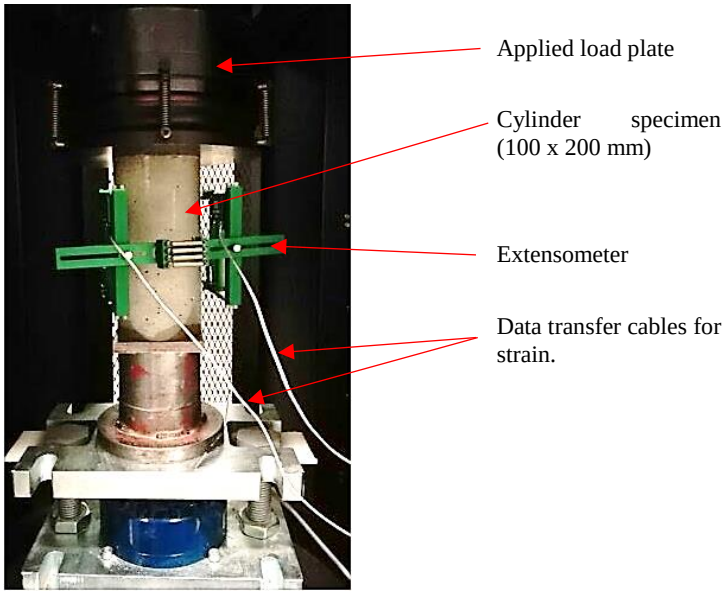

Figure 3.8: Static elastic modulus test set up in the Instron machine.

3.7.2. Creep and drying shrinkage test

The creep and drying shrinkage test was performed according to ISO 1920-9:2009. It involved the determination of i) creep of concrete cylinders subjected to a sustained uniaxial compressive load, ii) drying shrinkage of concrete cylinders kept in the environment room at 23 ±3^{o}C and 60% RH.

Four concrete cylinders (per mix) of 100 mm diameter and 300 mm height with 0.5 w/b ratio, were cast and initially cured for 24 h. After demoulding, the specimens were standard moist cured for 6 days (7 days in total). At the age of 7 days, the top as-cast surface of the specimens was ground to produce a flat, smooth, and parallel surface, Afterwards, the targets of the 100 mm gauge length were fixed onto the specimens, with three sets of targets fixed on the vertical surface spaced at 120^{o} angle.

From the age of 7 days, the specimens were kept in the environment room set at 23 ±3^{o}C and 60% RH, while strain readings were taken at 3-day intervals up to 28 days. This was done to determine drying shrinkage of the specimens at early age up to 28 days.

At 28 days, two specimens from each mix (those prepared for loading) were placed in the creep frames shown in Figure 3.9, while the remaining shrinkage specimens (control/drying shrinkage specimens, unloaded) had their ends sealed by epoxy to prevent moisture loss. The frames were then loaded to not more than 10% of the lowest compressive strength of the four mixes (Table 3.10).

Table 3.10: Applied stress on the creep frame at the age of loading (28 days).

Mix	Metakaolin, %	Compressive strength at 28 days, MPa	10 % of compressive strength), MPa	Applied stress, MPa
1	0	52.7	5.27	6.00
2	10	63.3	6.33	6.00
3	15	66.7	6.67	6.00
4	20	74.8	7.48	6.00

The strain readings (for both shrinkage and creep specimens) were taken immediately before and after loading within 30 s to determine 'instantaneous' strains, which were used to determine 'instantaneous' elastic modulus. The creep strain readings were recorded again after 2 h and 6 h for a day; daily for a week; and weekly up to 3 months. Finally, shrinkage strain, creep strain, instantaneous elastic modulus, specific creep, and creep coefficient were determined and presented in their respective graph against time.

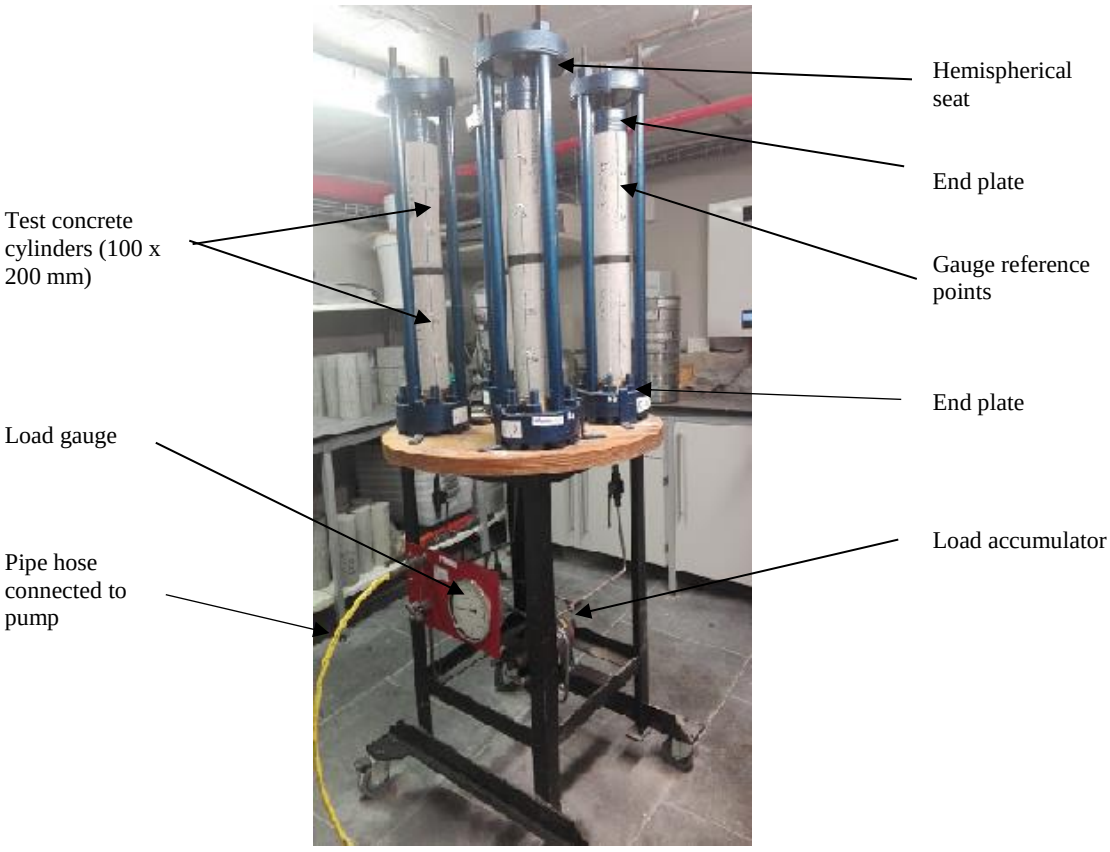

Figure 3.9: Creep frame loaded with concrete cylinders

3.8. DURABILITY PROPERTIES OF CONCRETE WITH METAKAOLIN

3.8.1. Durability index tests

Three durability index tests, i.e. oxygen permeability index (OPI), chloride conductivity index (CCI), and water sorptivity index (WSI) were carried out according to SANS 3001-CO3-2:2015;

SANS 3001-CO3-1:2015; and the UCT Durability Index Manual (Alexander 2017), respectively. Four 100 mm concrete cubes were cast for each concrete mix and wet-cured for 28 days. After 28 days curing, all concrete cubes were cut into concrete discs of 70 mm diameter and 30 mm thickness. Approximately eight discs were obtained for each mix. These discs were then marked and preconditioned at 50ºC for 7 days in preparation for the durability index tests.

3.8.1.1. Oxygen permeability index test

This test involves measuring the pressure decay of oxygen passed through the concrete disc which was placed in a falling head permeameter shown in Figure 3.10. Four discs were placed in four cells according to the test standard, and pressure readings were taken for 6 h or up to 50 kPa (whichever came), after which the test was stopped. The oxygen permeability index is defined as the negative log of the coefficient of permeability (k/ms).

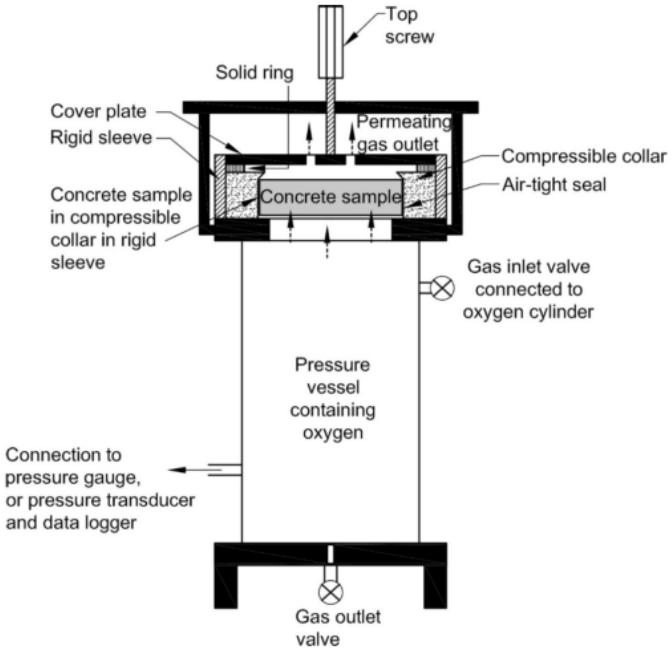

Figure 3.10: Schematic diagram of an oxygen permeameter

3.8.1.2. Water sorptivity index test

The specimens used in the OPI test were also used for this test. The test was performed by measuring the rate of absorption of calcium hydroxide-saturated solution through dry concrete discs under capillary action, regulated by their porosity. The test procedures were followed as described in the Manual.

3.8.1.3. Chloride conductivity index test

The aim of this test was to assess the resistance of concrete to chloride ingress, which reflects the performance of the same concrete when subjected to a high chloride environment. The remaining

four concrete discs were placed in the chloride conductivity cell (Figure 3.11), and the potential difference of 10 V was applied to initiate the movement of chloride ions. The chloride conductivity was determined by measuring the current flowing through each disc.

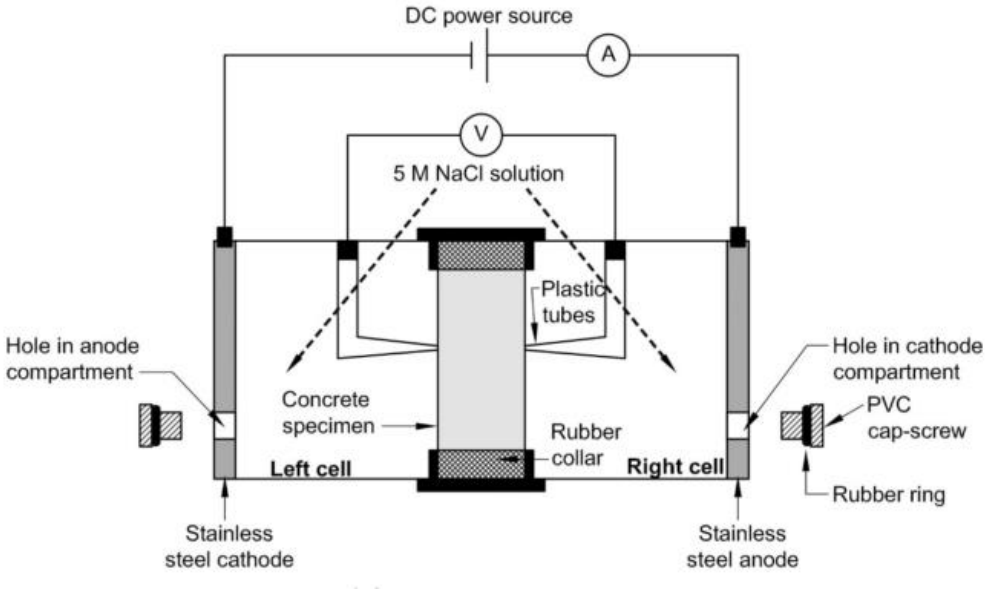

Figure 3.11: The chloride conductivity cell, where A stands for ammeter and V stands for the voltmeter.

3.8.2. Alkali-aggregate reaction testing: Accelerated mortar bar test (ASTM C 1567)

This is a test method used for evaluating the potential of SCMs to control deleterious internal expansion due to alkali-aggregate reaction (AAR), specifically ASR when reactive aggregates are intended for use in concrete. The test was conducted according to ASTM C 1567.

The mortar of 0.47 w/b ratio, and 1:2.25 binder: sand ratio was prepared. The sand used was the graded sand obtained by crushing greywacke aggregates according to the standard (for the reactive aggregate with a relative density of > 2.45). SP was used to achieve an adequate workability of the mortar. The flow test (SANS 5862) was conducted to attain a flow of 150 ± 5 mm.

Four mortar bars of 25 x 25 x 285 mm were cast for each replacement level (0%, 10%, 15% and 20% metakaolin), and initially cured for 24 h before demoulding. The specimens were protected against moisture loss and strain targets were placed. Initial strain readings were then read and recorded. Afterwards, the specimens were totally immersed in a storage container with sufficient water. The container was then sealed and placed in the oven at 80 ± 2^{o}C. After 24 h, the container was removed from the oven, the specimens were taken out and surface dried using a towel, and initial strain readings were taken. Finally, the specimens were immersed completely in the test container with a 1M NaOH solution at 80 ± 2^{o}C, and placed in the oven for 14 days.

The subsequent strain readings of the specimens were taken periodically, with at least three intermediate readings up to 14 days. The difference between the zero reading and reading at each period, for each specimen, was calculated and recorded as the expansion of the specimen. The expansion for the metakaolin-aggregate combination at a given period was taken as the average of the expansion of the four specimens for each replacement level to the nearest 0.01%.

3.8.3. Accelerated carbonation test

The aim of this test was to investigate carbonation effects on the concrete containing different replacement levels of metakaolin at the different w/b ratios. The method followed procedures given in Salvoldi (2010), see below.

Two 100 mm concrete cubes for each concrete mix were cast and cured for 28 days in the curing bath at 23 ± 3ºC. At the end of curing, the specimens were moved into the environment room at 45% ± 2.5% RH and 23ºC ± 3ºC. The specimens were left in this condition for 60 days to dry, while turned every week to ensure all sides dried. At this age, the internal relative humidity at a 10 mm depth of the specimen was assumed to be 70% - 65% RH according to prediction model shown in Figure 3.12. This was to ensure the drying rate of the specimens would not dictate the carbonation rate during the accelerated carbonation testing (Salvoldi, 2010). However, the prediction model used by Salvoldi (2010) did not account for w/b ratio, cement replacement levels, and type of SCM, therefore, the rate of mass loss of each specimen was recorded for 10 weeks until a constant mass loss rate of approximately 0.1% per week was achieved.

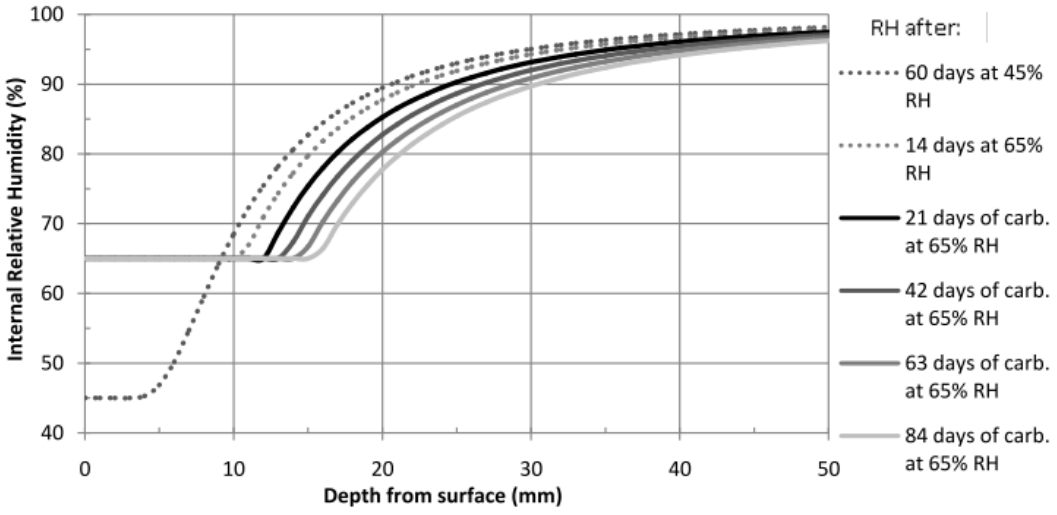

Figure 3.12: Internal RH for the concrete specimens after the drying and carbonation cycles indicated (Salvoldi, 2010)

The specimens were then sealed by epoxy on four sides, while two opposite sides (cast faces) were left unsealed to allow uniaxial, two-directional carbonation front progression. Thereafter, they

were preconditioned at 65% ± 5% RH and 20ºC ± 2ºC for 14 days (Figure 3.12), then transferred into the carbonation chamber with a controlled internal environment at a temperature of 20 ± 3°C, RH of 65±5%, and CO_2 concentration of 2 ± 0.1%. Carbonation is a relatively slow phenomenon, and so to achieve measurable results within an acceptable test duration, specimens must be subjected to an accelerated condition.

After completion of 28 days (4 weeks) in the carbonation chamber, a 20 mm thick slice for each specimen were cut and sprayed with a 1% phenolphthalein in isopropanol alcohol solution. After 24 h, the slices were sprayed again with phenolphthalein solution, and the depth to the identified interface was measured perpendicularly from the exposure face at six different locations of each specimen and an average carbonation depth was determined (RILEM CPC-18). The cut side of the remaining specimen was sealed by epoxy and returned to the chamber for further carbonation. After every 4 weeks i.e. at 56 and 84 days, the above procedure was repeated.

3.8.4. Bulk diffusion test

This test was conducted according to ASTM C 1556. The specimens were from the static elastic modulus test in section 3.7.1 since they were not damaged during the test. However, this breached the standard conditions that required a virgin specimen, but this was not considered problematic. Immediately after the static elastic modulus test at 56 days, the specimens were cut as shown in Figure 3.13. The top 75 mm was used as the test specimen and a 20 mm slice was used to determine an initial chloride-ion content, C_i.

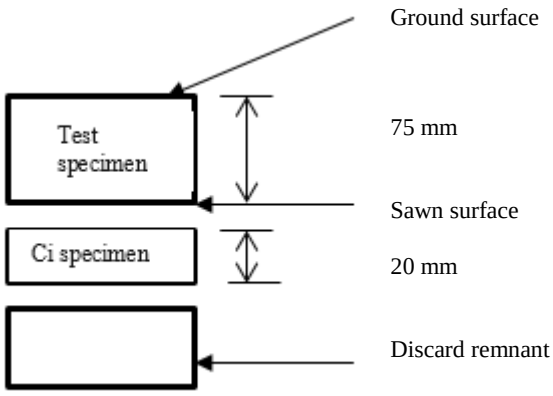

Figure 3.13: Example of the cut sample for Bulk diffusion (100 x 200 mm cylinder)

After air-drying, all sides except the ground surface (ground originally for the elastic modulus test) were sealed with epoxy. The initial mass of the specimen after epoxy sealing was determined followed by immersing the specimen in the saturated calcium hydroxide solution (approx. 3 g/L)) bath at 23±3°C, in a tightly closed plastic container for approximately 48 h. The specimens were then removed, rinsed with tap water and their masses were determined after surface drying.

Thereafter, the saturated specimens from the calcium hydroxide container were placed in the exposure container, see Figure 3.14, filled with a chloride solution (165±1 g NaCl per L= 2.8 M) in the environmental room maintained at 23±3°C and 50±5% for 90 days.

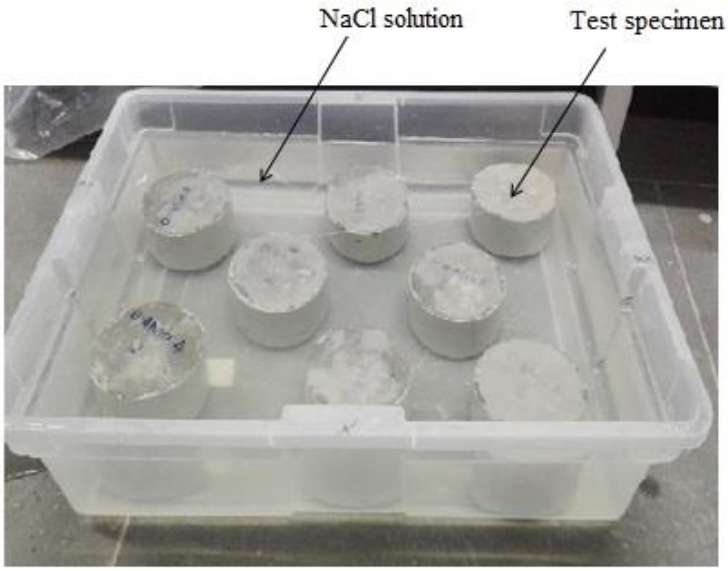

Figure 3.14: Bulk diffusion test: test specimens immersed in NaCl solution.

After 90 days, the specimens were removed from the solution, rinsed with tap water, cored to 70 mm diameter, and dried for 24 h in the laboratory at 23±3°C and 50±5% RH. The specimen was cored to remove the edge effect and disturbances from the coating. Thereafter, the specimen surfaces were profile-ground. A powder sample of 10 g from each layer shown in Table 3.11 was collected from the grinding process. Titration analysis was done to determine the amount of chloride ions in the powder samples.

Table 3.11: Depth intervals for profile grinding.

Profile depth	In mm		
w/b	0.4	0.5	0.6
1	0-2	0-2	0-1
2	2-4	2-4	1-2
3	4-6	4-6	2-3
4	6-8	6-8	3-4
5	8-10	8-10	4-5
6	10-12	10-12	5-6
7	12-14	12-14	6-8
8	-	14-16	8-10
9	-	16-18	10-15
10	-	18-20	15-20

3.9. SUMMARY OF EXPERIMENTAL INVESTIGATION

This chapter consists of eight (8) sub-sections. The Introduction presented the scope and context of the chapter. The section on Materials described the types of materials involved in the laboratory investigation, and included cement (CEM II A-L 52.5 N) and water, metakaolin, GGCS, silica fume and fly ash, fine aggregate (Philippi dune sand and greywacke crusher sand), and coarse aggregates (greywacke crusher stone). The Summary of Test Methods summarised all the methods performed. Pozzolanic Activity of Metakaolin described the techniques and methods used to characterize pozzolanic reactivity of metakaolin: SAI test, semi-adiabatic calorimetry, isothermal calorimetry, and TGA. The section on Concrete Mix Design and Fresh State Properties explained the techniques used to prepare concrete mixes, and the fresh state properties (setting time and workability) that were observed. Hardened Concrete Properties described properties of the concrete investigated after maturing. These tests included compressive strength and tensile splitting tests, and the MIP test. The section on Deformation Behaviour of Concrete entailed static elastic modulus, and creep and drying shrinkage tests. Finally, Durability Properties of Concrete with Metakaolin included four test methods: Durability index tests (OPI, WSI, and CCI), ASR testing (Acceleration mortar bar test), Acceleration carbonation test, and Bulk diffusion test. All tests performed in this study were conducted according to the recognised and accepted standards; where the corresponding standard could not be fulfilled, the reason was explained.

4. CHAPTER FOUR: ANALYSIS AND DISCUSSION OF RESULTS

4.1. INTRODUCTION

This chapter analyses and discusses the results obtained from laboratory experiments described in chapter 3. This chapter aims at meeting the specific objectives of the study, comparing the results with the literature review, and finally reasoning and commenting on the gaps addressed in the literature review. This chapter is divided into the following sections: morphology of cement, metakaolin and other SCMs, pozzolanic activity of metakaolin, properties of fresh concrete with metakaolin, properties of hardened concrete with metakaolin, deformation properties of concrete with metakaolin, and durability properties of concrete with metakaolin.

4.2. MORPHOLOGY OF CEMENT, METAKAOLIN AND OTHER SCMs

4.2.1. SEM analysis

The particle shape of cementitious materials used in this study were analysed by observing their morphology with a scanning electron microscope (SEM) and back-scatter detector. The scales used were 100 µm, 10 µm, and 2 µm depending on the magnification, where a clear image of the particles was clearly seen. The particles were studied to understand their particle shape, size and surface texture, and their differences from one another.

CEM II/A-L 52.5 N consists of angular and glassy particles with larger particles covered with fine particles as shown in Figure 4.1. The fine particles are limestone particles since the limestone was inter-ground with the clinker and gypsum, while the large particles are course clinker particles.

Figure 4.2 presents the spherical particle shape of the fly ash. Fly ash consists of large and small spheres, whereby the smaller spheres are attached to the larger spheres whose surface texture is smooth. The morphology of silica fume is shown in Figure 4.3. Its particles appear as agglomerates with fine spherical particles compared to fly ash particles.

Metakaolin appears as stacked particles with platy and some spherical shape as shown in Figure 4.4. These particles are indicative of halloysite. This morphology is identical to Figure 2.3 observed in the literature review chapter. GGCS particles are equant and chunky particles more likely as CEM II but with less fine particles, see Figure 4.5.

The morphology of these materials (exclude cement) has an impact on the microstructure of concrete since they act as filler. They enable filling the pore systems, and act as a nucleation site for intensifying kinetic energy of cement hydration.

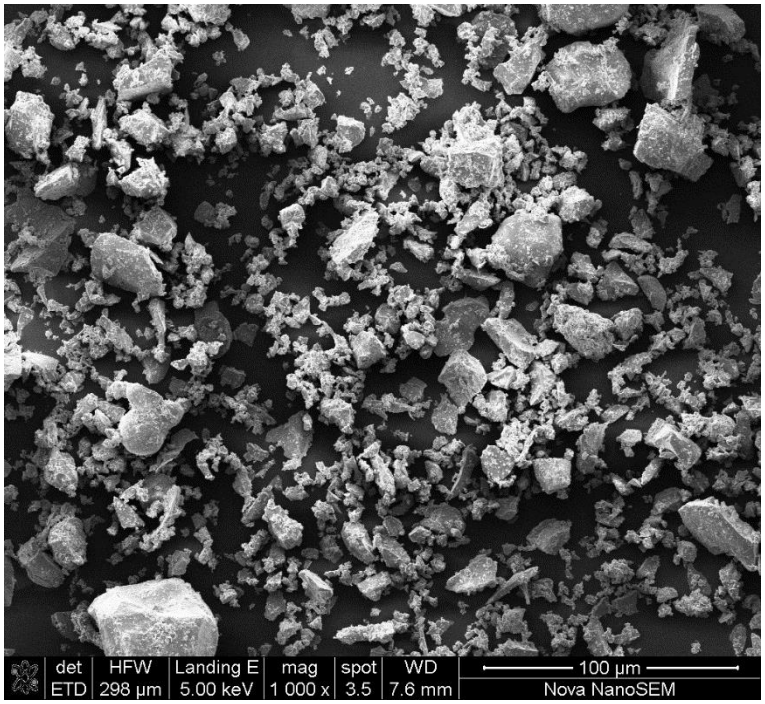

Figure 4.1: CEM II/ A-L 52.5 N

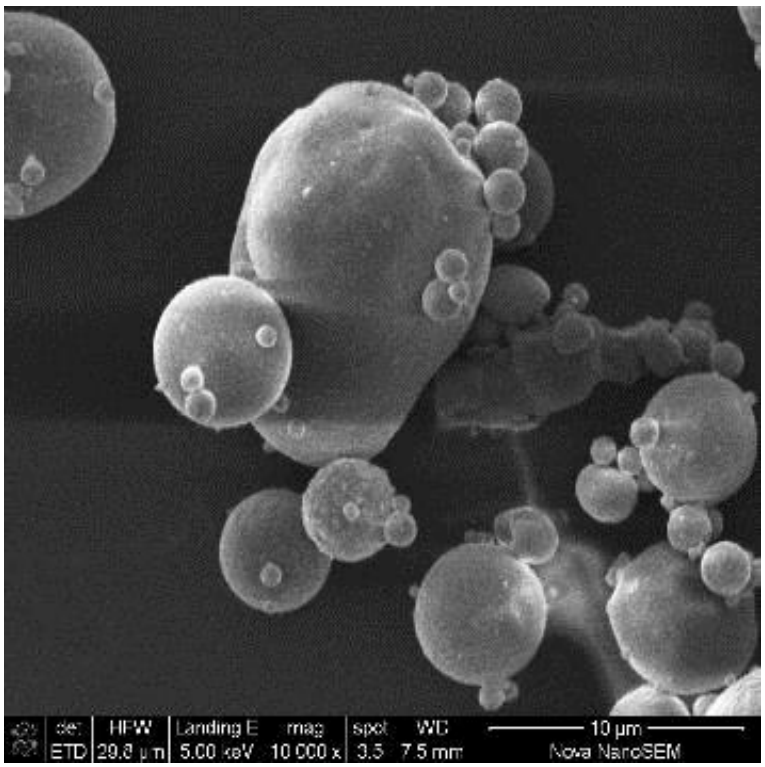

Figure 4.2: Fly ash

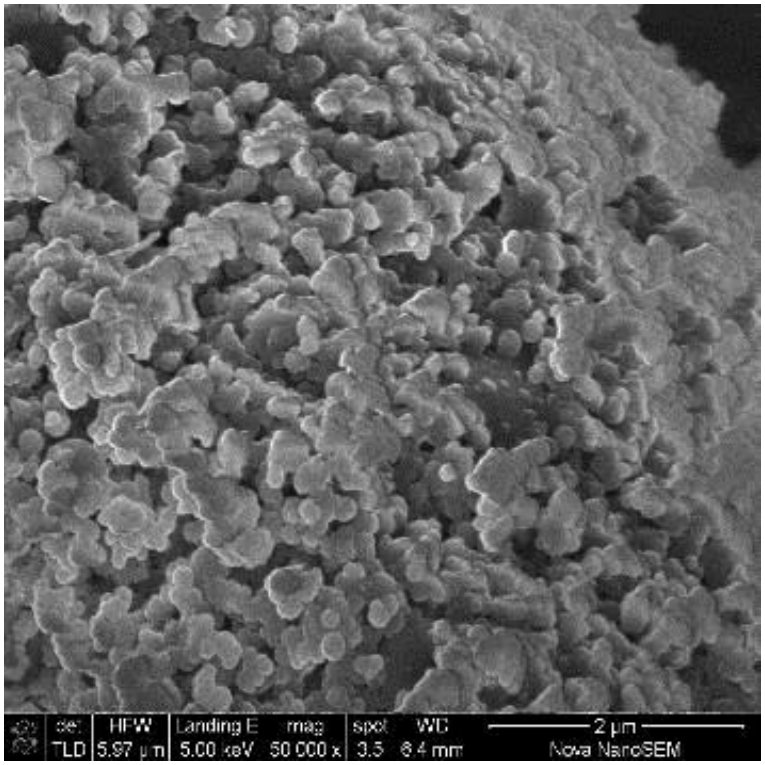

Figure 4.3: Silica fume

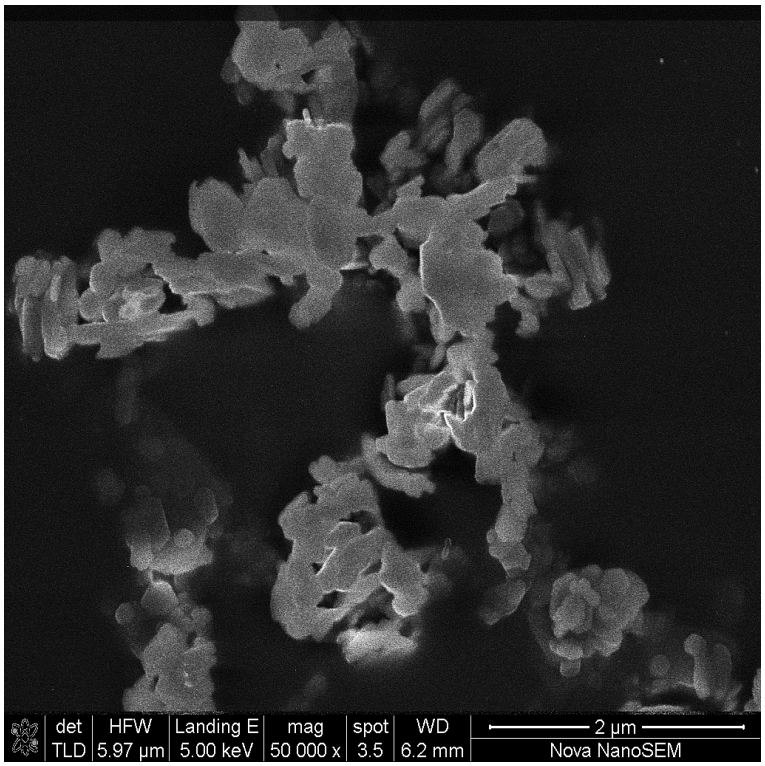

Figure 4.4: Metakaolin

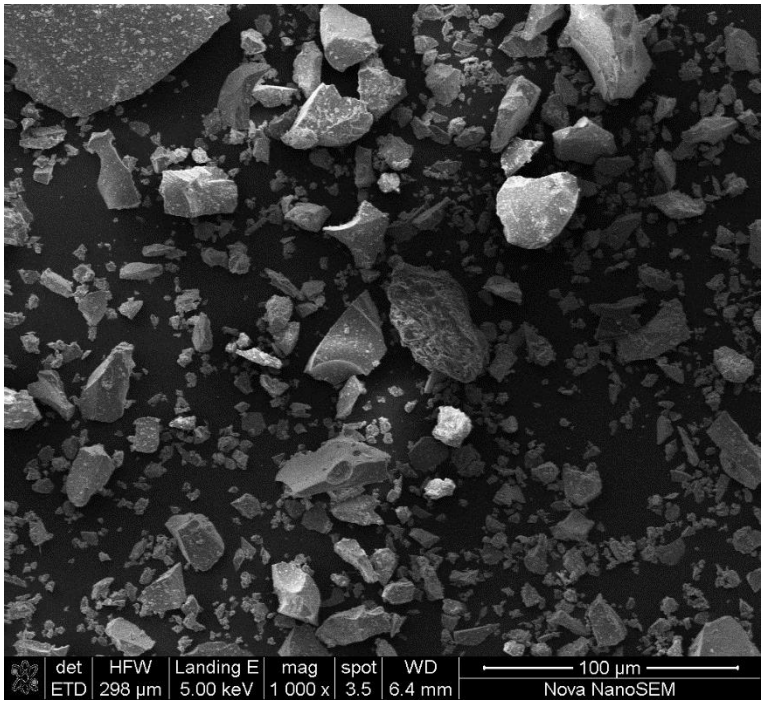

Figure 4.5: GGCS

4.3. POZZOLANIC ACTIVITY OF METAKAOLIN

Pozzolanic activity of metakaolin was evaluated, firstly, as the pozzolanic potential of metakaolin at different replacement levels in mortar on influencing strength, heat of hydration, CH consumption and chemically bound water, and secondly, as metakaolin performance in mk-portlandite systems in comparison with other SCM-portlandite systems such as GGCS, silica fume and fly ash on generating heat, consuming CH, and chemically bound water. The results are divided into four subsections; Strength Activity Index (SAI), heat of hydration (semi adiabatic and isothermal calorimetry results), Thermogravimetric analysis (TGA), and pozzolanic activity of metakaolin relative to other SCMs.

4.3.1. Strength Activity Index (SAI)

The mortars used for these tests were described in chapter 3, section 3.4.3. Results for compressive strength and strength activity index of mortar with different proportions of metakaolin are presented in Figure 4.6 and Figure 4.7, respectively. It was observed that compressive strength of mortar increased with curing age, as expected. As metakaolin content increased to 15%, the strength increased, while a further increase in metakaolin caused a decrease in strength. This was because the potential of metakaolin to utilise the CH from cement hydration was deemed to reach its limit, although another reason might be associated with the reduction of cement content in the mortar, the so-called dilution effect.

Figure 4.7 shows SAI values of metakaolin mortars. The SAI values were expressed relative to compressive strength of the control (i.e. 100%). An increase above 100% was regarded as strength boost due to metakaolin pozzolanic reaction. Pozzolanic reactivity of the metakaolin was found to be the highest at 15% mk followed by 20% mk, then 10% mk, at all curing ages. The maximum SAI values attained for 15%, 20%, and 10% mk were 136% at 14 days, 127% at 14 days, and 120% at 7 days, respectively. It was observed that the rate of strength development increased up to 14 days, and decreased afterwards, for metakaolin mortars. This was due to depletion of metakaolin pozzolanic potential.

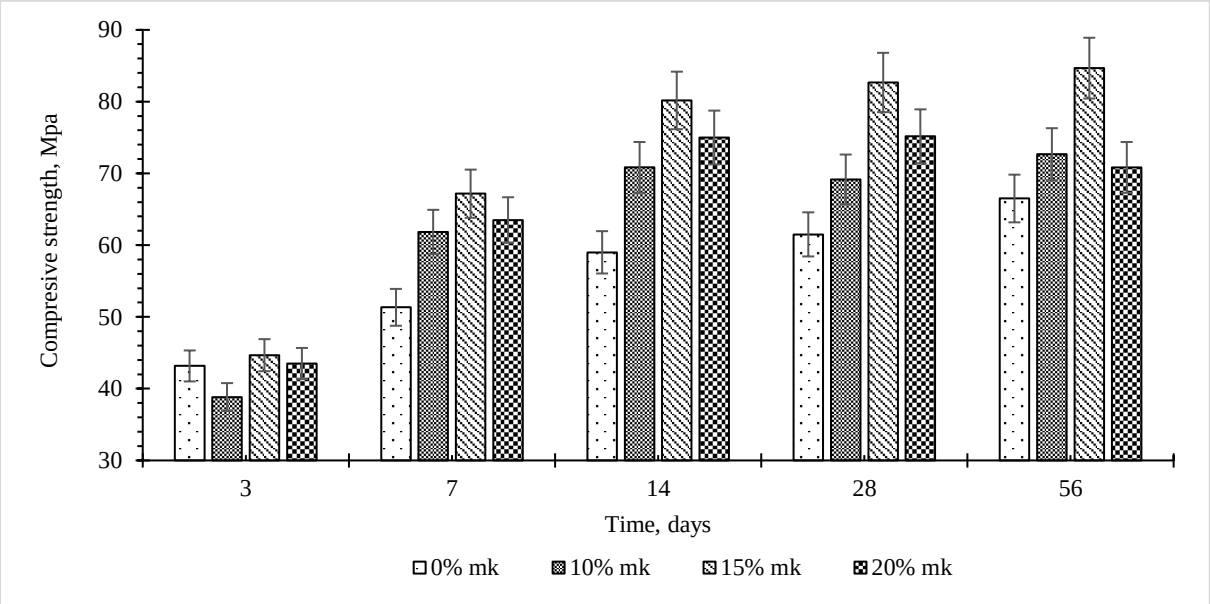

Figure 4.6: Compressive strength of the mortar mixes with metakaolin, at different curing ages

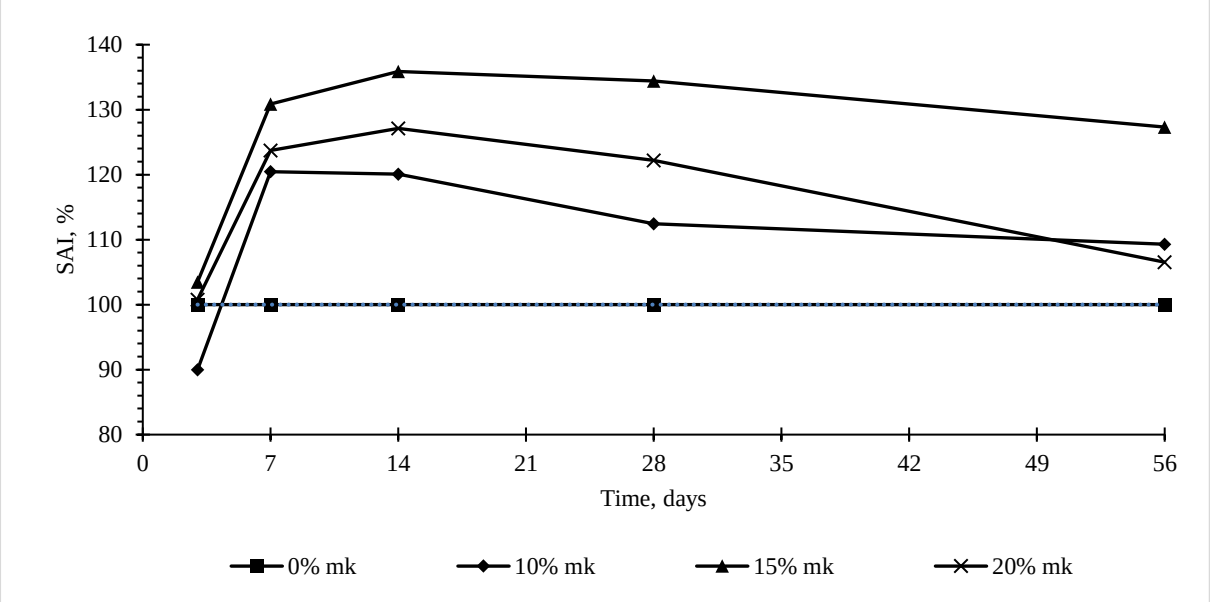

Figure 4.7: Strength activity index (SAI) of the mortars with metakaolin at different ages

4.3.2. Heat of hydration

Metakaolin influence on the heat of hydration was investigated using two methods for comparison purpose. These methods are described in Chapter 3, section 3.4.1 and 3.4.2. and the following is the discussion of their results;

4.3.2.1. Semi-adiabatic calorimetry results

Figure 4.8 shows temperature profiles of mortar with 0%, 10%, 15%, and 20% metakaolin. It should be noted that the results were collected in the environmental room at 23 ± 3^{o}C and 50 ± 5% of RH. Therefore, the initial temperature readings of all mortars were between 20^{o}C and 22^{o}C. The results show that the heat released raised the temperature to a peak, followed by a reduction in temperature as hydration rate decreased with time. This was expected since the hydration reaction is exothermic.

Substitution of cement with metakaolin appeared to affect the peak temperature. The peak temperatures were obtained at 13.3 h, 15.5 h, 15.5 h and 13.8 h of hydration with the magnitude of 35.1^{o}C, 33.8^{o}C, 33.1^{o}C, and 32.5^{o}C for 0%, 10%, 15%, and 20% mk, respectively (see Figure 4.9). It was observed that there was a drop of approximately 1^{o}C for each 'step' of increase of metakaolin content. Therefore, metakaolin reduced the peak temperature in the mortar. These results oppose the observations by Zhang and Malhotra, (1995) and Bai and Wild, (2002). They observed a higher temperature rise in the metakaolin mortars compared to control. They reasoned this as the effect of high pozzolanic activity of metakaolin, while in this study, the possible causes of temperature drop might be associated with cement substitution and the dilution effect of metakaolin (Newman & Choo 2003:13/26). These results are somewhat surprising in view of the significant strength increases brought about by the use of metakaolin in the concrete mixes, with the most likely explanation being that metakaolin improves the physical microstructure of the concrete.

The ascending order of temperature profiles up to about 20 h of hydration was 20%, 15%, 10%, and 0% mk. After 30 h of hydration, the order of the curves reversed. This indicated that mortars with metakaolin experienced later hydration than the main cement hydration and it became extreme as metakaolin content increased. A possible reason for this might be the additional exothermic reactions related to the formation of calcium aluminate phases due to the presence of high alumina content in metakaolin (Lagier and Kurtis, 2007).

Figure 4.10 shows the total heat evolved by mortars with metakaolin. It was observed that the total heat generated decreased with increase in metakaolin content. Consequently, at the end of 120 h, 0% mk had the highest heat followed by 10%, 15%, and 20% with the magnitude of 281.5, 264.1,

252.8, and 248.4 J/g, respectively. Referring to the contradiction observed in the literature review, section 2.7.4, it could be concluded that the current metakaolin decreases the total heat evolved in the mortars. This was supported by the results observed in isothermal calorimetry in the following section.

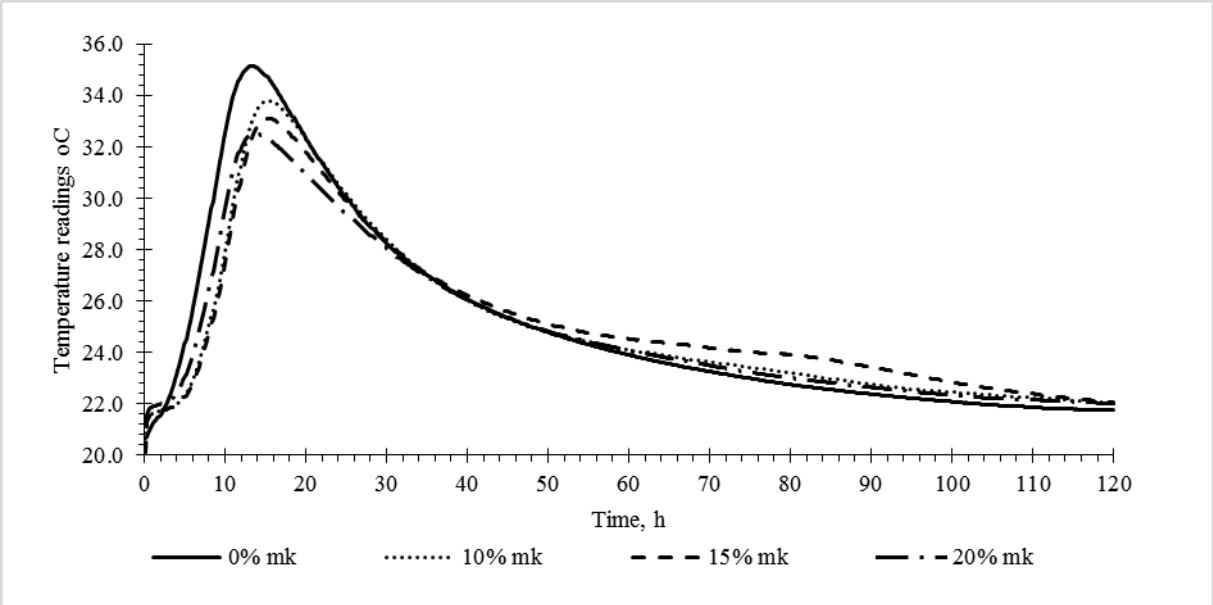

Figure 4.8: Temperature readings of mortar with metakaolin from semi-adiabatic calorimetry for 120 h

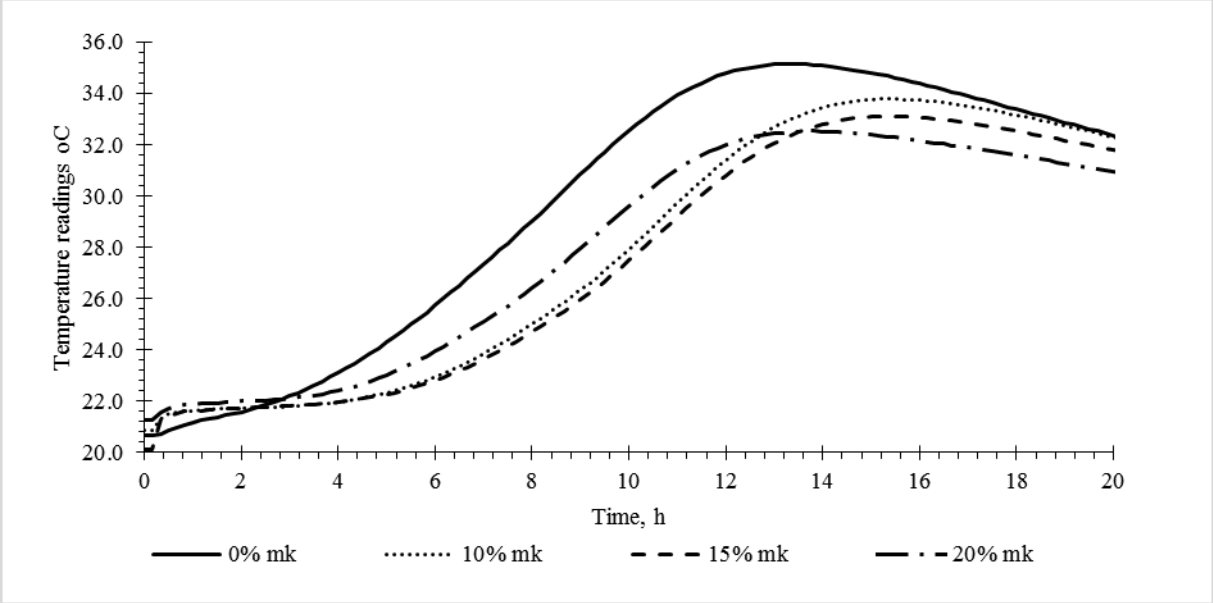

Figure 4.9: Temperature profile of mortar with metakaolin from semi-adiabatic calorimetry for 20 h

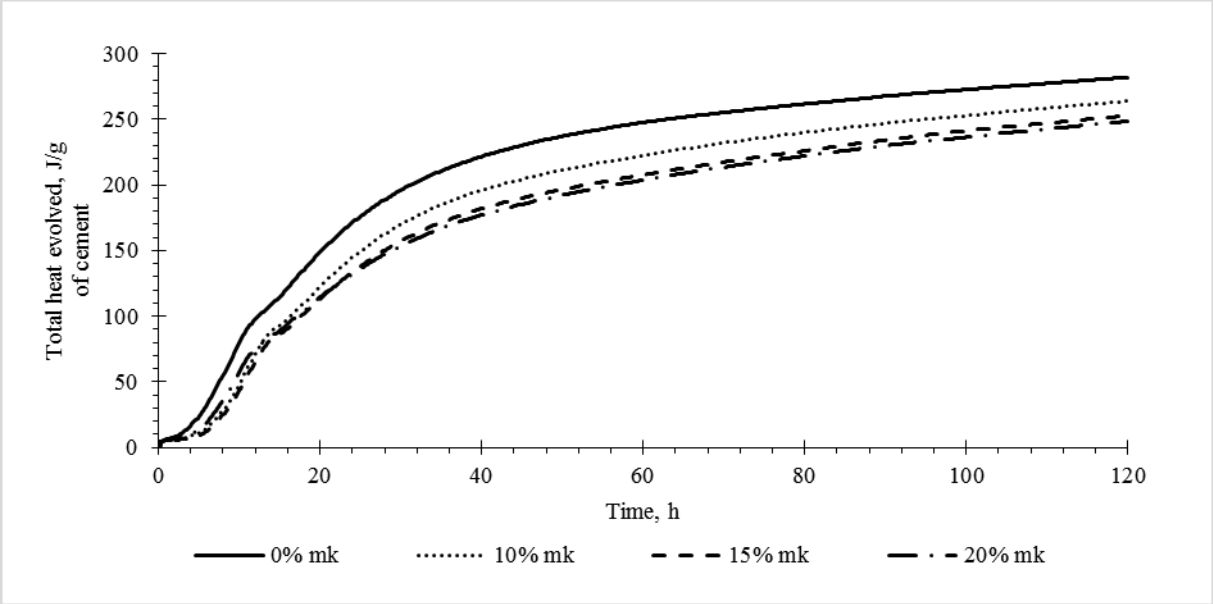

Figure 4.10: Total heat evolved by the mortar with metakaolin

4.3.2.2. Isothermal calorimetry results

Isothermal calorimetry is the most appropriate method that can clearly show five stages of the rate of heat of hydration of cement. These stages are well illustrated in Figure 4.11.

In this study, after conducting isothermal calorimetry test, thermal power curves for the mortars against hydration time up to 120 h (Figure 4.12) showed only four stages; 1) Induction period, 2) Acceleratory period, 3) Deceleratory period, 4) Period of slow continued reaction. The first stage could not be seen because the equipment was set by the manufacturer to display the thermal power results after a time of thermal equilibrium (1 h after starting the test) to the completion of test (ASTM C1679: Clause 14.2.2).

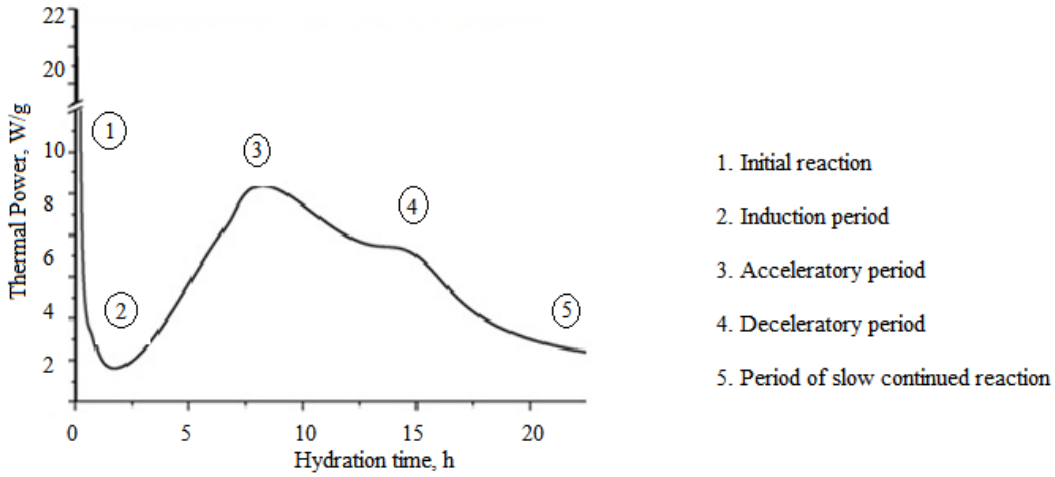

Figure 4.11: The rate of heat of evolution of cement hydration at 23^{o}C

The acceleratory period is controlled by the rate of low density CSH formation as hydration of C_3S takes place, and the first peak of hydration occurs. This is generally associated with the content of C_3S present in the system, meaning that any reduction of cement in the system affects the occurrence of this first peak. Referring to Figure 4.13, it was observed that the first peak was observed on the control curve, where none was observed in metakaolin mortars. However, the peak of control was reached first followed by 20%, and 10% and 15% mk which were very close to each other. This implied that the rate of formation of CSH was higher in the control than in metakaolin mortars. This might be associated firstly with the dilution effect, and secondly with metakaolin nucleation on cement particles which slowed down the formation of low density CSH.

In the deceleratory period, which is considered as the transition period from the chemical to diffusion control, 20% mk curve was below followed by 0%, 15%, and finally 10%. At this stage, the second peak which corresponds to hydration of C_3A occurs. The peak was dominant in metakaolin mortars. This was because of the reaction of alumina with CH to produce calcium aluminate hydrates (Lagier and Kurtis, 2007).

At the period of slow continuing reaction which is associated with porosity reduction and strength increase (due to the formation of high density CSH (Mostafa and Brown, 2005)), the curve of 20% mk was above those of 15%, 10% mk, and 0% mk. This portrayed a high metakaolin pozzolanic potential on heat development. A further description was depicted in Figure 4.14.

Figure 4.14 represents the difference in the rate of heat of evolution between the mortars with metakaolin and control, whereby the control is considered as a reference. This difference stands for the increased or decreased heat by the influence of metakaolin, and it is explained by three effects summarised as follow;

- Dilution effect; decreases heat due to the reduction of cement. This is attributed to the decrease of C_3S component which is responsible for heat generation.
- Acceleration effect; increases heat due to the influence of metakaolin on accelerating hydration reaction of C_3S.
- Pozzolanic effect; increases heat due to the reaction between metakaolin and CH.

The descending curves in Figure 4.14 represent the dilution effect, the ascending curves represent the acceleration effect, and the hogging curves represent the pozzolanic effect. The pozzolanic effect was observed between 15 h to 20 h of hydration, which agreed with Mostafa and Brown, (2005).

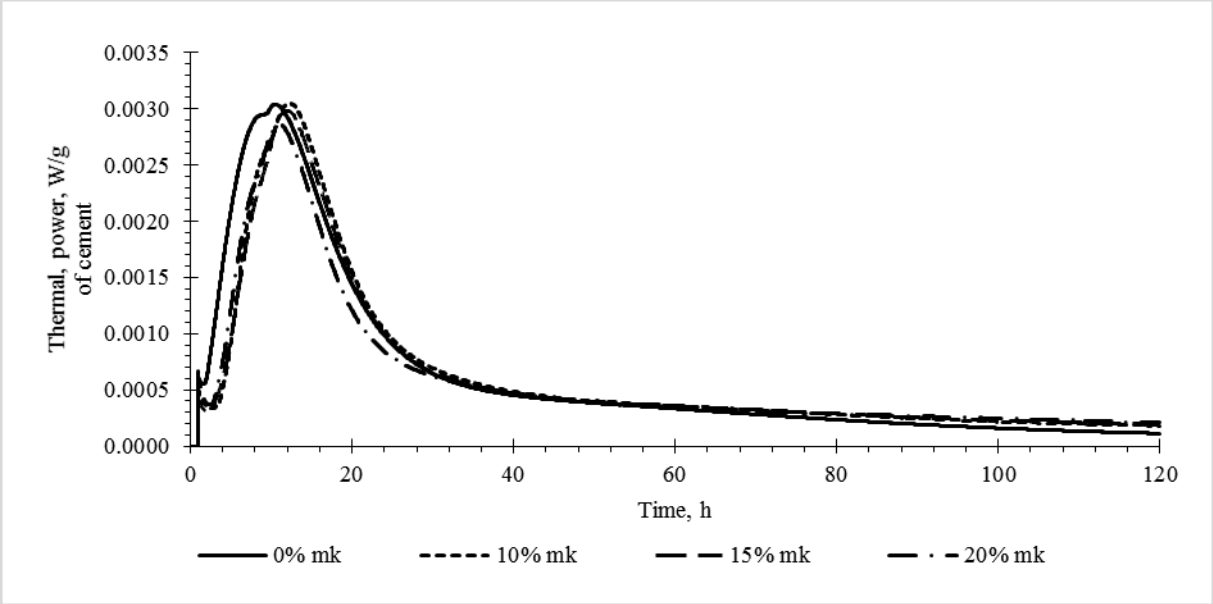

Figure 4.12: The rate of heat development in the metakaolin mortars for 120 h

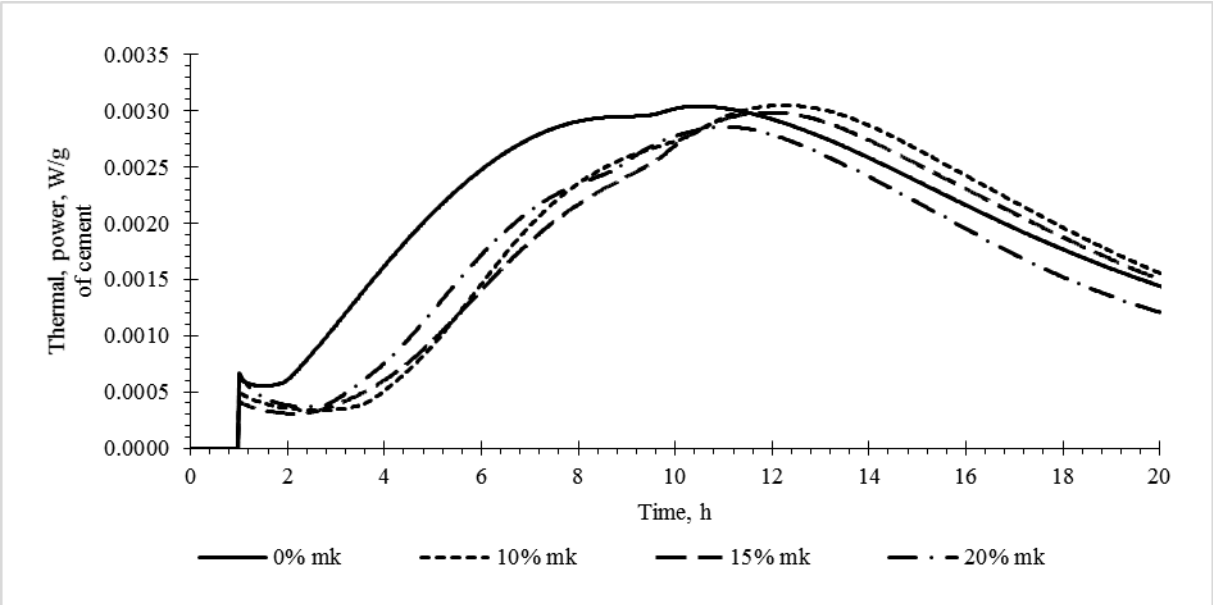

Figure 4.13: The rate of heat development in the metakaolin mortars for 20 h

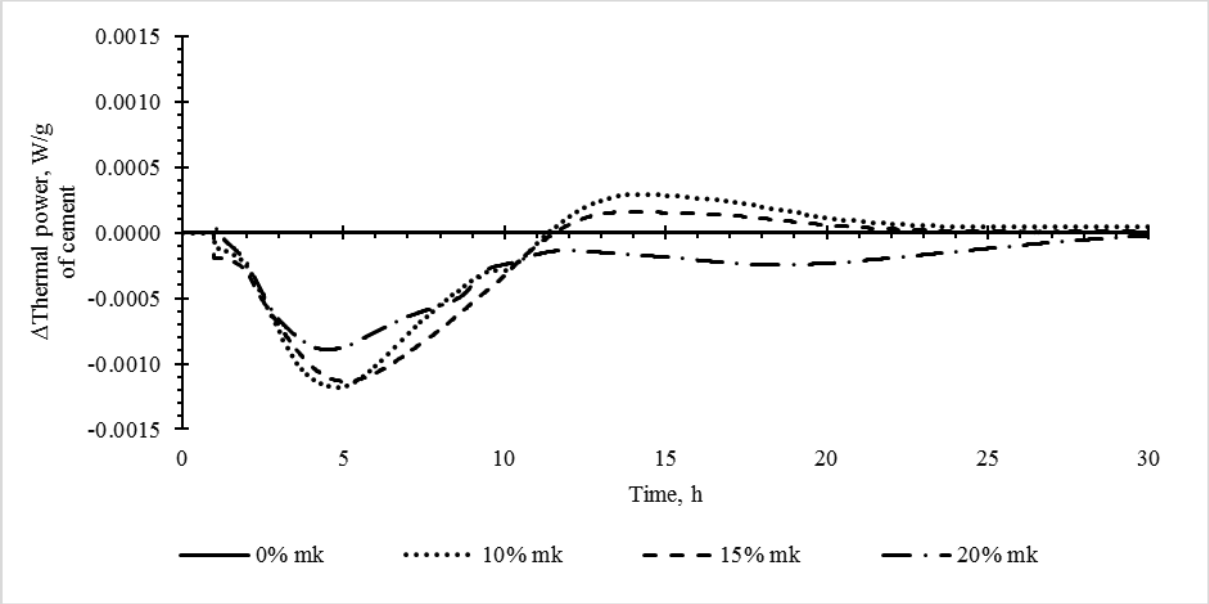

Figure 4.14: The difference in the rate of heat evolution of metakaolin mortars

Figure 4.15 shows that total heat generated with hydration time decreased with increase in metakaolin content. At the end of the test, total heat evolved was 274.7, 274.0, 267.9, and 258.8 J/g for 0%, 10%, 15%, and 20% mk, respectively. The differences of total heat generated between control and metakaolin mortars were approximately 1, 7, and 16 J/g for 10%, 15%, and 20% mk, respectively.

The curves of total heat generated by semi-adiabatic calorimetry (Figure 4.10) and Isothermal calorimetry (Figure 4.15) show a similar trend as the total heat evolved decreased with increasing metakaolin content. These two methods also had slightly different magnitudes of total heat evolved, see Table 4.1. In the semi adiabatic calorimetry, the control had a slightly higher heat than that in isothermal calorimetry, while metakaolin mortars had lower heat. The possible reason for this might be associated with the insulation effect of semi adiabatic calorimetry. Besides, the values were comparable since their ratios were above 0.90. With this knowledge, semi adiabatic calorimetry can be regarded as a trusted method to evaluate the total heat and to use as an indicator for comparing heat generated by various cementing materials.

Table 4.1: Total heat of hydration for two calorimetry

Mortar mix	Total heat of hydration, J/g in		Ratio of total heat generated ($\frac{SC}{IC}$)
	Semi adiabatic calorimetry (SC)	Isothermal calorimetry (IC)	
0% mk	281.5	274.7	1.02
10% mk	264.1	274.0	0.96
15% mk	252.8	267.9	0.94
20% mk	248.4	258.8	0.96

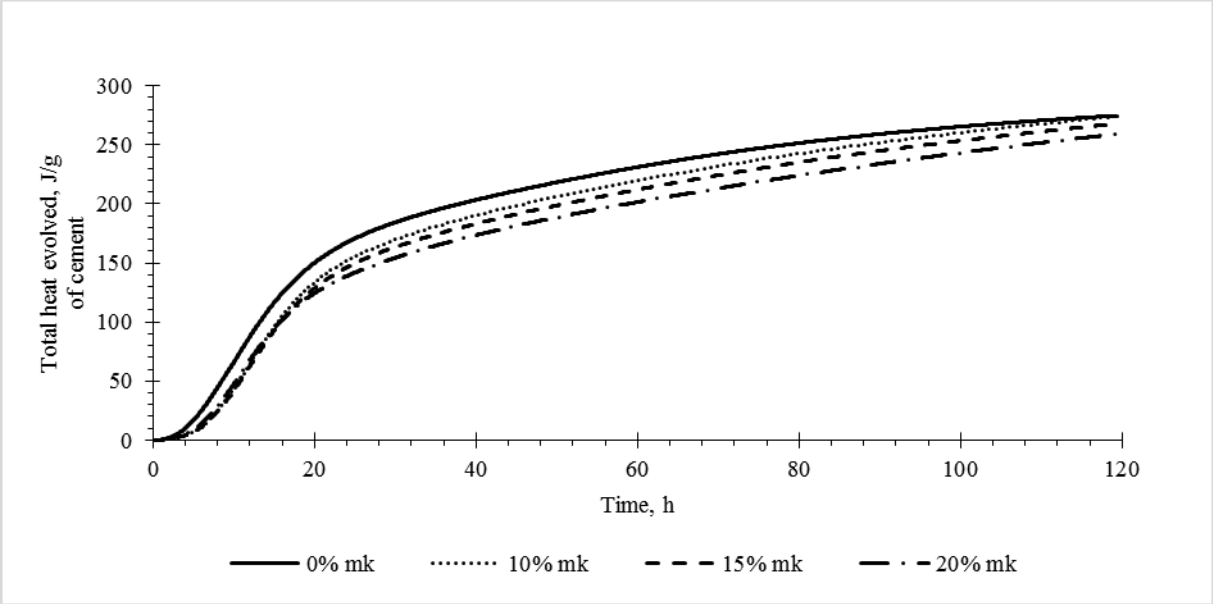

Figure 4.15: Total heat evolved by metakaolin mortars for 120 h

4.3.3. Thermogravimetric analysis (TGA) results

Results for thermogravimetric analyses are presented as CH content and chemically bound water in Figure 4.16 and Figure 4.17, respectively. Equation 4.1 was used to calculate CH content by taking into account the mass loss (ml) of samples due to the dehydroxylation of CH at 400°C to 500°C and the decomposition of $CaC0_3$ at 600°C to 800°C. The mass losses were evaluated from thermogravimetric (TG) analysis curves with the aid of Differential thermogravimetric (DTG) analysis curves which indicated the beginning and end of each step represented by the change in slope of the TG curve, see Figure 4.18.

$$\underset{\text{by mass of binder}}{CH\ content,\ \%} = \frac{1}{4} * \left(\frac{74}{18} * ml_{CH} + \frac{74}{44} * ml_{CaCO3} - \frac{74}{100} * CaCO_{3_{\text{in cement}}}\right) \qquad (4.1)$$

Whereby ¼ stands for the ratio of mass of binder to mass of mortar sample, and 74, 18, 44, and 100 g/mol stand for molar mass of CH, H_2O, CO_2, and $CaCO_3$, respectively.

The decomposition of $CaCO_3$ was considered in CH content calculation because firstly, the type of cement used contained 9% limestone, secondly, it was observed that during sample preparation carbonation might have taken place since the TG curves showed higher mass loss at $CaCO_3$ decomposition than at CH dehydroxylation. Therefore, the technique adopted by Kim and Olek, (2012) was used to analyse the results. The chemically bound water was considered as the total mass loss of the sample from 100°C to 1000°C minus the mass loss due to $CaCO_3$ decomposition.

The CH content and chemically bound water quantity observed in this test were underestimated compared to those observed in the literature, however, the study was more interested in comparison

purposes. The main source of errors was related to the presence of $CaCO_3$ component in the sand used (i.e. dune sand contained some sea shells) and the grinding and sieving process during the sample preparation (in the calculations, the mass of the sample was considered as mortar, while there was a possibility that it was only binder paste).

The CH contents of the control mix were generally affected by hydration time. With increasing hydration time, CH content increased. This effect was because of increase of degree of hydration. A slight difference of CH content between 7 and 28 days was observed, while a significant increase was observed at 56 days.

The influence of substituting cement with metakaolin on CH consumption was observed. With increasing metakaolin content, at each age, CH content decreased, with the lowest values at 20% mk. 10% mk showed the highest value at 56 days which might be explained as the result of the depletion of metakaolin content. At 15% and 20% mk, CH content did not increase significantly with hydration time. This was explained as the effect of the pozzolanic reaction which continued to consume CH with time. Another possible reason for this is the dilution effect, as replacing the cement resulted in the reduction of clinker content for hydration. The percentage of CH consumed at each replacement level are shown in Table 4.2. The CH consumption increased with metakaolin content, whereby 31% of CH produced by the control, at 56 days was consumed at 20% mk. This observation was supported by Paiva *et al.*, (2012), Bucher *et al.*, (2017) and Andrade *et al.*, (2018).

Chemically bound water was also investigated (Figure 4.17). Generally, all mortars showed an increase in bound water with hydration time. This signified that CSH formation increased with time. Different metakaolin contents showed different results as expected. The bound water decreased with increasing metakaolin content in the order of 10%, 15% and 20%. At the higher metakaolin content, lower bound water was observed except at 56 days. This was explained as the result of the filler effect that reduced hydration reaction.

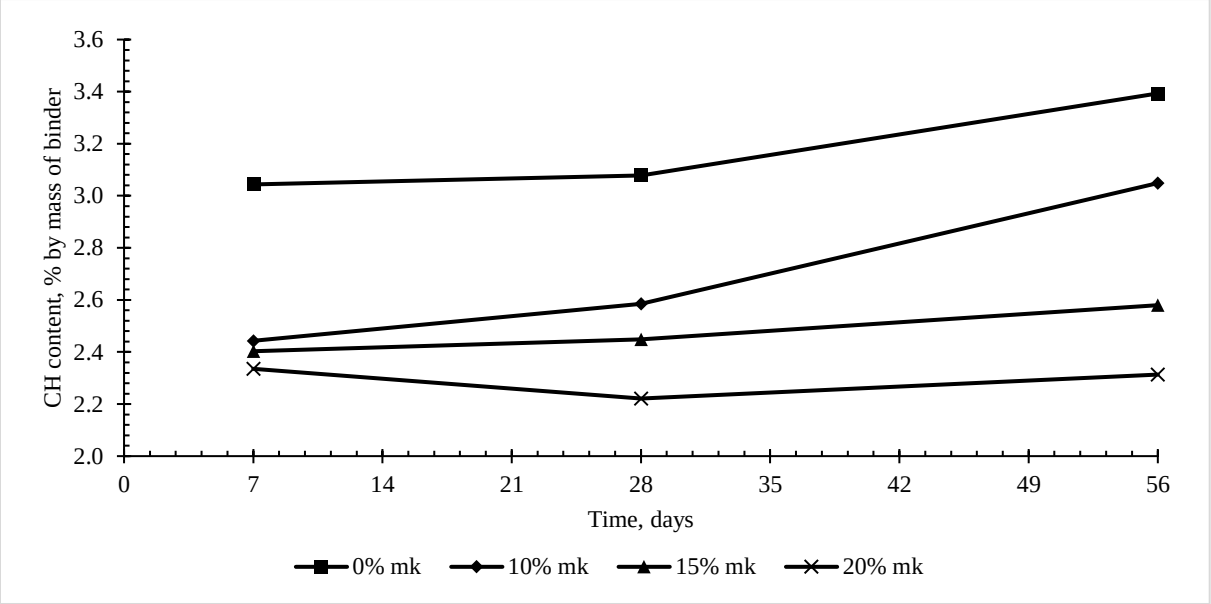

Figure 4.16: CH content in mortar mixes with metakaolin at three curing ages

Table 4.2: CH consumed by Metakaolin content in mortar at different hydration times

Curing time in days	7	28	56
Metakaolin		CH consumed, %	
0% mk	0.0	0.0	0.0
10% mk	19.7	16.0	10.1
15% mk	21.0	20.4	24.0
20% mk	23.3	27.8	31.8

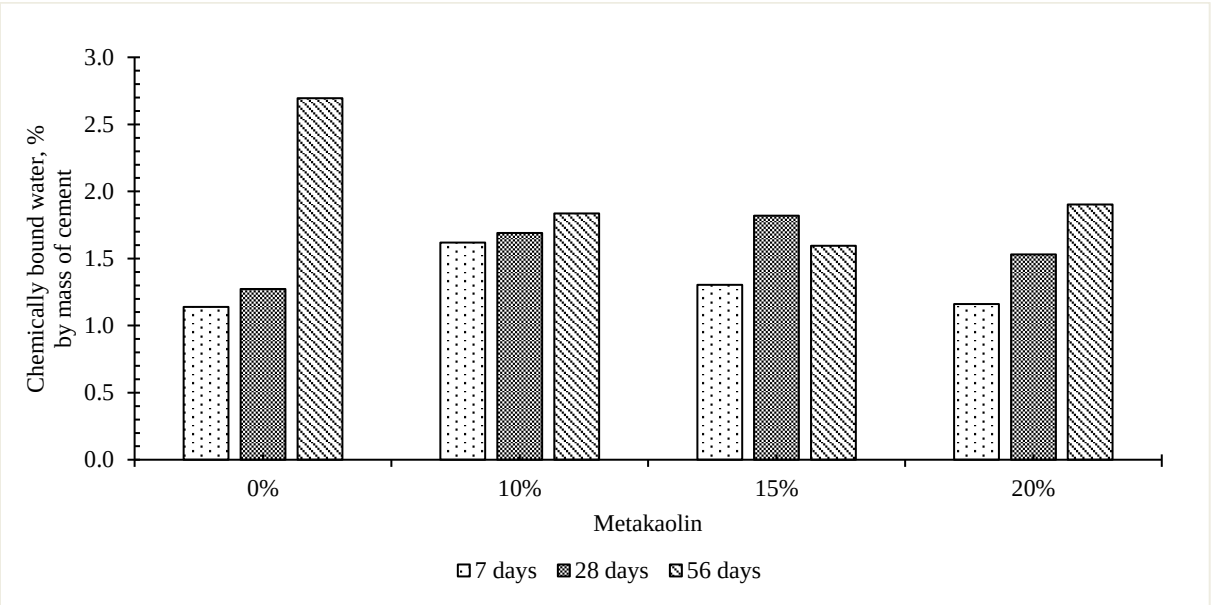

Figure 4.17: Chemically bound water in metakaolin mortar samples

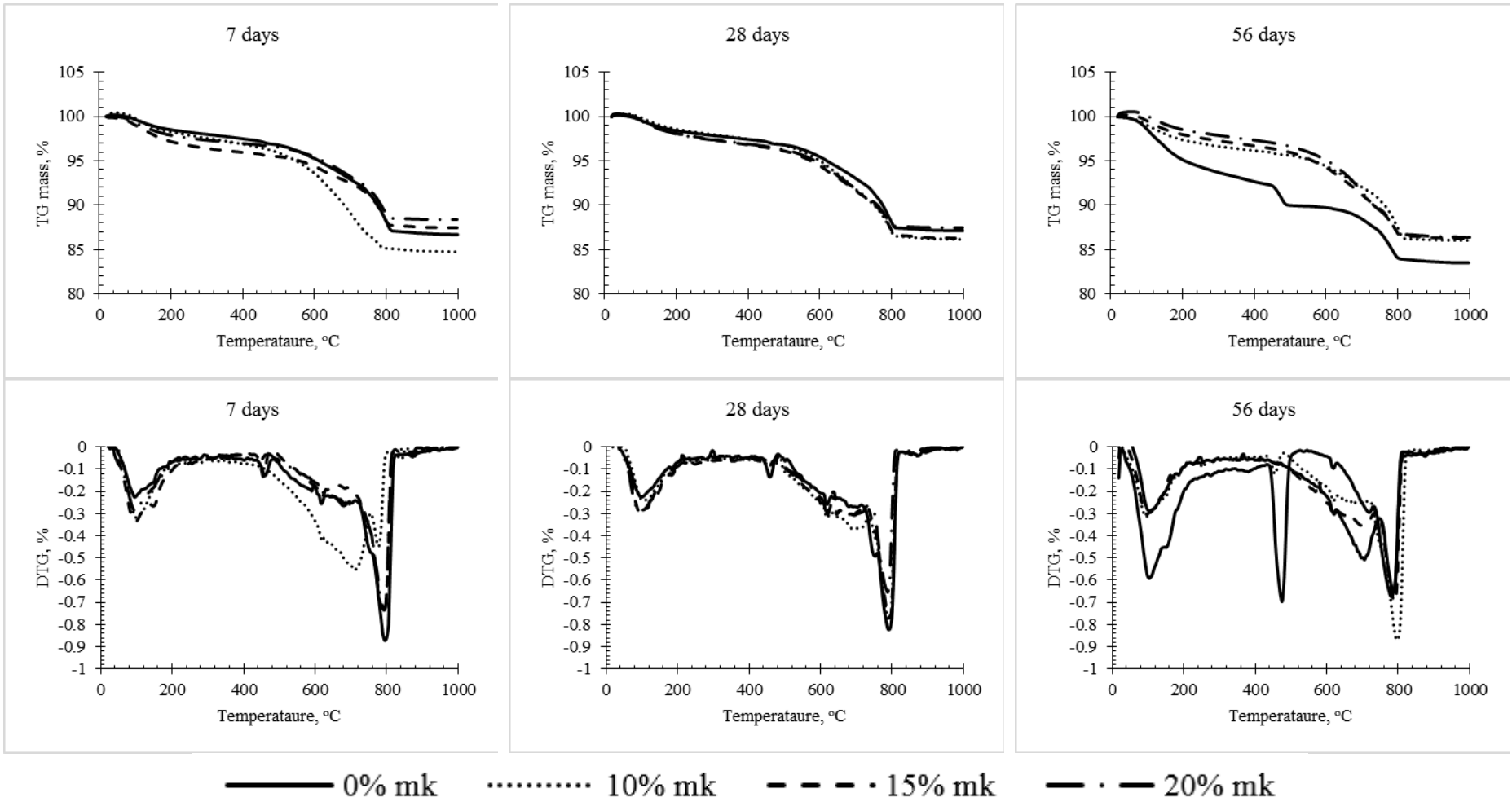

Figure 4.18: Thermogravimetric (TG) and Differential thermogravimetric (DTG) analysis of metakaolin mortar

4.3.4. Pozzolanic activity of metakaolin relative to other SCMs

Different SCMs (fly ash, GGCS, silica fume, and metakaolin) were studied to assess their pozzolanic activities in the SCM-portlandite system. The test methods used were isothermal calorimetry and TGA. After 160 h in the isothermal calorimetry test, their images were taken as shown in Figure 4.19. It was observed that the samples with fly ash and silica fume did not set, while GGCS and metakaolin samples were completely set and hardened.

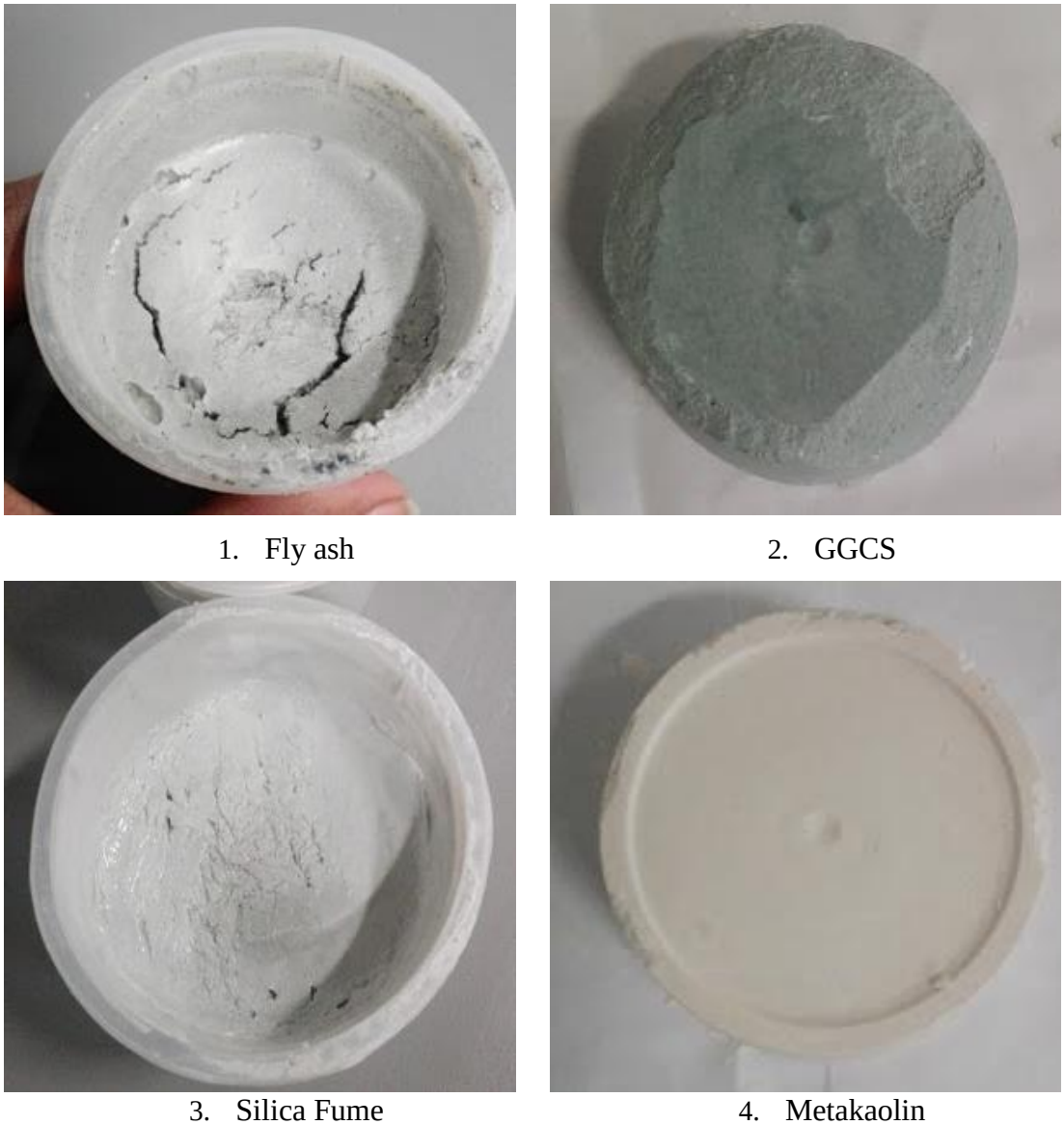

1. Fly ash
2. GGCS
3. Silica Fume
4. Metakaolin

Figure 4.19: Sample with SCMs after 160 h of hydration in isothermal Calorimetry

4.3.4.1. Isothermal calorimetry results for SCMs

Isothermal calorimetry results for SCM-portlandite samples are shown in Figure 4.20 and Figure 4.21, as thermal power and total heat evolved, respectively. It was observed that GGCS sample had a higher thermal power at the early age followed by metakaolin, while fly ash and silica fume

had the lowest thermal power. The low hydration rate of fly ash sample was associated, firstly, with poor solubility of its silica component, as its reactivity depends on external factor such as temperature, and secondly, with its low lime content, as this decelerated the pozzolanic reaction (Ma and Brown, 1997). In the case of silica fume, the slow hydration rate was due to its agglomerates that reacted slowly with CH, as observed by Mitchell, Hinczak and Day, (1998). The other reason might be related to the source of this silica fume.

Two hogging peaks and a sagging peak in between were observed in the metakaolin and GGCS isothermal hydration profiles. The first hogging peak represents the main hydration peak associated mainly with hydration reactions contributing to setting and early strength development. The sagging peak in the middle represents the sulphate depletion point, while the last hogging peak represents accelerated calcium aluminate activity (ASTM C 1679). The metakaolin sample showed a broadest distribution of isothermal hydration profile, while GGCS attained the highest main hydration peak at an earlier time.

The broad distribution in the metakaolin profile showed a continuous heat generation which persisted for several hours more than other mixes. This was associated with the higher silica and alumina contents. As the hydration reaction started, silica and alumina reacted with CH to form CSH and CAH. These reactions continued at a higher rate and for a longer time than GGCS. The general phenomenon showed a higher pozzolanic potential of metakaolin.

GGCS attained the highest main hydration peak because, in the CH solution, GGCS undergoes a two-stage reaction; the initial early hydration reaction i.e. immediately after adding water, the CaO component dissolve in water and react with other GGCS components to form cementitious hydrates, and the subsequent predominant reaction i.e. the silica and alumina components react with the CH solution. This two-stage reaction is hydraulic in nature, thus, it accelerated the heat formation. However, the GGCS profile showed the last hogging peak that lasted for a short time that inferred as the formation of CAH. This was generally associated with the depletion of alumina content in the system due to its low quantity.

The total heats generated by SCM- portlandite samples are shown in Figure 4.21. It is clear that at the end of the hydration period (160 h), metakaolin generated the highest total heat followed by GGCS, while silica fume and fly ash exhibited the lowest heat. The magnitudes of total heat generated were 70.3, 58.7, 26.0, and 24.0 J/ g of solid sample, respectively. This indicated that metakaolin had the highest pozzolanic reactivity.

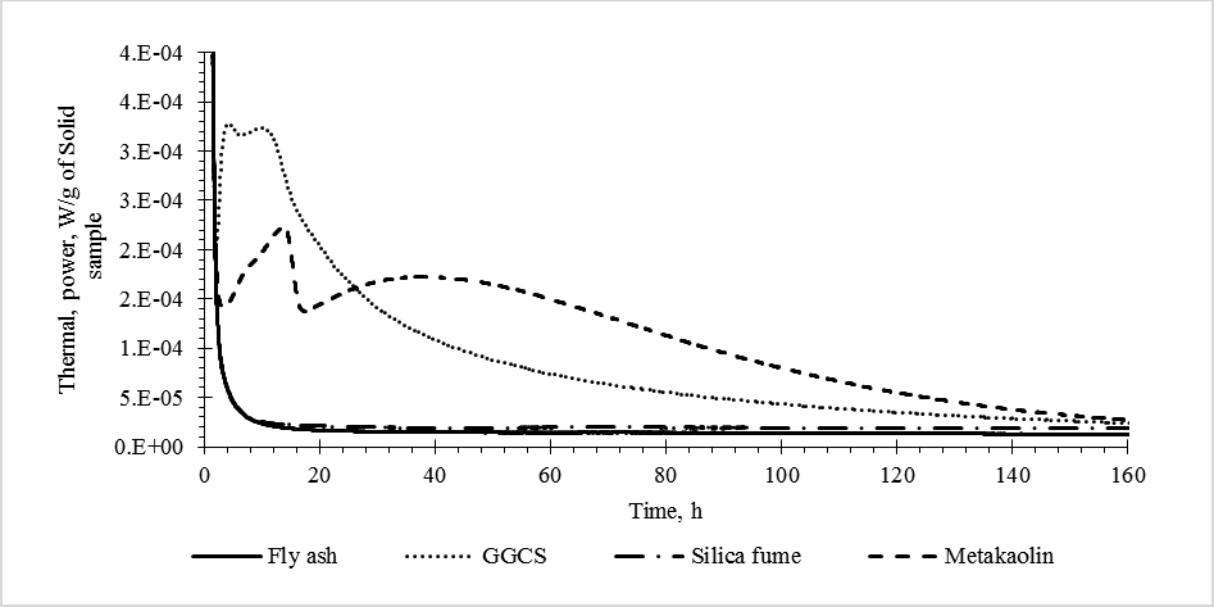

Figure 4.20: Isothermal hydration profile for the samples with different SCMs

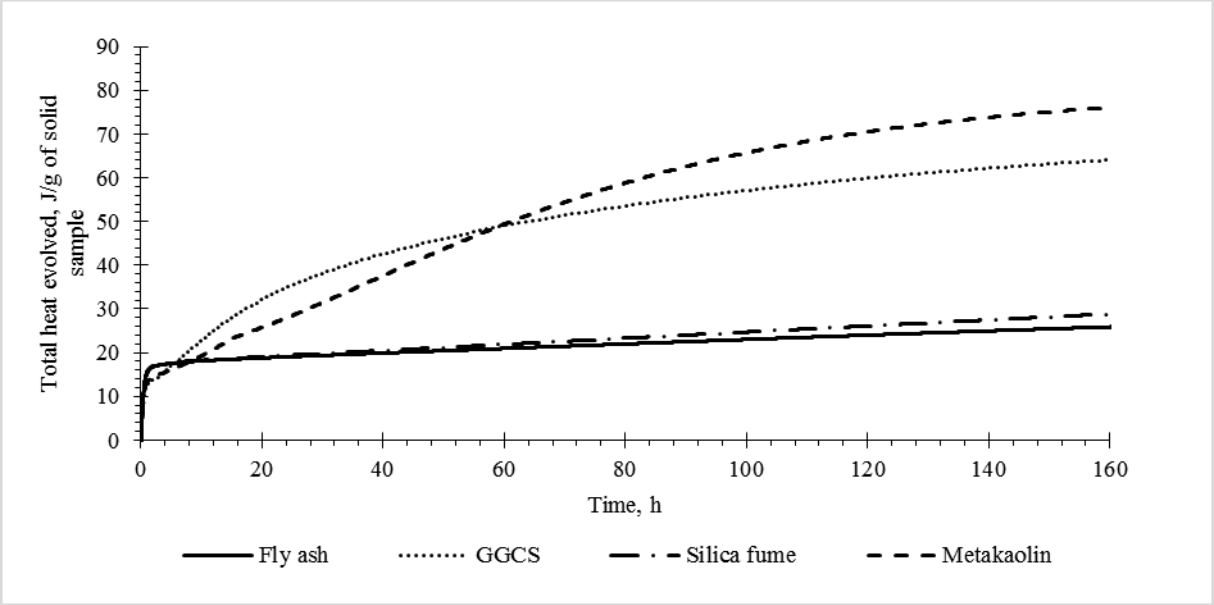

Figure 4.21: Total heat evolved by paste with different SCMs

4.3.4.2. Thermogravimetric analysis results of SCM-portlandite samples

The results of CH consumed by SCMs and chemically bound water in the SCM-portlandite mixture are shown in Figure 4.22. The results were evaluated from Figure 4.23 and Figure 4.24 using a similar technique as explained in section 4.3.3.

The order of CH consumption was as follows: fly ash< GGCS< silica fume< Metakaolin. The order of chemically bound water was as follows: fly ash< silica fume< GGCS < metakaolin. This order corresponded to the formation of cementitious hydrates i.e. the higher the chemically bound water, the higher the amount of cementitious hydrates formed. This order was also similar to that observed

in the isothermal calorimetry results. Generally, both orders implied that metakaolin had the highest pozzolanic activity while fly ash had the lowest.

By comparing the results of heat of hydration and TGA, it was concluded that metakaolin had the highest pozzolanic activity followed by GGCS, while silica fume and fly showed the lowest activities. The potential of GGCS could be directly linked to its high hydraulic activity. Silica fume and fly ash were ranked in the same level, although in terms of CH consumption and chemically bound water, silica fume had a higher potential than fly ash. These results also opposed those of Suraneni and Weiss, (2017), who observed that silica fume generated higher heat than fly ash and slag, although, they explained that its reactivity depended much on its origin and chemical composition.

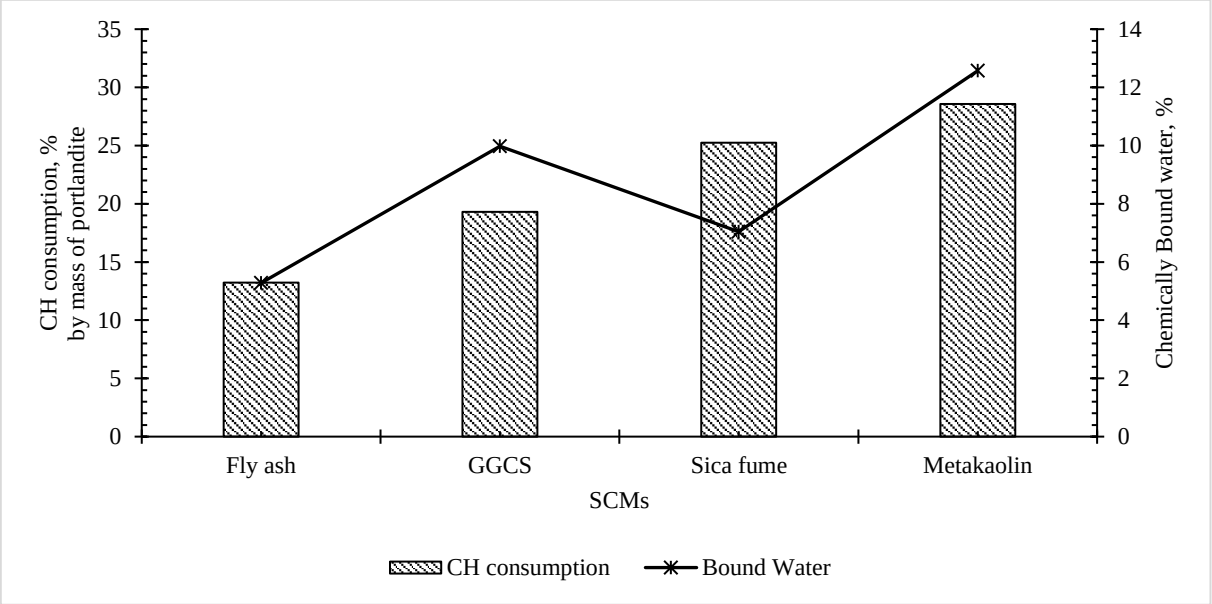

Figure 4.22: CH content and chemically bound water in the SCM-portlandite system

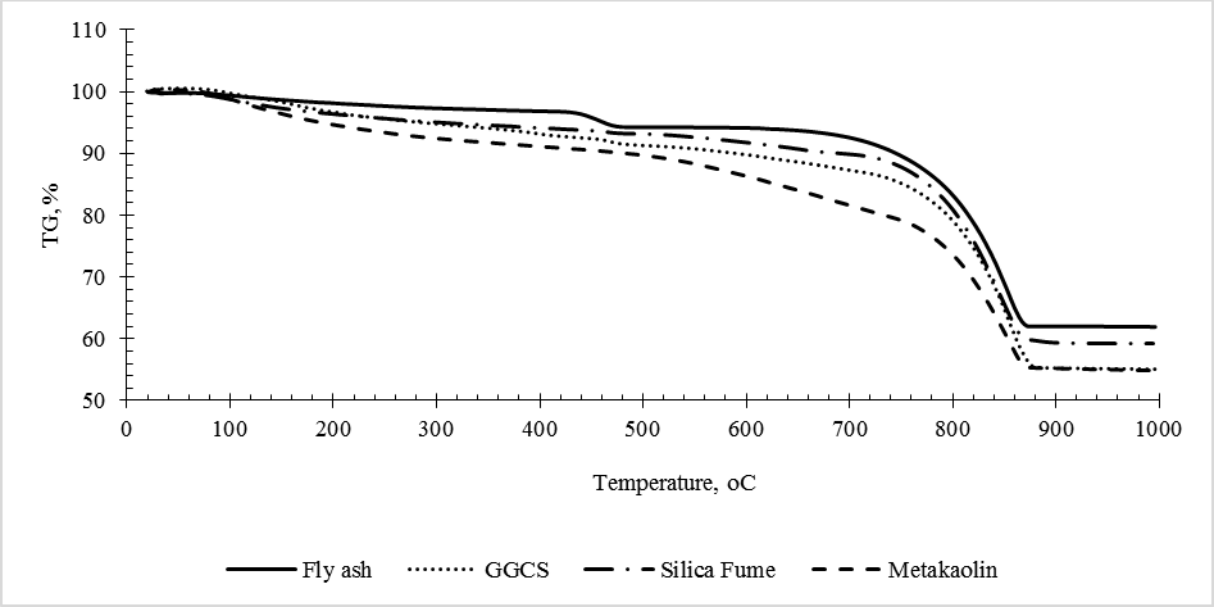

Figure 4.23: TG analysis of SCM-portlandite systems

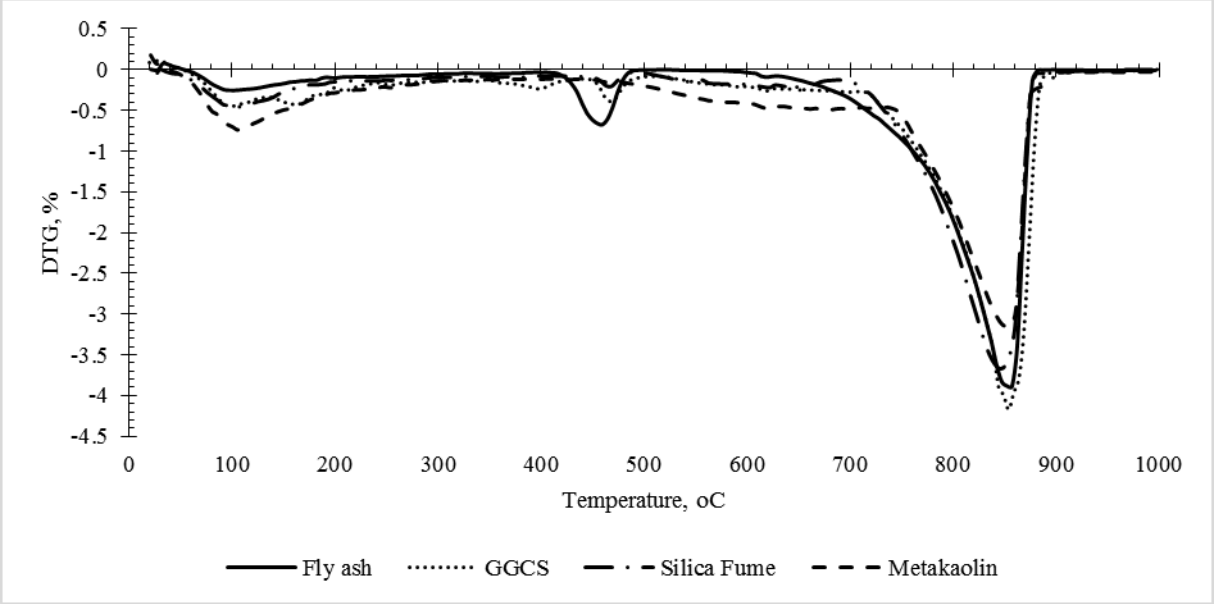

Figure 4.24: DTG analysis of SCM-portlandite systems

4.3.5. Closing remarks on the section

In the discussions that follow, certain pozzolanic and hydration mechanisms will be inferred as the causes of the behaviour observed. However, these were not actually independently measured, and so these can only be inferences

In terms of Strength Activity Index (SAI), firstly, the rate of strength development increased with hydration time up to 14 days and then reduced with time; secondly, the strength activity increased with metakaolin content up to 15% and then decreased at 20%. The increase was explained as the effect of pozzolanic reaction, while the decrease was considered to be caused by the dilution effect.

In terms of heat of hydration, the results of semi adiabatic and isothermal calorimetry methods supported each other. Both methods showed that metakaolin decreased the total heat generated by cement. The decrease was more observed in the mortar with higher metakaolin content which was caused by cement substitution and dilution effect. However, there was another observation that mortars with metakaolin showed a sign of continuing heat generation which was postulated as the results of calcium aluminate formation.

In term of CH content and chemical bound water, metakaolin mortars had a lower CH content than the control, which decreased with metakaolin content. The main reason for this was a high metakaolin pozzolanic potential. However, chemically bound water increased with hydration time, while decreased with metakaolin content as the result of the filler effect.

In comparing the pozzolanic activity of metakaolin in relation to other SCMs in the SCM-portlandite system, metakaolin exhibited the highest pozzolanic potential in terms of heat of hydration and chemically bound water followed by GGCS, while silica fume and fly ash were the last. However, metakaolin consumed more CH followed by silica fume, GGCS, then fly ash. The nature of their chemical compositions on reacting with CH solution was found to play a major role in their performances. Generally, it was concluded that metakaolin showed the best pozzolanic activity.

4.4. PROPERTIES OF FRESH CONCRETE MADE WITH METAKAOLIN

4.4.1. Setting times

The test results for setting time are shown in Figure 4.25 and Table 4.3. To obtain uniform consistency in the mixes, water content increased with the addition of metakaolin content by 22.9%, 31.4% and 39.8% for 10%, 15%, and 20% mk, respectively. This was also noted by Batis et al. (2005) and El-Diadamony *et al.*, (2016) who found that water demand increased with increase in metakaolin. They reasoned that this was due to high fineness and the amorphous structure of metakaolin.

Setting times (initial and final) of cement paste with metakaolin were higher compared to the control. This implied that metakaolin retarded the setting time. The possible cause of this was the reduction of cement content in the paste which results in a delay of hydration. However, El-Diadamony *et al.*, (2016) explained this by the coating effect of metakaolin particles on cement particle and the formation of ettringite. Besides, there was no direct proportionality relationship between the increase in metakaolin content and setting time. 10% mk showed the highest setting times, while a further increase of metakaolin to 15% and 20% resulted in a relative decrease in

setting times. The results agreed with Brooks, Megat Johari and Mazloom, (2000) who explained this as the result of higher water demand at higher metakaolin content which accelerated the hydration reaction and produced a denser binder phase. The results also agree with El-Diadamony *et al.*, (2016), although they had a different opinion from Brooks, Megat Johari and Mazloom, (2000); they explained setting time retardation as a result of decrease in water content as metakaolin content increased from 15% to 20% which was not observed in this study.

Table 4.3: Setting time results

Mix No	0% mk	10% mk	15% mk	20% mk
Water content, ml	118	145	155	165
Water content, % of binder	23.6	29.0	31.0	33.0
Initial setting time (min)	124	145	135	134
Final setting time (min)	139	165	153	150

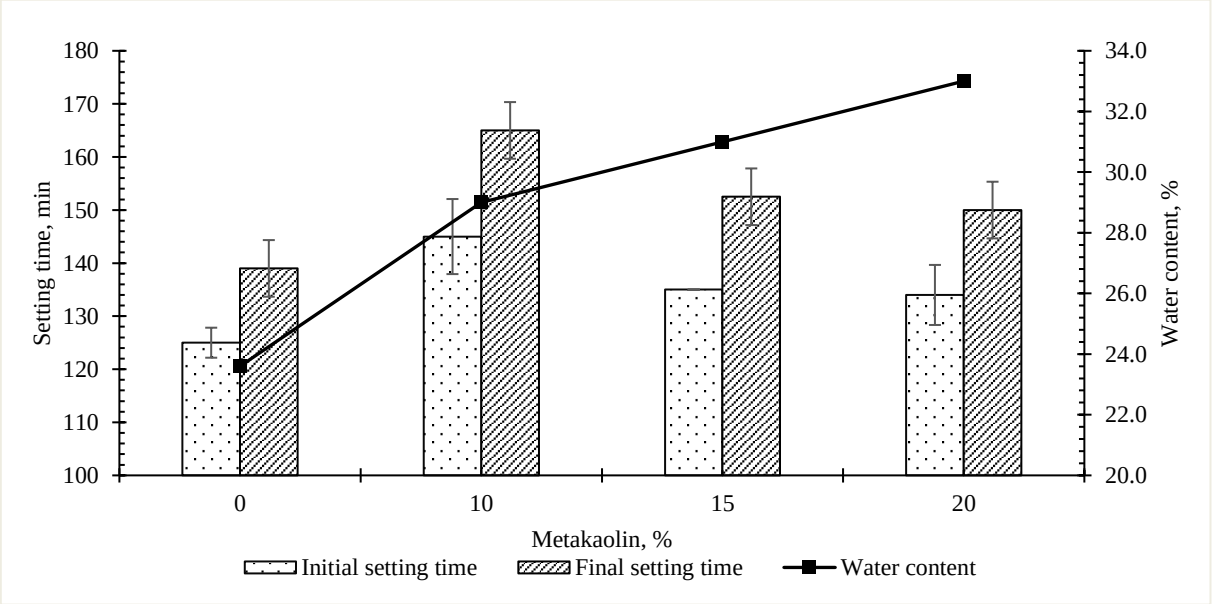

Figure 4.25: Setting times and water content of cement paste with metakaolin

4.4.2. Superplasticiser (SP) Dosage

Due to the greater fineness of metakaolin particles, when they replace cement in concrete, they tend to require more water to wet their surfaces. This results in an effective reduction of free water content, and consequently affects the workability of concrete. Since concrete designed for this study was proposed to use a constant amount of water at each w/b ratio and to achieve a slump of 100 ± 25 mm, the use of superplasticizer (SP) was required to disperse binder particles during mixing, and hence to achieve the same consistency. Thus, SP dosage was used as a final control to regulate the workability of the mixes.

Figure 4.26 shows SP dosage per mix with variation in w/b ratio. It was observed that as metakaolin increased from 0% to 20%, SP demand also increased. This was noted at each w/b; the control mix (0% mk) used less SP dosage followed by 10%, 15%, and 20% mk. The highest SP dosage was 1.34% (by mass of binder) for the mix with 20% mk at 0.4 w/b.

At the same replacement level, a trend of increase in SP dosage with w/b was observed, whereby the lowest values were observed for the mixes with 0.6 w/b ratio. This was because, at 0.4 w/b, there was effectively less 'free water' in the mix, and hence, more SP dosage was required to disperse the binder particles, and to obtain uniform consistency.

In the GGCS mixes, SP dosage was also affected by w/b ratio, and the values were similar to those of the control. As w/b ratio increased from 0.4 to 0.6, SP dosage also decreased. Thus, GGCS had less influence on the consistency of concrete. This was also observed by Jaufeerally, (2013) who noted a slump difference of 10-15 mm between concrete with 50% GGCS and control. Therefore, by comparing metakaolin and GGCS concretes, metakaolin mixes demanded more SP than those with GGCS.

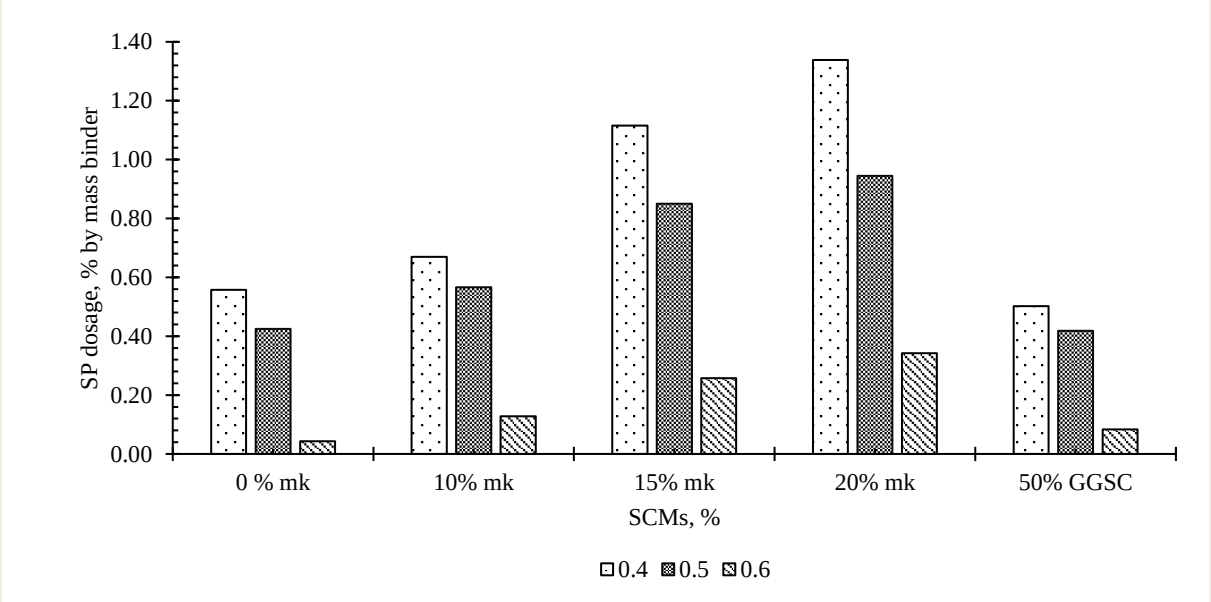

Figure 4.26: SP dosage (% by mass of binder) in the concrete mixes necessary to achieve a slump of 100 mm

4.5. HARDENED CONCRETE MADE WITH METAKAOLIN

4.5.1. Pore structure and refinement

MIP test results of concrete with different proportion of metakaolin at 0.6 w/b are presented in terms of cumulative porosity curve and differential pore volume curve. Cumulative porosity curve indicates the total porosity and threshold pore size. Total porosity corresponds to the maximum pore volume intrusion divided by the bulk volume of sample before the test. Dhandapani and

Santhanam, (2017) defined threshold pore size as the minimum continuous or breakthrough pore size for the sample, which serves as an indicator of durability (permeability and diffusion characteristics of concrete). Differential pore volume curve, also known as the 'frequency distribution curve', indicates the frequency of pores found at each pore size, whereby the pore size with the peak frequency is named 'critical pore size' of the system.

Pore size in this study referred to pore diameter which is categorized in three terms; nanopores with diameter < 0.01 µm, micropores with diameter between 0.01 and 0.10 µm, and macropores with diameter > 0.10 µm. It should be noted that the MIP test gives the information on the connectivity and capacity of the pore systems in hydrated cement, and not as an accurate measure of the actual pore sizes present (He, Li and Du, 2017). This is because the technique may involve breakdown of nanopores or break through to isolated pores as mercury is forced to intrude through the sample.

The influence of hydration time on pore development is shown in Figure 4.27. The total porosities filled by mercury for the whole range of concretes were less than 18%. These values were evaluated from mortar extracted from concrete. By assuming that mortar constitutes roughly 55% of concrete, the calculated total porosity of concrete is equal to 10%. This value is similar to total porosity obtained in concrete by the durability index test, WSI (Section 4.7.1). At 0% mk, a clear trend of decrease in total porosity with curing age was observed. Concrete contained more macropores, mainly at 7 and 28 days than at 56 days. This was obviously associated with densification of the hydrated matrix as a result of CSH production that fills space in the pore system.

For metakaolin concretes, there was no clearly defined relationship between total porosity and curing age. At 10% mk, total porosities at all ages were similar with the values lying between 13% and 14%, while at 15% and 20% mk, 28-day old concretes were found to have maximum porosities of 15% and 16%, respectively, and the minimum porosity at 56 days with magnitudes of 10% and 14%, respectively. It was observed that 20% mk had slightly higher porosity, and nanopores started to develop at all ages. This simply implied that, at higher metakaolin content, less total hydration reaction might occur, although total porosity might still be similar.

The differential curves are marked as (b) in Figure 4.28. The initial peaks appeared in the finer range (nanopores section) in all curves. These peaks indicated intrusion in the nanopore range which occurs mostly in the pozzolanic systems. With hydration time, more hydration products are

deposited near macropore region and refined the pores, consequently, increasing intrusion in the finer range.

Also, there was the transformation of peak shapes from sharp to blunt, critical pore size shift, and appearance and growth of initial rounded peak with curing age. The sharp peak indicated penetration of mercury through a continuously connected pore network from the sample surface (Cook and Hover, 1999). This implied that as curing age increased, the connectivity of pores in the hydrated matrix became discontinued. However, the critical pore size shift indirectly associated with the growth of the initial peak resulted in a wide distribution in pore size. This phenomenon was thought by Cook and Hover, (1999) to be either associated with crushing pressure of hydrated products that impeded the intrusion of mercury. Therefore, by observing the distribution curves in Figure 4.28 and Figure 4.29, the initial rounded peaks were more dominant at 15% mk, and at 56 days of curing for all concretes, respectively. This meant that, at 15% replacement rate and 56 days of curing, more hydration products were produced to hinder the intrusion.

The influence of metakaolin was separately observed by comparing concrete with and without metakaolin at different ages as shown in Figure 4.29. It was found that metakaolin significantly altered pore size distribution in concrete, particularly at early ages. At 7 days, metakaolin concretes had less total porosities than control, although the porosity decreased with decrease in metakaolin content in the order of 20%, 15%, and 10% mk. Threshold pore sizes for metakaolin concretes were smaller than that of the control, and they also decreased with metakaolin content in the same trend as total porosity. At 28 days, all concretes had pore size distributions seemingly to almost falling in the same region. Critical pore size for 0% mk was found in the macropore range, while for metakaolin concretes, it occurred in the micropore range, meaning that metakaolin concretes had more micropores than macropores. At 56 days, critical and threshold pore sizes for concretes occurred in the micropore range except for 10% mk, which might be associated with the location where the representative sample was taken. Therefore, this study agreed with the literature, that metakaolin refines pore size, while had less influence on total porosity.

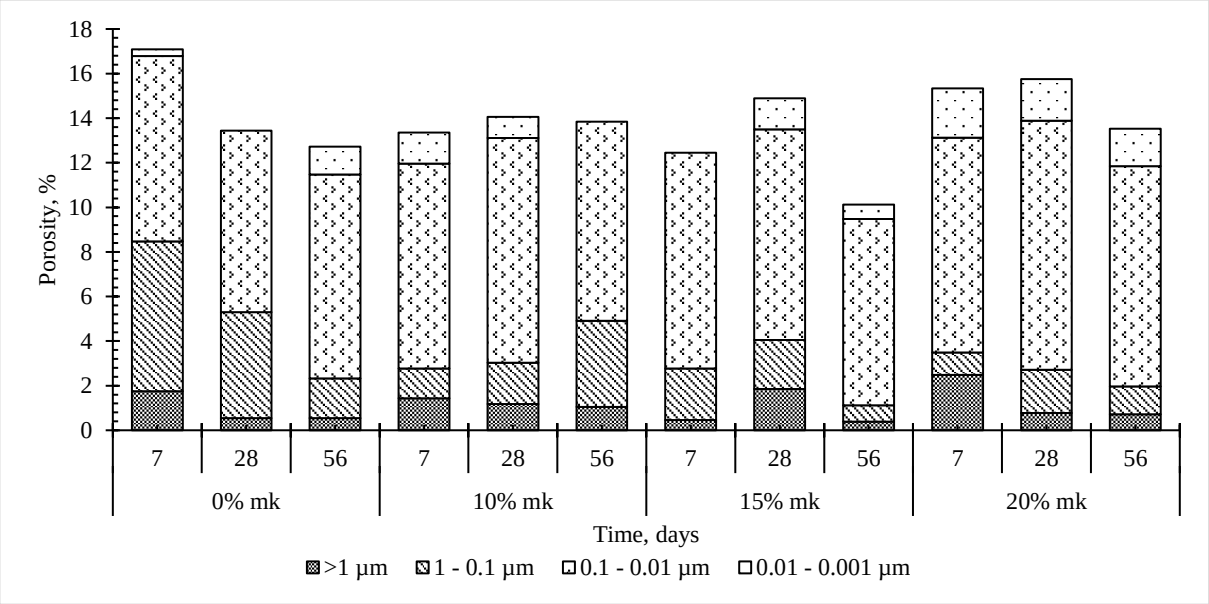

Figure 4.27: Total porosity distribution with curing age for concrete with different proportional of metakaolin.

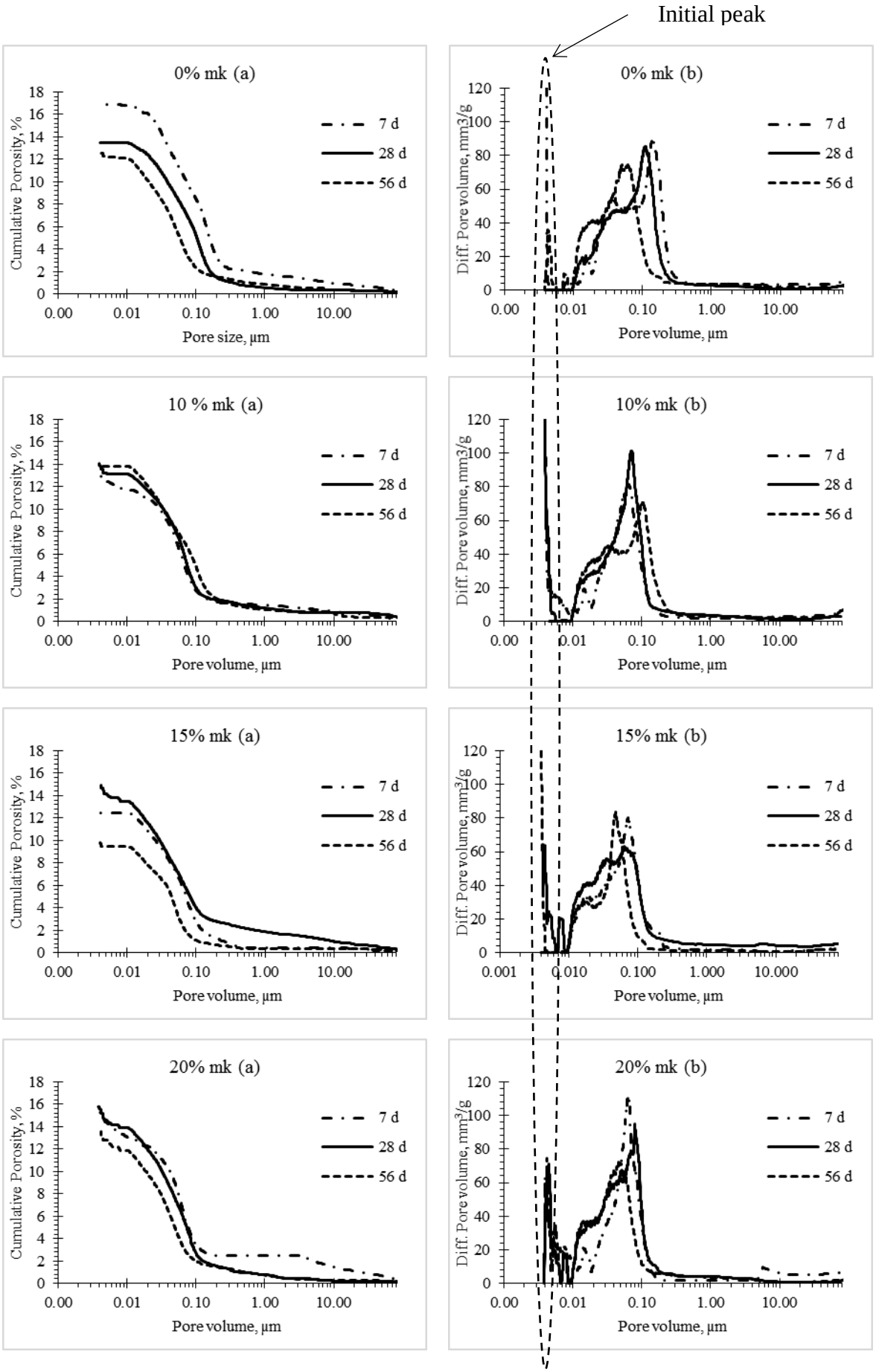

Figure 4.28: Pore development with hydration time in concrete containing metakaolin

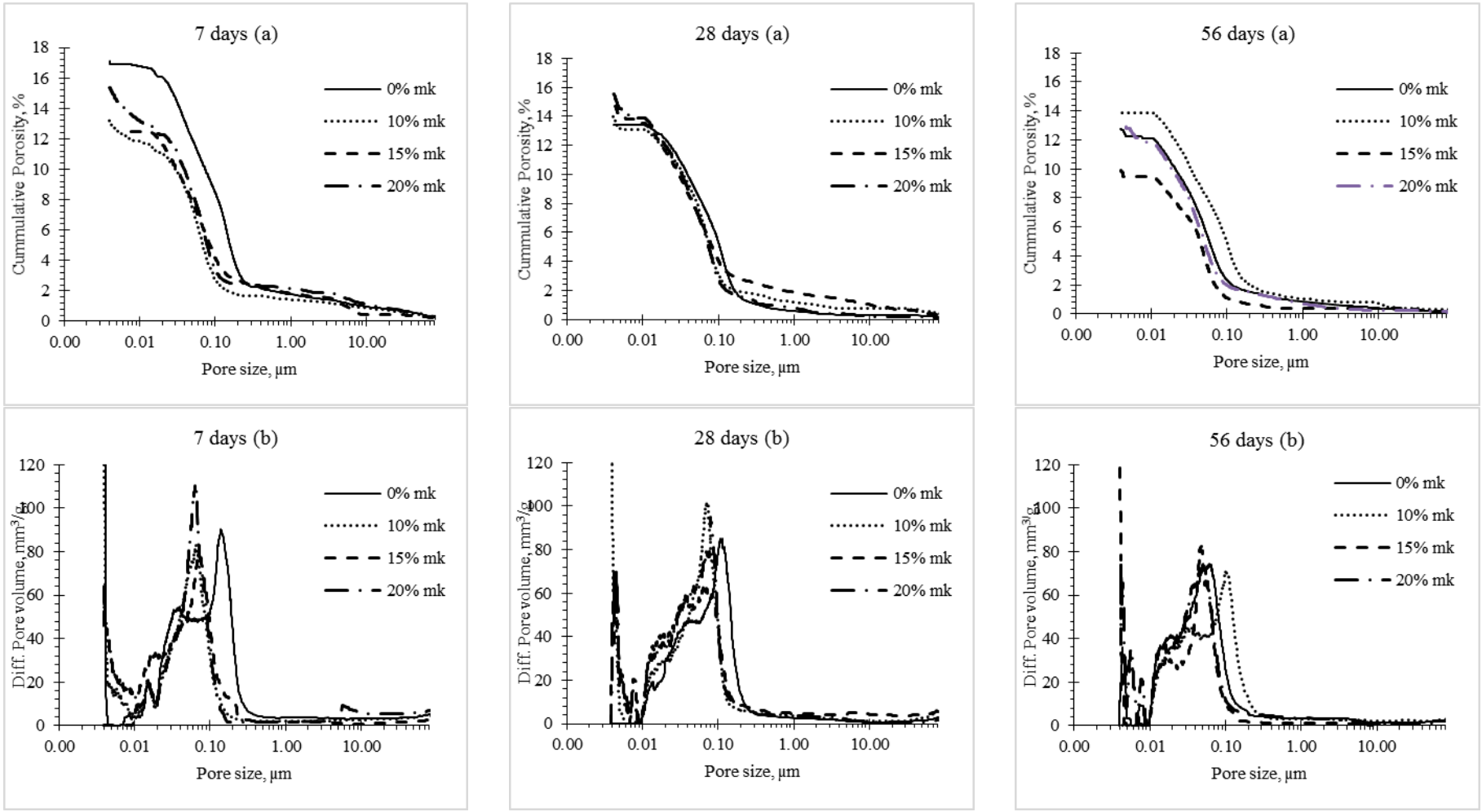

Figure 4.29: Porosity of concrete with different proportion of metakaolin at 0.6 w/b

4.5.2. Compressive strength

Compressive strength results of concrete containing different proportions of metakaolin at three w/b ratios are shown in Figure 4.30 with progressive curing age. A trend of decrease of compressive strength with increase in w/b ratio was observed in all mixes. Concretes with 0.4 w/b showed the highest compressive strength followed by 0.5 then 0.6 w/b. This study covered all range of concrete types, whereby 0.4 w/b concrete represented high-strength concrete and 0.6 w/b represented low-strength concrete. This assisted in observing the influence of metakaolin in different strength ranges of concrete.

Concrete incorporating metakaolin showed higher strength with increasing metakaolin content at 7, 28, and 56 days. A high rate of strength increase with metakaolin was observed for concrete with 0.4 and 0.5 w/b ratios, while at 0.6 w/b, the rate slowed down as metakaolin content increased. This might be postulated as the depletion of CH content with time at a high w/b ratio that led to run-out of pozzolanic potential, consequently, low strength development. It was observed that compressive strength was very high for 20% mk, achieving strengths of 70.3, 86.7, and 85.5 MPa for 0.4 w/b, 62.0, 74.8, and 75.5 MPa for 0.5 w/b, 46.7, 57.0, and 58.3 MPa for 0.6 w//b, at 7, 28, and 56 days, respectively. Thus, the replacement level of 20% gave the maximum compressive strength of concrete.

This observation was similar to that of Dadsetan and Bai, (2017) for self-compacting concrete with metakaolin at 0.4 and 0.45 w/b. They reasoned this high strength development was associated with the higher amount of silica in metakaolin that increased CSH gel in fresh concrete and also affected the hardened properties at early and later ages. However, the observation opposed the results observed by Aiswarya *et al*, (2013), Wild, Khatib and Jones,(1996), Kim, Lee and Moon, (2007), and (Khatib, 2008) who deemed that 20% mk reduced compressive strength of concrete due to a dilution effect. The results also opposed compressive strength of mortar observed in section 4.3.1. It was observed that 15% mk in mortar resulted in the highest compressive strength, while a slight decrease of strength was observed at 20% mk. This might infer that metakaolin has a high influence on the Interfacial Transition Zone (ITZ).

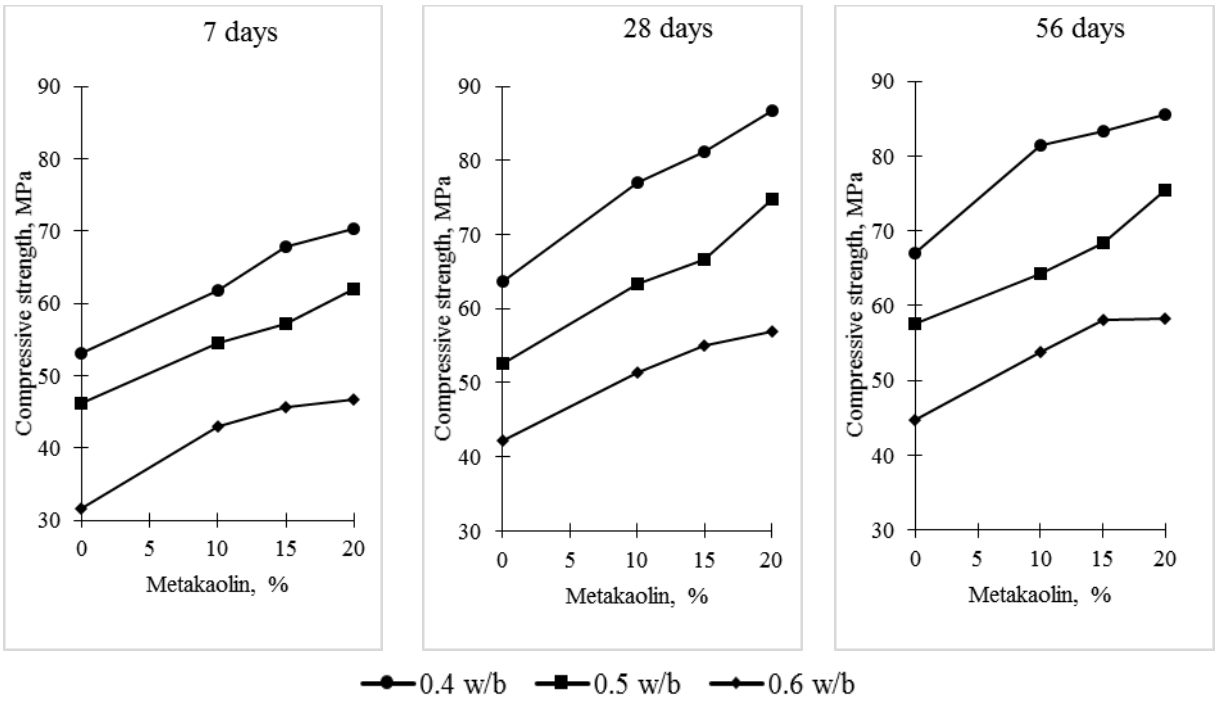

Figure 4.30: Compressive strength development of concrete containing different proportions of metakaolin with curing ages at three w/b ratios

Figure 4.31 presents compressive strength results of all range of concretes covered in this study. The error bar shows the standard deviation of compressive strength obtained from crushing three concrete cubes. The curve constructed by dashed lines represents the difference in the material batches (sand and aggregates) which were used in preparing the corresponding mixes. The results were used to compare compressive strength of concrete with different proportion of metakaolin and 50% GGCS at three w/b ratios. The magnitudes of compressive strength of control, 0% mk, were 53.2, 63.7, and 67.0 MPa for 0.4 w/b, 46.2, 52.7, and 57.5 MPa for 0.5 w/b, and 31.7, 42.2, and 44.7 MPa for 0.6 w/b, at the corresponding curing period of 7, 28, and 56 days. These values were used as the references to establish relative compressive strength of concrete with metakaolin and GGCS, and control, in Figure 4.32.

For metakaolin concretes, the relative strength increased with curing age, from 7 to 28 days at all w/b ratios, then, decreased from 28 to 56 days at 0.4 and 0.5 w/b, while remaining constant at 0.6 w/b. The initial increase of strength was associated with pozzolanic activity and acceleration of hydration reaction by metakaolin, and the decrease was due to decelerations of pozzolanic reaction (Wild and Khatib, 1997).

Concrete containing 50% GGCS exhibited the lowest compressive strength compared to control and metakaolin concretes, especially at the early age. Their strengths, at all w/b ratios, were very similar to the control. The high relative compressive strengths achieved were 103% at 56 days for 0.4 w/b, 92% at 28 and 56 days for 0.5 w/b, and 102% at 28 and 56 days for 0.6 w/b.

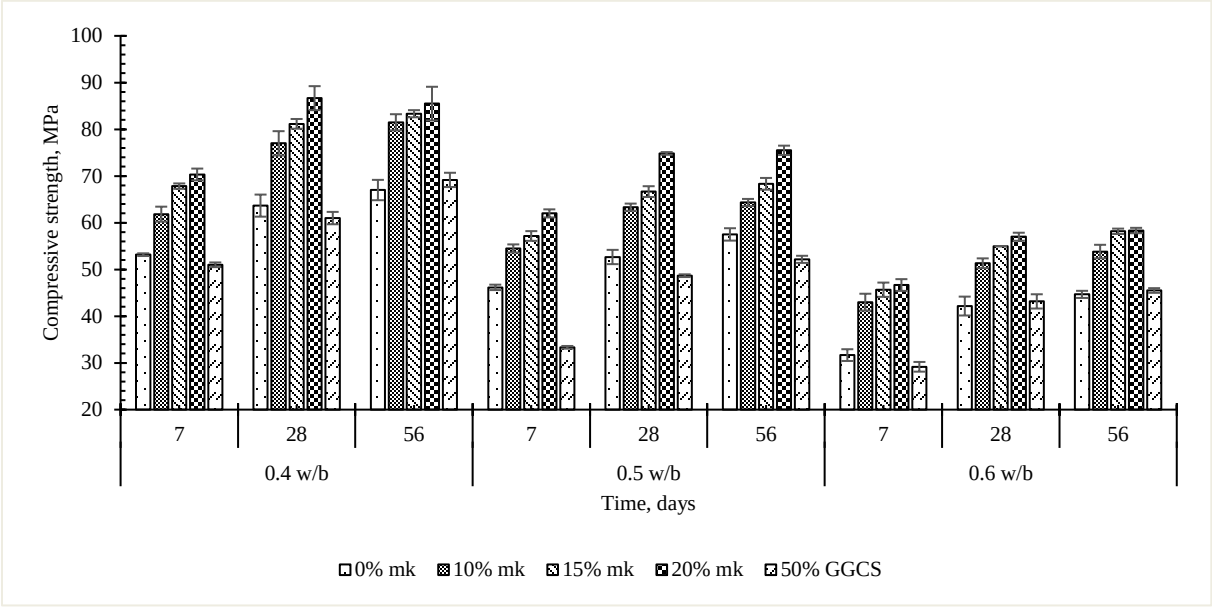

Figure 4.31: Compressive strength of concrete containing metakaolin and GGCS at three w/b ratios

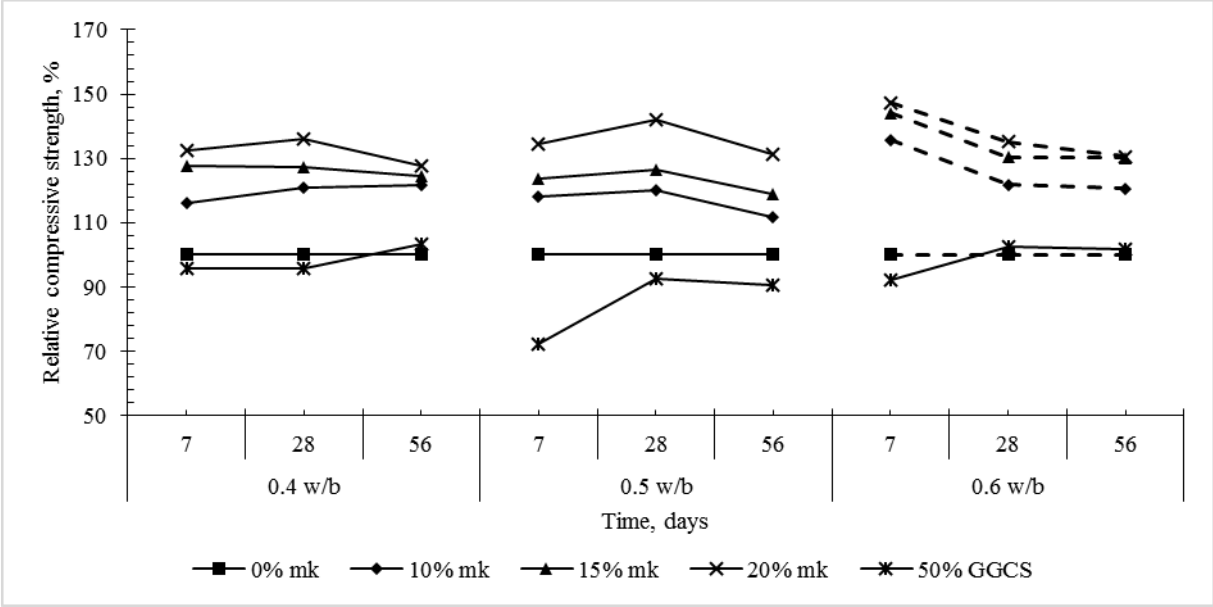

Figure 4.32: Relative compressive strength of concrete with metakaolin and GGCS at three w/b ratios

4.5.3. Tensile splitting strength

The results of tensile splitting strength of metakaolin concretes are presented in Figure 4.33. It was observed that tensile splitting strength increased with increase in metakaolin content from 0% to

20% at three w/b ratios. It was clearly observed that 20% mk had the highest tensile splitting strength as observed in the results of compressive strength. These results varied from those observed in the literature review, section 2.7.3. It was claimed that the highest tensile splitting strength of concrete with metakaolin would be achieved at a replacement rate between 10% and 15%, and a further increase would decrease the strength.

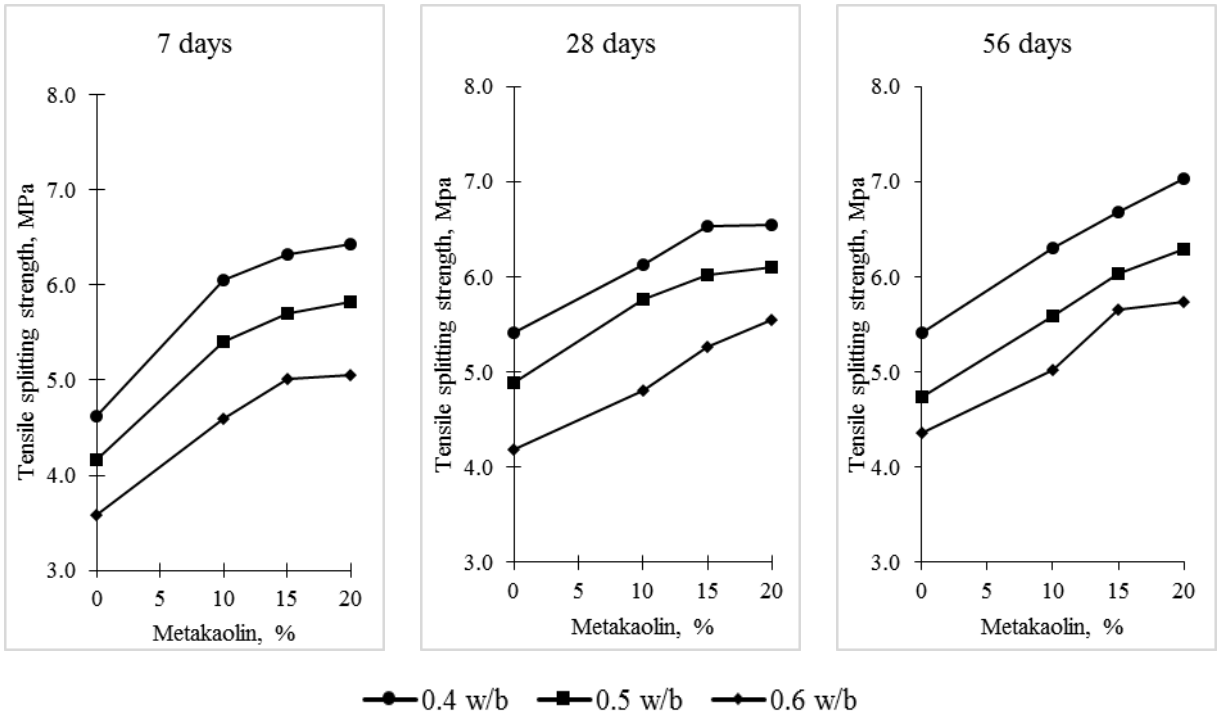

Figure 4.33: Tensile splitting strength development of concrete containing different proportions of metakaolin with progressive curing ages at three w/b ratios

Figure 4.34 presents tensile splitting strength of the range of concrete studied, whereby the error bars represent the standard deviation of tensile splitting strength of three concrete cubes. A similar trend as for compressive strength was observed, where metakaolin concretes had extraordinary strength compared to control and GGCS concretes. However, there was only a slight increase in tensile splitting strength with curing age. At all w/b ratios, the maximum strength gain with curing time, ranged between 0.1 and 0.7 MPa for metakaolin concretes, 0.6 and 0.8 MPa for control, 0.6 and 1.9 MPa for GGCS concretes. It could be seen that GGCS concrete gained strength at the highest rate followed by control, then metakaolin concrete.

The relative tensile splitting strengths of all concretes are presented in Figure 4.35. The strengths of control concrete were considered as the reference with 100% relative strength. The control

strength magnitudes at 7, 28, and 56 days were 4.6, 5.4, and 5.4 MPa for 0.4 w/b, 4.2, 4.9, and 4.6 MPa for 0.5 w/b, and 3.6, 4.2, and 4.4 MPa for 0.6 w/b, respectively. Relative tensile splitting strength at all ages and w/b ratios ranged between 113 and 131% for 10% mk, 121 and 140% for 15% mk, and 121 and 141% for 20% mk. It was seen that 20% mk had the highest relative tensile strength which was similar to that of 15% mk.

The behaviour of GGCS concretes varied from other concretes. At 0.4 w/b, there were insignificant differences in relative tensile strength which seemed to be similar to control. At 0.5 w/b, the relative strength decreased to 84% at 7 days, then increased to 104% and 113% at 28 and 56 days, respectively. At 0.6 w/b, there was a decrease to 88% at 7 days and an increase to 107% and 104% at 28 and 56 days, respectively. This type of trend was similar to that in compressive strength that led to a general conclusion that GGCS showed un-improvement of strength with time.

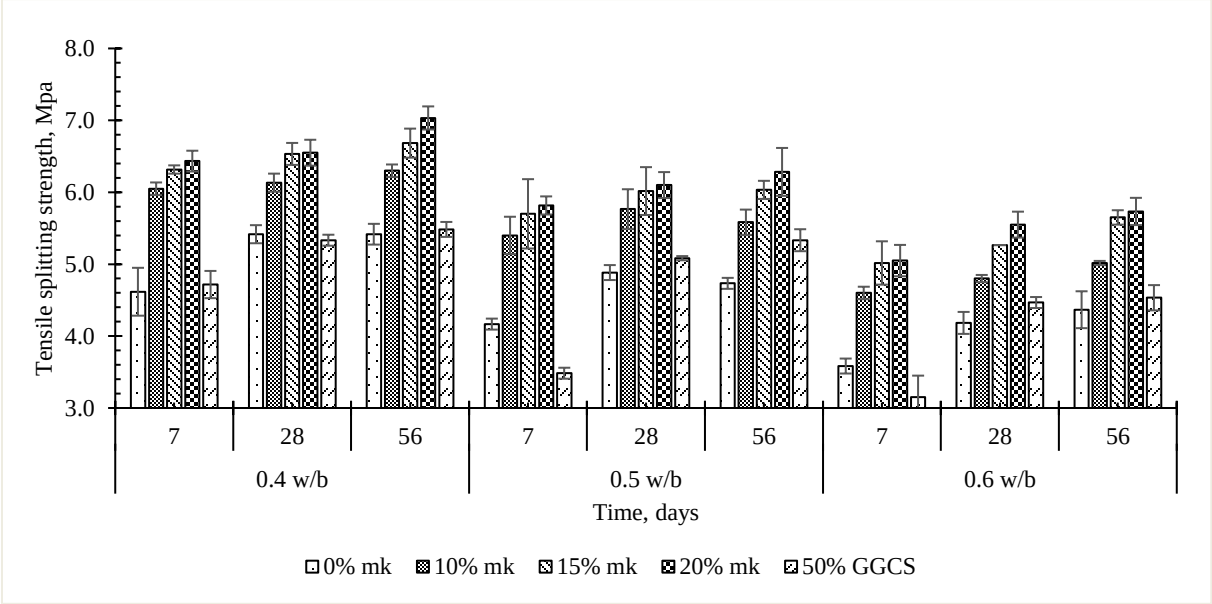

Figure 4.34: Tensile splitting strength of concrete containing metakaolin and GGCS at three w/b ratios

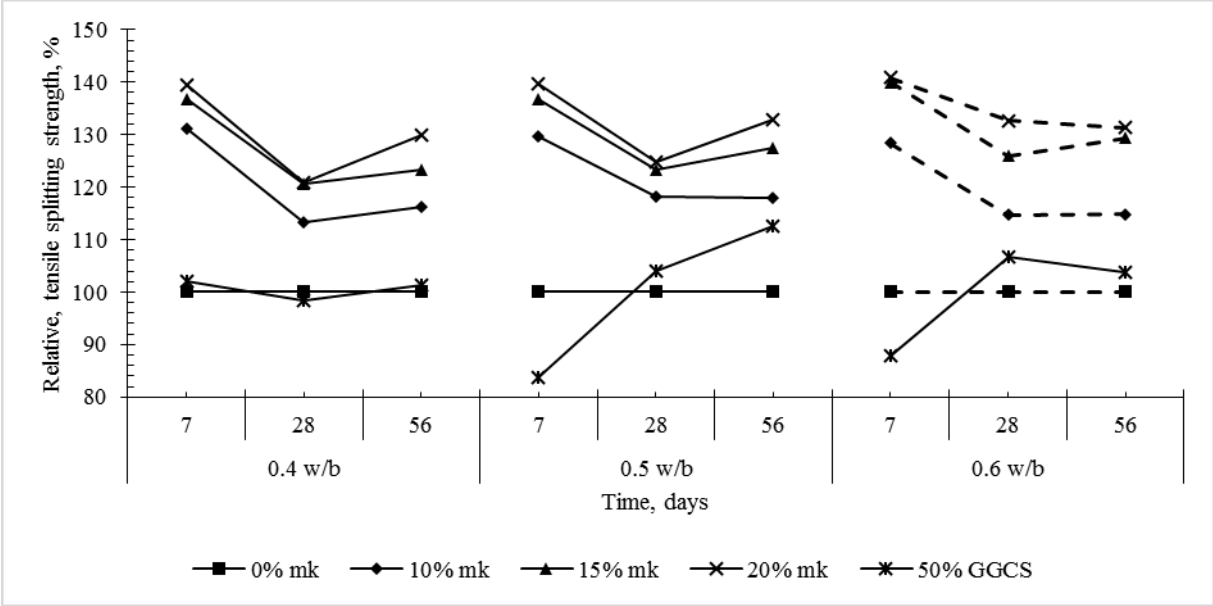

Figure 4.35: Relative tensile splitting strength of concrete with metakaolin and GGCS at three w/b ratios

Relationship between tensile splitting strength and compressive strength of metakaolin concrete in Table 4.4 indicates the ratios of tensile splitting strength to compressive strength of metakaolin concretes at all w/b ratios and curing ages. The ratios range between 7.6% and 11.3% and indicate that, at low compressive strength, tensile splitting strength was as high as 11.3% of compressive strength, while at high compressive strength, the ratio reduced to 7.6% (Arioglu, Girgin and Arioglu, 2006; Dinakar, Sahoo and Sriram, 2013). These ratios are similar to the ratio suggested by Mindess, Young and Darwin, (2003:317) and Mehta and Monteiro, (2006:77). It is clear that these ratios were more affected by w/b ratio and curing time than metakaolin content. The average ratios increased with w/b ratios, and decreased with curing time.

Table 4.4: Tensile splitting strength to compressive strength of concrete

	0.4 w/b			0.5 w/b			0.6 w/b		
Days	7	28	56	7	28	56	7	28	56
0% mk	8.7%	8.5%	8.1%	9.0%	9.3%	8.2%	11.3%	9.9%	9.8%
10% mk	9.8%	8.0%	7.7%	9.9%	9.1%	8.7%	10.7%	9.4%	9.3%
15% mk	9.3%	8.0%	8.0%	10.0%	9.0%	8.8%	11.0%	9.6%	9.7%
20% mk	9.1%	7.6%	8.2%	9.4%	8.2%	8.3%	10.8%	9.7%	9.8%
Ave	9.2%	8.0%	8.0%	9.6%	8.9%	8.5%	11.0%	9.7%	9.7%

The relationship between tensile splitting strength (f_{st}) and compressive strength (f_{cs}) for metakaolin concretes at all w/b ratios is expressed in equation 4.1. The equation fits 2/3 power of

f_{cs} relationship which correlated with CEB-FIP model (Arioglu, Girgin and Arioglu, 2006). Figure 4.36 shows the power model fit of the data collected of compressive and tensile splitting strengths.

$$f_{st} = 0.3561 f_{cs}^{2/3} \qquad R^2 = 0.8658 \tag{4.1}$$

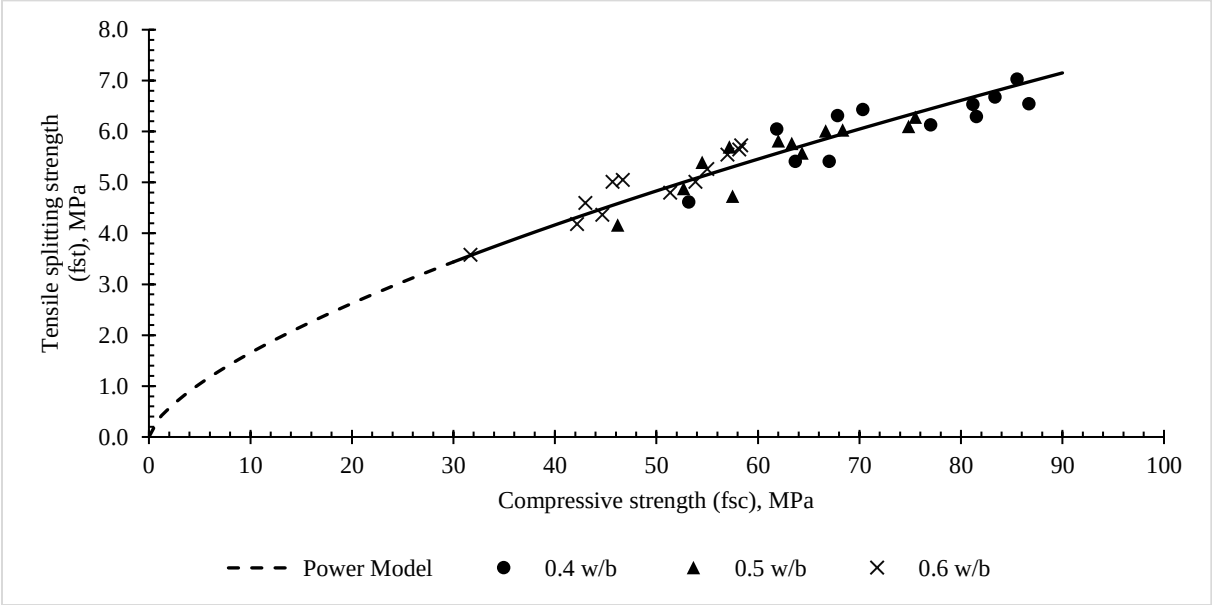

Figure 4.36: Power relationship model between tensile splitting strength and compressive strength of metakaolin concretes

4.5.4. Closing remarks of the section

Generally, metakaolin concretes exhibited excellent hardened properties at all replacement levels used. Metakaolin altered the microstructure of concrete, firstly by refining the pores and reducing pore connectivity, but it had less effect on total porosity. The mechanical properties i.e. compressive and tensile splitting strengths were more improved by metakaolin than GGCS. These properties increased with increase in metakaolin content, whereby the highest replacement level showed the highest strength. The compressive strength and tensile splitting strength of the 20% mk concrete gave premiums of approximately 47% and 41% over the control concrete, respectively. By relating the influence of w/b ratio and metakaolin content, metakaolin showed more of its potential at a higher w/b. The relative strengths were increased with w/b ratio, although not at a greater rate. Thus, it was concluded that, with a high replacement level of metakaolin and high w/b, the desired hardened properties of concrete can be achieved.

4.6. DEFORMATION BEHAVIOUR OF CONCRETE WITH METAKAOLIN.

4.6.1. Static elasticity modulus

The results for static elastic modulus (E_c) of concrete at 28 and 56 days of curing are presented in Figure 4.37 and Figure 4.38, respectively. At 28 days, elastic modulus decreased with increase in w/b ratio which revealed a less stiff matrix due to higher porosity. At all w/b ratios, metakaolin increased E_c of concrete as also observed by Zhang and Malhotra, (1995). However, there was no definite relationship between metakaolin content and elastic modulus. It was observed that 10% mk, at 0.4 w/b, had the highest E_c which then gradually decreased with increase in metakaolin content. At 0.6 w/b, the highest E_c was observed at 15% mk, whereas, at 0.5 w/b, E_c of control and metakaolin concretes were similar, although 15% mk tended to have a slightly lower E_c values.

E_c also increased with curing age since the values at 56 days were higher than those at 28 days. At 56 days, E_c of metakaolin concretes with 0.4 w/b were very high and had a similar trend to that at 28 days. This agreed with the argument of Ramezanianpour, (2014:236) that metakaolin might have a greater effect on elastic modulus at lower w/b. However, the trend at 0.4 w/b was different from the results obtained by Ayub, Khan and Memon, (2014). They found that at the age of 60 days, metakaolin concrete with 0.4 w/b had similar values as was observed in this study at 0.5 and 0.6 w/b. The average E_c increase from 28 to 56 days were 1.0, 1.9, and 6.6 GPa for 0.4, 0.5, and 0.6 w/b, respectively. A maximum increase was observed at 0.6 w/b, which implied that as pozzolanic and hydration reactions took place, 0.6 w/b concretes became stiffer.

To support the behaviour of metakaolin in concrete with 0.5 w/b, Figure 4.39 shows a comparison of compressive elastic modulus as tested on the Instron machine and 'instantaneous' elastic modulus from the creep test of metakaolin concrete at 28 days. It was observed that instantaneous elastic moduli were slightly higher than compressive elastic modulus, although the differences were small. This was possibly associated with the test method since the creep equipment was manually controlled. In the compressive elastic modulus (Instron machine), the stress was automatically applied at a constant loading rate that led to a constant increase in strain with a corresponding higher strain, consequently, a slightly lower elastic modulus (Mehta and Monteiro, 2006:95). However, the differences were minor and the trends of metakaolin influence were similar.

Comparing 50% GGCS and metakaolin concretes, at 28 days for 0.4 and 0.5 w/b, E_c of GGCS was similar to that of 20% mk, while at 0.6 w/b, GGCS had a very high E_c above all concretes. At 56 days, GGCS behaved similar to metakaolin concretes. Therefore, between these two SCMs, there was little to choose.

The relationship between E_c and compressive strength is presented in Figure 4.40. The values of elastic modulus obtained after testing the concrete cylinders at 28 and 56 days were correlated with the predicted E_c obtained from the ACI empirical formula shown in equation 4.3, whereby ρ stands for a density of metakaolin concrete, 2460 kg/m^3. However, E_c is highly depending on the aggregate type. Equation 4.3 from Fulton, (2009:114-116) was used to establish $E_{c,28}$ in relation to aggregate type and compressive strength at 28 days, whereby 24 GPa stands for stiffness factor of greywacke aggregate, and 0.25 GPa/Mpa is a coefficient. The ratio of E_c tested at 28 days on the Instron machine to $E_{c,28}$ calculated from the equation were shown in Table 4.5. All the ratios approached 1.0 with a standard deviation of 0.06. With these ratios, it was concluded that the results in this study were reasonable since they showed small deviations from those calculated based on aggregate type.

$$E_c = 0.043(\rho^3 f_{cs})^{1/2} \ (GPa) \qquad R^2 = 0.7073 \tag{4.2}$$

$$E_{c,28} = 24 + 0.25 f_{cs,28} \ (GPa) \tag{4.3}$$

Table 4.5: The ratio of E_c tested at 28 days on the Instron machine to $E_{c,28}$ calculated based on aggregate type

w/b	0.4	0.5	0.6
0% mk	1.05	1.09	0.94
10% mk	1.10	1.06	0.99
15% mk	1.05	1.00	0.98
20% mk	1.00	0.97	0.90

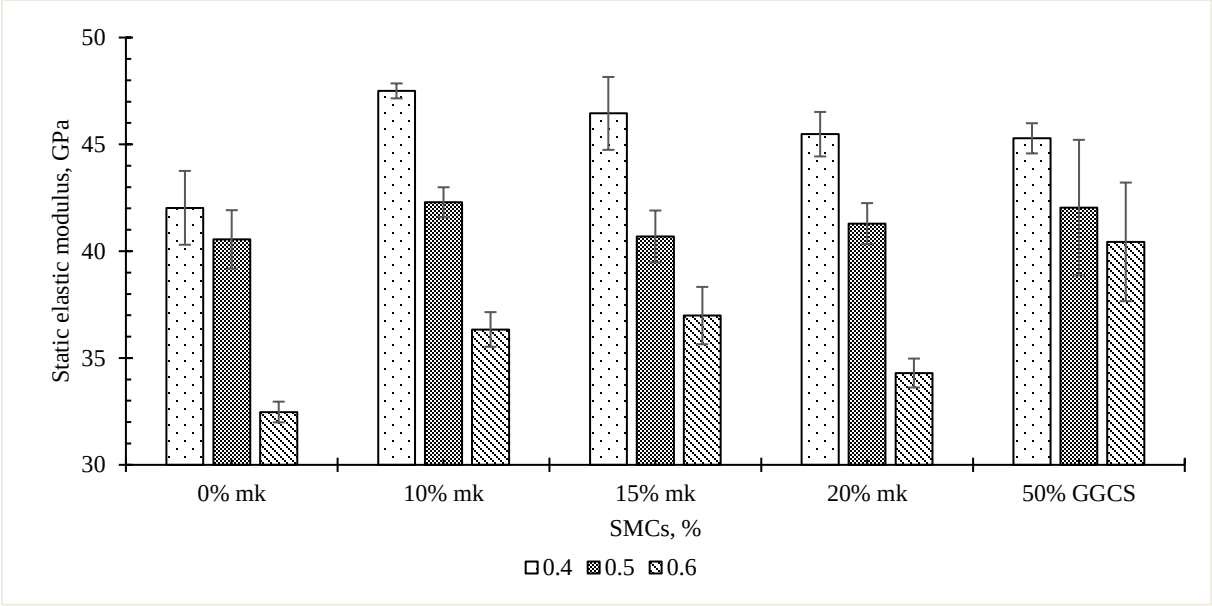

Figure 4.37: Static elastic modulus of concrete with metakaolin and GGCS at 28 days of curing

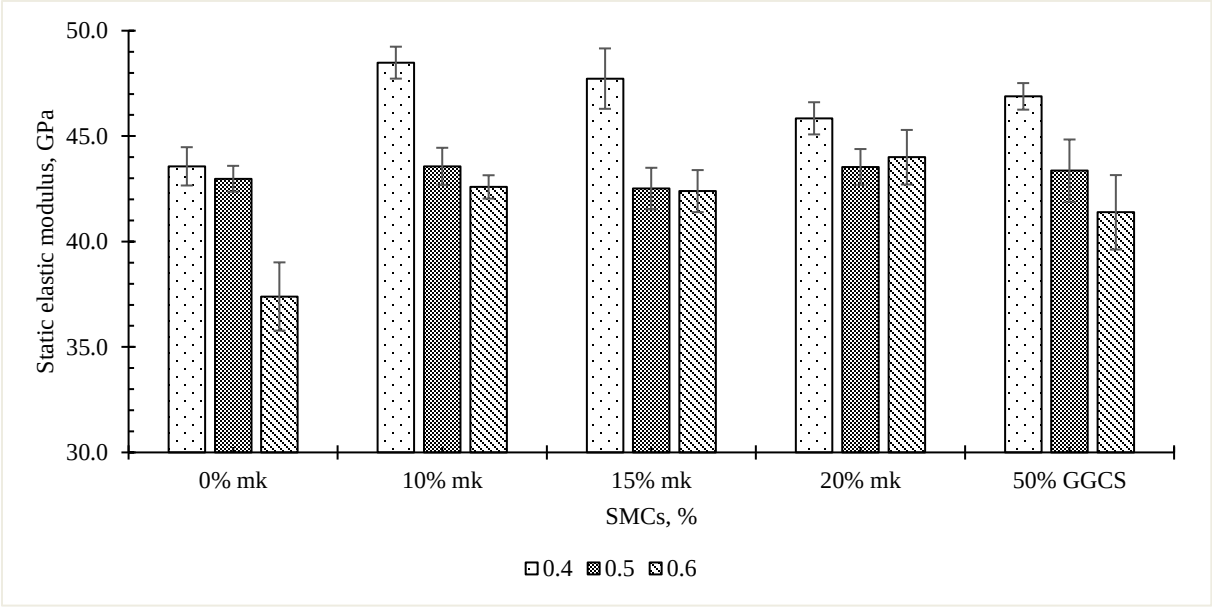

Figure 4.38: Static elastic modulus of concrete with metakaolin and GGCS at 56 days of curing

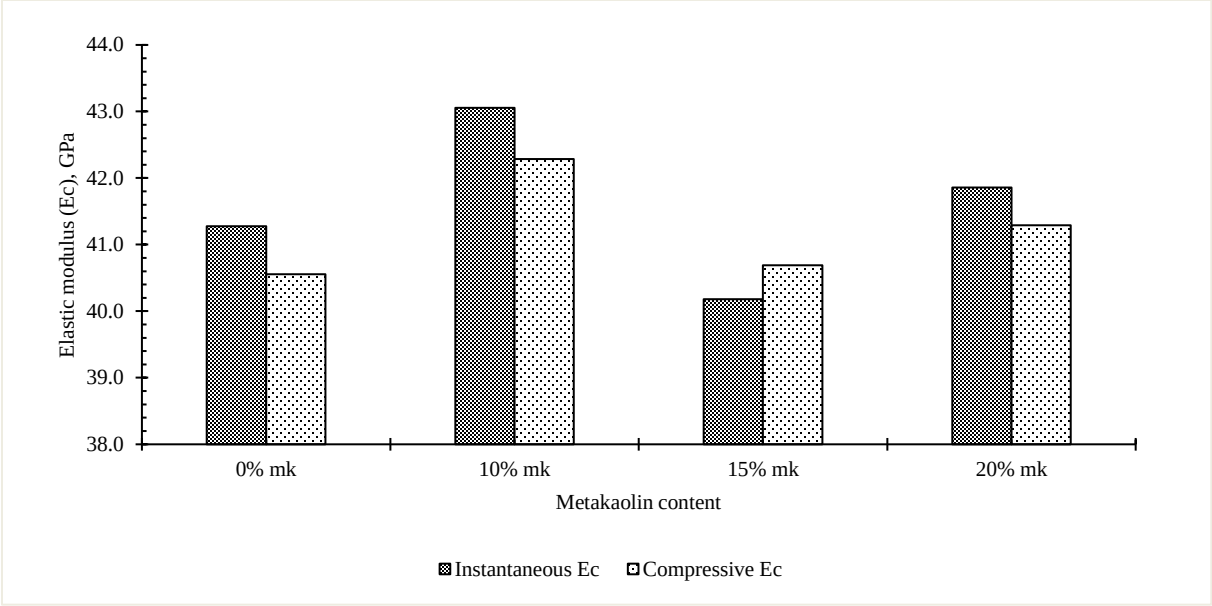

Figure 4.39: Comparisons of compressive elastic modulus and instantaneous elastic modulus from creep test of metakaolin concrete with 0.5 w/b

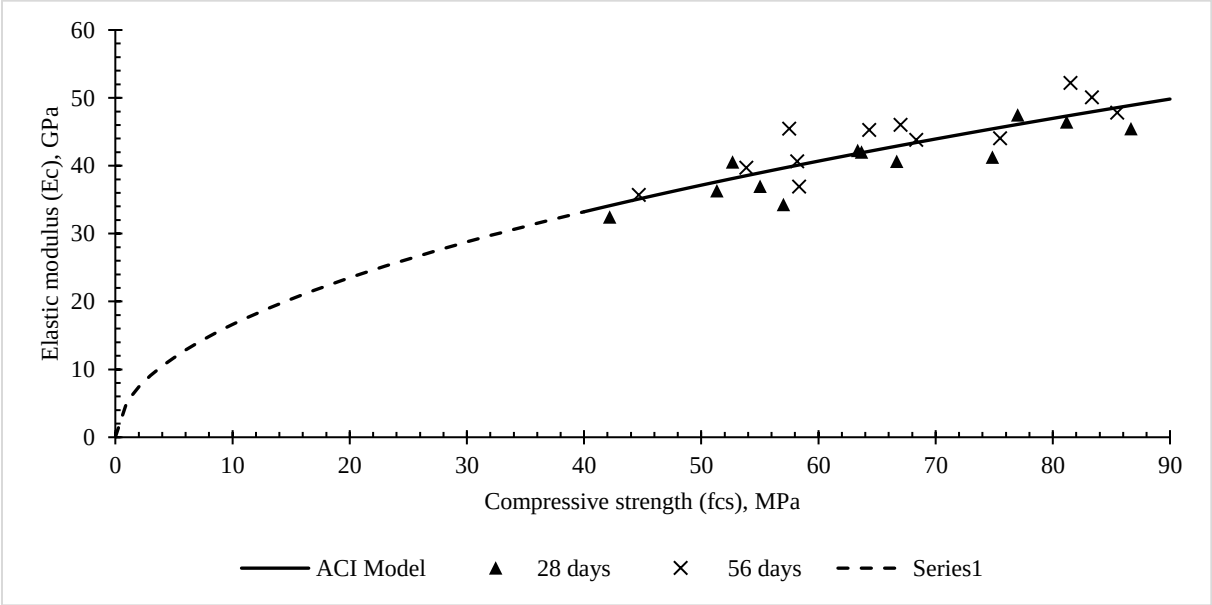

Figure 4.40: Relationship between elastic modulus and compressive strength of metakaolin concretes fitting in the ACI prediction model

4.6.2. Creep

Creep decreases as the strength and modulus of elasticity of concrete increase. The inclusion of metakaolin in concrete tends to strengthen and stiffen concrete as observed in section 4.5. It is definitely due to the influence of metakaolin in refining macropores in concrete by filling with the secondary cementitious products from pozzolanic reaction as discussed in section 4.3. These

influences are expected to affect the behaviour of concrete when it is long-term loaded under a constant stress, thereby reducing creep strain.

Figure 4.41 and Figure 4.42 present the results of creep test in terms of creep strains and specific creep, respectively. The results were calculated from when concretes had the age of 28 days, born in mind that the applied stresses on all concretes were equal and constant throughout the test. It was observed that the control attained the highest creep from its early ages to the later ages. The influence of metakaolin was exhibited even at the lowest replacement level. As the replacement level increased creep strain also decreased, whereby the lowest creep was achieved at 20% mk. The creep reduction, at 100 days, was 6.1%, 14.6%, and 26.5% for 10%, 15% and 20% mk, respectively. For specific creep, the reduction was 5.8%, 14.4%, and 26.5% for 10%, 15% and 20% mk, respectively. This inverse proportionality relationship between creep and metakaolin content was also observed by Brooks and Johari, (2001) as discussed in the literature review, chapter 2.

The rate of increase in creep strain with time was higher at early ages which kept decreasing with time. It was hypothesised that a high initial rate was due to the fact that concretes were not well dried when loaded, although, they were initially stored under initial drying condition in the environmental room set at 23 ± 3^{o}C and 50% RH for 21 days. It was possible that this duration was not sufficient to overcome the effect of thermodynamic moisture exchange between the interior and the outer surfaces of concrete. Therefore, simultaneous drying or escape of internal moisture from the concrete under applied stress accelerated creep, which was then decreased as the rate of moisture escape decreased. The rate was also proved higher on the control, which decreased with increase in metakaolin.

The effect of metakaolin on creep coefficient was also studied. Referring to Figure 4.43 which shows the increase of creep coefficient of metakaolin concrete with time, it was observed that the remarkable influence of metakaolin on creep coefficient was achieved when metakaolin replaced cement by the rate above 15%. The insignificant difference was observed between 0% and 10% mk, both concretes showed similar values. There was a huge variation of creep coefficient between concretes with less and more than 15% metakaolin. This variation was generally attributed to the fluctuation in elastic strain with metakaolin content. The instantaneous elastic strain measured was 1.45e-2, 1.39e-2, 1.49e-2, and 1.43e-2 for 0%, 10%, 15% and 20% mk, respectively. Besides, the

coefficients, at 100 days, were 2.12, 2.08, 1.77, and 1.58 for 0%, 10%, 15% and 20% mk, respectively. This implied that despite the fact that there was no defined relationship between metakaolin content and elastic strain yet the coefficient decreased with increase in metakaolin content.

Figure 4.44 shows specific creep of concrete per unit compressive strength at the age of 28 days. This figure is intended to show the influence of metakaolin after normalizing for the effect of compressive strength, i.e. it recognises that stronger concretes also creep less, and by normalising for strength, the 'intrinsic' creep potential of metakaolin can be better explored. The results show that the creep curves of metakaolin concretes tend to 'bunch' together into the same envelope, for all metakaolin contents, indicating that metakaolin replacement ratio does not have a strong influence on creep intrinsically. The Figure also shows that, marginally, the metakaolin concretes have slightly higher creep intrinsically, then, the control concrete, indicating further that there is no mechanism by which metakaolin reduces creep of concretes. The conclusion is thus that the main factor that influences metakaolin creep is a higher compressive strength.

Therefore, by understanding the factors that affect creep in concrete i.e. i) the removal of adsorbed water from hydrated cement by sustained applied stress, ii) additional microcracking in the ITZ associated owning to drying shrinkage, ii) the occurrence of delayed elastic response in aggregate due to bond between aggregates and cement paste, that declines stress transfer to the concrete (Mehta and Monteiro, 2006:97). The addition of metakaolin thus held on reducing creep by firstly, densifying pore structure, hence less exchange of adsorbed water from the concrete matrix to the surrounding environment, while encouraging self-desiccation. Secondly. Improving paste matrix in the ITZ, thus reduction of additional microcracking in the ITZ. Finally, increasing the bonding between cement paste and aggregate, that increases the occurrence of delayed elastic response in aggregate.

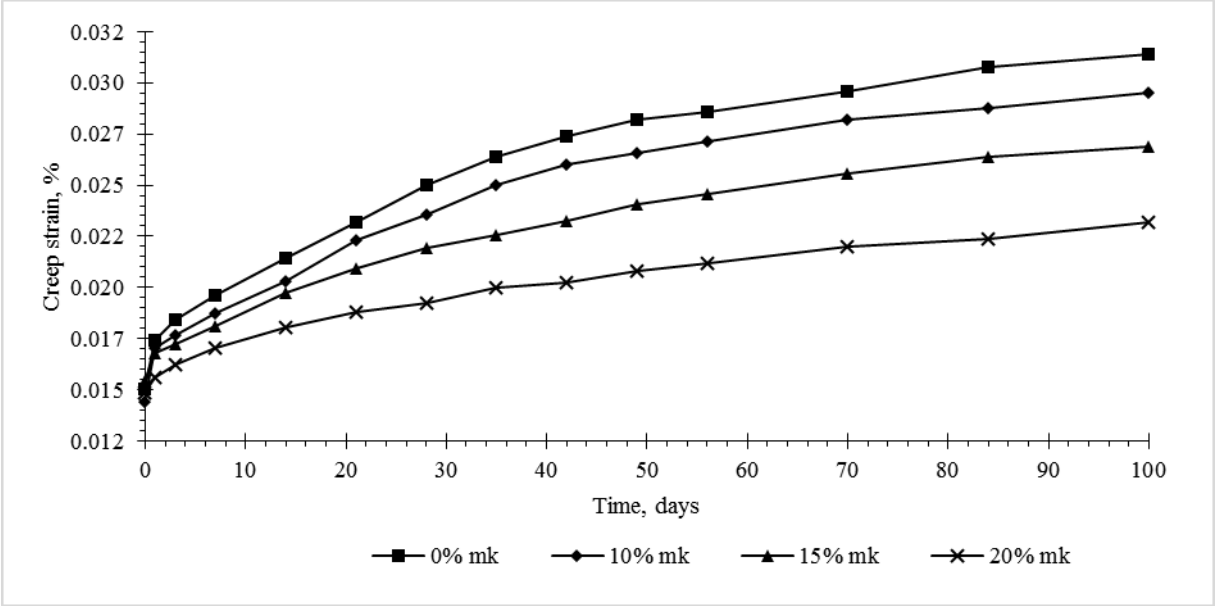

Figure 4.41: Creep strain of metakaolin concretes

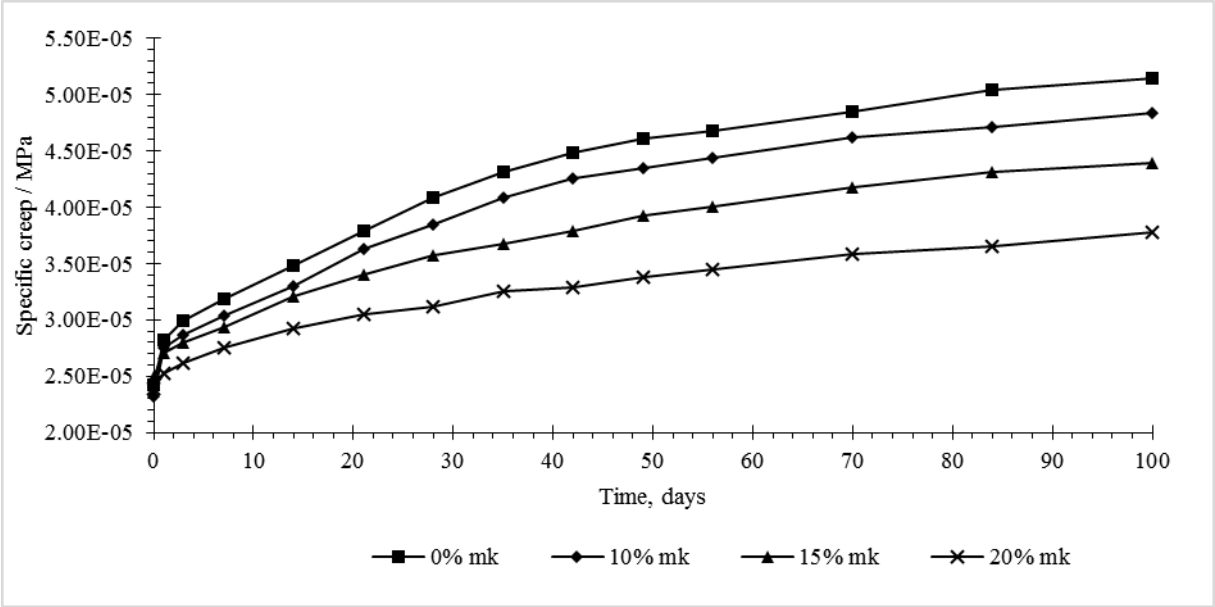

Figure 4.42: Specific creep of metakaolin concretes

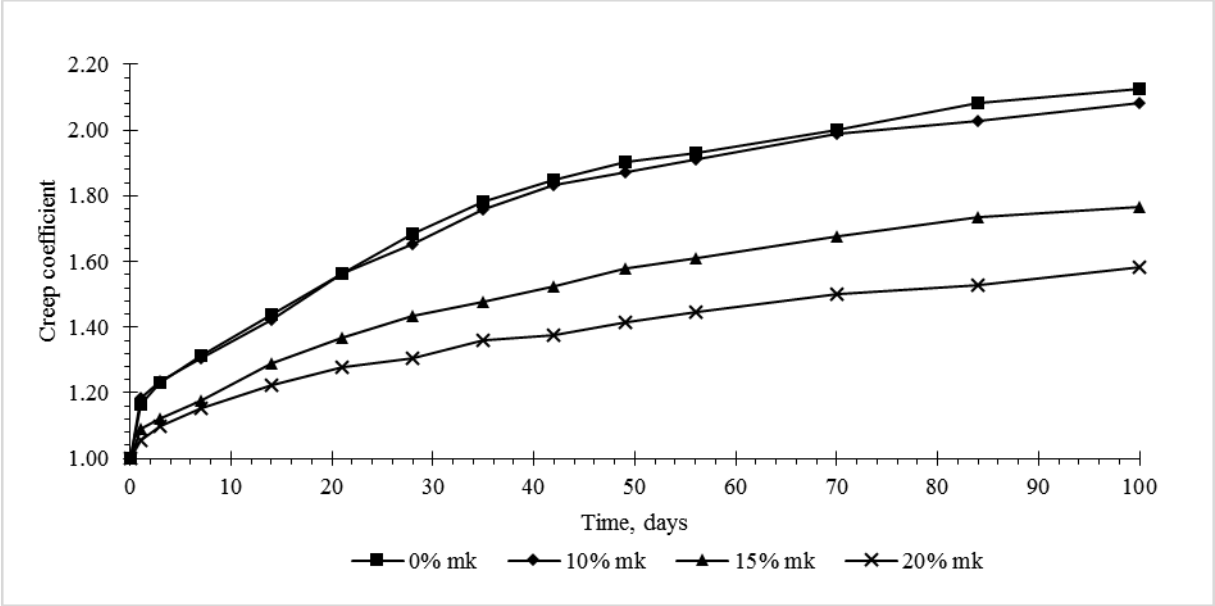

Figure 4.43: Creep coefficient of metakaolin concretes

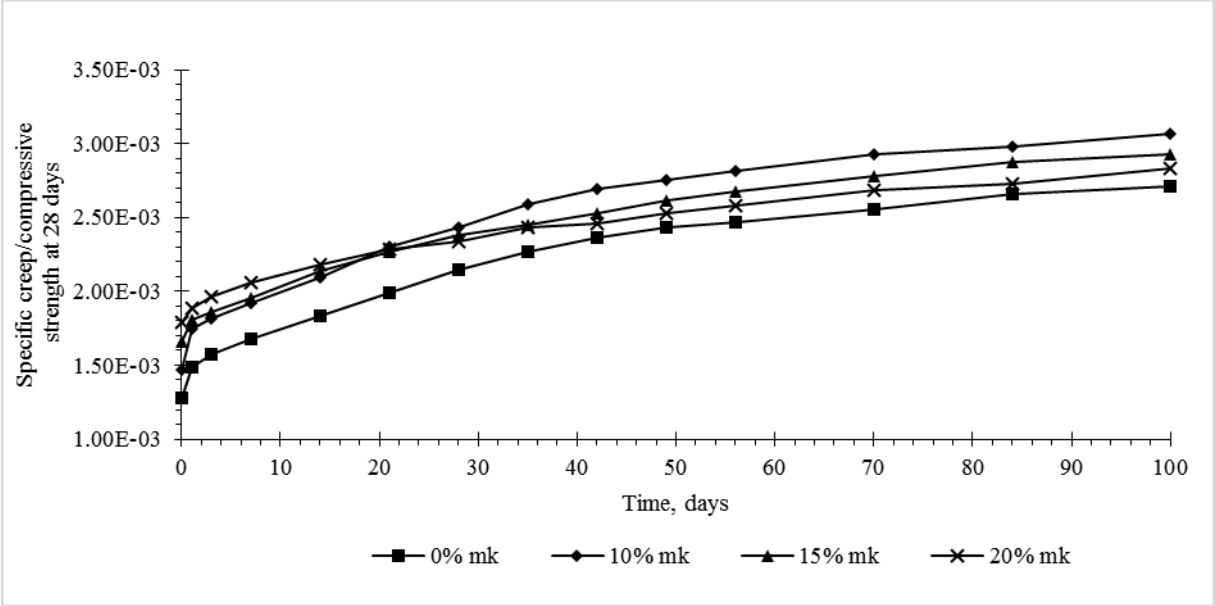

Figure 4.44: Specific creep per unit compressive strength of control and metakaolin concretes at 28 days

4.6.3. Drying shrinkage

The results of drying shrinkage of concrete with different proportions of metakaolin at 0.5 w/b ratio are shown in Figure 4.45. It was clear that drying shrinkage strain and creep strain (Figure 4.41) had similar tendency. As the amount of metakaolin increased drying shrinkage also decreased. 20% mk exhibited the lowest drying shrinkage, while 0% mk (control) exhibited the highest. The highest percentage of drying shrinkage reduction was 39.3% for 20% mk, 30.2% for

15%mk and 30.0% for 10% mk at 118 days. This generally attributed to the reason explained before about the potentiality of metakaolin on densifying and stiffening the microstructure of concrete, thereby, reducing the exchange of adsorbed water by allowing self-desiccation. Drying shrinkage also increased with time regardless of metakaolin content as it is a time dependent. At early age, drying shrinkage increased rapidly, then slowed down in long term. These results were also supported by Brooks and Johari, (2001) and Khatib, (2008).

As far as drying shrinkage was concern, it was concluded that drying shrinkage is inversely proportional to metakaolin content, while directly proportional to drying time. It should be noted that this study did not undergo any laboratory experiment to clear out the contradiction observed in the literature review of whether metakaolin decreased or increased autogenous shrinkage.

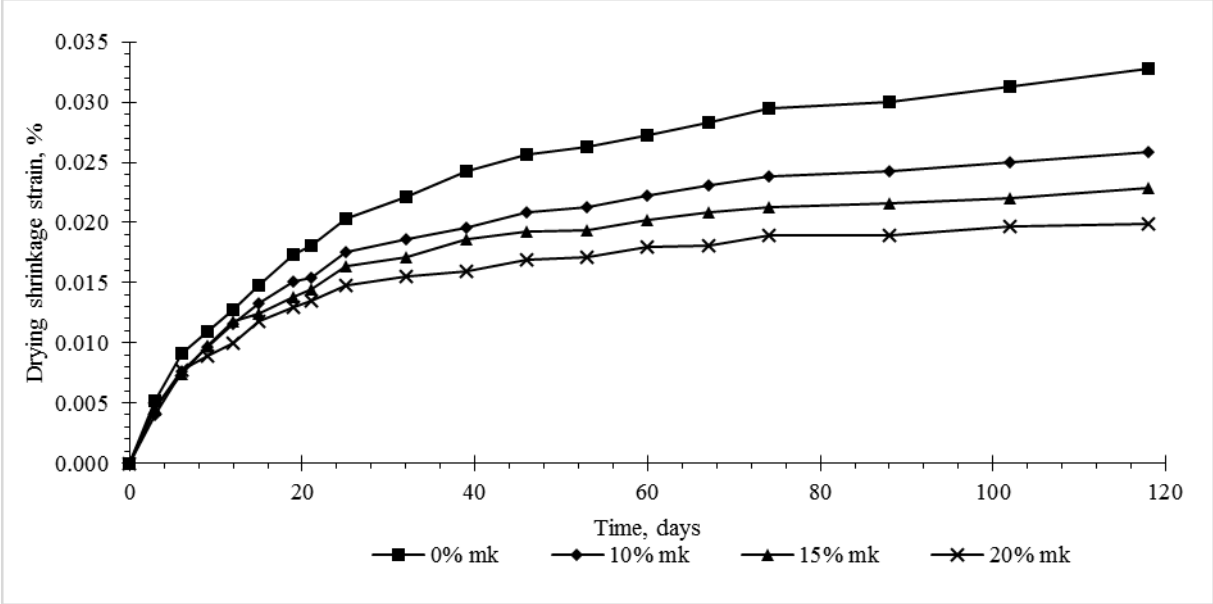

Figure 4.45: Drying shrinkage of metakaolin concrete obtained from control specimens for creep test

4.6.4. Closure remarks of the section

Time dependent behaviour of concrete i.e. static elastic modulus, creep, and drying shrinkage were improved by the inclusion of metakaolin. Static elastic modulus of concrete was generally increased by metakaolin despite replacement levels and w/b ratios, although there was no defined relationship between metakaolin content and static elastic modulus. The influence of metakaolin on creep and drying shrinkage was tremendous. As metakaolin content increased, both creep and drying shrinkage decreased in similar trend, whereby the lowest strain was observed at 20%

replacement. These effects were mostly associated with physical and chemical alterations of metakaolin on concrete. Generally, the results correlated well with the literature.

4.7. DURABILITY PROPERTIES OF CONCRETE WITH METAKAOLIN

This section expresses the potential of metakaolin on enhancing durability of concrete. It presents the results and discussions of durability indexes i.e. permeability, sorptivity and porosity, and chloride conductivity in comparison to GGCS concretes. It also discusses the result of incorporating metakaolin in concrete to mitigate ASR, and to reduce carbonation effect and diffusion of chloride ions.

4.7.1. Durability index results

Durability index test results were evaluated for oxygen permeability, water sorptivity and chlorides conductivity, at 28 days of curing. The results obtained are discussed in related to Table 4.6.

Table 4.6: Criteria to judge the quality of concrete from the results of durability index (DI) test (Alexander, Mackechnie and Ballim, 1999)

Quality of concrete	Oxygen permeability Index (OPI) log scale	Water sorptivity index (WSI) mm/h$^{0.5}$	Chloride conductivity index (CCI) mS/ cm
Excellent	>10	< 6	< 0.75
Good	9.5 - 10	6 - 10	0.75 - 1.50
Poor	9.0 - 9.5	10 - 15	1.50 - 2.50
Very Poor	< 9	> 15	> 2.50

The dashed lines shown in Figure 4.46 to Figure 4.52 represent the difference in casting time and material batches (i.e. coarse aggregates and fine aggregates) used in preparing concrete mixes. The points connected by dashed lines represent concretes which were cast four months earlier than those presented by the points connected by solid lines. Hence, the influence of different material batches was suspected to induce some variations in the results obtained.

4.7.1.1. Oxygen permeability index (OPI) results

Figure 4.46 presents the results obtained from the OPI test. As explained in the methodology chapter, section 3.8.1.1, OPI is the negative log of the Darcy coefficient of permeability (k) of the specimen. Figure 4.47 shows the coefficient of permeability of concrete with SCMs (metakaolin and GGCS) at different w/b ratios. By definition, OPI is a measure of the capacity of concrete to transfer gas by permeation, and the value depends on the microstructure of concrete and moisture

condition of the concrete. According to Table 4.6, all concretes showed "excellent" quality despite having different types and quantities of SCMs, and w/b ratios. All OPI values were above 10, and it was observed that control concretes (0% mk) had the lowest OPI values, whilst the addition of SCMs increased the values.

At 0.4 w/b ratio, OPI value increased with the addition of metakaolin, whereby 20% and 15% mk showed the highest values followed by 10% and 0%. A similar trend was also observed at 0.5 w/b ratio. At 0.6 w/b ratio, OPI values were expected to be less than those at 0.4 and 0.5 w/b ratio, but since the materials used in preparing these concretes were different, their OPI values were slightly higher. However, a trend of increase of OPI values was similar to that observed at 0.4 and 0.5 w/b ratio. Thus, OPI values increased with increase in metakaolin content, whereby the highest value was observed at 20% mk.

Comparing the influence of metakaolin to GGCS in concrete, at 0.4 and 0.6 w/b, concretes with 50% GGCS had OPI values lower than those of concretes containing metakaolin. However, at 0.5 w/b, 50% GGCS had OPI value slightly higher than 10% metakaolin. Generally, concretes with metakaolin showed the highest OPI values at all w/b ratios. This implies that the concrete with metakaolin had the highest resistance to gas permeability which was definitely associated with the fact that metakaolin reduces pore connectivity in concrete, refer section 2.9.1.

A reasonably linear correlation was observed between the coefficient of permeability and replacement levels of metakaolin, as shown in Figure 4.48. 0.6 and 0.5 w/b showed the best correlation fits with $R^2 = 0.93$, and 0.4 w/b with $R^2 = 0.87$.

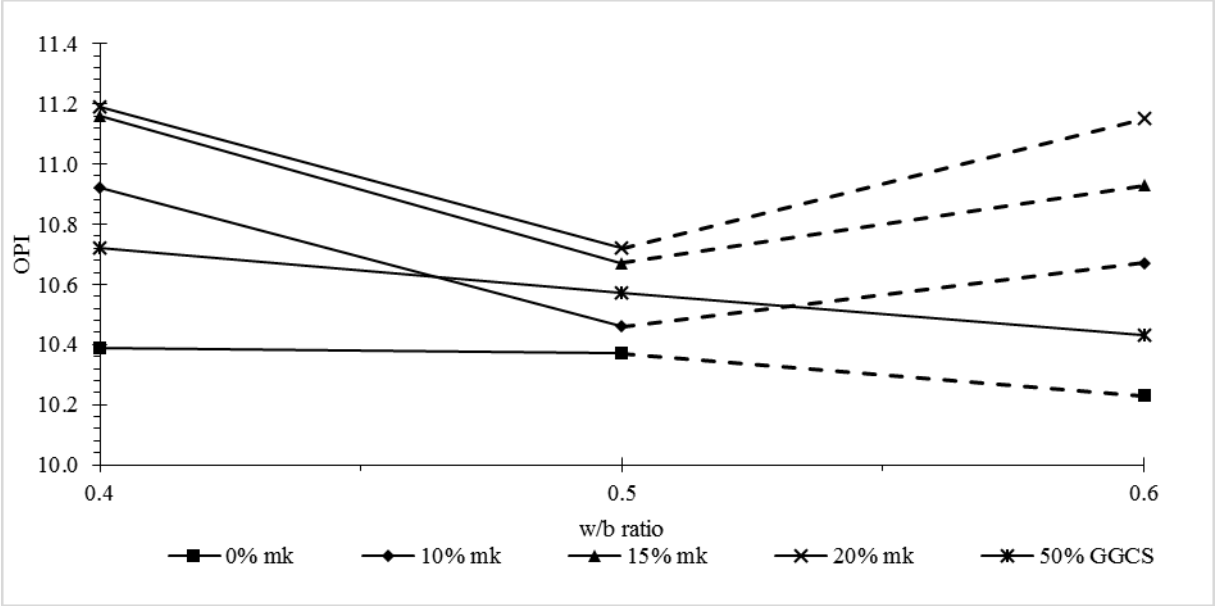

Figure 4.46: Oxygen permeability index (OPI) of concrete at different w/b ratio

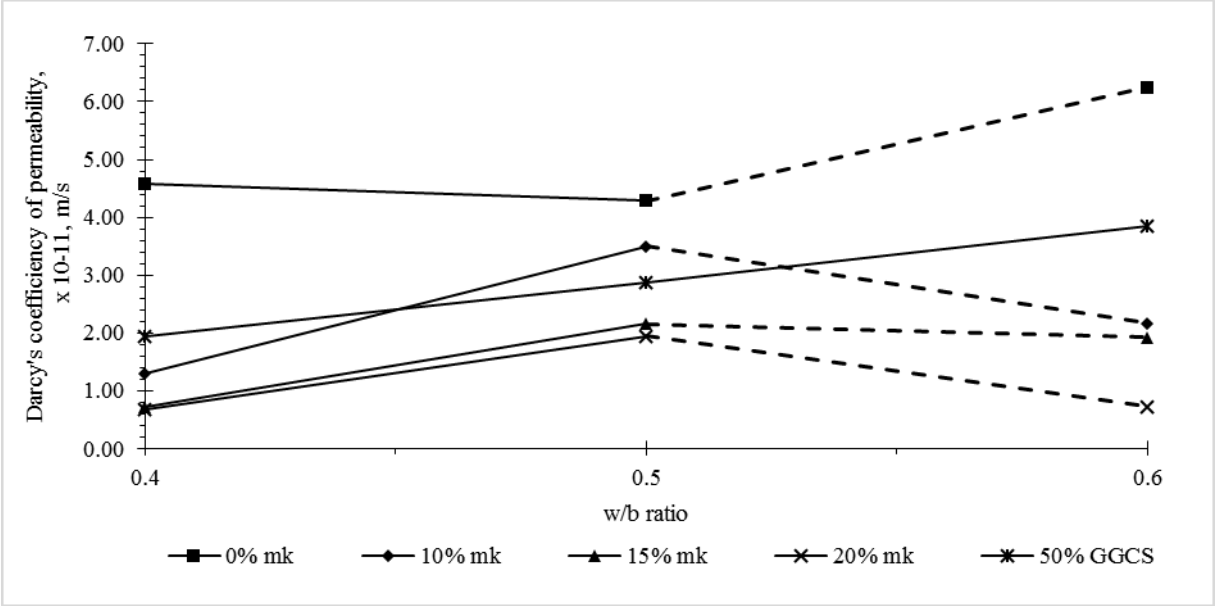

Figure 4.47: Darcy coefficient of permeability of concrete at different w/b ratio

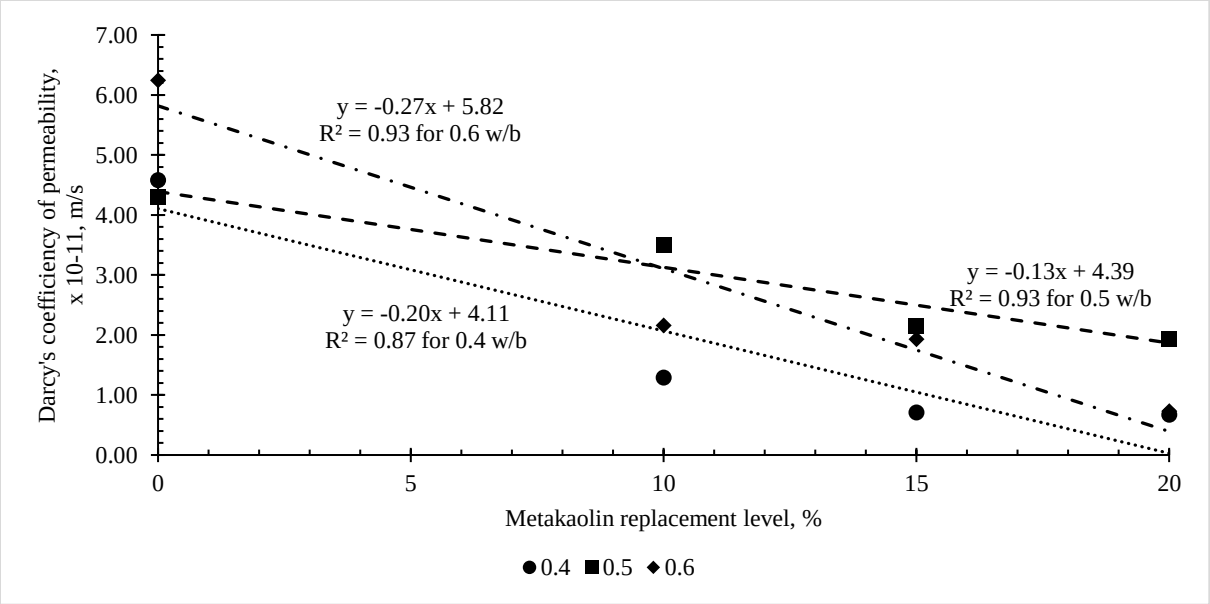

Figure 4.48: Darcy's coefficient of permeability of concrete with metakaolin at different w/b ratio

4.7.1.2. Water sorptivity index (WSI) results

WSI results present rate of capillary suction as well as water-penetrable porosity of concrete. WSI values shown in Figure 4.49, ranged between 5.5 and 7.5 mm/h$^{0.5}$ which indicated 'excellent' to 'good' quality concrete. The control concretes (0% mk) showed the highest WSI which implied that the concrete had a high rate of capillary suction and less resistance to water absorption. This was observed at all w/b ratios (0.4, 0.5, and 0.6). Sorptivity values decreased with increase in metakaolin, where the lowest values were observed at 20% mk, at all w/b ratios.

According to Razak, Chai and Wong, (2004), metakaolin reduces water sorptivity of concrete by firstly, reducing porosity, and secondly, reducing capillary pore connectivity. This was well verified in Figure 4.50 which presents porosity of concrete with SCMs (metakaolin and GGCS) at different w/b ratios. The porosity decreased with increase in metakaolin content. Figure 4.51 shows the slope of porosity decrease with increase in metakaolin content. The highest negative slope is observed in concrete with 0.6 w/b (-0.20) followed by 0.5 w/b (-0.12) and finally 0.4 w/b (-0.03), see Figure 4.51. It was clear that metakaolin had a higher potential for reducing porosity in concrete with high w/b than in low w/b.

The result of porosity of metakaolin concrete at 0.6 w/b was related to MIP results discussed in section 2.9.1. Considering that porosity measured by vacuum water saturation (Figure 4.50) were calculated on concrete, and total porosity measured by MIP test on mortar extracted from concrete.

By roughly assuming that 55% of concrete consists of mortar, then, converting the maximum porosity measured in 0.6 w/b concrete i.e. 10.54%, the value obtained is similar to 18% of the maximum total porosity obtained by MIP test on the same concrete. This concludes that vacuum water saturation method is a trusted method on evaluating porosity of concrete.

The performance of GGCS was not as good as expected since its sorptivity values were higher than those of the control concrete, especially at 0.4 and 0.5 w/b. However, in relation to porosity, GGCS decreased the porosity of concrete. The porosity values were 5.60%, 7.39%, and 7.35% at 0.4, 0.5, and 0.6 w/b ratio, correspondingly, which still were low values. At 0.4 w/b, the value was equal to that of 10% mk, although, at 0.5 and 0.6 w/b, the values ranged between those of 15% and 20% mk.

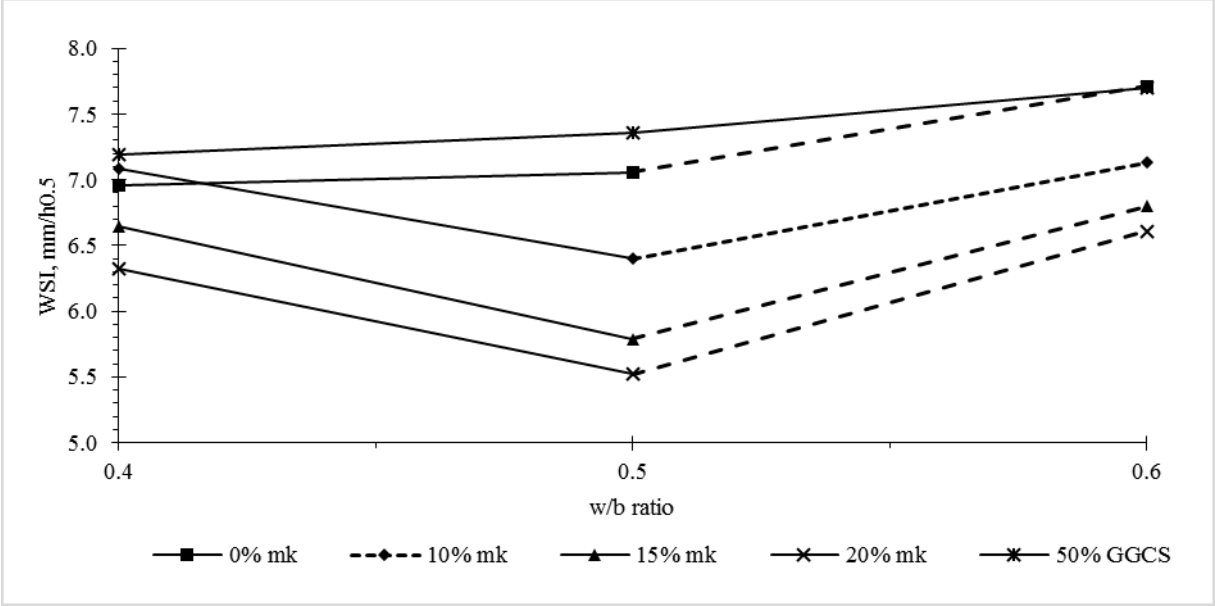

Figure 4.49: Water sorptivity index of concrete with w/b ratio

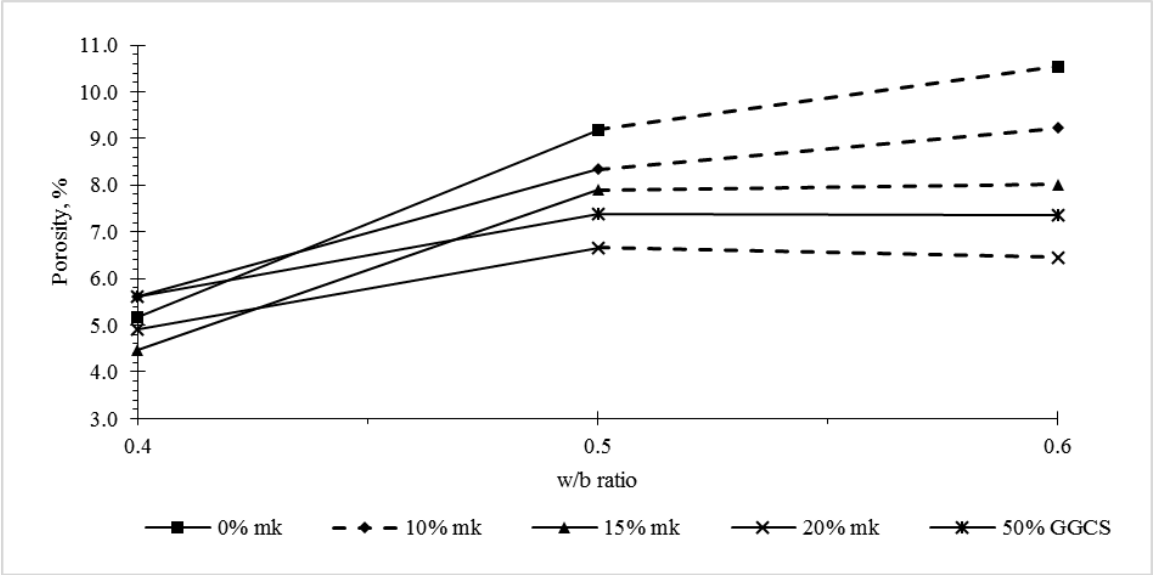

Figure 4.50: Porosity of concrete with metakaolin at different replacement levels and GGCS at 50% replacement level

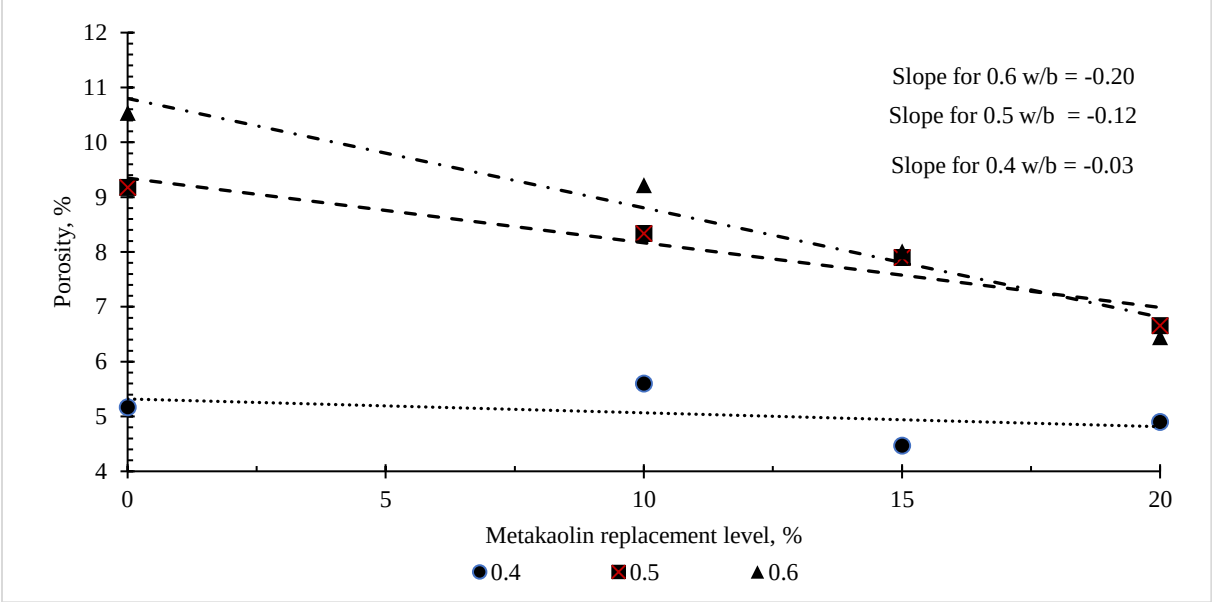

Figure 4.51: Relationship between porosity and metakaolin replacement levels

4.7.1.3. Chloride conductivity index results

As explained in the literature review chapter, section 2.9, the main factor that decreases the penetrability of chloride ion in concrete is a good quality of concrete with low permeability. This is enhanced by metakaolin and w/b ratio by altering pore structure of concrete. However, when metakaolin concrete is immersed in NaCl solution, metakaolin tends to increase chloride binding

capacity due to its high composition of alumina, thus, reducing the amount of free chloride ions for conductivity (Thomas *et al.*, 2012). In that case, the influences of w/b ratio and metakaolin content were found to play a key role in reducing penetrability of chloride ions, as shown in Figure 4.52.

The average CCI values decreased with decrease in w/b ratio as well as increase in metakaolin content. All concretes had CCI values below 0.75 mS/cm which ranked them as 'excellent' quality concrete, except the control concrete, at 0.6 w/b, which had a value between 0.75 and 1.50 mS/cm, although, it was still regarded as good quality concrete (Table 4.6). The CCI values of metakaolin at 0.4 w/b had magnitudes of 0.15, 0.11 and 0.10 mS/cm for 10%, 15%, and 20% mk, respectively. According to these values, it could be concluded that metakaolin concrete with low w/b had a very high resistance to chloride ion transport.

It was observed that as metakaolin replaced cement in concrete, CCI values decreased, whereby 20% mk had the lowest values. At 0.5 w/b, the values were still low, although the decrease of chloride conductivity with increase in metakaolin content was well defined. A similar trend was observed at 0.6 w/b, although the values were significantly higher compared to those at 0.5 and 0.4 w/b.

GGCS concretes also behaved well, their CCI values were 0.16, 0.26, and 0.31 mS/cm at 0.4, 0.5, and 0.6 w/b, respectively. These values were similar to those of 10% mk at 0.4 and 0.5 w/b. At 0.6 w/b, the value was similar to that of 15% mk, which could be inferred as the consequence of material differences. Generally, GGCS concrete behaved similar to 10% mk in terms of CCI.

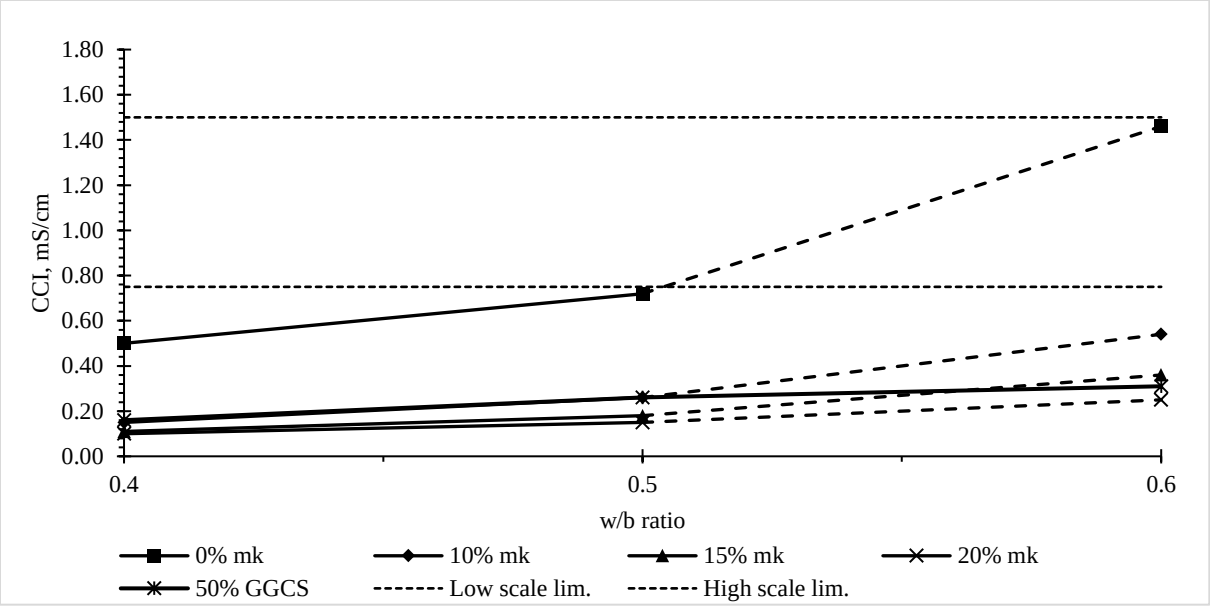

Figure 4.52: Chloride conductivity index (CCI) values of concrete at different w/b ratio

4.7.2. Alkali Silica Reaction (ASR), results

The results of ASR expansion of greywacke-mortar with different levels of metakaolin content were discussed as per ASTM C 1567. The level at which the expansion at 16 days was equal to an acceptable level, ASR was considered suppressed. The acceptable level is the expansion of tested mortar below 0.10% at 16 days after casting (this is the total of 24 h of casting and demoulding, 24 h of curing in the hot water, at 80ºC, and 14 days of immersion in NaOH solution). At this expansion, concrete with SCM is expected to have a low risk to deleterious expansion in the field. The expansion above 0.10% is indicative of potentially deleterious expansion.

From Figure 4.53, at 3 days of testing, a control mix had ASR expansion greater than 0.10%, whereby at 14 days, the expansion was considerably higher of 0.27%. This was true since the type of aggregate used was a known deleteriously reactive. For that reason, it was expected that the addition of metakaolin would reduce this deleterious behaviour.

The use of metakaolin at different levels showed excellent results. All mortar bars with metakaolin had an expansion less than 0.10% at 14 days, except that of 10% mk. The expansion values of the mortar with 10% mk at 12 and 14 days were slightly greater than 0.10%. This was similar to the results obtained by Ramlochan, Thomas and Gruber, (2000) at 10% mk replacement level. They postulated this was due to alkalinity increase in the pore solution over time, which was observed in pore solution analysis of the mortar containing 10% mk.

The expansion decreased with increase in metakaolin replacement levels to 20%. The reduction percentages shown in Table 4.7 indicated that 20% mk had the highest reduction of 89%. Its expansion was 0.03% at 14 days which could be regarded as insignificant. It was also observed that 10% mk (which had an expansion of approximately 0.10%) could reduce the expansion up to 61%, which was almost half of the control expansion. Despite that, 10% mk could still be considered as a potential replacement level to suppress ASR, only if the nature of aggregate was considered (Ramlochan, Thomas and K. a Gruber, 2000)

The possible reason of the high reduction behaviour in ASR was a high pozzolanic activity of metakaolin that reduced the alkalis in the pore solution, consequently, ASR was restricted to take place since there were fewer alkalis to react with. This phenomenon became more effective with increase in metakaolin content. The higher the metakaolin content, the higher the consumption of Na and K alkalis, and CH, subsequently, the reduction in the alkalinity in the pore solution.

In conclusion, metakaolin replacement levels above 10% were effective in suppressing ASR. However, 10% replacement level can also be considered since it was capable of reductions virtually to the 'sate' limit. The replacement level of metakaolin required to suppress deleterious expansion in concrete will significantly depend on the nature of the reactive aggregate (Ramlochan, Thomas and K. a Gruber, 2000). Therefore, it is recommended that before considering using metakaolin to suppress ASR, an effective replacement level must be established in combination with the given aggregate.

Table 4.7: ASR expansions at 14 days and metakaolin potential of expansion reduction

Mix	Expansion, % at 14 days	Reduction, %
0% mk	0.27	0%
10% mk	0.10	61%
15% mk	0.08	71%
20% mk	0.03	89%

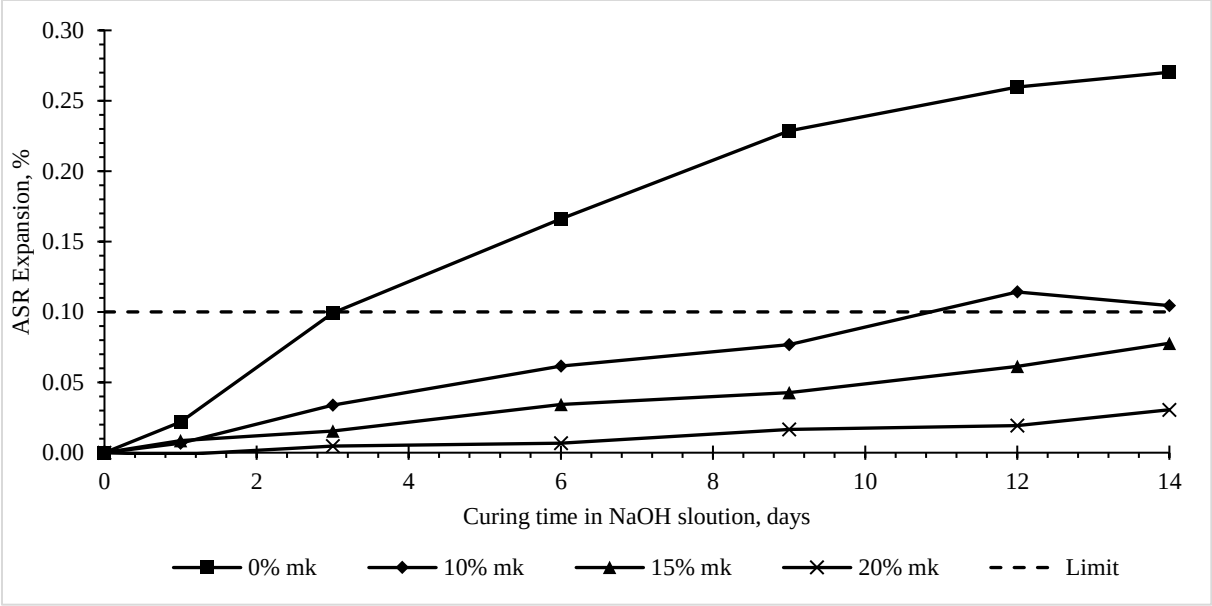

Figure 4.53: ASR expansion of mortar bars with metakaolin

4.7.3. Accelerated carbonation results

Chapter 3, section 3.8.3 give details of the accelerated carbonation testing. To summarise, the CO_2 concentration used in the tests was 2 ± 0.1%, and the environment of exposure was 20 ± 2°C, and RH of 65±1%. The depths of carbonation were calculated as the average of twelve measurements on the surfaces of two 20 mm concrete cuts (six measurements on each, see Figure 4.54) at 28, 56, and 90 days of CO_2 exposure, using the phenolphthalein indicator method. It was observed that at the end of 90 days of exposure, concretes with 0.4 w/b ratio had no measurable carbonation regardless of the type and quantity of SCMs used. This was attributed to the fact that at a low w/b ratio, concrete had high resistance to gas permeability, as observed in the OPI test (section 4.7.1).

Carbonation occurred in concretes with 0.5 and 0.6 w/b ratios as shown in Figure 4.55 and Figure 4.56. The error bars represent the standard deviation of the twelve carbonation depth measurements. The rate of carbonation was higher for the concrete with 0.6 w/b than that with 0.5 w/b. The depth also increased with time of carbonation exposure, whereby the highest depths were observed at 90 days of exposure. The high carbonation rate in the 0.6 w/b concretes was associated directly with the influence of high porosity that accelerated the permeability of CO_2. As w/b ratio decreased, the porosity also reduced, hence, there was higher resistance to permeability.

The influence of metakaolin on carbonation was observed in these studies. The observations in this study differed from the literature. For example, these results opposed those of Kim, Lee and

Moon, (2007) who observed a higher carbonation depth by as much as 100 to 370% for concretes with metakaolin. Metakaolin undergoes pozzolanic reaction by consuming CH that is responsible for decelerating the carbonation reaction, hence, the higher a carbonation effect is expected for concrete with metakaolin. However, in this study, it was observed that at 0.6 w/b, the control and metakaolin concretes had similar carbonation depths at the ages of 56 and 90 days of exposure, while at 28 days, carbonation depths decreased with metakaolin content. At 0.5 w/b, carbonation depths, at all exposure ages, decreased with metakaolin, whereby 20% mk had very low depths of between 1 to 3 mm.

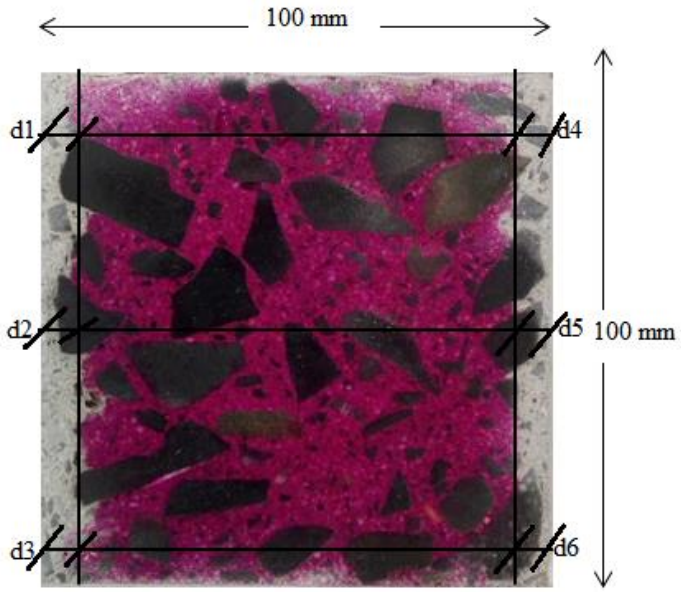

Figure 4.54: Measurement of carbonation depth on 0.6 w/b concrete with 10% mk, at 56 days of exposure

The observed high potential of metakaolin for resisting carbonation was attributed in this work to its influence on reducing concrete permeability as observed in section 4.7.1 (Bucher *et al.*, 2017). This implied that metakaolin had a less detrimental carbonation effect since the chemical process was compensated by a physical process – that od matrix densification and improved impermeability. Generally, it can be concluded that metakaolin concrete with high resistance to gaseous permeation has a high potential in resisting diffusion of CO_2.

Carbonation of concretes with metakaolin and GGCS was also compared. GGCS concretes was found to have substantially higher carbonation compared to the control and metakaolin concretes at 0.5 and 0.6 w/b. This was because the matrix densification of GGCS concretes was not marked as for metakaolin concretes, thus, it accelerated carbonation by allowing the diffusion of CO_2 gas.

Therefore, as far as carbonation was concerned, metakaolin performed better in resisting carbonation than GGCS, provided that the low permeability of concrete was ensured.

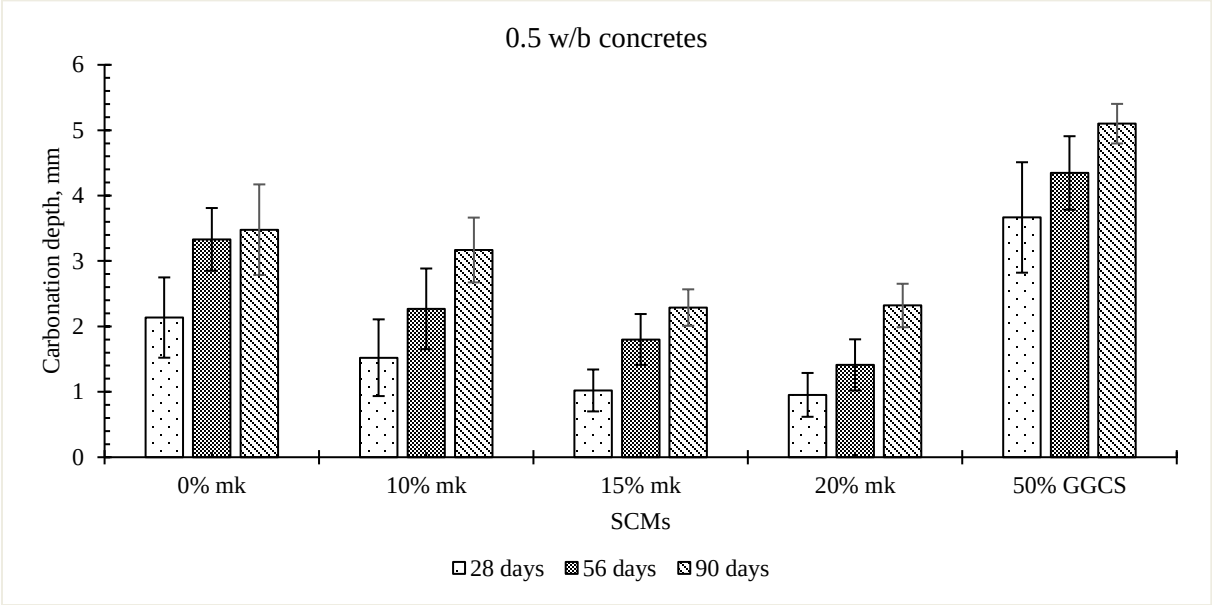

Figure 4.55: Carbonation depths of concrete at 0.5 w/b ratio, after 28, 56, 90 days of accelerated carbonation

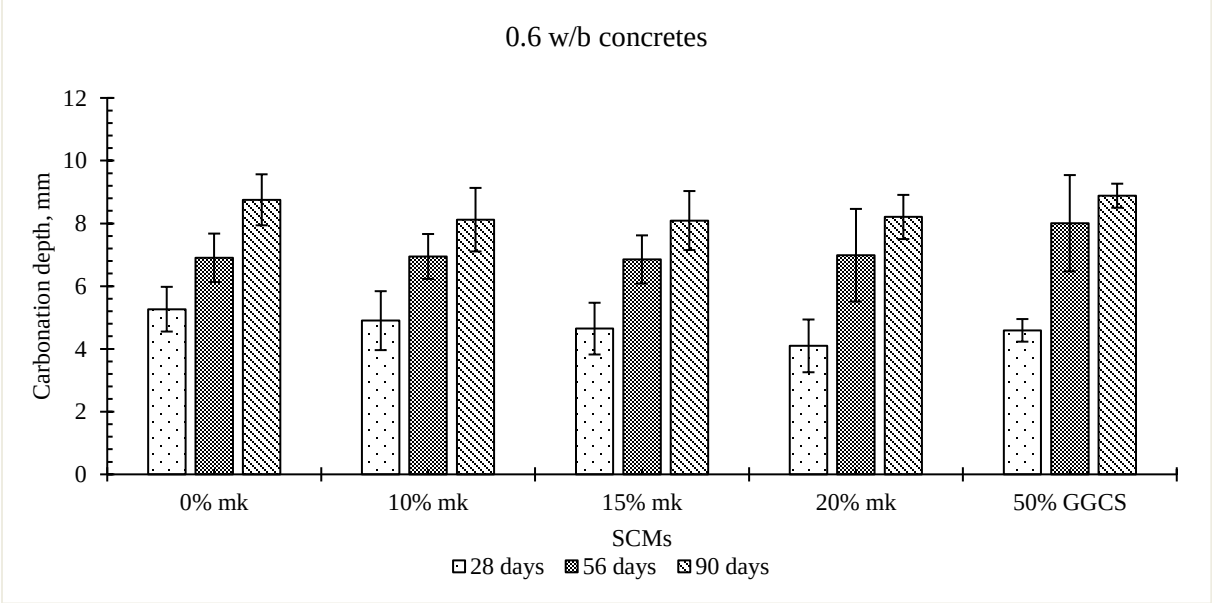

Figure 4.56: Carbonation depths of concrete at 0.6 w/b ratio, after 28, 56, 90 days of accelerated carbonation

4.7.4. Bulk chloride diffusion results

The results of chloride diffusion are presented in Figure 4.57, Figure 4.58, and Figure 4.59 for 0.4, 0.5 and 0.6 w/b ratios, respectively. The chloride ion (CI^-) content by mass of cement was measured by using titration method and the profile was drawn using Fick's second law of diffusion from CI concentration–depth profiles after 90 days of ponding concrete cylinders in the NaCl solution. It was observed that CI concentration generally increased with w/b ratio. At a lower w/b, there was less CI concentration compared to that at a higher w/b ratio. This was generally associated with the low penetrability (as a function of low porosity) of concrete with low w/b ratio (Stanish, Hooton and Thomas, 1997).

At 0.4 w/b, the control mix profile had the highest values which illustrated the highest rate of chloride ingress, while the profiles of metakaolin concretes were bunched together. At 0.5 w/b, a clear influence of metakaolin on reducing the rate of chloride diffusion was observed. As metakaolin content increased, the diffusion decreased at a greater rate. Also, metakaolin concrete profiles showed a steeper slope compared to the control. This illustrated the greater influence of metakaolin on reducing CI penetration. At 0.6 w/b, the control profile had the highest values, followed by 10% and 15% mk, while 20% mk had the lowest values.

Table 4.8 shows the CI penetration depth in all concretes. CI penetration depth was derived by observing a profile depth at which the initial CI content was initially detected. It was observed that the penetration depth increased with w/b ratio, while decreased with metakaolin content. The control concrete with high w/b ratio had the highest depth of penetration. The addition of metakaolin reduced the penetration at a higher degree. The lowest penetration depth was observed in 0.4 w/b concrete with 15% and 20% metakaolin contents, although it was observed that the effect of metakaolin was similar independent of replacement rate. It was observed that metakaolin had no much positive effect at 0.6 w/b as it was previously observed in other concrete properties such as strength.

Table 4.8: CI penetration depth of concrete with metakaolin at different w/b ratios; bulk diffusion tests, after period of 90 days in chloride solution

	CI penetration depth, mm			
Metakaolin, %	0	10	15	20
0.4 w/b	8.0	6.4	4.8	4.8
0.5 w/b	15.2	10.4	10.4	9.6
0.6 w/b	19.2	18.0	18.0	16.8

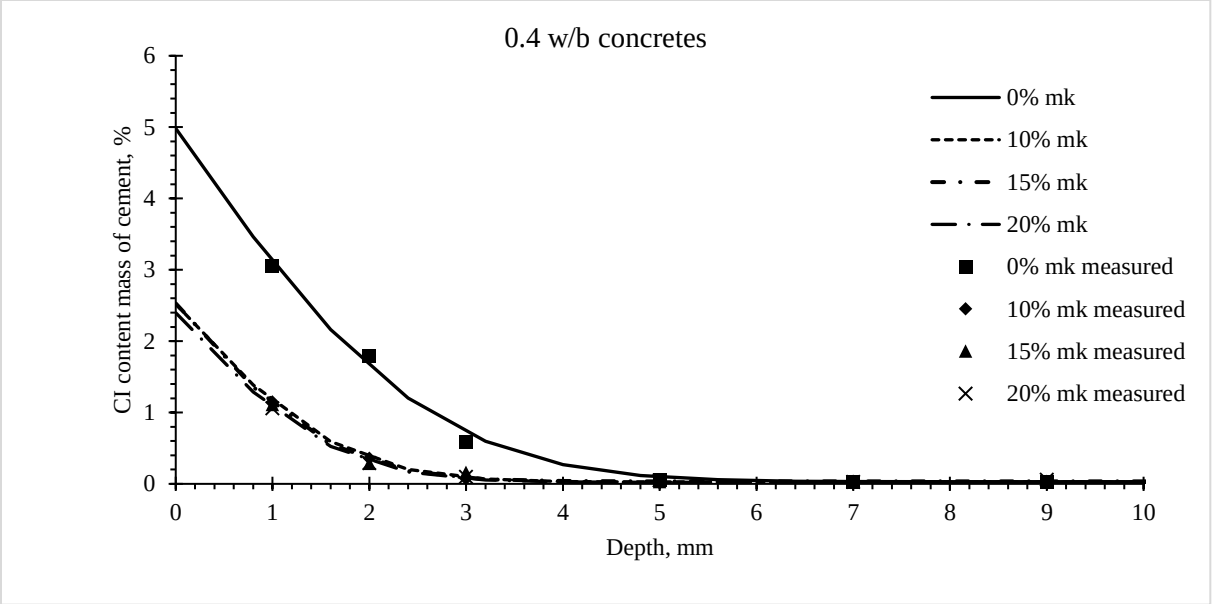

Figure 4.57: Chloride ion (CI) diffusion profiles for 0.4 w/b concretes after 90 days of immersion in NaCl solution

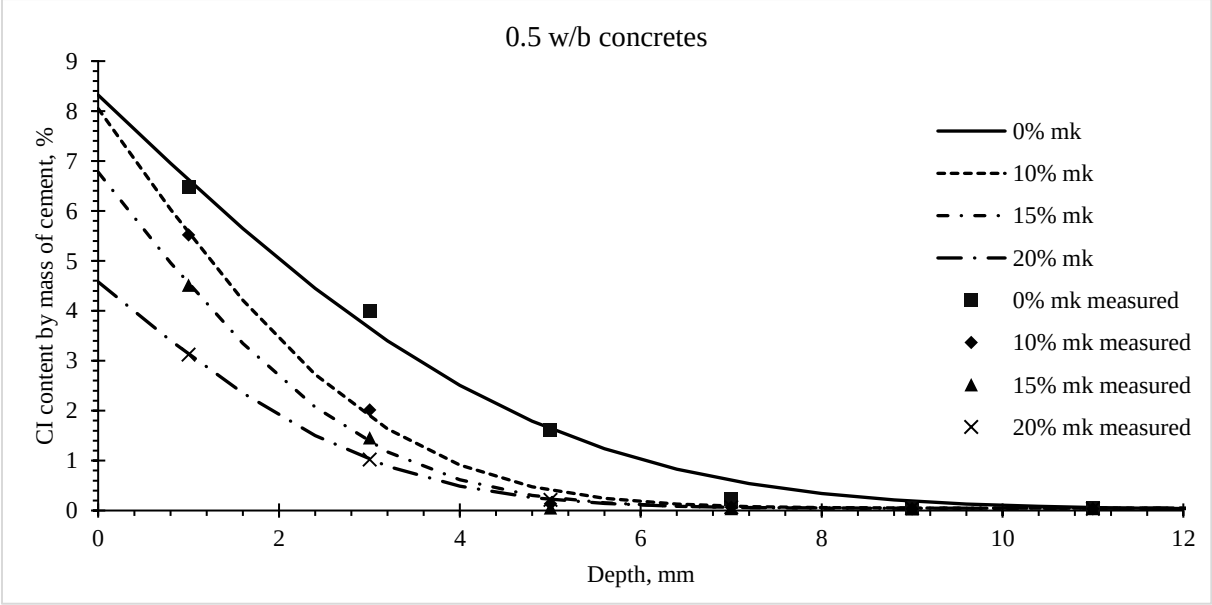

Figure 4.58: Chloride ion (CI) diffusion profiles for 0.5 w/b concretes after 90 days of immersion in NaCl solution

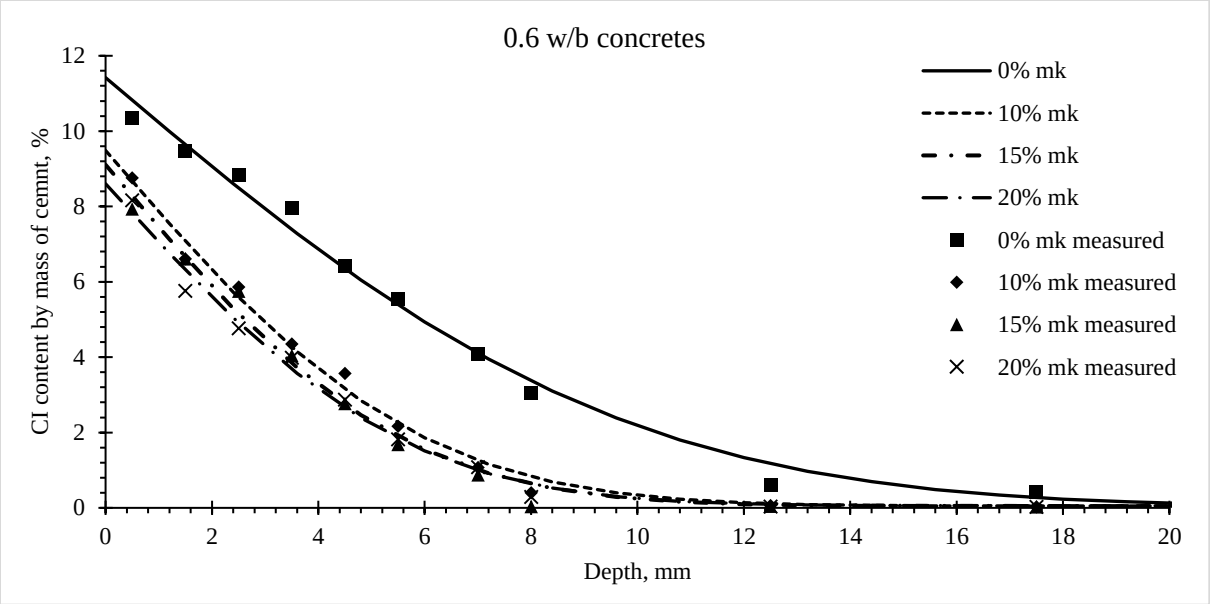

Figure 4.59: Chloride ion (CI) diffusion profiles for 0.6 w/b concretes after 90 days of immersion in NaCl solution

Figure 4.60 shows the apparent chloride diffusion coefficients of concretes with metakaolin at different w/b ratios. It was observed that 0.6 w/b had the highest diffusion coefficients which substantially decreased with metakaolin content. At 0.4 and 0.5 w/b ratios, the diffusion coefficient and metakaolin content were also inversely related. As metakaolin content increased up to 15%, diffusion coefficient decreased, while an insignificant increase was observed at 20% mk.

The reduction of apparent CI diffusion coefficient of the control with increasing metakaolin content is shown in Table 4.9. It is clearly seen that approximately 60% of CI diffusion coefficient of the control concretes was decreased by the additions of metakaolin. The highest reductions were observed at 15% mk at all w/b ratios followed by 20% then 10%.

This influence of metakaolin in reducing the ingress of chloride ions in concrete by diffusion is associated with two factors. Firstly, the potential of metakaolin on affecting the pore structure of concrete by the refinement and discontinuation of pore networks (see section 4.5.1) and densification of concrete matrix by the influence of its pozzolanic and filler effects. As the microstructure of concrete was improved by metakaolin, the chloride diffusivity was reduced, hence, less CI was detected along the profile of metakaolin concrete. Secondly, the capacity of metakaolin to physically and chemically bind with free chloride ions dissolved in the pore solution (Chloride binding capacity). This was associated with the quantity of alumina component in metakaolin that binds with free chloride ions, thereby reducing the diffusion rate. The higher the

metakaolin content, the higher the chloride binding capacity, and the lower the diffusion rate (Stanish, Hooton and Thomas, 1997; Thomas *et al.*, 2012).

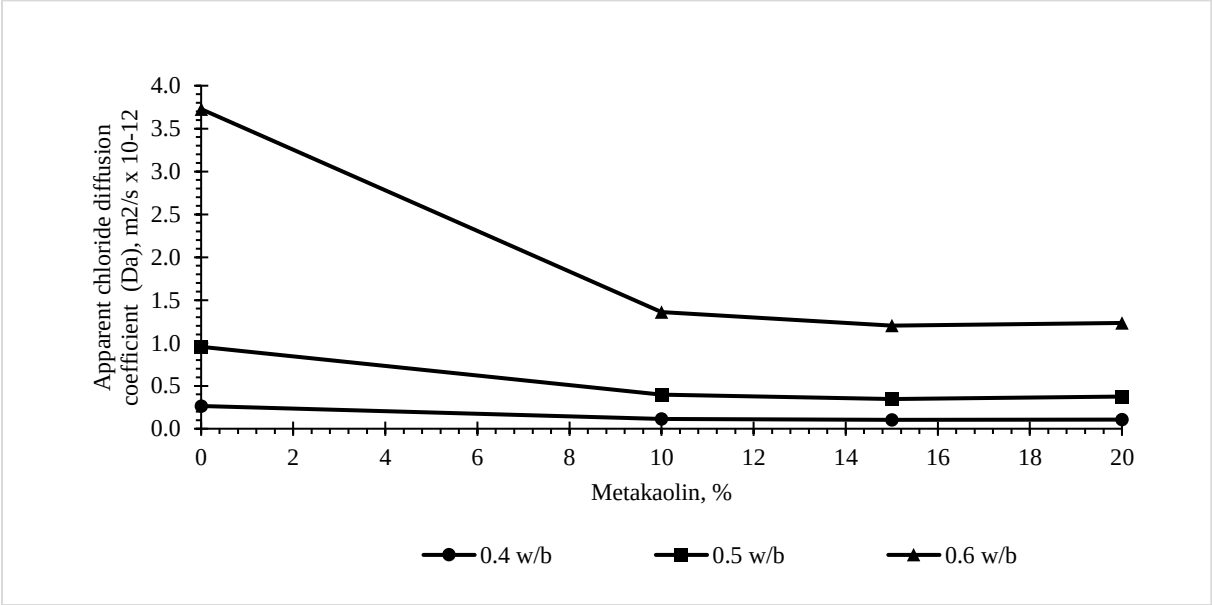

Figure 4.60: Apparent CI diffusion coefficient of metakaolin concretes at different w/b ratio

Table 4.9: Reduction of apparent CI diffusion coefficient of metakaolin concretes

	Reduction of Apparent CI diffusion coefficient, %		
Metakaolin, %	10	15	20
0.4 w/b	57.6	60.9	60.0
0.5 w/b	58.3	63.8	60.6
0.6 w/b	63.5	67.7	66.9

4.7.5. Closing remarks of the section

Generally, it was concluded that the inclusion of metakaolin in concrete significantly improved durability of concrete. In terms of durability index, three transport properties (sorptivity, permeability and conductivity) were observed. The results showed that metakaolin produced concretes with excellent quality. This was influenced by metakaolin potential on altering concrete microstructure, both chemically and physically. The substantial effects were pronounced when metakaolin was incorporated in concrete with high w/b ratio. This remarkable behaviour was also noticed in the strength properties of concretes.

The potential of metakaolin on mitigating ASR was also studied, whereby greywacke aggregates were used. The results showed that ASR expansion of these aggregates reduced with increasing metakaolin content. The highest expansion reduction was observed at 20% replacement rate, although more than 50% reduction was also achieved at the lowest replacement rate. It was then advised that before considering using metakaolin for suppressing ASR of a certain deleterious reactive aggregate, the effective replacement rate must be established.

In terms of carbonation, metakaolin was found having a less detrimental issue on concrete. The results showed that carbonation depth was affected by metakaolin depending on w/b ratio. At 0.4 w/b ratio, no carbonation was observed, at 0.5 w/b, carbonation depth decreased with metakaolin content, while at 0.6 w/b, all concretes showed approximately equal depths. This was attributed to the compensation of carbonation effect by the physical effects of metakaolin in concrete.

Moreover, metakaolin reduced chloride bulk diffusion in concrete. With increasing metakaolin content and decreasing w/b ratio, CI diffusion coefficient decreased. CI penetration depth was remarked higher for control concretes, while showing similar depth for metakaolin concretes at the same w/b ratio. This potential of metakaolin on reducing chloride diffusion in concrete was inferred to be caused by metakaolin chloride binding capacity and its ability to alter concrete microstructure.

The potential of GGCS on improving durability of concrete in comparison to metakaolin was also studied. In terms of durability index, GGCS produced good quality concretes, while in terms of carbonation, GGCS increased carbonation depth. This was because the matrix densification of GGCS concretes was not as marked as for metakaolin concretes.

4.8. CLOSURE

This chapter was divided into seven sections. The Introduction presented the scope and context of the chapter. The Morphology of Cement, Metakaolin and other SCMs described the morphology of cementing materials used in this study (metakaolin, CEM II A-L 52.5 N, GGCS, silica fume and fly ash). The Pozzolanic Activity of Metakaolin was discussed to meet two objectives; metakaolin reactivity i) in mortar at different replacement rate, in terms of strength development, heat of hydration, and CH consumption, and ii) in mk-portlandite system by comparing with the performance of other SCMs-portlandite system (fly ash, GGCS, and silica fume), in terms of heat of hydration and CH consumption. The Properties of Fresh Concrete with Metakaolin discussed

the results obtained in the setting time and slump (workability) test. The Hardened Concrete Made with Metakaolin discussed the results of MIP test, compressive strength, and tensile splitting strength tests. The Deformation of Behaviour of Concrete with metakaolin discussed the results of static elastic modulus, creep, and drying shrinkage tests of metakaolin concrete. Finally, the Durability Properties of Concrete with Metakaolin discussed the results of DI tests, acceleration mortar bar test, acceleration carbonation test and chloride bulk diffusion.

5. CHAPTER FIVE: CONCLUSIONS AND RECOMMENDATION

5.0. INTRODUCTION

This chapter draws conclusions based on the objectives, literature review, and results obtained in this study. The main intentions are firstly, to clarify that this study has met its main objective that is divided into four compressed specific objectives, and secondly, to show that the gaps highlighted in the literature are filled, at least in terms of the scope of this study. Therefore, the chapter discusses and draws conclusions based on the specific objectives. At the end of the chapter, recommendations are provided.

5.1. SPECIFIC CONCLUSIONS

The followings are the discussion and conclusions of this study based on the specific objectives.

5.1.1. Characterization of metakaolin in terms of its morphology and pozzolanic activity

5.1.1.1. Metakaolin in comparison to other SCMs

The morphology of metakaolin particles was identical to that of halloysite. Fly ash and silica fume particles were identified mainly as spheres, although the size of fly ash particles was larger than silica fume. GGCS particles were more like cement particles in shape and texture, i.e. angular and glassy, but different in sizes.

In terms of pozzolanic activity which was analysed by two methods, isothermal calorimetry and TGA on the special paste mixtures of SCMs and portlandite (SCM-portlandite system), it was found that metakaolin generated more heat of hydration followed by GGCS, while fly ash and silica fume seemed to generate lower heat. Metakaolin also was found to consume more CH in the mixture followed in order by silica fume, GGCS, and fly ash. In terms of chemically bound water, metakaolin had the highest amount followed by GGCS, silica fume, and fly ash. Through this analysis, it was concluded that metakaolin had the highest pozzolanic activity. Generally, this was associated with its high reactivity which was contributed by various factors such as the means of its production, producing highly reactive particles and the origin of its raw material (kaolin clay).

5.1.1.2. Pozzolanic activity of metakaolin at different replacement levels

This was analysed on the mortar mixes which were prepared by replacing PC with metakaolin at replacements of 0%, 10%, 15%, and 20%. The pozzolanic indices used for analysis were the strength activity index (SAI), heat of hydration, and CH consumption.

The results of the SAI showed that mortar containing 15% metakaolin had the highest SAI over mortar with 20% mk. This was generally attributed to the dilution effect.

In terms of heat of hydration, two methods; semi-adiabatic calorimetry and isothermal calorimetry, were used for analysis. The results from both methods gave the same conclusion that the total heat of hydration of the cement blend decreased with increasing metakaolin content. Three effects i.e. pozzolanic reaction, dilution and acceleration effects were inferred as the main causes of this decrease. It was also observed that isothermal calorimetry generated a higher total heat than semi-adiabatic calorimetry. The difference was associated with the insulation effect on the semi-adiabatic calorimetry, that caused heat loss.

The potential of metakaolin to consume CH generated by hydration of cement, the so-called 'pozzolanic reaction' was also studied relative to the chemically bound water. It was found that the consumption of CH increased with metakaolin content in the cement blend. The maximum consumption was observed at 20% replacement level, where more than half of CH produced at 56 days was consumed by metakaolin. The chemically bound water was found to increase with time of hydration, as the degree of hydration increased, while it decreased with metakaolin content as a result of the dilution effect. However, this contrasted with the literature since the inclusion of metakaolin was expected to increase the chemically bound water as the result of metakaolin potential in increasing the hydrated products.

Generally, it was concluded that the pozzolanic activity of metakaolin in mortar in terms of strength activity index, heat of hydration, CH consumption and chemically bound water increased with metakaolin content, although some variations were observed in strength activity. Also, a further study on understanding the influence of metakaolin on consuming CH content and chemically bound water is required. This was because the results in certain respects contradicted and did not support the literature.

5.1.2. Influence of metakaolin on fresh and hardened concrete properties, and comparison of performance with GGCS concretes

5.1.2.1. Setting times

The literature generally indicates that the inclusion of metakaolin in concrete affects setting times by increasing the final setting time, while some contradictions exist on its influence on the initial setting time. It was also noted that there was no clear relationship between increasing metakaolin content and setting times. In this study, it was found that, at any replacement level starting from 10%, metakaolin increased both initial and final setting times. This was attributed to the metakaolin dilution effect and coating effect on the cement particles that delayed the hydration reaction. It was observed that there was no clear relationship between metakaolin content and setting times since the highest setting times were observed at 10% mk, and a further increase in metakaolin resulted in the reduction of setting times. This agreed with some literature, where it was reasoned as the result of decreasing water content with increasing metakaolin content, although this was not experienced in this study.

5.1.2.2. Workability

The inclusion of metakaolin in concrete, in the literature, was found to decrease the workability. This was totally supported by this study. It was observed that the workability of concrete decreased proportionally with increasing metakaolin. This was revealed by the quantity of SP dosage used to achieve a slump of 100 mm in all concrete mixes. The SP dosage increased with decrease in w/b ratio and increase in metakaolin content, with the highest quantity observed at 20% mk for 0.4 w/b concrete. This was caused by the fineness of metakaolin particles with higher water demand to wet the surfaces, therefore, to overcome the effect, more SP dosage was required to disperse the particles. By comparing metakaolin and GGCS, it was found that GGCS had less effect on workability compared to metakaolin since its SP dosage was nearly equal to that in control concretes.

5.1.2.3. Pore structure and refinement

The observation on the effect of metakaolin on concrete pore structure agreed with the literature despite the limitation on the number of samples for testing. Metakaolin was found to improve the microstructure of concrete by firstly, altering the pore structure, particularly at the early age, thereby reducing pore size from macropore to nanopores, and secondly, by creating discontinuous

pore connectivity. This was attributed to metakaolin pozzolanic and filler effects that increased the hydrated products in concrete that filled macropores and densified the concrete matrix. The effects were more marked with increasing metakaolin content. The total porosity of concrete was less affected by metakaolin content, although it was affected by hydration time. As hydration time increased, total porosity decreased. This was because of on-going hydration reaction producing more hydrated products to fill the pores. Finally, it was concluded that the inclusion of metakaolin in concrete has little effect on decreasing total porosity, instead, it improved the pore microstructures by reducing pore size from large diameter to the small diameter and discontinuing the pore networks.

5.1.2.4. Compressive strength

Compressive strength as one of the key properties of concrete was studied with metakaolin at different replacement levels, and compared to concrete with 50% GGCS. The observations showed vary marked differences since it turned out that this metakaolin was very reactive. Metakaolin potential on compressive strength increased with its content, with the highest strength observed at 20% replacement level regardless of the w/b ratio. It was also interesting and noteworthy that metakaolin had the greatest influence on the concrete with the higher w/b ratio, especially at early ages. This was attributed to its high pozzolanic activity and acceleration of the hydration reaction. GGCS concrete had less potential in enhancing compressive strength since its strengths were very similar to those of the control. Therefore, it was concluded that metakaolin had an enhanced strength effect compared with GGCS, which could give it an advantage to be used as a substitute for GGCS in concrete.

5.1.2.5. Tensile splitting strength

In the literature, it was observed the addition of metakaolin improved tensile splitting strength of concrete, with maximum strength being achieved at 10% and 15%; a further increase in metakaolin content caused a strength decrease. This was reasoned as the result of dilution effect. The conclusion made in the literature was not supported by the results obtained in this study. It was observed that tensile splitting strength of concrete increased with increase in metakaolin content, with an approximately 41% increase in the strength of control concrete at a 20% metakaolin content in 0.6 w/b concrete at 7 days. GGCS concretes in comparison to metakaolin had lower strengths especially at early ages, with GGCS concretes experiencing a decrease in tensile strength

below the control. Because of this, metakaolin was considered superior to GGCS in terms of enhancing tensile splitting strength.

It was observed that tensile splitting strength of metakaolin concrete followed a $2/3^{rd}$ power law with compressive strength. Therefore, it was concluded that tensile splitting strength of metakaolin concrete could be well predicted by using the CEB-FIP model expression (equation 4.1).

5.1.3. Influence of metakaolin on the deformation behaviour of concrete

5.1.3.1. Static elastic modulus

The literature had a limited number of studies on the influence of metakaolin on elastic modulus of concrete. However, the few studies found raised some contradictions on whether elastic modulus was directly proportional to metakaolin content. In this study, it was found that metakaolin increased the elastic modulus of concrete, although there was no definite relationship between metakaolin content and elastic modulus. Apart from that, elastic modulus of metakaolin concretes was affected by the w/b ratio, with a lower w/b ratio metakaolin concrete achieving high but predictable elastic modulus values. Moreover, the maximum elastic modulus increase with hydration time was observed at a higher w/b, which implied that as pozzolanic and hydration reactions took place, concretes with higher w/b became stiffer. However, comparing GGCS and metakaolin concretes, both SCMs showed good performance, therefore, there was little to choose.

It was also found that the elastic modulus of metakaolin concrete could be predicted by using the ACI empirical formula shown in equation 4.2, if its compressive strengths were known. Further, the elastic modulus of metakaolin concrete depends on the type of aggregates used, so by knowing the type of aggregate and compressive strength achieved, elastic modulus can also be predicted by using equation 4.3 which was evaluated from Fulton, (2009:114-116).

5.1.3.2. Creep and drying shrinkage of metakaolin concrete

Studying the influence of metakaolin on concrete creep was emphasized by a limited number of studies found in the literature, which made it difficult to draw conclusions about metakaolin effects on enhancing creep. Only one study was found, and it concluded that metakaolin decreased both basic and total creep of concrete (Brooks and Johari, 2001). This finding was supported by this study, as it showed that with increasing metakaolin content, creep strain, specific creep and creep coefficient were decreased. However, by normalising the effect of compressive strength in metakaolin concrete, it was found that metakaolin influence had no strong effect on creep

intrinsically, but the main factor that influences metakaolin creep was a higher compressive strength.

In terms of drying shrinkage, it was concluded that drying shrinkage decreased with increasing metakaolin content, while it increased with hydration time. This generally supported various studies reviewed in the literature. The scope of this study precluded a focus on filling the gap highlighted on the influence of metakaolin on autogenous shrinkage. Therefore, a further study on this is required.

5.1.4. Durability of concrete containing metakaolin in terms of its potential to reduce concrete penetrability and to mitigate ASR

5.1.4.1. Concrete penetrability

The penetrability of concrete with metakaolin was studied in terms of its potential to improve transport properties such as sorption, permeation, conductivity, and diffusion. The results were obtained by studying durability indexes (OPI, WSI, and CCI) and chloride bulk diffusion.

The literature concluded that water sorptivity was inversely related to metakaolin content, supported by this study. It was observed that metakaolin reduced water sorptivity by refining concrete porosities. This was evidenced by the results of porosity calculated by vacuum water saturation which decreased with increasing metakaolin content. Moreover, the porosities calculated by this technique correlated well with total porosities calculated by MIP test on the mortars extracted from similar concretes. It was concluded that the vacuum water saturation method is a reliable method to evaluate porosity of concrete.

In terms of gas permeability and chloride conductivity, the study supported the literature by concluding that metakaolin had a significant influence on reducing gas permeability and chloride ion conductivity. By comparing metakaolin and GGCS for both gas permeability and chloride conductivity, it was found that the potential of GGCS to improve these transport properties of concrete was equivalent to the potential of metakaolin when used in concrete at 10% replacement level. Generally, both SCMs performed well in improving concrete permeability and conductivity.

In terms of chloride ion diffusion, it was found that the inclusion of metakaolin decreased the rate of chloride diffusion which resulted in the decrease of chloride penetration depth. The chloride diffusion coefficient decreased with increasing metakaolin content and decreasing w/b ratio,

although 15% mk showed the highest reduction followed by 20% mk. The influence of metakaolin on the concrete microstructure and its high chloride binding capacity were considered as the main factors for the reduction. Finally, it was concluded that incorporating metakaolin in concrete would generally improve concrete penetrability.

5.1.4.2. Alkali silica reaction (ASR)

The potential for metakaolin to suppress ASR in concrete with reactive greywacke aggregates was effectively illustrated by increasing metakaolin content in the mortar. With increasing metakaolin content ASR expansion decreased, such that at 20% mk, almost 90% of ASR expansion of control concrete was reduced. This was attributed to the effectiveness of metakaolin to consume alkali ions in the concrete, thus reducing the susceptibility of concrete to ASR attack. This supported the literature, however, it was suggested that before using metakaolin in concrete to suppress ASR, an effective replacement level must be established in combination with the given aggregate.

5.1.4.3. Carbonation effect

CH content in concrete is responsible for retarding carbonation. The inclusion of any pozzolanic material is therefore regarded as a 'carbonation accelerator' since it consumes CH. With this fact, metakaolin concretes were expected to have higher carbonation depths than the control mix, although the results in this study observed the opposite. Using accelerated carbonation tests, it was found that the influence of metakaolin on carbonation depended on w/b ratio, since at 0.4 w/b, all concretes experienced no carbonation, at 0.5 w/b, carbonation depths decreased with increasing metakaolin content, while at 0.6 w/b, all concrete had similar carbonation depths. The influence of metakaolin on densifying the concrete matrix was attributed as the main reason for the potential to resist carbonation. In comparison to metakaolin, GGCS was found to accelerate carbonation. Generally, it was concluded that metakaolin had no detrimental effect on carbonation.

5.2. CONCLUSION SUMMARY.

Metakaolin that is locally available in the Western Cape has mostly positive influences on enhancing properties of concrete;

i. It has a high pozzolanic activity in terms of heat of hydration and CH consumption and chemically bound water in comparison to GGCS
ii. It decreases heat of hydration when blended with cement. With increasing metakaolin content, total heat generated decreases.

iii. It is effective in consuming CH produced by the hydration reaction. With increasing metakaolin content, the CH consumption increases.

iv. It affects fresh properties of concrete by increasing the setting times and reducing workability of concrete.

v. It alters the microstructure of concrete by refining the pores and reducing pore connectivity. However, it has no effect on the reduction of total porosity.

vi. It substantially increases the compressive strength and tensile splitting strength of concrete, with compressive strength and tensile splitting strength increasing with increase in metakaolin content.

vii. It slightly increases the static elastic modulus of concrete, the trend being independent of the replacement level.

viii. It decreases creep strain, specific creep and creep coefficient, with the influence being attributed to the increased compressive strength. The higher the metakaolin content, the higher the reduction in both creep and drying shrinkage.

ix. The influence of metakaolin on reducing penetrability of concrete is excellent. Metakaolin decreases gas permeability and sorptivity of concrete with increase in metakaolin content. It also increases the resistance to chloride ion transport, with higher resistance being achieved at higher metakaolin contents.

x. Metakaolin shows a high potential in suppressing ASR expansion in concrete with a reactive greywacke aggregate. Its potential was evident even at the lowest replacement level, however, increased content resulted in very low expansions.

xi. Metakaolin retards carbonation by reducing concrete permeability. Its potential is more pronounced in concretes with low w/b ratio.

By comparing metakaolin and GGCS, metakaolin generally exhibits better concrete properties than GGCS. Thus, at the scarcity of GGCS, metakaolin can be considered as a suitable substitute for GGCS in Western Cape concrete. However, the replacement level of metakaolin is less compared to that of GGCS. This raises a question on the reduction of cement quantity in the construction industry.

5.3. RECOMMENDATIONS

The followings are the recommendations:

i. A further study on understanding the influence of metakaolin on consuming CH content and chemically bound water is required. This is because the values observed were underestimated. Therefore, proper techniques must be employed to obtain the desired results.
ii. The scope of this study precluded a focus on filling the gap highlighted on the influence of metakaolin on autogenous shrinkage and flexural strength. Therefore, further studies on these areas are required.
iii. Carbonation prediction model of concrete with metakaolin was not studied. It will have a huge contribution to the body of knowledge to study the influence of metakaolin on carbonation by establishing the prediction model.
iv. A single metakaolin derived from one source in the Western Cape was studied, although it will make a difference to study various metakaolin from other sources. Studying this will be beneficial and economical since it will allow the utilization of various kaolin deposits found in South Africa that are not yet exploited.
v. Study on the effect of metakaolin in the environment and sustainability is also required. This is to evaluate its contribution to serving the world against CO_2 emission and utilization of natural resources.
vi. The questions on the cost-effectiveness, and the awareness and willingness of industry to incorporate metakaolin suggest for further studies on the economic comparison of metakaolin with GGCS, and the use of calcined clay which is not manufactured in a sophisticated way as metakaolin should be considered.

This study adds to the body of knowledge of metakaolin use as an SCM in comparison to GGCS. This leads to awareness of its potential in the Western Cape. Consequently, its utilization can assist in addressing the possible scarcity of SCMs.

REFERENCES

Advanced Cement Technologies (2017) *Metakaolin and Silica Fume - USA & Worldwide Supplier - Projects*. Available at: http://www.advancedcementtechnologies.com/projects (Accessed: 23 February 2017).

Aiswarya, S. *et al.* (2013) 'Experimental investigation on concrete containing Nano Metakaolin', *IRACST – Engineering Science and Technology: An International Journal*, 3(1), pp. 2250–3498.

Alexander, M. . (2017) 'Durability Index Testing Procedure Manual 2017', *Department of Civil Engineering department, University of Cape Town*, Ver. 4, p. 43.

Alexander, M. ., Jaufeerally, H. and Mackechnie, J. (2003) 'Structural and durability properties of concrete made with Corex slag', *Department of Civil Engineering , UCT*. (Research monograph), Research m, p. 30.

Alexander, M. and Beushausen, H. (2009) 'Deformation and volume change of hardened concrete', in *Fulton's concrete technology*, pp. 111–154.

Alexander, M. G., Mackechnie, J. R. and Ballim, Y. (1999) 'Guide to the use of durability indexes for achieving durability in concrete structures', *Research monograph*, p. 36.

Andrade, D. da S. *et al.* (2018) 'Chemical and mechanical characterization of ternary cement pastes containing metakaolin and nanosilica', *Construction and Building Materials*, 159, pp. 18–26.

Argeco DéveloppementCompany (2017) *Demeter Technologies - Flash calcination, Couleur Pollen*. Available at: http://www.demeter-technologies.fr/calcination.avantages.php (Accessed: 30 April 2017).

Arioglu, N., Girgin, Z. C. and Arioglu, E. (2006) 'Evaluation of ratio between splitting tensile strength and compressive strength for concretes up to 120 MPa and its application in strength criterion', *ACI Materials Journal*, 103(1), pp. 18–24.

Asbridge, H. A., Jones, R. T. and Osborne, G. J. (1996) 'High-performance metakaolin concrete: Results of large-scale trials in aggressive environments', in *Concrete in the service of Mankind*. Dundee: Radical Concrete Technology, pp. 35–48.

ASTM C 1202-12 (2012) 'Standard Test Method for Electrical Indication of Concrete's Ability to Resist Chloride Ion Penetration 1', *America Society for Testing and Material*, pp. 1–8.

ASTM C 1293 (2015) ‘Standard Test Method for Determination of Length Change of Concrete Due to Alkali- Silica Reaction’, *Annual Book of ASTM Standards*, pp. 1–7.

ASTM C 1556 (2017) ‘Standard Test Method for Determining the Apparent Chloride Diffusion Coefficient of Cementitious Mixtures by Bulk Diffusion 1’, pp. 1–7.

ASTM C 1567-13 (2008) ‘Standard Test Method for Determining the Potential Alkali-Silica Reactivity of Combinations of Cementitious Materials and Aggregate (Accelerated Mortar - Bar Method)’, *Annual Book of ASTM Standards*, pp. 1–6.

ASTM C 1679 (2014) ‘Standard Practice for Measuring Hydration Kinetics of Hydraulic Cementitious Mixtures Using Isothermal Calorimetry 1’, *America Society for Testing and Material*, 13, p. 15.

ASTM C 1702 (no date) ‘Standard Test Method for Measurement of Heat of Hydration of Hydraulic Cementitious Materials Using Isothermal Conduction Calorimetry 1’. doi: 10.1520/C1702-17.

ASTM C 1753 - 15 (2015) ‘Standard Practice for Evaluating Early Hydration of Hydraulic Cementitious Mixtures Using Thermal Measurements’, (September), pp. 1–19.

ASTM C 618 (2010) ‘Standard Specification for Coal Fly Ash and Raw or Calcined Natural Pozzolan for Use’, *Annual Book of ASTM Standards*, pp. 3–6.

Avet, F. *et al.* (2016) ‘Development of a new rapid, relevant and reliable (R 3) test method to evaluate the pozzolanic reactivity of calcined kaolinitic clays Hydration (A) Calorimetry (A) CaCO 3 (D) Thermal treatment (A)’, *Cement and Concrete Research*, 85, pp. 1–11.

Ayub, T., Khan, S. U. and Memon, F. A. (2014) ‘Mechanical characteristics of hardened concrete with different mineral admixtures: A review’, *The Scientific World Journal*, 2014, pp. 1–16.

Badogiannis, E. *et al.* (2015) ‘Evaluation of chloride -penetration resistance of metakaolin concrete by means of a diffusion -Binding model and of the k-value concept’, *Cement and Concrete Composites*, 63, pp. 1–7.

Badogiannis, E. G. *et al.* (2015) ‘Durability of metakaolin Self-Compacting Concrete’, *Construction and Building Materials*. Elsevier Ltd, 82, pp. 133–141.

Badogiannis, E. and Tsivilis, S. (2008) 'Exploitation of poor Greek kaolins: Durability of metakaolin concrete', *Cement and Concrete Composites*, 31, pp. 128–133.

Bai, J. and Wild, S. (2002) 'Investigation of the temperature change and heat evolution of mortar incorporating PFA and metakaolin', *Cement & Concrete Composites*, 24, pp. 201–209.

Baker, J. . *et al.* (1990) *Durability of Building Materials and Components: Proceedings of the 5th International Conference Held in Brighton, UK, 7-9 November 1990*, *Spon Press,Taylor & Francis Group*.

Ballard, Z. J., Caires, W. S. and Peters, S. R. (2008) 'Alternative mitigation materials for Alkali-silica reaction (ASR) in concrete', *Colorado Department of Transportation DTD Applied Research and Innovation Branch*, CDOT-2008-, p. 74.

Ballim, Y., Alexander, M. and Beushausen, H. (2009) 'Durability of concrete', in Owens, G. (ed.) *Fulton's concrete technology,9th edition*. Midrand, South Africa: Cement & Concrete Institute, pp. 155–188.

Bapat, J. D. (2013) *Mineral Admixtures in Cement and Concrete*. London and New York: Taylor & Francis Group.

Bareuther, E. *et al.* (1976) 'Process fro preparing a metakaolin wite pigment from kaolinite.', *United States Patent*.

Barnes, P. and Bensted, J. (2002) *Structure and Performance of Cements, 2nd edition*, *Spon Press,Taylor & Francis Group*. London and New York: Spon Press Taylor & Francis Group.

Batis, G. *et al.* (2005) 'The effect of metakaolin on the corrosion behavior of cement mortars', *Cement & Concrete Composites*, 27, pp. 125–130.

Blight, G. . and Alexander, M. . (2011) *Alkali-aggregate reaction and structural damage to concrete*. London, UK: Taylor & Francis Group. doi: 10.1201/b10773.

Bloodworth, a J., Highley, D. E. and Mitchell, C. J. (1993) 'Industrial Mineral laboratory Manual; KAOLIN', *Mineralogy and Petrology Group, British Geological Survey @NERC*, (Technical report WG/93/1), p. 75.

Boddy, A., Hooton, R. D. and Gruber, K. A. (2001) 'Long-term testing of the chloride penetration

resistance of concrete containing high-reactivity metakaolin', *Cement and Concrete Research*, 31, pp. 759–765.

Brooks, J. J. and Johari, M. A. M. (2001) 'Effect of metakaolin on creep and shrinkage of concrete', *Cement & Concrete Composites*, 23, pp. 495–502.

Brooks, J. J., Megat Johari, M. A. and Mazloom, M. (2000) 'Effect of admixtures on the setting times of high-strength concrete', *Cement and Concrete Composites*, 22(4), pp. 293–301.

BS 1881 : Part 121 : 1983 (no date) 'British standard for testing concrete. Part 121: Method for determination of static modulus of elasticity in compression'.

BS 3892:1:1997 (no date) 'British Standard Pulverized-fuel ash for use with Portland cement'.

BS EN 196-9:2010 (no date) 'British standard methods of testing cement Part 9: Heat of hydration - Semi-Adiabatic method.'

Bucher, R. *et al.* (2017) 'Service life of metakaolin-based concrete exposed to carbonation: Comparison with blended cement containing fly ash, blast furnace slag and limestone filler', *Cement and Concrete Research*, 99, pp. 18–29. doi: 10.1016/j.cemconres.2017.04.013.

Bucher, R., Cyr, M. and Escadeillas, G. (2015) 'Carbonation of Blended Binders Containing Metakaolin', *RILEM Bookseries*, 10, pp. 27–33.

Calmetrix, I. (2016) 'I-Cal 2000 HPC isotheral calorimeter for concrete and cement, User Manual', p. 47. Available at: http://downloads.calmetrix.com/Manuals/ICal2000UserManual.pdf.

Carles-Gibergues, A. *et al.* (2008) 'A simple way to mitigate alkali-silica reaction', *Materials and Structures*, 41(73–83).

Cassagnabère, F. *et al.* (2010) 'Metakaolin, a solution for the precast industry to limit the clinker content in concrete: Mechanical aspects', *Construction and Building Materials*. Elsevier Ltd, 24(7), pp. 1109–1118.

Cassagnabère, F., Escadeillas, G. and Mouret, M. (2008) 'Study of the reactivity of cement/metakaolin binders at early age for specific use in steam cured precast concrete', *Construction and Building Materials*, 23, pp. 775–784.

Chakraborty, A. K. (2013) 'Dehydroxylation Mechanism', in *Phase Transformation of Kaolinite*

Clay. Illustrate. New York: Springer New Delhi Heidelberg, pp. 313–322.

Claverie, M. *et al.* (2015) 'Structural and chemical changes in kaolinite caused by flash calcination: Formation of spherical particles', *Applied Clay Science*. Elsevier B.V., 114, pp. 247–255.

Cole, D. I., Ngcofe, L. and Halenyane, K. (2014) *Mineral commodities in the Western Cape province, South Africa, Council for Geoscience*. Report Number 2014-0012. Western Cape: Council of Geoscience.

Cook, R. A. and Hover, K. C. (1999) 'Mercury porosimetry of hardened cement pastes', *Cement and Concrete Research*, 29(6), pp. 933–943.

Courard, L. *et al.* (2003) 'Durability of mortars modified with metakaolin', *Cement and Concrete Research*, 33, pp. 1473–1479.

Cyr, M., Rivard, P. and Labrecque, F. (2009) 'Reduction of ASR-expansion using powders ground from various sources of reactive aggregates', *Cement and Concrete Composites*, 31, pp. 438–446.

Dadsetan, S. and Bai, J. (2017) 'Mechanical and microstructural properties of self-compacting concrete blended with metakaolin, ground granulated blast-furnace slag and fly ash', *Construction and Building Materials*, 346, pp. 658–667.

Davidovits, J. (2015) *Geopolymer chemistry and applications : 4th edition*. Edited by J. Davidovits. Saint-Quentin, France: nstitut Géopolymère 16 rue Galilée F-02100.

Dhandapani, Y. and Santhanam, M. (2017) 'Assessment of pore structure evolution in the limestone calcined clay cementitious system and its implications for performance', *Cement and Concrete Composites*, 84, pp. 36–47.

Diao, J. *et al.* (2016) 'System assessment of recycling of steel slag in converter steelmaking', *Journal of Cleaner Production*, 125, pp. 159–167. doi: 10.1016/j.jclepro.2016.03.040.

Diko, M., Ekosse, G. and Ogola, J. (2016) 'Fourier transform infrared spectroscopy and thermal analysis of kaolinitic clays from South Africa and Cameroon.', *Acta Geodynamica et Geomaterialia*, 13(2182), pp. 149–158.

Dinakar, P., Sahoo, P. K. and Sriram, G. (2013) 'Effect of Metakaolin Content on the Properties of High Strength Concrete', *International Journal of Concrete Structures and Materials*, 7, pp.

215–22.

Ding, J. T. and Li, Z. (2002) ‘Effects of metakaolin and silica fume on properties of concrete’, *ACI Materials Journal*, 99(4), pp. 393–398.

Dippenaar, R. (2004) ‘Industrial uses of slag. The use and re-use of iron and steelmaking slags’, in *VII International Conference on Molten Slags Fluxes and Salts, The South African Institute of Mining and Metallurgy*, pp. 57–69. doi: 10.1179/174328105X15805.

Donatello, S., Tyrer, M. and Cheeseman, C. R. (2010) ‘Comparison of test methods to assess pozzolanic activity’, *Cement and Concrete Composites*. Elsevier Ltd, 32(2), pp. 121–127.

DSTN Suriname N.V. (2017) *New U.S. Embassy Building, Paramaribo - Moengo Minerals N.V., Moengo Minerals N.V. Alle rechten voorbehouden*. Available at: http://www.moengominerals.com/en/power-pemba/projects/new-building-for-american-embassy-paramaribo/ (Accessed: 23 February 2017).

Duan, P. *et al.* (2013) ‘Effects of metakaolin, silica fume and slag on pore structure, interfacial transition zone and compressive strength of concrete’, *Construction and Building Materials*, 44, pp. 1–6.

Ekosse, G. I. E. (2010) ‘Kaolin deposits and occurrences in Africa: Geology, mineralogy and utilisation’, *Applied Clay Science*, 50, pp. 212–236.

El-Diadamony, H. *et al.* (2016) ‘Hydration and characteristics of metakaolin pozzolanic cement pastes’, *HBRC Journal*. Housing and Building National Research Center, (May), pp. 1–9.

Fernandes, I. and Broekmans, M. A. T. M. (2013) ‘Alkali-Silica Reactions: An Overview. Part I’, *Metallography, Microstructure, and Analysis*, 2(4), pp. 257–267.

Frías, M. and Cabrera, J. (2000) ‘Pore size distribution and degree of hydration of metakaolin±cement pastes’, *Cement and Concrete Research*, 30, pp. 561–569.

Frías, M., Sánchez de Rojas, M. and Cabrera, J. (2000) ‘The effect that the pozzolanic reaction of metakaolin has on the heat evolution in metakaolin-cement mortars’, *Cement and Concrete Research*, 30, pp. 209–216.

Gleize, P. J. P., Cyr, M. and Escadeillas, G. (2006) ‘Effects of metakaolin on autogenous shrinkage

of cement pastes'.

Gruber, K. A. *et al.* (2001) 'Increasing concrete durability with high-reactivity metakaolin', *Cement & Concrete Composites*, 23, pp. 476–484.

Güneyisi, E. *et al.* (2012) 'Strength, permeability and shrinkage cracking of silica fume and metakaolin concretes', *Construction and Building Materials*, 34, pp. 120–130.

Hassan, A. A. A., Lachemi, M. and Hossain, K. M. A. (2012) 'Effect of metakaolin and silica fume on the durability of self-consolidating concrete', *Cement and Concrete Composites*. Elsevier Ltd, 34(6), pp. 801–807.

He, Z., Li, L. and Du, S. (2017) 'Creep analysis of concrete containing rice husk ash', *Cement and Concrete Composites*. Elsevier Ltd, 80, pp. 190–199.

Hewlett, P. (2004) *Lea's Chemistry of Cement and Concrete*. 4th edn. Oxford, UK: Butterworth-Heinemann.

Hosterman, J. W., Patterson, S. H. and Good, E. E. (1990) 'world nonbauxite Aluminium resources excluding Alunite (U.S geological survey professional papers)', in *Geology and Resources of Aluminum. USA Government*. Washington, p. 352.

Illston, J. M. and Domone, P. (2002) *Construction Materials: Their Nature and Behaviour, Third Edition*. London and New York: Taylor & Francis Group.

ISO 1920-9:2009 (no date) 'International Standard. Testing of concrete. Part 9: Determination of creep of concrete cylinders in compression.'

Jaufeerally, H. (2013) 'Performance and properties of structural concrete made with Corex slag', *Msc dessertation, University of Cape Town*, p. 168.

Jiang, G., Rong, Z. and Sun, W. (2015) 'Effects of metakaolin on mechanical properties, pore structure and hydration heat of mortars at 0.17 w/b ratio', *Construction and Building Materials*, 93, pp. 564–572.

Khatib, J. M. (2008) 'Metakaolin concrete at a low water to binder ratio', *Construction and Building Materials*, 22(8), pp. 1691–1700.

Khatib, J. M. and Clay, R. M. (2004) 'Absorption characteristics of metakaolin concrete', *Cement*

and Concrete Research, 34(1), pp. 19–29.

Khatib, J. M. and Hibbert, J. J. (2004) 'Selected engineering properties of concrete incorporating slag and metakaolin'.

Khatib, J. M. and Mangat, P. S. (1995) 'Absorption characteristics of concrete as a function of location relative to casting position', *Cement and Concrete Research*, 25(5), pp. 999–1010.

Khatib, J. M. and Wild, S. (1996) 'Pore size distribution of metakaolin paste', *Cement and Concrete Research*, 26(10), pp. 1545–1553.

Khatib, J. M. and Wild, S. (1998) 'Sulphate resistsnce of metakaolin mortar', *Cement and Concrete Research*, 28(1), pp. 83–92.

Kim, H.-S., Lee, S.-H. and Moon, H.-Y. (2007) 'Strength properties and durability aspects of high strength concrete using Korean metakaolin', *Construction and Building Materials*, 21, pp. 1229–1237.

Kim, T. and Olek, J. (2012) 'Effects of sample preparation and interpretation of thermogravimetric curves on calcium hydroxide in hydrated pastes and mortars', *Transportation Research Record*, (2290), pp. 10–18.

Lagier, F. and Kurtis, K. E. (2007) 'Influence of Portland cement composition on early age reactions with metakaolin', *Cement and Concrete Research*, 37(10), pp. 1411–1417.

Li, H.-J., Hideaki, S. and Tokuda, M. (1995) 'ThermodynamicAnalysis of Slag Recycling Using a Slag Regenerator', *ISIJ International*, 35(9), pp. 1079–1088. Available at: https://www.jstage.jst.go.jp/article/isijinternational1989/35/9/35_9_1079/_pdf/-char/en (Accessed: 3 July 2018).

Liu, X. Y. (2000) 'Heterogeneous nucleation or homogeneous nucleation?', *The Journal of Chemical Physics Journal of Chemical Physics*, 112(10).

Lothenbach, B., Scrivener, K. and Hooton, R. D. (2011) 'Supplementary cementitious materials', *Cement and Concrete Research*. Elsevier Ltd, 41(12), pp. 1244–1256.

Ma, W. and Brown, P. W. (1997) 'Hydrothermal reaction of fly ash with Ca(OH)* AND CaSOc2H20', *Cement and Concrete Research*. Elswier Science Ltd, 27(8), pp. 1237–1248.

Mcpolin, D. O. *et al.* (2007) 'New Test Method to Obtain pH Profiles due to Carbonation of Concretes Containing Supplementary Cementitious Materials', *Journal of Materials in Civil Engineering*, 19(11), pp. 936–946.

Mehta, P. K. and Monteiro, P. J. M. (2006) *Concrete: microstructure, properties, and materials*. 3rd edn. New York: McGraw-Hill.

Meier, S. A. *et al.* (2007) 'Dynamics of the internal reaction layer arising during carbonation of concrete', *Chemical Engineering Science*, 62, pp. 1125–1137.

Mindess, S., Young, J. F. and Darwin, D. (2003) 'Concrete', *Prentice Hall*. USA: Pearson Education, p. 644.

Mitchell, D. R. G., Hinczak, I. and Day, R. A. (1998) 'Interaction of silica fume with Calcium hydroxide solutions and hydrated cement pastes', *Cement and Concrete Research*, 28(11), pp. 1571–1584.

Mobasher, B. *et al.* (2010) 'Transport properties in metakaolin blended concrete', *Construction and Building Materials*. Elsevier Ltd, 24(11), pp. 2217–2223.

Mostafa, N. Y. and Brown, P. W. (2005) 'Heat of hydration of high reactive pozzolans in blended cements: Isothermal conduction calorimetry', *Thermochimica Acta*, 435(2), pp. 162–167.

Murray, H. H. (1981) *Applied Clay Mineralogy, Volume 2: Occurrences, Processing and Applications of Kaolins, Bentonites, Palygorskitesepiolite, and Common Clays (Developments in Clay Science), 1st edition., Development in science clay*. Amsterdam: Elsevier Science.

Naik, T. R. (1997) 'Concrete durability as influenced by density and/or porosity.', in *World of concrete-Mexico*. mexico, p. 29.

Newman, J. and Choo, B. S. (2003) *Advanced Concrete Technology 3: Processes*, *Butterworth-Heinemann*. Amsterdam: Elsevier B.H.

Nicolas, R. S., Cyr, M. and Escadeillas, G. (2013) 'Characteristics and applications of flash metakaolins', *Applied Clay Science*, 83–84, pp. 253–262.

Nicolas, R. S., Cyr, M. and Escadeillas, G. (2014) 'Performance-based approach to durability of concrete containing flash-calcined metakaolin as cement replacement', *Construction and Building*

Materials. Elsevier Ltd, 55, pp. 313–322.

Owens, G. (2009) *Fulton's concrete technology, 9th edition.*, *Cement and Concrete Institute*. Edited by G. Owens. Midland. South Africa.

Paiva, H. *et al.* (2012) 'Effect of metakaolin dispersion on the fresh and hardened state properties of concrete', *Cement and Concrete Research*, 42, pp. 607–612.

Pera, J. and Amrouz, A. (1998) 'Development of Highly Reactive Metakaolin from Paper Sludge', *Advance Cement Based Materials*, 7, pp. 49–56.

Poon, C.-S. *et al.* (2001) 'Rate of pozzolanic reaction of metakaolin in high-performance cement pastes', *Cement and Concrete Research*, 31, pp. 1301–1306.

Qian, X. and Li, Z. (2001) 'The relationships between stress and strain for high-performance concrete with metakaolin', *Cement and Concrete Research*, 31, pp. 1607–1611.

Ramezanianpour, A. A. (2014) *Cement Replacement Materials; Properties, Durability, Sustainability*. Springer Berlin Heidelberg.

Ramlochan, T., Thomas, M. and Gruber, K. A. (2000) 'The effect of metakaolin on alkali±silica reaction in concrete', *Cement and Concrete Research*, 30, pp. 339–344.

Ramlochan, T., Thomas, M. and Gruber, K. a (2000) 'The effect of metakaolin on alkali ± silica reaction in concrete', *Cement and Concrete Research*, 30, pp. 339–344.

Rashad, A. M. (2013) 'Metakaolin as cementitious material: History, scours, production and composition-A comprehensive overview', *Construction and Building Materials*, 41, pp. 303–318.

Ravi, V. *et al.* (2017) 'An Overview of Polymer / Clay Nanocomposites', in Jlassi, K., Chehimi, M. M., and Thomas, S. (eds) *Clay-Polymer Nanocomposites*. Amsterdam: Elsevier Ltd, pp. 29–81.

Razak, H. A., Chai, H. K. and Wong, H. S. (2004) 'Near surface characteristics of concrete containing supplementary cementing materials', *Cement and Concrete Composites*, 26(7), pp. 883–889.

RILEM CPC-18 (1984) 'CPC-18 Measurement of hardened concrete carbonation depth', *RILEM Reommendation*.

Robayo-Salazar, R. A., Mejía de Gutiérrez, R. and Puertas, F. (2016) 'Effect of metakaolin on natural volcanic pozzolan-based geopolymer cement', *Applied Clay Science*. Elsevier B.V., 132–133, pp. 491–497.

Sabir, B., Wild, S. and Bai, J. (2001) 'Metakaolin and calcined clays as pozzolans for concrete: A review', *Cement and Concrete Composites*, 23(6), pp. 441–454.

Saillio, M., Baroghel-Bouny, V. and Pradelle, S. (2015) 'Various Durability Aspects of Calcined Kaolin-Blended Portland Cement Pastes and Concretes', *RILEM Bookseries*, 10, pp. 401–409.

Salvador, S. (1995) 'Pozzolanic properties of flash-calcined kaolinite: A comparative study with soak-calcined products', *Cement and Concrete Research*, 25(1), pp. 102–112.

Salvoldi, B. G. (2010) *Modelling the Carbonation of Concrete Using Early Age Oxygen Permeability Index Tests*. University of Cape Town.

SANS 201:2008 (2008) 'Sieve analysis, fines content and dust content of aggregates', *South African National Standards*.

SANS 3001-CO3-1:2015 (2015) 'Civil engineering test methods Part CO3-1: Concrete durability index testing — Preparation of test specimens', *South African National Standards*.

SANS 3001-CO3-2:2015 (2015) 'Civil engineering test methods Part CO3-2: Concrete durability index testing — Oxygen permeability test', *South African National Standards*.

SANS 50196-3:2006 (2006) 'Methods of testing cement Part 3 : Determination of setting times and soundness', *South African National Standards*.

SANS 5844:2014 (2006) 'Particle and relative densities of aggregates', *South African National Standards*.

SANS 5845:2006 (2006) 'Bulk densities and voids content of aggregates', *South African National Standards*.

SANS 5860 : 2006 (2006) 'Concrete tests — Dimensions, tolerances and uses of cast test specimens', *South African National Standards*.

SANS 5861-1:2006 (2006) 'Concrete tests Part 1: Mixing fresh concrete in laboratory', *South African National Standards*.

SANS 5861-2:2006 (2006) ‘Concrete tests Part 2: sampling of freshly mixed concrete.’, *South African National Standards*.

SANS 5862-1:2006 (2006) ‘Concrete tests-Consistence of freshly mixed concrete-Slump test’, *South African National Standards*.

SANS 5862-2:2006 (2006) ‘Concrete tests - Consistence of freshly mixed concrete - Flow test.’, *South African National Standards*.

SANS 5863:2006 (2006) ‘Concrete tests- Compressive strength of hardened concrete’, *South African National Standards*.

SANS 6253:2006 (2006) ‘Concrete tests - Tensile splitting strength of concrete.’, *South African National Standards*.

Sarfo-Ansah, J. *et al.* (2014) ‘Calcined Clay Pozzolan as an Admixture to Mitigate the Alkali-Silica Reaction in Concrete’, *Journal of Materials Science and Chemical Engineering*, 2, pp. 20–26.

Scrivener, K. L. (2014) ‘Options for the future of cement’, *The indian concrete journal*, (July), pp. 11–21.

Scrivener, K. L. and Kirkpatrick, R. J. (2008) ‘Innovation in use and research on cementitious material’, *Cement and Concrete Research*, 38, pp. 128–136.

Shah, M. and Jamani, A. (2017) ‘Experimental study on mechanical and durability properties of High strength concrete containing Nano silica and Metakaolin’, *International Journal For Technological Research In Engineering ISSN*, 4(8), pp. 2347–4718.

Shehab El-Din, H. K. *et al.* (2017) ‘Mechanical performance of high strength concrete made from high volume of Metakaolin and hybrid fibers’, *Construction and Building Materials*, 140, pp. 203–209.

Shi, Z. *et al.* (2015) ‘Durability of Portland Cement Blends Including Calcined Clay and Limestone: Interactions with Sulfate, Chloride and Carbonate Ions’, *RILEM Bookseries*, 10, pp. 133–145.

Siddique, R. (2008) *Waste materials and by-products in concrete*. Deblik, Berlin: Springer Berlin

Heidelberg.

Siddique, R. and Khan, M. I. (2011) *Supplementary cementing materials*, *Engineering materials*. London, New York: Springer Berlin Heidelberg.

Stanish, K. D., Hooton, R. D. and Thomas, M. D. (1997) 'Testing the Chloride Penetration Resistance of Concrete: A Literature Review', *Department of Civil Engineering, University of Toronto, Canada*.

Statista (2018) *Major countries in worldwide cement production from 2012 to 2017 (in million metric tons), The statistic Portal*. Available at: https://www.statista.com/statistics/267364/world-cement-production-by-country/ (Accessed: 23 March 2018).

Subaşı, A. and Emiroğlu, M. (2015) 'Effect of metakaolin substitution on physical, mechanical and hydration process of White Portland cement', *Construction and Building Materials*, 95, pp. 257–268.

Suraneni, P. and Weiss, J. (2017) 'Examining the pozzolanicity of supplementary cementitious materials using isothermal calorimetry and thermogravimetric analysis', *Cement and Concrete Composites*. Elsevier Ltd, 83, pp. 273–278.

Tafraoui, A., Escadeillas, G. and Vidal, T. (2016) 'Durability of the Ultra High Performances Concrete containing metakaolin', *Construction and Building Materials*. Elsevier Ltd, 112, pp. 980–987.

Teklay, A. *et al.* (2015) 'Experimental and modeling study of flash calcination of kaolinite rich clay particles in a gas suspension calciner', *Applied Clay Science*. Elsevier B.V., 103, pp. 10–19.

Thomas, M. *et al.* (2006) 'Test methods for evaluating preventive measures for controlling expansion due to alkali – silica reaction in concrete', 36, pp. 1842–1856.

Thomas, M. (2011) 'The effect of supplementary cementing materials on alkali-silica reaction: A review', *Cement and Concrete Research*, 41(12), pp. 1224–1231.

Thomas, M. (2013) *Supplementary Cementing Materials in Concrete*. Boca Raton London New York: CRC Press; Taylor & Francis Group.

Thomas, M. D. *et al.* (2012) 'The effect of supplementary cementitious materials on chloride

binding in hardened cement paste', *Cement and Concrete Research*. Elsevier Ltd, 42(1), pp. 1–7.

Thomas, M. D. A., Fournier, B. and Folliard, K. J. (2013) 'Alkali-Aggregate Reactivity (AAR) Facts Book', p. 211.

Tironi, A. *et al.* (2013) 'Assessment of pozzolanic activity of different calcined clays', *Cement and Concrete Composites*, 37, pp. 319–327.

TradingEconomics (2018) *South Africa Production 2014-2018, Trading Economics*. Available at: https://tradingeconomics.com/south-africa/steel-production (Accessed: 23 March 2018).

Visser, J. H. M. (2012) 'Accelerated carbonation testing of mortar with supplementary cementing materials - Limitation of the acceleration due to drying', *HERON*, 57(3).

Wadsö, L. (2003) *An experimental comparison between isothermal calorimetry, semi-adiabatic calorimetry and solution calorimetry for the study of cement hydration*.

Walker, R. and Pavı´a, S. (2011) 'Physical properties and reactivity of pozzolans, and their influence on the properties of lime–pozzolan pastes', *Materials and Structures*, 44, pp. 1139–1150.

Wang, H. and Gillott, J. E. (1991) 'Mechanism of Alkali-silica reaction and the significance of calcium hydroxide', *Cement and Concrete Research*, 21, pp. 647–654.

Wild, S. and Khatib, J. M. (1997) 'Portlandite consumption in metakaolin cement pastes and mortars', *Cement and Concrete Research*, 27(1), pp. 137–146.

Wild, S., Khatib, J. M. and Jones, A. (1996) 'Relative strength, pozzolanic activity and cement hydration in superplasticised metakaolin concrete', *Cement and Concrete Research*, 26(10), pp. 1537–1544.

Yusuf, T. O. *et al.* (2014) 'Impact of Blending on Strength Distribution of Ambient Cured Metakaolin and Palm Oil Fuel Ash Based Geopolymer Mortar', *Advances in Civil Engineering*, 2014, pp. 1–8.

Zhang, M. H. and Malhotra, V. M. (1995) 'Characteristics of a thermally activated alumino-silicate pozzolanic material and its use in concrete', *Cement and Concrete Research*, 25(8), pp. 1713–1725.

A. APPENDICES

A.1. STRENGTH ACTIVITY INDEX

Table A.1 shows compressive strength of mortar containing metakaolin. These data were used to evaluate strength activity index of metakaolin at different replacement levels.

Table A.1: Average compressive strength of mortar containing metakaolin, MPa

Time in days	3	7	14	28	56
0% mk	43.2	51.3	59.0	61.5	66.5
10% mk	38.8	61.8	70.8	69.2	72.7
15% mk	44.7	67.2	80.2	82.7	84.7
20% mk	43.5	63.5	75.0	75.2	70.8

A.2. SEMI ADIABATIC CALORIMETRY

The analysis of the data collected from semi adiabatic calorimetry;

The temperature readings were collected from three channels one containing inert sample and other two containing mortar samples. Equation A2.1 to A2.10 and Table A.2 explain how total heat of hydration of the mortar was calculated from temperature readings.

$$\mathrm{qi} = \mathrm{abs}(\mathrm{inert} - \mathrm{average})\mathrm{sample\ temperatures} \quad \textit{(A2.1)}$$

$$\mathrm{Cqi} = \mathrm{Cumulative\ of\ qi} \quad \textit{(A2.2)}$$

$$\mathrm{Qi} = \mathrm{successive\ mean\ of\ Cqi} \quad \textit{(A2.3)}$$

$$\mathrm{A} = \mathrm{C_p} * \mathrm{Cqi}\frac{\mathrm{Ms}}{\mathrm{Mc}}, \mathrm{where\ M\ stands\ for\ mass\ ,\ s\ for\ sample\ and\ c\ for\ cement} \quad \textit{(A2.4)}$$

$$\mathrm{B} = \mathrm{Cummulative}\left(\frac{\propto * \mathrm{ti} * \mathrm{Qi}}{\mathrm{Mc}}\right), \mathrm{where\ ti\ is\ time\ elapse} \quad \textit{(A2.5)}$$

$$\mathrm{Total\ heat} = \mathrm{A} + \mathrm{B} \quad \textit{(A2.6)}$$

Calculations for Coefficient of heat loss, α;

Coefficient of heat loss in the semi adiabatic calorimetry was obtained by allowing hot water (100^{o}C) to cool in the semi adiabatic calorimetry for 24 h. The temperature readings collected were used to draw a logarithmic curve. The process was done three times and three equations (A2.7,

A2.8, and A2.9) were obtained which were equivalent to equation A2.10. Using the average of their slope values, the coefficient of heat loss was calculted using equation A2.11. Noted that the value should be less than 100 J/(h·K).

$$\text{In T} = -0.0358\text{t} + 4.278 \quad \textit{(A2.7)}$$

$$\text{In T} = -0.0359\text{t} + 4.242 \quad \textit{(A2.8)}$$

$$\text{In T} = -0.0360\text{t} + 4.253 \quad \textit{(A2.9)}$$

$$\text{In T} = -\frac{\propto}{\text{C}_\text{w}}\text{t} + \text{InA} \quad \textit{(A2.10)}$$

$$\propto = 0.0359 * \text{C}_\text{w} * \text{Mw} = 97.75\text{K/h} \quad \textit{(A2.11)}$$

Where by mass of water (Mw)=650 g, and Cw= 4.186 J/g.K

Table A.2: example of total heat calculation using the data collected from semi adiabatic calorimetry

Mortar with 0% mk											
Raw data, temperature readings in ^{o}C					Data calculations						
Time	Inert sample	Mortar samples			qi	Cqi	Qi	A	ti	B	A+B
min		1	2	Ave	^{o}C	^{o}C	^{o}C	J/g	h	J/g	J/g
0	20.0	20.5	20.8	20.6	0.69	0.69	0.35	3.943	0	0	3.943
10	20.0	20.5	20.8	20.6	0.69	0.69	0.69	3.943	0.17	0.0	3.976
20	20.0	20.6	20.9	20.7	0.73	0.73	0.71	4.146	0.17	0.1	4.212
30	20.0	20.7	21.0	20.9	0.83	0.83	0.78	4.752	0.17	0.1	4.854
40	20.1	20.8	21.1	21.0	0.91	0.91	0.87	5.215	0.17	0.1	5.358
50	20.1	20.9	21.2	21.1	0.97	0.97	0.94	5.535	0.17	0.2	5.722
60	20.1	21.0	21.3	21.2	1.03	1.03	1.00	5.861	0.17	0.2	6.095
70	20.2	21.1	21.4	21.2	1.06	1.06	1.04	6.078	0.17	0.3	6.361
80	20.2	21.2	21.5	21.3	1.09	1.09	1.08	6.241	0.17	0.3	6.574
90	20.2	21.2	21.5	21.4	1.14	1.14	1.12	6.515	0.17	0.4	6.901
100	20.3	21.3	21.6	21.5	1.18	1.18	1.16	6.755	0.17	0.4	7.196
110	20.3	21.4	21.7	21.5	1.23	1.23	1.21	7.021	0.17	0.5	7.518
120	20.3	21.4	21.7	21.6	1.28	1.28	1.25	7.312	0.17	0.6	7.868
130	20.3	21.5	21.8	21.7	1.33	1.33	1.31	7.621	0.17	0.6	8.238
140	20.4	21.6	21.9	21.8	1.40	1.40	1.37	8.021	0.17	0.7	8.702

A.3. THERMOGRAVIMETRIC ANALYSIS

Weight losses (ml) evaluated from the TG and DTG curves (as shown in Figure A.1) and Equation A3.1 and A3.2 were used to calculate CH content and chemically bound water of mortar samples containing metakaolin, respectively. Table A.3 shows evaluation of the data for all mortars.

$$\text{CH content, \%}_{\text{by mass of binder}} = \frac{1}{4} * \left(\frac{74}{18} * \text{ml}_{\text{CH}} + \frac{74}{44} * \text{ml}_{\text{CaCO}_3} - \frac{74}{100} * \text{CaCO}_{3\,\text{in cement}}\right) \quad \text{(A3.1)}$$

$$Chemically\ bound\ water_{by\ mass\ of\ binder} = \frac{1}{4}(WL - ml_{CaCO3}) \quad \text{(A3.2)}$$

Table A.3: CH content and chemically bound water of mortar containing metakaolin by using data collected from TGA

Mixes	Curing days	Mass of sample, mg	Mass loss(ml) in TG curve, %		$CaCO_3$ in mortar due to cement, %	Total CH, % (by mass of binder)	Mass loss (WL), (100-1000)°C %	Chemically bound water, %
			CH	$CaCO_3$				
0% mk	7	63.94	0.13	7.90	2.25	3.04	12.46	1.14
	28	61.68	0.18	7.86	2.25	3.08	12.95	1.27
	56	64.83	1.93	4.33	2.25	3.39	15.11	2.70
10% mk	7	65.08	0.05	6.57	2.03	2.44	13.05	1.62
	28	63.49	0.00	7.03	2.03	2.59	13.79	1.69
	56	65.83	0.16	7.74	2.03	3.05	15.08	1.84
15% mk	7	64.80	0.04	6.45	1.91	2.40	11.67	1.31
	28	64.55	0.24	6.07	1.91	2.45	13.35	1.82
	56	65.43	0.04	6.87	1.91	2.58	13.25	1.60
20% mk	7	64.96	0.04	6.24	1.80	2.34	10.88	1.16
	28	64.56	0.06	5.92	1.80	2.22	12.04	1.53
	56	64.00	0.08	6.09	1.80	2.31	13.70	1.90

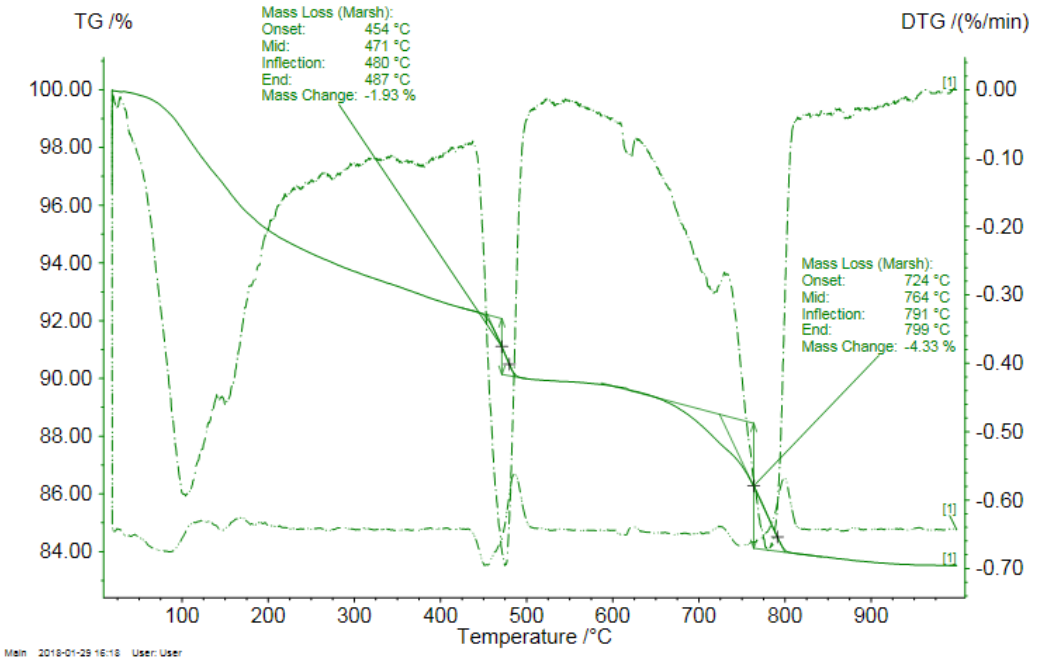

Figure A.1: TGA and DTG curves of control mortar at 56 days of curing showing calculation of weight losses

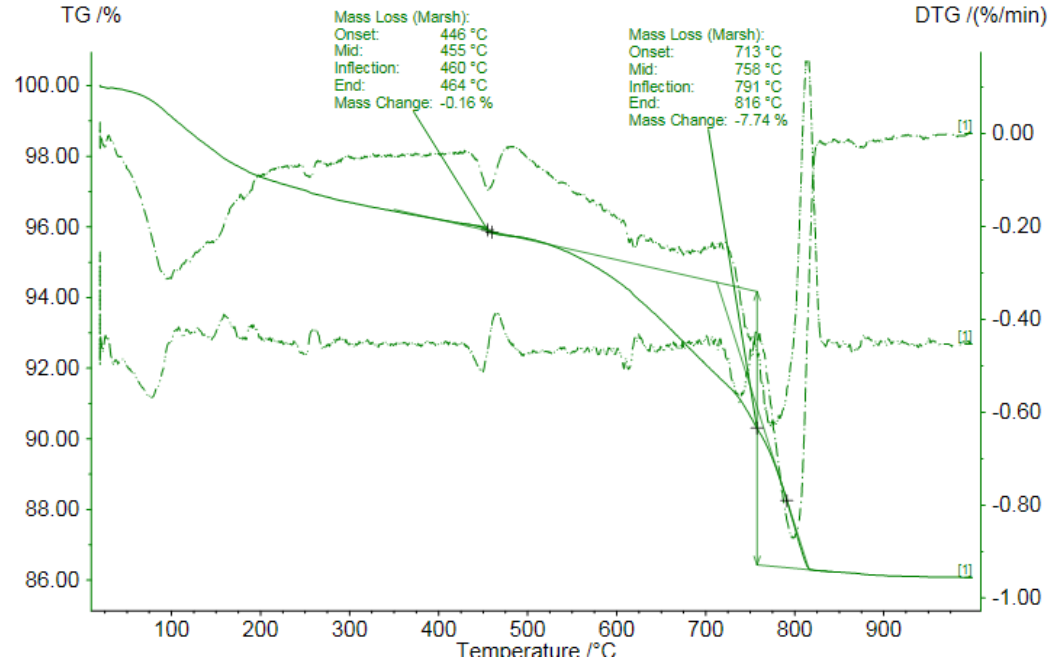

Figure A.2TGA and DTG curves of 10% mk mortar at 56 days of curing showing calculation of weight losses

A.4. COMPRESSIVE STRENGTH

Table A.4 to Table A.7 show the summary of collected data used to evaluated compressive strength of concretes with different w/b ratios.

Table A.4: Summary of compressive strength data of metakaolin concretes with 0.4 w/b ratio

Mixes	Days	Ave. Dimension, mm			Ave. Load	Ave. Compressive strength	Ave. density	Stdev of Comp. strength	Stdev of Av. Density
		Height	Breadth	Width	[kN]	[MPa]	[kg/m^3]		
0.4 w/b 0% mk	7	100.6	100.5	100.1	536	53.2	2386.9	0.3	18.3
	28	100.4	100.4	101.1	659	63.7	2424.5	2.4	21.4
	56	100.3	100.3	100.7	671	67.0	2433.6	2.2	9.5
0.4 w/b 10% mk	7	100.3	100.3	99.5	619	61.8	2403.7	1.6	10.9
	28	100.3	100.3	100.5	776	77.0	2402	2.6	14.1
	56	100.3	100.2	99.7	816	83.3	2386.4	0.8	41.8
0.4 w/b 15% mk	7	100.3	100.3	100.3	682	67.8	2369.2	0.6	10.6
	28	100.3	100.3	99.8	813	81.2	2371.8	1.0	42.0
	56	100.2	100.2	100.8	841	83.3	2386.4	0.8	41.8
0.4 w/b 20% mk	7	100.5	100.5	100.4	710	70.3	2349.8	1.3	20.1
	28	100.2	100.2	100.7	875	86.7	2392.8	2.6	13.9
	56	100.2	100.1	100.0	855	85.5	2385.8	3.6	9.1

Table A.5: Summary compressive strength data of metakaolin concretes with 0.5 w/b ratio

Mixes	Days	Ave. Dimension, mm			Ave. Load	Ave. Compressive strength	Ave. density	Stdev of Comp. strength	Stdev of Av. Density
		Height	Breadth	Width	[kN]	[MPa]	[kg/m^3]		
0.5 w/b 0% mk	7	100.1	100.1	101.2	467	46.2	2349.4	0.6	26.7
	28	100.0	100.0	100.2	544	52.7	2390.4	1.5	14.4

	56	100.0	100.0	100.7	561	57.5	2368.2	1.3	23.3
0.5 w/b 10% mk	7	100.1	100.2	100.7	550	54.5	2387.1	0.9	24.7
	28	100.1	100.1	101.1	641	63.3	2363.2	0.8	42.8
	56	100.1	100.1	102.0	657	68.3	2374.7	1.3	18.7
0.5 w/b 15% mk	7	100.0	100.0	100.7	575	57.2	2379.3	1.0	9.0
	28	100.0	100.0	100.3	669	66.7	2368.3	1.2	4.7
	56	100.0	100.0	100.9	689	68.3	2374.7	1.3	18.7
0.5 w/b 20% mk	7	100.2	100.2	100.7	625	62.0	2363	0.9	18.7
	28	100.2	100.2	100.4	753	74.8	2353.8	0.3	28.6
	56	100.2	100.2	100.6	760	75.5	2396.4	1.0	40.7

Table A.6: Summary of compressive strength data of metakaolin concretes with 0.6 w/b ratio

Mixes	Days	Ave. Dimension, mm			Ave. Load	Ave. Compressive strength	Ave. density	Stdev of Comp. strength	Stdev of Av. Density
		Height	Breadth	Width	[kN]	[MPa]	[kg/m^3]		
0.6 w/b 0% mk	7	100.4	100.4	99.9	316	31.7	2373.9	1.3	24.4
	28	100.2	100.2	99.6	433	42.2	2406.2	2.0	8.1
	56	100.2	100.1	99.9	438	44.7	2386.7	0.8	12.3
0.6 w/b 10% mk	7	100.5	100.4	101.0	436	43.0	2371.6	1.8	6.1
	28	100.5	100.5	102.0	525	51.3	2392.1	1.0	16.9
	56	100.2	100.2	100.3	541	58.2	2365.8	0.6	17.5
0.6 w/b 15% mk	7	100.5	100.5	100.4	461	45.7	2367.2	1.5	9.6
	28	100.2	100.1	100.4	554	55.0	2384.7	0.9	22.5
	56	100.2	100.2	100.9	589	58.2	2365.8	0.6	17.5
0.6 w/b 20% mk	7	100.3	100.3	100.9	473	46.7	2350.7	1.3	11.6
	28	100.0	100.1	100.6	575	57.0	2353	0.9	17.3
	56	100.5	100.4	101.8	595	58.3	2348	0.6	16.2

Table A.7: Compressive strength of GGCS concretes with three w/b ratios

Mixes	Days	Ave. Dimension, mm			Ave. Load	Ave. Compressive strength	Ave. density	Stdev of Comp. strength	Stdev of Av. Density
		Height	Breadth	Width	[kN]	[MPa]	[kg/m^3]		
0.4 w/b 50% GGCS	7	100.1	100.1	100.1	511	51.0	2397.4	0.5	9.9
	28	99.8	99.8	100.2	643	61.0	2400.3	1.3	1.6
	56	100.0	100.0	100.5	663	69.2	2440.6	1.5	14.6
0.5 w/b 50% GGCS	7	100.4	100.4	99.6	332	33.3	2373	0.3	29.2
	28	100.2	100.2	99.6	485	48.7	2381.7	0.3	18.4
	56	100.2	100.2	100.4	525	45.5	2372	0.5	50.2
0.6 w/b 50% GGCS	7	100.2	100.2	99.4	289	29.2	2405.5	1.0	23.2
	28	100.4	100.4	100.9	438	43.2	2364.6	1.5	6.5
	56	100.2	100.2	101.1	461	45.5	2372	0.5	50.2

A.5. TENSILE STRENGTH

Table A.8 to Table A.11 show the summary of collected data used to evaluated tensile splitting strength of concretes with different w/b ratios.

Table A.8: Tensile splitting strength of metakaolin concretes with 0.4 w/b ratio

Mixes	Days	Ave. Dimension, mm			Ave. Load	Ave. Tensile split. strength	Ave. density	Stdev of Tens. strength	Stdev of Av. Density
		Height	Breadth	Width	[kN]	[MPa]	[kg/m^3]		
0.4 w/b 0% mk	7	100.5	100.6	101.5	74	4.6	2412.4	0.3	6.8
	28	100.3	100.3	100.8	87	5.4	2422.4	0.1	15.1
	56	100.4	100.3	100.6	86	5.4	2427.8	0.1	26.7
0.4 w/b 10% mk	7	100.4	100.4	102.2	97	6.1	2365.9	0.1	33.5
	28	100.2	100.2	101.2	98	6.1	2400.4	0.1	3.6
	56	100.0	100.0	99.3	98	6.7	2358.4	0.2	35.5
0.4 w/b 15% mk	7	100.1	100.1	100.8	100	6.3	2369.1	0.1	36.4
	28	99.9	100.0	100.0	102	6.5	2378.3	0.2	22.8
	56	100.0	100.0	101.3	106	6.7	2358.1	0.2	35.5
0.4 w/b 20% mk	7	100.1	100.1	100.3	102	6.4	2378.5	0.1	4.3
	28	100.0	100.0	100.1	103	6.6	2382.2	0.2	26.2
	56	100.1	100.1	99.2	110	7.0	2365.8	0.2	32.3

Table A.9: Tensile splitting strength of metakaolin concretes with 0.5 w/b ratio

Mixes	Days	Ave. Dimension, mm			Ave. Load	Ave. Tensile split. strength	Ave. density	Stdev of Tens. strength	Stdev of Av. Density
		Height	Breadth	Width	[kN]	[MPa]	[kg/m^3]		
0.5 w/b 0% mk	7	100.0	100.0	101.1	66	4.2	2404	0.1	17.3
	28	100.0	100.0	100.3	77	4.9	2395.9	0.1	10.5
	56	100.0	100.0	100.3	75	4.7	2398.7	0.1	14.6
0.5 w/b 10% mk	7	100.1	100.1	101.7	86	5.4	2377.6	0.3	29.6
	28	100.1	100.1	99.6	90	5.8	2360.7	0.3	48.6
	56	100.0	100.0	100.9	88	6.0	2377.6	0.1	18.8
0.5 w/b 15% mk	7	100.0	100.0	100.1	90	5.7	2377.5	0.5	13.1
	28	100.1	100.1	99.4	94	6.0	2391.2	0.3	1.4
	56	100.0	100.0	100.0	95	6.0	2377.6	0.1	18.8
0.5 w/b 20% mk	7	100.0	100.0	100.3	92	5.8	2400.5	0.1	6.5
	28	100.2	100.2	100.7	97	6.1	2351.1	0.2	33.0
	56	100.1	100.1	100.5	99	6.3	2394.9	0.3	57.4

Table A.10: Tensile splitting strength of metakaolin concretes with 0.6 w/b ratio

Mixes	Days	Ave. Dimension, mm			Ave. Load	Ave. Tensile split. strength	Ave. density	Stdev of Tens. strength	Stdev of Av. Density
		Height	Breadth	Width	[kN]	[MPa]	[kg/m^3]		
0.6 w/b 0% mk	7	100.3	100.3	100.3	57	3.6	2381.6	0.1	13.2
	28	100.6	100.5	100.3	65	4.2	2381.5	0.2	14.2
	56	100.4	100.5	100.5	68	4.4	2382.6	0.3	33.7
	7	100.2	100.2	100.7	73	4.6	2370.8	0.1	29.8

0.6 w/b 10% mk	28	100.4	100.3	100.2	76	4.8	2385.4	0.1	11.8
	56	100.3	100.3	100.4	79	5.7	2360.3	0.1	36.8
0.6 w/b 15% mk	7	100.2	100.1	100.9	80	5.0	2374.3	0.3	3.3
	28	100.3	100.3	100.6	83	5.3	2382.5	0.1	19.0
	56	100.3	100.3	101.0	90	5.7	2360.3	0.1	36.8
0.6 w/b 20% mk	7	100.2	100.1	100.9	80	5.1	2350.9	0.2	21.7
	28	100.2	100.1	101.0	88	5.6	2373.1	0.2	22.3
	56	100.2	100.2	101.3	92	5.7	2367.9	0.2	16.4

Table A.11: Tensile splitting strength of metakaolin concretes with 0.6 w/b ratio

Mixes	Days	Ave. Dimension, mm			Ave. Load	Ave. Tensile split. strength	Ave. density	Stdev of Tens. strength	Stdev of Av. Density
		Height	Breadth	Width	[kN]	[MPa]	[kg/m^3]		
0.4 w/b 50% GGCS	7	100.0	100.0	99.9	74	4.7	2398.6	0.2	19.1
	28	100.0	100.0	100.2	86	5.3	2420.4	0.1	15.8
	56	100.1	100.1	99.9	86	5.5	2445.2	0.1	20.5
0.5 w/b 50% GGCS	7	100.2	100.2	99.6	55	3.5	2398.1	0.1	22.1
	28	100.3	100.3	100.7	80	5.1	2416.3	0.0	11.4
	56	100.1	100.1	99.5	83	4.5	2378.6	0.2	17.3
0.6 w/b 50% GGCS	7	100.1	100.1	100.6	50	3.2	2406.5	0.3	21.9
	28	100.1	100.1	100.0	70	4.5	2408.8	0.1	25.7
	56	100.3	100.3	100.2	72	4.5	2378.6	0.2	17.3

A.6. ELASTIC MODULUS

Table A.12: Elastic modulus of concrete at different w/b ratio

Static elastic modulus of concrete (GPa)							
w/b		0.4		0.5		0.6	
Mixes/Days	No.	28	56	28	56	56	56
0% mk	1	40.5	42.9	39.8	42.5	33.0	39.2
	2	41.7	43.2	42.1	42.8	32.3	37.1
	3	43.9	44.6	39.7	43.7	32.1	36.0
	Ave.	42.0	43.6	40.6	43.0	32.5	37.4
10% mk	1	47.5	48.9	43.1	44.6	36.9	41.9
	2	47.2	49.0	41.9	42.9	35.8	43.0
	3	47.9	47.6	41.8	43.2		42.9
	Ave.	47.5	48.5	42.3	43.6	36.3	42.6
15% mk	1	48.4	49.4	40.3	42.9	36.0	43.2
	2	45.5	46.9	42.1	43.2	37.9	41.3
	3	45.5	46.9	39.8	41.4		42.7
	Ave.	46.5	47.7	40.7	42.5	37.0	42.4
20% mk	1	45.4	46.2	40.3	44.4	34.9	44.1
	2	46.6	46.4	42.2	42.7	34.4	42.6
	3	44.5	45.0	41.3	43.5	33.6	45.2
	Ave.	45.5	45.8	41.3	43.5	34.3	44.0
50% GGCS	1	44.6	46.4	38.4	41.9	37.4	39.6
	2	46.0	47.3	43.3	43.4	41.0	41.5
	3	45.2		44.4	44.8	42.9	43.1
	Ave.	45.3	46.9	42.0	43.4	40.4	41.4

A.7. DURABILITY INDEX

Table A.13: Data collected for DI test

Oxygen Permeability Index, OPI results							
	Average OPI				Standard deviation		
w/b	0.4	0.5	0.6	w/b	0.4	0.5	0.6
0% mk	10.39	10.37	10.23	0% mk	0.23	0.05	0.16
10% mk	10.92	10.46	10.67	10% mk	0.18	0.08	0.06
15% mk	11.16	10.67	10.93	15% mk	0.12	0.05	0.30
20% mk	11.19	10.72	11.15	20% mk	0.11	0.12	0.13
50% GGCS	10.72	10.57	10.43	50% GGCS	0.11	0.14	0.14
Average Coefficient of permeability, k (m/s), x 10^{-11}					Standard deviation		
w/b	0.4	0.5	0.6	w/b	0.4	0.5	0.6
0% mk	4.58	4.29	6.25	0% mk	2.56	0.51	2.40
10% mk	1.29	3.50	2.16	10% mk	0.49	0.63	0.28
15% mk	0.71	2.15	1.93	15% mk	0.19	0.26	1.46
20% mk	0.67	1.94	0.73	20% mk	0.19	0.51	0.22
50% GGCS	1.94	2.87	3.85	50% GGCS	0.48	1.03	1.20
Water Sorptivity Index, WSI results, in mm/$hr^{0.5}$							
	Average WSI				Standard deviation		
w/b	0.4	0.5	0.6	w/b	0.4	0.5	0.6
0% mk	6.96	7.06	7.71	0% mk	0.82	0.30	0.51
10% mk	7.08	6.40	7.13	10% mk	0.42	1.32	0.58
15% mk	6.65	5.79	6.80	15% mk	1.27	0.43	0.47
20% mk	6.32	5.52	6.61	20% mk	1.30	0.70	0.31
50% GGCS	7.19	7.36	7.70	50% GGCS	0.65	0.82	1.37
	Average Porosity, %				Standard deviation		
w/b	0.4	0.5	0.6	w/b	0.4	0.5	0.6
0% mk	5.17	9.18	10.54	0% mk	0.82	0.59	0.78
10% mk	5.60	8.34	9.22	10% mk	0.74	0.32	0.71
15% mk	4.47	7.90	8.01	15% mk	0.65	0.27	0.57
20% mk	4.90	6.66	6.45	20% mk	0.47	0.99	0.96
50% GGCS	5.60	7.39	7.35	50% GGCS	0.32	0.90	0.98
Chloride Conductivity index, CCI results in mS/cm							
	Average CCI, mS/cm				Standard deviation		
w/b	0.4	0.5	0.6	w/b	0.4	0.5	0.6
0% mk	0.50	0.72	1.46	0% mk	0.04	0.03	0.10
10% mk	0.15	0.26	0.54	10% mk	0.02	0.02	0.06
15% mk	0.11	0.18	0.36	15% mk	0.01	0.03	0.06
20% mk	0.10	0.15	0.25	20% mk	0.01	0.02	0.04
50% GGCS	0.16	0.26	0.31	50% GGCS	0.01	0.03	0.04

A.8. CREEP AND DRYING SHRINKAGE TEST

Analysing creep and shrinkage results

$$Creep\ strain = Average\ loaded\ strain - Drying\ shrinkage\ strain - Applied\ instanteneous\ strain \quad \text{(A8.1)}$$

$$Instanteneous\ elastic\ modulus = \frac{Applied\ stress}{Average\ immediate\ strain} \quad \text{(A8.2)}$$

$$Specific\ Creep = \frac{Creep\ strain}{Applied\ stress} \quad \text{(A8.3)}$$

$$Creep\ coeficient = Specific\ creep * Instanteneous\ Elastic\ modulus \quad \text{(A8.4)}$$

$$Drying\ shrinkage = Average\ strain\ at\ time\ t - Average\ starin\ at\ time\ zero \quad \text{(A8.5)}$$

Applied stress 6 MPa	Instantaneous elastic modulus, GPa
0% mk	41.3
10% mk	43.1
15% mk	40.2
20% mk	41.9

Table A.14: Strain readings of metakaolin creep and shrinkage samples for 100 days

Laboratory Readings, 2017			28-Sep	28-Sep	28-Sep	29-Sep	01-Oct	05-Oct	12-Oct	19-Oct	26-Oct	02-Nov	09-Nov	16-Nov	23-Nov	07-Dec	21-Dec	06-Jan
Calibration readings			487	487	487	488	488	486	488	489	490	488	487	490	489	488	487	487
Location	Sample	Lb	Unloaded	Loaded	2 h loaded	1	3	7	14	21	28	35	42	49	56	70	84	100
0.5 w/b 0% mk	11 Creep	A	380	368	367	365	363	360	356	354	348	345	343	341	339	338	336	334
		B	464	448	447	446	445	444	441	435	434	433	432	431	430	429	425	422
		C	446	432	431	430	428	423	419	413	410	408	405	404	403	402	400	398
	12 Creep	A	440	425	425	424	421	417	413	410	407	405	403	401	399	397	395	393
		C	472	456	455	452	451	447	444	441	438	436	434	431	429	426	424	422
		B	440	440	440	440	440	439	437	434	433	432	431	430	429	428	427	426
		C	469	469	469	469	468	462	462	461	459	459	458	458	456	456	454	452
	14 Shrinkage	A	452	452	452	452	451	450	448	446	445	444	443	442	441	440	439	437
		B	513	513	513	513	512	510	508	506	505	504	503	501	500	499	498	497
		C	455	455	455	455	454	453	450	447	445	445	444	443	442	442	441	439
0.5 w/b 10% mk	21 Creep	A	448	435	430	429	429	427	425	422	420	418	416	414	412	410	408	406
		B	469	458	455	454	454	451	449	446	442	441	440	439	438	437	436	434
		C	472	460	457	457	456	454	452	451	448	446	444	443	442	440	438	436
	22 Creep	A	448	430	430	430	429	424	420	415	414	413	410	408	407	406	405	404
		B	451	435	435	435	432	428	425	422	419	416	414	413	411	410	409	408
	23 Shrinkage	A	430	430	430	430	430	427	426	424	423	423	422	421	420	420	420	420
		B	504	504	504	504	504	502	501	501	498	498	497	496	495	495	494	492
		C	454	454	454	454	454	452	451	450	449	448	447	446	445	444	443	442
	24 Shrinkage	A	463	463	463	463	461	460	459	458	457	456	455	454	453	453	452	451
		B	543	543	543	543	543	541	540	539	538	538	537	537	536	536	535	534
		C	473	473	473	473	473	470	469	468	467	467	466	465	465	464	463	463
0.5 w/b 15% mk	31 Creep	A	440	426	425	425	424	421	419	415	414	414	413	412	410	408	406	405
		B	449	436	435	435	434	430	427	424	423	423	421	420	419	417	416	415
		C	466	449	448	448	447	444	442	440	439	438	437	436	435	434	432	430

32 Creep	A	461	446	445	444	442	439	437	433	431	429	427	426	425	424	423	422
	B	445	432	432	430	429	426	425	423	420	419	418	416	416	415	414	412
	C	410	392	391	391	390	389	385	384	382	381	379	376	376	375	374	373
33 Shrinkage	A	456	456	456	456	456	455	454	453	453	453	452	452	451	450	450	449
	B	450	450	450	450	449	446	446	445	444	444	443	443	443	443	442	441
	C	453	453	453	453	452	449	448	447	446	445	445	444	444	443	443	442
34 Shrinkage	A	445	445	445	445	445	444	443	441	440	440	439	437	437	437	437	436
	B	441	441	441	441	440	439	438	436	435	435	434	433	433	433	432	432
	C	470	470	470	470	469	466	466	464	464	464	463	463	462	462	461	460
	B	463	451	451	450	449	447	446	444	443	442	441	440	439	438	437	436
	C	462	447	447	446	445	444	442	441	440	439	438	437	436	435	434	433
42 Creep	A	458	443	443	442	441	439	436	435	434	433	432	431	430	429	428	427
	B	427	412	412	411	410	408	406	405	404	403	402	401	399	398	397	396
	C	475	460	460	460	458	455	454	453	450	449	448	448	447	447	445	444
43 Shrinkage	A	457	457	457	457	457	456	455	455	454	454	453	453	452	452	451	451
	B	415	415	415	415	414	414	413	412	411	410	409	408	408	408	408	408
44 Shrinkage	A	467	467	467	467	467	466	465	465	464	464	464	464	463	463	462	461
	B	458	458	458	458	457	455	455	454	453	453	452	452	451	451	450	450
	C	456	456	456	456	455	453	452	452	451	451	450	450	449	449	448	448

Table A.15: Creep strains calculated data

Samples	Unloaded	loaded	Creep strain												
Date 2017	28-Sep	28-Sep	29-Sep	01-Oct	05-Oct	12-Oct	19-Oct	26-Oct	02-Nov	09-Nov	16-Nov	23-Nov	07-Dec	21-Dec	06-Jan 2018
Time, days	0	0	1	3	7	14	21	28	35	42	49	56	70	84	100
0% mk	0.00E+00	1.45E-02	1.69E-02	1.79E-02	1.91E-02	2.09E-02	2.27E-02	2.45E-02	2.59E-02	2.69E-02	2.77E-02	2.81E-02	2.91E-02	3.03E-02	3.09E-02
10% mk	0.00E+00	1.39E-02	1.65E-02	1.72E-02	1.82E-02	1.98E-02	2.18E-02	2.31E-02	2.45E-02	2.55E-02	2.61E-02	2.66E-02	2.77E-02	2.83E-02	2.90E-02
15% mk	0.00E+00	1.49E-02	1.63E-02	1.68E-02	1.76E-02	1.92E-02	2.04E-02	2.14E-02	2.21E-02	2.27E-02	2.36E-02	2.41E-02	2.51E-02	2.59E-02	2.64E-02
20% mk	0.00E+00	1.43E-02	1.51E-02	1.57E-02	1.65E-02	1.75E-02	1.83E-02	1.87E-02	1.95E-02	1.97E-02	2.03E-02	2.07E-02	2.15E-02	2.19E-02	2.27E-02

Table A.16: Specific creep calculated data

Samples	loaded	Specific creep (strain/MPa)												
Date 2017	28-Sep	29-Sep	01-Oct	05-Oct	12-Oct	19-Oct	26-Oct	02-Nov	09-Nov	16-Nov	23-Nov	07-Dec	21-Dec	06-Jan 2018
Time, days	0	1	3	7	14	21	28	35	42	49	56	70	84	100
0% mk	2.42E-05	2.82E-05	2.99E-05	3.19E-05	3.48E-05	3.78E-05	4.08E-05	4.31E-05	4.48E-05	4.61E-05	4.68E-05	4.85E-05	5.05E-05	5.14E-05
10% mk	2.32E-05	2.75E-05	2.86E-05	3.04E-05	3.30E-05	3.63E-05	3.84E-05	4.09E-05	4.25E-05	4.35E-05	4.44E-05	4.62E-05	4.71E-05	4.84E-05
15% mk	2.49E-05	2.71E-05	2.79E-05	2.93E-05	3.21E-05	3.40E-05	3.57E-05	3.68E-05	3.79E-05	3.93E-05	4.01E-05	4.18E-05	4.31E-05	4.40E-05
20% mk	2.39E-05	2.52E-05	2.62E-05	2.75E-05	2.92E-05	3.05E-05	3.12E-05	3.25E-05	3.28E-05	3.38E-05	3.45E-05	3.58E-05	3.65E-05	3.78E-05

Table A.17: Creep coefficient calculated data

Samples	loaded	Creep coefficient												
Date 2017	28-Sep	29-Sep	01-Oct	05-Oct	12-Oct	19-Oct	26-Oct	02-Nov	09-Nov	16-Nov	23-Nov	07-Dec	21-Dec	06-Jan 2018
Time, days	0	1	3	7	14	21	28	35	42	49	56	70	84	100
0% mk	1.00	1.16	1.23	1.32	1.44	1.56	1.69	1.78	1.85	1.90	1.93	2.00	2.08	2.12
10% mk	1.00	1.19	1.23	1.31	1.42	1.56	1.65	1.76	1.83	1.87	1.91	1.99	2.03	2.08
15% mk	1.00	1.09	1.12	1.18	1.29	1.37	1.43	1.48	1.52	1.58	1.61	1.68	1.73	1.77
20% mk	1.00	1.06	1.10	1.15	1.22	1.28	1.31	1.36	1.37	1.42	1.44	1.50	1.53	1.58

Table A.18: Drying shrinkage strains calculated data

	Drying shrinkage strain from day 21												
Time	0	21	25	32	39	46	53	60	67	74	88	102	118
0% mk	0.00E+00	1.81E-02	2.03E-02	2.21E-02	2.43E-02	2.57E-02	2.63E-02	2.73E-02	2.83E-02	2.95E-02	3.01E-02	3.12E-02	3.28E-02
10% mk	0.00E+00	1.54E-02	1.76E-02	1.86E-02	1.96E-02	2.09E-02	2.12E-02	2.22E-02	2.31E-02	2.39E-02	2.42E-02	2.50E-02	2.59E-02
15% mk	0.00E+00	1.44E-02	1.64E-02	1.71E-02	1.86E-02	1.92E-02	1.94E-02	2.02E-02	2.09E-02	2.12E-02	2.16E-02	2.21E-02	2.29E-02
20% mk	0.00E+00	1.35E-02	1.47E-02	1.55E-02	1.59E-02	1.69E-02	1.71E-02	1.79E-02	1.81E-02	1.89E-02	1.89E-02	1.97E-02	1.99E-02

A.9. Acceleration carbonation test results

Table A.19: Carbonation depth of concrete at 0.5 and 0.6 w/b ratios

		Carbonation depth, mm			
		0.5 w/b		0.6 w/b	
Exposure duration	Concrete type	Average depth	Stdev	Average depth	Stdev
	0% mk	2.14	0.61	5.27	0.71
	10% mk	1.52	0.59	4.90	0.94
	15% mk	1.02	0.32	4.65	0.82
	20% mk	0.95	0.34	4.10	0.84
28 days	50% GGCS	3.67	0.84	4.59	0.36
	0% mk	3.33	0.48	6.90	0.77
	10% mk	2.27	0.62	6.95	0.72
	15% mk	1.80	0.39	6.85	0.77
	20% mk	1.41	0.39	6.99	1.48
56 days	50% GGCS	4.35	0.56	8.01	1.53
	0% mk	3.48	0.69	8.75	0.81
	10% mk	3.17	0.50	8.12	1.01
	15% mk	2.29	0.28	8.09	0.94
	20% mk	2.32	0.33	8.21	0.70
90 days	50% GGCS	5.10	0.30	8.88	0.38

A.10. Chloride bulk diffusion

$$Chloride\ content\ \%\ (by\ mass\ of\ concrete) = \frac{Molar\ mass\ of\ Cl * volume\ of\ titrant\ consumed * Molarity\ of\ titrant}{Mass\ of\ sample * 10}$$

$$Chloride\ content, \%\ (by\ mass\ of\ cement) = \frac{Chloride\ content, \%\ (by\ mass\ of\ concrete) * density\ of\ concrete}{Cement\ content}$$

Table A.20: Titration results and CI content data used for analysis of Bulk diffusion results

Core Label	Depth (mm)	Average depth (mm)	mass of sample (g)	Volume of titrant consumed (ml)	Chloride Content % (by mass of concrete)	Chloride Content % (by mass of cement)
0.4 w/b 0% mk	0-2	1	2.311	3.740	0.5737	3.061
	2-4	3	2.319	2.201	0.3365	1.795
	4-6	5	2.462	0.757	0.1090	0.581
	6-8	7	2.402	0.069	0.0101	0.054
	8-10	9	2.205	0.027	0.0044	0.023
	10-12	11	2.381	0.036	0.0053	0.028
	12-14	12	2.229	3.740	0.5737	3.061
	ci		2.246	0.035	0.0055	0.030
0.4 w/b 10% mk	0-2	1	2.359	1.436	0.2149	1.146
	2-4	3	2.359	0.446	0.0670	0.358
	4-6	5	2.372	0.091	0.0136	0.073
	6-8	7	2.349	0.056	0.0084	0.045
	8-10	9	2.183	0.040	0.0065	0.035
	10-12	11	2.353	0.038	0.0057	0.031
	12-14	12	2.323	0.037	0.0056	0.030
	14-16	13	2.356	0.033	0.0050	0.026
	ci		2.263	0.032	0.0051	0.027

Concrete type	0.4 w/b	0.5 w/b	0.6 w/b
Concrete Density (kg/m^3)	2470	2470	2470
Cement Content (kg/m^3)	463	370	308
Molarity of titrant (M)	0.1	0.1	0.1
Molar mass of Cl (g)	35.45	35.45	35.45

Core Label	Depth (mm)	Average depth (mm)	mass of sample (g)	Volume of titrant consumed (ml)	Chloride Content % (by mass of concrete)	Chloride Content % (by mass of cement)
0.4 w/b 15% mk	0-2	1	2.291	1.350	0.2089	1.114
	2-4	2	2.291	0.350	0.0542	0.289
	4-6	3	2.225	0.190	0.0303	0.161
	6-8	5	2.418	0.042	0.0061	0.033
	8-10	7	2.215	0.031	0.0049	0.026
	10-12	9	2.261	0.044	0.0070	0.037
	12-14	11	2.213	0.028	0.0045	0.024
	14-16	13	2.203	0.027	0.0043	0.023
	ci		2.153	0.039	0.0065	0.035
0.4 w/b 20% mk	0-2	1	2.463	1.380	0.1986	1.060
	2-4	2	2.463	0.380	0.0547	0.292
	4-6	3	2.463	0.128	0.0185	0.098
	6-8	5	2.283	0.058	0.0090	0.048
	8-10	7	2.478	0.035	0.0050	0.027
	10-12	9	2.191	0.070	0.0113	0.060
	12-14	11	2.118	0.037	0.0062	0.033
	14-16	13	2.393	0.031	0.0047	0.025
	ci		2.225	0.025	0.0040	0.022

Core Label	Depth (mm)	Average depth (mm)	mass of sample (g)	Volume of titrant consumed (ml)	Chloride Content % (by mass of concrete)	Chloride Content % (by mass of cement)
0.5 w/b 0% mk	0-2	1	2.328	6.370	0.9700	6.4754
	2-4	3	2.131	3.590	0.5972	3.9868
	4-6	5	2.271	1.551	0.2421	1.6162
	6-8	7	2.144	0.218	0.0360	0.2401
	8-10	9	2.421	0.050	0.0073	0.0488
	10-12	11	2.129	0.046	0.0077	0.0511
	12-24	13	2.351	0.033	0.0050	0.0332
	14-16	15	2.307	0.029	0.0044	0.0294
	16-18	17	2.268	0.021	0.0033	0.0222
	18-20	19	2.388	0.046	0.0069	0.0460
	ci		2.393	0.025	0.0037	0.0246
0.5 w/b 10% mk	0-2	1	2.135	4.980	0.8269	5.520
	2-4	3	2.245	1.910	0.3016	2.013
	4-6	5	2.385	0.138	0.0206	0.137
	6-8	7	2.321	0.067	0.0102	0.068
	8-10	9	2.218	0.032	0.0051	0.034
	10-12	11	2.258	0.031	0.0048	0.032
	12-24	13	2.316	0.028	0.0042	0.028
	14-16	15	2.255	0.039	0.0061	0.040
	16-18	17	2.206	0.030	0.0048	0.032
	18-20	19	2.144	0.029	0.0047	0.032
	ci		2.253	0.046	0.0072	0.048

Core Label	Depth (mm)	Average depth (mm)	mass of sample (g)	Volume of titrant consumed (ml)	Chloride Content % (by mass of concrete)	Chloride Content % (by mass of cement)
0.5 w/b 15% mk	0-2	1	2.191	4.180	0.6763	4.515
	2-4	3	2.227	1.370	0.2181	1.456
	4-6	5	2.237	0.047	0.0074	0.050
	6-8	7	2.462	0.043	0.0061	0.041
	8-10	9	2.390	0.035	0.0052	0.034
	10-12	11	2.113	0.034	0.0056	0.038
	12-24	13	2.223	0.043	0.0068	0.045
	14-16	15	2.195	0.051	0.0082	0.055
	ci		2.39	0.046	0.0068	0.045
0.5 w/b 20% mk	0-2	1	2.280	3.010	0.4680	3.124
	2-4	3	2.338	1.010	0.1531	1.022
	4-6	5	2.338	0.213	0.0323	0.216
	6-8	7	2.295	0.065	0.0101	0.067
	8-10	9	2.335	0.045	0.0068	0.045
	10-12	11	2.207	0.030	0.0048	0.032
	12-24	13	2.190	0.029	0.0046	0.031
	14-16	15	2.147	0.025	0.0041	0.027
	16-18	17	2.198	0.026	0.0043	0.028
	18-20	19	2.381	0.021	0.0031	0.021
	ci		2.231	0.044	0.0070	0.047

Core Label	Depth (mm)	Average depth (mm)	mass of sample (g)	Volume of titrant consumed (ml)	Chloride Content % (by mass of concrete)	Chloride Content % (by mass of cement)
0.6 w/b 0% mk	0-1	0.5	2.208	8.030	1.2892	10.339
	1-2	1.5	2.276	7.577	1.1802	9.464
	2-3	2.5	2.221	6.906	1.1023	8.840
	3-4	3.5	2.245	6.290	0.9932	7.965
	4-5	4.5	2.458	5.554	0.8010	6.424
	5-6	5.5	2.341	4.566	0.6914	5.544
	6-8	7.0	2.430	3.496	0.5100	4.090
	8-10	8.0	2.384	2.555	0.3799	3.046
	10-15	12.5	2.437	0.526	0.0765	0.614
	15-20	17.5	2.384	0.366	0.0544	0.436
	20-25	22.5	2.150	0.037	0.0061	0.049
	ci		2.216	0.021	0.0033	0.027
0.6 w/b 10% mk	0-1	0.5	2.135	6.580	1.0926	8.762
	1-2	1.5	2.258	5.250	0.8242	6.610
	2-3	2.5	2.130	4.390	0.7306	5.859
	3-4	3.5	2.137	3.270	0.5424	4.350
	4-5	4.5	2.161	2.713	0.4451	3.569
	5-6	5.5	2.405	1.830	0.2697	2.163
	6-8	7.0	2.279	0.860	0.1338	1.073
	8-10	8.0	2.506	0.352	0.0498	0.399
	10-15	12.5	2.307	0.046	0.0071	0.057
	15-20	17.5	2.408	0.023	0.0034	0.027
	20-25	22.5	2.186	0.023	0.0038	0.030
	ci		2.157	0.037	0.0061	0.049

Core Label	Depth (mm)	Average depth (mm)	mass of sample (g)	Volume of titrant consumed (ml)	Chloride Content % (by mass of concrete)	Chloride Content % (by mass of cement)
0.6 w/b 15% mk	0-1	0.5	2.167	6.050	0.9897	7.937
	1-2	1.5	2.268	5.270	0.8237	6.606
	2-3	2.5	2.392	4.840	0.7173	5.752
	3-4	3.5	2.139	3.040	0.5038	4.040
	4-5	4.5	2.517	2.450	0.3451	2.767
	5-6	5.5	2.413	1.430	0.2101	1.685
	6-8	7.0	2.299	0.710	0.1095	0.878
	8-10	8.0	2.124	0.025	0.0041	0.033
	10-15	12.5	2.465	0.034	0.0048	0.039
	15-20	17.5	2.261	0.022	0.0035	0.028
	20-25	22.5	2.302	0.025	0.0039	0.031
	ci		2.25	0.038	0.0060	0.048
0.6 w/b 20% mk	0-1	0.5	2.311	6.639	1.0184	8.167
	1-2	1.5	2.209	4.472	0.7177	5.755
	2-3	2.5	2.412	4.046	0.5947	4.769
	3-4	3.5	2.247	3.147	0.4965	3.982
	4-5	4.5	2.514	2.540	0.3582	2.872
	5-6	5.5	2.352	1.501	0.2262	1.814
	6-8	7.0	2.219	0.840	0.1342	1.076
	8-10	8.0	2.434	0.250	0.0363	0.291
	10-15	12.5	2.466	0.033	0.0047	0.037
	15-20	17.5	2.505	0.026	0.0037	0.030
	20-25	22.5	2.434	0.022	0.0031	0.025
	ci		2.328	0.045	0.0069	0.055

APPLICATION FORM

Please Note:
Any person planning to undertake research in the Faculty of Engineering and the Built Environment (EBE) at the University of Cape Town is required to complete this form **before** collecting or analysing data. The objective of submitting this application *prior* to embarking on research is to ensure that the highest ethical standards in research, conducted under the auspices of the EBE Faculty, are met. Please ensure that you have read, and understood the **EBE Ethics in Research Handbook** (available from the UCT EBE, Research Ethics website) prior to completing this application form: http://www.ebe.uct.ac.za/ebe/research/ethics1

APPLICANT'S DETAILS		
Name of principal researcher, student or external applicant		Alice Titus Bakera
Department		Civil Engineering
Preferred email address of applicant:		Bkrali003@myuct.ac.za
If Student	Your Degree: e.g., MSc, PhD, etc.	MSc (Eng)
	Credit Value of Research: e.g., 60/120/180/360 etc.	120
	Name of Supervisor (if supervised):	Emeritus Prof Mark Alexander
If this is a researchcontract, indicate the source of funding/sponsorship		CoMSIRU
Project Title		Properties of Western Cape concrete with metakaolin

I hereby undertake to carry out my research in such a way that:
- there is no apparent legal objection to the nature or the method of research; and
- the research will not compromise staff or students or the other responsibilities of the University;
- the stated objective will be achieved, and the findings will have a high degree of validity;
- limitations and alternative interpretations will be considered;
- the findings could be subject to peer review and publicly available; and
- I will comply with the conventions of copyright and avoid any practice that would constitute plagiarism.

SIGNED BY	Full name	Signature	Date
Principal Researcher/ Student/External applicant	Alice Titus Bakera		**31 Jan 2018**

APPLICATION APPROVED BY	Full name	Signature	Date
Supervisor (where applicable)	Emeritus Prof Mark Alexander		**31 Jan 2018**
HOD (or delegated nominee) Final authority for all applicants who have answered NO to all questions in Section1; and for all Undergraduateresearch (Including Honours).	Click here to enter text.		Click here to enter a date.
Chair : Faculty EIR Committee For applicants other than undergraduate students who have answered YES to any of the above questions.	R Behrens		12 Feb 2018